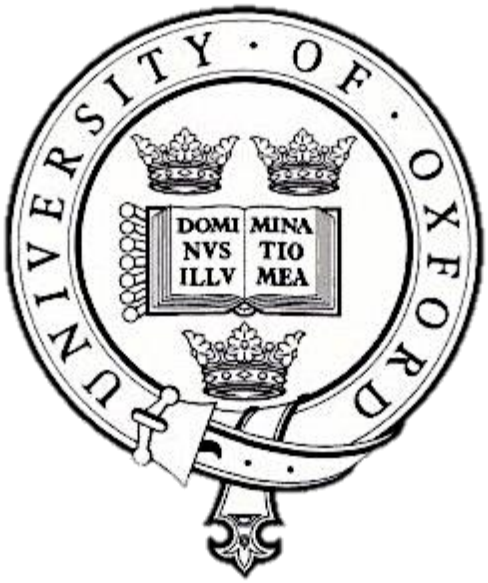
Second Generation Superagonistic Anti-PD-1 Antibodies



Susan Yangshan Yu

Linacre College

Supervisor: Simon J. Davis

Thesis submitted for the degree of Doctor of Philosophy

Trinity Term, 2019

The work described in this thesis was supported by the Medical Research Council [grant number 1238220].



Abstract

Second Generation Superagonistic Anti-PD-1 Antibodies

Susan Yangshan Yu, Linacre College

Thesis submitted for the degree of Doctor of Philosophy

Trinity Term, 2019

Antibodies known as 'superagonists', such as those raised against CD28, induce high levels of signalling activity. Based on the kinetic-segregation model, a hypothesis arose: the greater potency of superagonists arises from their ability to more effectively exclude large phosphatases from the vicinity of CD28, favouring its phosphorylation. This hypothesis can be further extrapolated so that any immobilized antibody binding to a membrane-proximal epitope on a receptor with tyrosine phosphorylation motifs should induce signalling by that receptor. Previous studies indicated that antibody epitope positions are related to their signalling induction abilities. Earlier findings demonstrated that strong inhibitory signalling could also be induced by 1st generation anti-PD-1 antibodies that bind close to the membrane with high affinity, or away from the membrane with very low affinity. We have combined the apparently advantageous features of both sets of antibodies into a single 2nd generation anti-PD-1 antibody using a mutagenesis approach and subsequently tested their binding to PD-1 *via* surface plasmon resonance (SPR). We generated a new model of the superagonistic complex from our mutational SPR data and previous mutational data on PD-1. This model confirmed that it is indeed the position of the epitope, not the chemistry of binding, that dictates whether an antibody is an effective agonist and a blocker of TCR signalling or not. We then devised different *in vitro* assay formats, plate-bound and in solution, to investigate the effects of these anti-PD-1 antibodies on cytokine generation and cell proliferation. By adding higher levels of anti-PD-1 antibodies, greater IL-2 suppression was observed, regardless of the antibody presentation method. Synergistic inhibitory effects were further observed with combinations of these antibodies. Similarly, we studied the inhibitory effects of our antibodies on germinal centre B cell formation, primary antibody response, antibody affinity maturation and $CD8^+$ T cell response *in vivo*. Our *in vivo* assays showed that a higher concentration of anti-PD-1 antibody application led to larger inhibitory effects, therefore dose optimisation will also be key for maximisation of antibody inhibitory potential. Compared to the 1st generation antibodies, the 2nd generation antibodies displayed reduced PD-1 cell surface downregulation *in vivo*. Our results provided evidence that PD-1 downregulation can be uncoupled from receptor triggering by altering affinity. This could potentially help deliver sustained inhibitory PD-1 signalling. The experiments demonstrated in this thesis provide a foundation for generating a novel class of potentially therapeutic antibodies, the inhibitory superagonists.

Acknowledgements

A DPhil thesis cannot be completed without the generous help of numerous people.

First and foremost, I would like to thank my caring and wonderful family. I'm eternally grateful for my mum, dad, and brother, for providing me with ample wisdom, incredible support, guidance, steadfast and unconditional love. Thank you so much for always being there for me and for bringing me immense laughter and joy. Your unwavering strength and immense patience have helped me weather many storms. I'm grateful for my grandparents, uncles and aunts, for their endless support, despite the oceans that separate us. Thank you all for making me bolder, stronger, and hopefully wiser. Thank you for inspiring me to be the best that I can be!

I'm indebted to Prof. Simon Davis, my supervisor who has guided me through the years. I would also like to thank Prof. Richard Cornall and Consuelo for their support. My immediate thanks need to go every member of the Davis and the Cornall lab, past, and present. Thank you for teaching me new skills and knowledge. I'm grateful for the advice and support shown by everyone, and also for the fun times we've had inside and outside the lab. Special thanks need to go to Oliver, Jan, Dongdong, Heather and Mai, for their support and guidance with my DPhil project.

Undoubtedly, I would like to thank all of my friends for enriching my life. Thank you for your encouragements and for inspiring me to stay strong and be a better person. I wish to express my gratitude to Amy, Elizabeth, and Xiaoxiao for their invaluable support and friendship. I'm especially grateful for Alec, for helping me to learn and transform. Thank you for your love, fellowship, and support along this unpredicatable odyssey. May we continue to learn, flourish, and transform together!

Finally, I wish to dedicate this thesis to my dearly beloved family.

Contents

Chapter 1 General introduction 1

I. Overview of the immune system 1

II. The innate immune response 2

III. The adaptive immune response 4

III.A. T-cell mediated immunity 4

III.B. $CD4^+$ T cells 5

III.C. $CD8^+$ T cells 6

III.D. Regulatory T cells 7

III.E. Natural killer T cells 7

III.F. Memory T cells 8

III.G. Antigen presentation 8

III.H. B cell mediated immunity 9

IV.A. Antibody structure and function 10

IV.B. Fc receptors 12

V. Immunoreceptors and signalling 13

V.A. The TCR complex 14

V.B. TCR downstream signalling 15

V.C. Models of T cell activation 15

V.D. The aggregation model 16

V.E. Conformational change models 18

V.F. Kinetic segregation and redistribution-based models 21

V.G. B-cell activation 23

V.H. Superagonistic antibody signalling 23

VI. Costimulatory pathway 24

VI.A. CD28 24

a. Structure/ligands 24

VI.A.b. Signalling 27

VI.B. CTLA-4 28

a. Structure/ligands **28**
VI.B.b. Signalling **28**
VI.C. BTLA **29**
a. Structure/ligands **29**
VI.C.b. Signalling **29**
VI.D. ICOS **30**
a. Structure/ligands **30**
VI.D.b. Signalling **30**
VII. PD-1 ..... **31**
A. PD-1 structure **31**
VII.B. Regulation of PD-1 expression **31**
VII.C. PD-1 ligands **33**
a. Structure **33**
VII.C.b. Expression **33**
VII.D. PD-1 Signalling **34**
VII.E. PD-1 polymorphisms **35**
VIII. Costimulation and therapy **36**
A. Non PD-1 costimulatory pathways **36**
VIII.B. PD-1 ..... **39**
VIII.B.a. Chronic viral infections **40**
VIII.B.b. Transplantation immunity **40**
VIII.B.c. Anti-tumour immunity **42**
VIII.B.d. Autoimmunity **43**
VIII.B.d.(i) Type I diabetes **43**
VIII.B.d.(ii) Experimental autoimmune encephalomyelitis **44**
VIII.B.d.(iii) Inflammatory bowel disease **45**
VIII.B.d.(iv) Rheumatoid arthritis **46**
VIII.B.d.(v) Systemic lupus erythematosus **47**
IX. Work preceding the project **48**
X. Objectives of this thesis **55**

Chapter 2 Materials and methods 56
I. Molecular cloning techniques 56
I.A. Overview of cloning method.....56
I.B. Polymerase chain reaction (PCR) 56
I.C. Agarose gel electrophoresis 58
I.D. Restriction enzyme digestion of DNA.....59
I.E. Ligation of inserts into vectors. 59
I.F. Competent bacterial cell transformation.....60
I.G. Vector production and purification.....61
I.H. DNA sequencing and analysis.....61
I.I. Glycerol stocks of transformed bacteria.....62
I.J. Colony PCR.....62
I.K. Generating Cl19BirAHis WT and mutant Fabs.....62
II. Mammalian cell culture.....64
II.A. General techniques.....64
II.B. Cell culture media 64
II.C. Thawing of cells 65
II.D. Cell freezing 65
II.E. Cell counting 65
II.F. Sub-culturing of cells.....68
II.G. Plating of cells for transient transfection 68
II.H. PEI Co-transfection of HEK 293T cells for Cl19 Fab production 68
II.I. Production of soluble His-tagged protein in mammalian cell lines 69
II.J. Stable cloning and large scale soluble protein production with CHOK1 cells 69
II.K. pEE14 expression vector for stable transfections.....70
II.L. Stable transfection of CHOK1 cells for the production of first generation and second generation whole anti-PD-1 antibodies.....70
II.M. Methionine sulfoxamine (MSX) Selection 72
II.N. Dot blot for highly expressing clone identification 73

II.O. Large-scale cell culture of the chosen clone for protein generation 73
III. Protein techniques 76
III.A. Extraction of His tagged protein from tissue culture supernatant.....76
III.B. Extraction of antibodies from tissue culture supernatant using protein G.....77
III.C. Protein purification by gel filtration.....78
III.D. Sodium dodecyl sulphate polyacrylamide gel electrophoresis (SDS-PAGE) for detecting the purity of antibodies.....78
III.E. Western blotting.....79
III.F. Biotinylation of protein.....79
IV. Surface Plasmon Resonance (SPR) using Biacore.....80
V. Flow cytometry 81
VI. Mouse Model: humanized PD-1 knock-in (hPD-1 k.i.) mice 82
VII. Cell purification: ficoll stratification of mouse splenocytes.....83
VIII. *In vitro* assays 83
VIII.A. CFSE cell proliferation assay 83
VIII.B. Sheep red blood cell specific enzyme-linked immunosorbent assays (ELISAs) 84
VIII.C. Anti-mouse IL-2, TNF-α, IFN-γ ELISAs.....85
VIII.D. NP5-BSA and NP25-BSA ELISAs 86
Chapter 3 PD-1 and Cl19 Fab production for binding analysis.....88
I. Introduction.....88
II. Results.....89
II.A. PD-1FcHis expression and purification.....89
II.B. PD-1FcHis cleavage and deglycosylation.....91
II.C. Anti-PD-1 Cl19 Fab transient expression and purification.....94
II.D. Test for PD-1FcHis and Cl19 Fab complex formation and binding using FPLC.....98
II.E. Stable expression and purification of Cl19 Fab.....98
II.F. Analysis of the kinetics of binding of PD-1 to Cl19 Fab using a surface

plasmon resonance-based assay.....102
III. Discussion.....102
Chapter 4 Production and characterisation of new fast off-rate Cl19 antibody derivatives.....105
I. Introduction.....105
II. Results.....106
II.A. Production of anti-PD-1 Cl19 FabBirAHis.....106
II.B. Mutant anti-PD-1 Cl19BirAHis Fabs.....109
II.C. First set of mutant anti-PD-1 Cl19 Fabs and their binding kinetics.....112
II.D. Kinetic analysis of the Cl19 R3M2L and R3M3L mutants.....112
II.E. Second-round mutations of anti-PD-1 Cl19 FabBirAHis.....118
II.F. Expression of intact forms of the 1st generation Cl19 antibody and 2nd generation anti-PD-1 antibodies.....119
II.G. Testing of Cl19 isotype control antibody on the Biacore.....127
III. Discussion.....127
Chapter 5 Analysis of the inhibitory effects of anti-PD-1 antibodies *in vitro*.....134
I. Introduction.....134
II. Results.....136
II.A. PD-1 cell surface downregulation upon activation *in vitro*.....136
II.B. Effects of 1st generation antibodies on cytokine production.....137
II.C. Effects of 2nd generation antibodies and antibody combinations on cytokine production.....143
II.D. Effects of different types of immobilisation on IL-2 suppression.....145
II.E. Suppression of proliferation with single immobilised anti-PD-1 antibodies.....152
II.F. Suppression of proliferation with combinations of immobilised anti-PD-1 antibodies.....154
II.G. IL-2 production in the solid-phase assay.....154
III. Discussion.....157

Chapter 6 Analysis of the inhibitory effects of anti-PD-1 antibodies *in vivo*.....162

I. Introduction.....162

II. Results.....165

II.A. Effects of single anti-PD-1 antibody administration on GC B cell formation following SRCB challenge.....165

II.B. SRBC challenge and inhibitory effects of anti-PD-1 antibodies on the GC response with a combination of anti-PD-1 antibodies.....165

II.C. The effects of anti-PD-1 Cl19 antibodies on the primary antibody response following SRBC challenge.....166

II.D. NP-CGG challenge and effects of anti-PD-1 antibodies on antibody affinity maturation.....170

II.E. Effects of anti-PD-1 antibody administration on cell surface PD-1 downregulation following SRCB challenge.....170

II.F. The effects of anti-PD-1 antibody administration on the antigen specific $CD8^+$ T cell response.....179

II.G. Reduced PD-1 downregulation with 2nd generation antibodies and lack of cytotoxicity *in vivo*.....180

III. Discussion.....183

Chapter 7 General discussion.....188

I. Results from this thesis.....189

I.A. Mutational analysis of the Cl19 PD-1 binding site.....189

I.B. Production and characterisation of new fast off-rate Cl19 derivatives.....190

I.C. The properties of the Cl19 Fab/PD-1 interaction.....191

I.D. Inhibitory effects of anti-PD-1 antibodies *in vitro*.....196

I.E. Inhibitory effects of anti-PD-1 antibodies *in vivo*.....199

I.F. PD-1 receptor downregulation.....201

I.G. Signalling implications.....204

II. Concluding remarks.....207

Abbreviations

APC	Antigen-presenting cell
BCR	B-cell receptor
BLAST	Basic local alignment search tool
BTLA	B and T lymphocyte attenuator
CD	Cluster of differentiation
CDR	Complementary-determining region
CHO	Chinese hamster ovary
CMV	Cytomegalovirus
CTLA-4	Cytotoxic T-lymphocyte-associated protein 4
DAM	Donkey anti-mouse Fc antibody
DC	Dendritic cell
DMEM	Dulbecco's modified eagle medium
DNA	Deoxyribonucleic acid
dNTP	Deoxynucleotide
ECL	Enhanced chemiluminescence
EDTA	Ethylenediaminetetraacetic acid
EIA	Enzyme-immunoassay
ELISA	Enzyme-linked immunosorbent assay
ER	Endoplasmic reticulum
Fab	Fragment antigen-binding
FACS	Fluorescence-activated cell sorting
Fc	Fragment crystallisable
FcR	Fragment crystallisable receptor
FPLC	Fast protein Liquid Chromatography
h	Human
HBS	HEPES-buffered saline
HEK	Human embryonic kidney
His	Histidine

HIV	Human immunodeficiency virus
HRP	Horse radish peroxidase
ICOS	Inducible T-cell costimulator
Ig	Immunoglobulin
IL-2	Interleukin-2
IFN-γ	Interferon-γ
ITAM	Immunoreceptor tyrosine-based activation motif
ITIM	Immunoreceptor tyrosine-based inhibitory motif
ITSM	Immunoreceptor tyrosine-based switch motif
K_D	Dissociation constant
k_{off}	Dissociation rate constant
k_{on}	Association rate constant
KS	Kinetic segregation
m	Mouse
MFI	Mean fluorescence intensity
MHC	Major histocompatibility complex
MSX	Methionine sulphoximine
NK	Natural killer
N-terminus	Amine-terminus
NFAT	Nuclear factor of activated T-cells
Ni-NTA	Nickel-nitrilotriacetic acid
PAMPs	Pathogen associated molecular patterns
PBS	Phosphate-buffered saline
PCR	Polymerase chain reaction
PD-1	Programmed cell death-1
pH	Potential hydrogen
pMHC	peptide-bound MHC protein
RPMI	Roswell Park Memorial Institute medium
SDS-PAGE	Sodium dodecyl sulphate polyacrylamide gel electrophoresis
SH2	Src homology 2

SPR	Surface plasmon resonance
TAP	Transporter associated with antigen presentation
Tapasin	TAP-associated glycoprotein
TCR	T-cell receptor
TIB	Type I diabetes
TNF	Tumour necrosis factor
TSS	Transformation and storage solution
ZAP-70	Zeta-chain associated protein of 70 kDa

Chapter 1
General introduction

I. Overview of the immune system

We are constantly being exposed to organisms that are being swallowed, inhaled or dwell on our mucous membranes or skin. The pathogenicity of the organisms and the integrity of host defence mechanisms determine whether such organisms can penetrate and cause disease or not [1]. The immune system consists of an interactive network of cells, humoral factors, cytokines and lymphoid organs. The immune system functions to provide immunity against disease through the detection of disease causing agents and subsequent induction of suitable responses. The critical function of the immune system in host defence is best illustrated when it goes wrong. Underactivity can result in severe infections and tumours whilst over-activity leads to autoimmunity and allergic responses.

The first unicellular organism emerged more than 3.5 billion years ago. This is when, almost concurrently, the earliest form of immunity began developing [2]. The most primitive type of immunity allowed amoeba to make distinctions between food and other amoebas. This, over time, has evolved into a key host defence mechanism. It has been shown through genomic analysis of multicellular organisms that efficient mechanisms of host immunity were already in existence prior to the divergence of plants and animals [3]. Multicellular organisms (metazoans) sense conserved products on myriad classes of pathogens named pathogen associated molecular patterns (PAMPs), that are highly conserved and enable the detection of "microbial non-self" [4]. Jawed vertebrates developed a more complex method of host defence through rearrangement of germline encoded specific sensors. This enabled them to distinguish varying non-self elements from the other. The discovery of the

recombination activation gene (RAG) proteins, RAG-1 and RAG-2, helped to explain the mechanism of this adaptive form of immunity. These proteins facilitate the recombinatorial gene rearrangement of immunoglobulins and T cell receptors, helping to generate immense diversity [5]. Immunity is divided into two parts distinguished by the specificity and the speed of the reaction. They are called the innate and the adaptive responses, although in reality, there is a great deal of interaction between them. The more primitive arm comprises innate immunity, where a constitutively produced, highly conserved sensing mechanism and fast-acting effector cells operate, whilst the other, adaptive arm relies on the great diversity of reactivity of the immune system.

II. The innate immune response

The innate immune response includes chemical, physical and microbiological barriers as well as pivotal elements of the immune system comprised of monocytes, macrophages, neutrophils, complement, acute phase proteins, cytokines and chemokines, which provide immediate host defence mechanisms [1]. This arm of the immune system is highly conserved in nature, and observed in even the simplest animals, thereby confirming its great importance for survival.

A fundamental feature of the innate reaction is neutrophil recruitment and their activation at infection sites for the eradication of pathogens [6]. When neutrophil activity is dysregulated, this leads to vasculitis, systemic inflammatory immune response syndrome and inflammation, *e.g.* in connective tissue diseases. There is great interest in understanding mechanisms underlying such processes for the development of new anti-inflammatory immunotherapies [7, 8].

The complement system has various essential roles in innate immunity. It is comprised of at least twenty serum glycoproteins, some of which are regulatory [1]. These glycoproteins are activated in a sequential cascade of enzymatic reactions that is amplified at different stages. This means that the activation of a single molecule

causes thousands of other molecules to be produced as a consequence. Potent anaphylatoxins C3a and C5a are produced, they can elicit a plethora of physiological responses including pathogen opsonisation and their removal by phagocytes, chemoattraction, in addition to cell lysis [9]. The complement system can be activated by three pathways: gram negative bacteria, *via* a classical pathway by antigen antibody reactions and *via* an alternative pathway involving, *e.g.* yeast polysaccharides.

The central physiological role for eosinophils is providing protection against parasitic infections, in particular against nematodes. Such infections cause IgE to be produced by plasma cells which then coats the pathogen. Eosinophils are able to bind to these antibodies using their low affinity receptor $Fc_{\varepsilon}RII$, and release highly cytotoxic substances from their granules including major basic protein, eosinophilic cationic protein, eosinophil derived neurotoxin and eosinophil peroxidase onto pathogen surfaces [1].

Natural killer (NK) cells possess the morphology of lymphocytes but have no specific antigen receptor. They can recognise abnormal cells in two ways. Firstly, they express immunoglobulin receptors (FcR) that bind to antibody-coated pathogens, which culminates in antibody dependent cellular cytotoxicity. Secondly, they can recognise MHC Class I *via* their surface receptors. Upon interaction with a cell, if this receptor is not bound, the NK cells will lyse the target *via* perforin secretion which generates holes in the cell membrane, allowing co-released granzyme to get into the target cell, leading to apoptosis [1].

Cytokines are small molecular weight protein messengers that are produced by virtually all cells. They have a diverse array of immunological functions and are secreted by one cell to change the behaviour of itself or another cell, acting as autocrine, paracrine or endocrine messengers. Intracellular signalling is initiated by binding to specific cell membrane receptors. Most cytokines are soluble but some are also membrane bound. The biological function varies depending on the cell type and

the actual cytokine involved. These include the induction of cell division, activation, movement and apoptosis. Interleukins are a group of cytokines produced by leucocytes and largely have effects on other immune cells. Chemokines are cytokines that have chemoattractant activity. Colony stimulating factors cause differentiation and proliferation of stem cells whilst interferons block viral replication [1].

III. The adaptive immune response

The adaptive immune response is highly specific and is mediated by lymphocytes which express very specific receptors that recognise an enormous variety of antigens due to the way they are assembled. Following successful responses against the pathogen, a fraction of the effector cells differentiates into memory cells which can generate accelerated responses upon re-exposure to the same antigens. Conversely, self-antigens can become targets for adaptive immunity and when dysregulated, destructive damage occurs in the host, leading to autoimmune conditions.

The two key cell types involved in adaptive immunity are the B lymphocytes and T lymphocytes. Both cell types originate from early lymphoid progenitors in the bone marrow. The cells that stay in the bone marrow initially develop into B cells whilst others migrate to the thymus and become T cells [10]. The receptors of these lymphocytes are characterised by their assembly through the recombination of large numbers of variable (V), diversity (D) and joining (J) gene segments. This produces very high levels of diversity for antigen recognition [11].

III.A. T-cell mediated immunity

A constraint of the humoral immunity involving antibodies and the complement system is that cancer antigens and intracellular pathogens often are not accessible. Contrastingly, T-cell-mediated immunity facilitated by antigen presentation *via* MHC can overcome this problem. Within the thymus, β-selection allows the development of double negative ($CD8^-CD4^-$) thymocytes. At this thymocyte selection checkpoint, selection is based on successful rearrangement and pairing of the β chain to the pre-

TCRα chain to generate a pre-TCR. Effective signalling *via* the functional pre-TCR complex leads to CD4 and CD8 co-receptor expression in addition to cellular proliferation [12]. Consequently, thymocytes develop into double positive ($CD8^+CD4^+$) once they pass this checkpoint. Subsequently, the TCRα chain is rearranged and a mature TCR is generated.

In the thymus cortex, cells are exposed to the major histocompatibility complex (MHC)/self-peptide complexes that are expressed by cortical thymic epithelial cells (cTECs). Cells which are unsuccessful in forming interactions with the MHC/peptide complex undergo apoptosis. In contrast, those that successfully interact gain a survival signal (positive selection). Such positively selected cells are thus committed to single positive ($CD8^+CD4^-$ or $CD8^-CD4^+$) lineages. Specifically, cells that form interactions with the MHC class II complex differentiate into CD4 single positive cells while those which interact with the MHC class I complex differentiate into CD8 single positive. Thereafter, these single positive cells migrate to the medulla where they are subject to another round of selection. At this stage of negative selection, cells with high affinity for the MHC/self-peptide complex presented by medullary dendritic cells and TECs (mTECs) undergo elimination. Negative selection is fundamental for the prevention of autoimmune disorders and in the maintenance of tolerance to self-peptides [13, 14].

III.B. $CD4^+$ T cells

T helper (Th) cells are $CD4^+$ T cells which play significant roles in facilitating the adaptive immune response. Upon antigenic stimulation through peptide/MHC class II complexes, naive CD4 T cells proliferate and undergo differentiation into various lineages including Th1, Th2, Th17 and induced regulatory T cells (iTreg). The type of differentiation is mostly dependent upon the cytokine environment. Studies have demonstrated that Th1 differentiation is induced by Interleukin-12 (IL-12) and interferon-gamma (IFN-γ), Th2 cells by IL-4 and IL-2, Th17 cells by transforming growth factor beta (TGF-β) and IL-6, whilst IL-2 and TGF-β can promote iTreg cell

induction [15, 16]. Interestingly, each Th cell lineage has "signature" cytokine production. IFN-γ and tumour necrosis factor-beta (TNF-β) are secreted by Th1; IL-4, IL-5 and IL-13 by Th2; IL-17A, IL-7F and IL-22 by Th17; and TGF-β and IL-10 by iTreg [16, 17]. The generation of such distinct signature cytokines has endowed each cell type with unique functions. Th1 cells are responsible for cell-mediated immune responses through facilitating macrophage and cytotoxic $CD8^+$ Th17 cell activation. They also play a crucial role in fighting against intracellular pathogens and viruses. Conversely, Th2 cells play their part in the humoral immune response. They provide defence against extracellular pathogens by helping to induce B cell immunoglobulin generation. Furthermore, they help to mediate the activation of mast cells and eosinophils [18-21]. Despite the fact that earlier studies have suggested that Th17 cells are responsible for defence against extracellular pathogens such as fungi and bacteria, emerging investigations have shed light on Th17 cells' highly pro-inflammatory nature. This in turn is suggestive of their propensity to induce severe auto-immune disorders [22]. In contrast to the helper T cells, iTregs are able to downregulate the immune response and prevent autoimmunity through suppression of the initial priming and proliferation of auto-reactive T cells [23].

III.C. $CD8^+$ T cells

Cytotoxic T lymphocytes (CTLs; cytotoxic $CD8^+$ T cells) are recognised for their capacity to mediate cytotoxicity. Following antigenic stimulation by peptide/MHC class I complexes, these cells can cause target cell apoptosis by secreting granzymes and perforin. Perforin inserts into the target cell surface membrane and polymerises. This generates a pore, leading to cell lysis and destruction. Granzymes are a family of serine proteases that are released from cytoplasmic granules within the CTLs. They help protect against viral infections and cellular transformations. Once a receptor mediated conjugate is formed between a granzyme containing cell and transformed or infected target cells, granzymes will enter the target cell *via* endocytosis and cause apoptosis. Granzyme B is the most potent pro-apoptotic member of the granzyme family [24]. Furthermore, CTLs can induce apoptosis of the target cell through the

binding of Fas ligand (FasL) to the Fas molecule expressed on target cells [25, 26]. CTLs can also respond through their T cell receptors to myriad antigens by proliferating and secretion of cytokines and chemokines [27].

III.D. Regulatory T cells

Naturally occurring regulatory T cells (nTregs) are characterised by their expression of CD25 (the IL-2 receptor α-chain) and transcription factor forkhead box P3 (FOXP3). Surprisingly, these cells only constitute approximately 5% of $CD4^+$ T cells. They are mainly responsible for the prevention of auto-immunity, maintenance of self-tolerance in addition to regulating immune responses to pathogens. They function *via* the suppression of the activation, proliferation and effector functions of a broad spectrum of immune cells including T cells, B cells, antigen presenting cells and NK cells. Some putative suppressive mechanisms have been shown. These include secretion of immune-suppressive cytokines such as IL-10 and TGF-β, suppression of the activating capacity of dendritic cells and induction of cytolysis [28, 29].

III.E. Natural killer T cells

CD1d-restricted natural killer T (NKT) cells are a unique subset of T cells. Upon T cell activation through TCR engagement, they swiftly generate an array of cytokines including the signature cytokines produced by Th1, Th2 and Th17 cells. CD1d is an MHC class I-related antigen-presenting molecule which is expressed by a wide range of cell types including B cells, DCs, macrophages and hepatocytes. NKT cells play an essential role in the regulation of various immune responses. NKT cells are classified into two groups. This is determined by differences in the T cell receptor (TCR) usage. Type I invariant NKT (iNKT) cells have an invariant TCRα-chain and are easily detected by α-galactosylceramide (α-GalCer)-loaded CD1d tetramers. In contrast, Type II non invariant NKT (non-iNKT) cells have a broader TCR repertoire and thus are not readily identifiable. iNKT cells recognise only glycolipid antigens whilst non-iNKT cells are capable of recognizing non-lipid small molecules.

These two groups of NKT cells in addition to several CD1d-expressing cell types can be found in the intestine. Seemingly, their interactions are modulated by commensal and pathogenic microbes, helping to contribute to intestinal immune reactions in health and disease [30].

III.F. Memory T cells

Immunological memory is a crucial aspect of adaptive immunity. Following the resolution of a primary immune response, lymphocytes no longer undergo clonal expansion. Consequently, the contraction phase ensues whereby the majority of the effector cells undergo apoptosis. A tiny proportion of these effector cells become memory cells with increased life spans. Strikingly, they have a lowered activation threshold and enhanced effector functions. IL-15 and IL-7 are involved in the maintenance of a low level of T-cell proliferation. Upon secondary exposure to the same pathogen, memory T cells undergo reactivation and thus can generate a much faster and stronger response than previously [31, 32].

III.G. Antigen presentation

A key interaction which is integral to the adaptive immune system involves the T cell and an antigen presenting cell (APC). The APCs present foreign peptides on specialized receptors called major histocompatibility complex (MHC) Class I and Class II protein [33]. They are able to bind peptide through the interactions that form between pockets in the MHC protein binding groove and peptide anchor residues. Humans normally express six varying alleles of the highly polymorphic Class I and eight of the Class II, each of which is able to bind 10^3-10^4 unique peptides [34]. Consequently, in principle, any given protein can be presented. These peptides originate from degraded self and pathogen proteins and are selected, processed and get delivered to the cell surface *via* MHC [35]. Some of them are derived from engulfed and degraded microbes which were endocytosed and presented by MHC Class II proteins. Others may have originated from viruses or self proteins that have been imported from the endoplasmic reticulum through the transporter associated

with antigen presentation (TAP). These peptides are loaded onto the class I MHC proteins with the assistance of tapasin, a TAP-associated glycoprotein [33]. The MHC protein has a quaternary structure which is stabilized through the interactions with the antigenic peptide. In the ER, with the help of tapasin, MHC Class I proteins over time swap low affinity peptides for higher binding peptides and can only reach the cell surface once stable folding is achieved. This prevents them from being recycled into the ER *via* calreticulin [36]. MHC class I is ubiquitously expressed on cell membranes of all nucleated cells and is required for their survival by suppression of cytotoxic activity of natural killer cells [37, 38]. In contrast, MHC class II expression is limited to professional APCs, such as B cells, DCs and macrophages [33].

III.H. B cell mediated immunity

Following antigen binding and activation, B cells differentiate into antibody-producing plasma cells. Antibodies comprise soluble forms of the BCR. In contrast, to the TCR, the BCR is not restricted to MHC-presented antigen and is able to recognise almost any structure. This includes organic or inorganic molecules such as a structure on cell or pathogen surfaces, in addition to soluble toxins. In this way, toxins are neutralised. Neutrophils perform opsonisation of microbes by phagocytosis, which then triggers complement system activation. When antigens on the surface of infected or transformed cells are bound by antibody, this causes Fc-receptor bearing cells such as NK cells to destroy the target cell through antibody-dependent cell-mediated cytotoxicity [39]. Such a mechanism actively lyses the abnormal target cell, acting to limit and contain infection.

B cells, in contrast to the Th cells, do not undergo direct activation upon ligation with cognate antigen. Instead, they require signals from a T cell [40-43]. In general, B cells are located in lymph nodes. Sampling of their environment is performed with their BCR. Following antigen binding, the antigen is then internalised, processed and presented to a Th cell using MHC class II. The primed Th cell which has previously

undergone activation *via* the same antigen, then produces cytokines. As a consequence, B cell division ensues, culminating in plasma cell differentiation. Dissimilarly, without T cell help, memory B cells can undergo activation following the recognition of complexed antigen bound to Fc receptors by follicular dendritic cells [1, 44]. This allows for rapid and effective recall antibody responses. Such memory B cells are able to persist in the human body over decades. Thus, they permit memory maintenance for a given antigen without the requirement for constant antigenic stimulation or proliferation. Interestingly, memory B cells are greatly abundant in the human spleen, comprising 45% of the total B cell population.

IV.A. Antibody structure and function

Antibodies are composed of two light (~25 kDa) and two heavy chains (~55 kDa), forming a homodimeric structure which is stabilized by disulphide bonds. Papain treatment of antibodies has helped to elucidate the functional elements of antibodies. Two identical fragments are responsible for antigen binding (Fab) whilst the fragment crystallizable (Fc) is utilized for effector functions. The light chain consists of only one variable and one constant domain whilst the heavy chain is comprised of a variable and three or four constant domains (CH1-CH-4) [45]. Both light and heavy chain variable domains are in the form of immunoglobulin folds, made up of "beta sandwich" domains stabilised by intrachain disulphide bonds. Interchain disulphide bonds are located at the hinge regions of antibodies, where the Fc joins the Fab. Importantly, antibodies are glycoproteins, can be N or O linked [46]. These sugar residues contribute to antibody stability and effector function such as Fc receptor binding. Normally, immunoglobulins are expressed in two distinct states: a secreted form, *i.e.* the antibody or a membrane bound form, *i.e.* the BCR. They are both the result of alternative splicing of the heavy chain constant domains. The ϰ and λ gene loci encode different light chains [45].

Mature B cells express two BCR isotypes, IgD and IgM. The BCR is comprised of membrane immunoglobulin (mIg); a structure of four (in the case of IgD) or five

(IgM) immunoglobulin domains in the heavy chain joined by a hinge region, and a short intracellular domain made up of three amino acids: lysine, valine, lysine (KVK). The mIg itself does not possess any signalling capacities since it doesn't contain any signalling motifs. However, it is linked to the Igα/Igβ heterodimer which contains potent immunoreceptor tyrosine-based activation motifs (ITAMs): a conserved sequence of four amino acids whereby a tyrosine is separated from a leucine or isoleucine by any two amino acids (YxxL/I). This conserved sequence is normally repeated twice in the cytoplasmic domain of ITAM-containing proteins and is separated by 7 to 12 amino acids, producing the recognisable signature $YxxL_{7–12}YxxL$ [47].

Immense diversity is generated among immunoglobulins through VDJ recombination of variable segments. In contrast, some diversity also derives from constant regions of heavy chains, therefore permitting a spectrum of effector functions. Class switch recombination involves VDJ heavy chain variable domain splicing; this maintains antigenic specificity but alters effector functions, leading to varied immunoglobulin isotype generation. There are five different isotypes: IgG, IgM, IgA, IgD and IgE [45].

At the beginning of development, B cells only express IgM BCRs. This isotype has fairly low affinity and is polyreactive; capable of binding various distinct epitopes. This ensures that a greater range of antigens will be able to be recognized in early immune reactions. IgM antibodies are predominantly secreted as pentamers and stabilization is achieved by an additional J chain. This helps to enhance their avidity, leading to effective pathogen opsonisation, mainly in the form of immobilized antigens. Once the B cell is activated, they switch to the production of IgD which is frequently co-expressed along with IgM. IgD is able to interact with bacteria proteins with their constant regions, further enhancing B cell activation [45]. Cytokine signalling concurrent with B cell activation through antigen binding can culminate in antibody class switching to IgA, IgE and IgG. Strikingly, the BCR gene is subjected

to somatic hypermutation. This is an essential process whereby under conditions of selection through antigen mediated activation, it induces the production of BCRs with increasing affinities, consequently eliciting a process named affinity maturation. IgA is commonly found in the mucosa and is expressed as dimers whereas IgG is mostly secreted in the serum [45]. IgA is implicated in toxin and viral neutralization, plays a key role in antigen dependent cell mediated cytotoxicity and prevention of pathogen binding to the mucosa. Lastly, IgE is responsible for protection against worms and parasites and is implicated in many allergies. A variety of subclasses exist and bind with different affinities to Fc receptors [45].

IV.B. Fc receptors

Immunoglobulin molecules are made up of two copies of a variable Fab region and various constant Fc region which form interactions with effector molecules including complement proteins and Fc receptors (FcRs). Particular FcRs usually show specificity for only one or two of the mammalian Ig isotypes. FcγRs are specific for IgG whilst FcεRs specifically bind to IgE. The polymeric immunoglobulin receptor (pIgR) binds to pentameric IgM and dimeric IgA [48]. FcRs are transmembrane proteins that help to link cell-mediated and humoral immunity [45]. A wide spectrum of immune cells from both the adaptive and innate immune arms express this receptor. These include T cells, B cells, macrophages, DCs, neutrophils and natural killer cells [49]. Interestingly, FcRs can be both activating and inhibitory. They vary in the antibody subclass and isotype they bind to, their expression pattern, the affinity with which they bind and the responses they induce [49]. Some of them possess signalling motifs which depend on external kinases for signal propagation *via* phosphorylation. In contrast, others form associations with adapter proteins that bear these motifs [49]. FcR signalling can trigger a host of responses. These include immune cell triggering, cell differentiation, phagocytosis, degranulation and chemokine or cytokine secretion, internalisation for processing and presentation of antigens for antibody-dependent cell-mediated cytotoxicity as well as alterations in migratory behaviour [50]. Furthermore, some Fc receptors facilitate the uptake and

transport of antibodies [45]. Notably, X-ray crystallography studies of FcRs bound to antibodies have shown that they form highly compact complexes. FcRs bind to the lower hinge regions of antibodies, the resultant configuration causes the Fc regions to face downward, giving a compact structure [51, 52].

V. Immunoreceptors and signalling

Immunoreceptors are non-catalytic tyrosine-phosphorylated receptors with mostly small ectodomains [53]. They are a subset of leukocyte receptors possessing no intrinsic enzymatic activity and thus are dependent on external kinases and tyrosine phosphorylation to trigger signalling cascades [53]. Activation is by cell surface bound ligands, the interactions are quite weak but specific [53, 54]. Immunoreceptors share modest sequence homology and they vary because of their assorted ligands. Interestingly, they engage a common downstream signalling machinery, suggesting that their triggering may be through a shared mechanism [53, 55]. Such receptors are able to instigate either inhibitory or activating signals. This is related to particular signalling motifs they, or their associated adaptors express. Thus, downstream signalling proteins are recruited which can allow for different types of signalling to ensue.

Numerous receptors express semi-conserved motifs containing the tyrosine residues which become phosphorylated by extrinsic kinases upon ligand binding. These include immunoreceptor tyrosine-based activation, inhibitory, or switch motifs (ITAMs, ITIMs, and ITSMs) [56-59]. Kinase action is brought into check by receptor-type protein tyrosine phosphatases such as CD45 and CD148. These are expressed at the cell surface in large numbers [55]. Normally, a mixture of immunoreceptors form simultaneous engagements or bind within a short period of time. Their synergistic or antagonistic signalling is then integrated downstream of the immunoreceptor [53, 60-62]. Examples of immunoreceptors include the TCR, the BCR, the Fc receptor family and the CD28 family [53, 55].

V.A. The TCR complex

The T cell receptor (TCR) is composed of an α and a β polypeptide chain. A disulphide bond in the stalk section of their extracellular domains allows covalent binding between the chains [63]. Each chain consists of a small cytoplasmic region, a helical transmembrane domain in addition to two membrane proximal invariant Ig domains that are attached to the transmembrane region *via* an extracellular stalk region [54]. The membrane-distal variable Ig domains, Vα and Vβ bind to the pMHC complex through the complementarity determining regions (CDRs) [54]. The αβTCR forms non covalent associations with three dimeric signalling modules: CD3δε, CD3γε, and ζζ [64].

Studies of the crystal structure of the TCR complex have shown that the CDRs and in particular, the CDR3, exhibit considerable conformational flexibility [65-67]. This allows one TCR to putatively recognise approximately 10^5 different pMHC ligands [54, 68]. It has also been revealed that there are no conserved contacts between the CDRs and specific MHC residues [69]. However, conservation is shown for the overall geometry of the TCR/pMHC interaction [54, 70]. The TCR/pMHC interaction has a reasonably high affinity in comparison to other immunoreceptor/ligand interactions and is characterised by slow kinetics in solution [54]. The TCR itself does not possess enzymatic activity and signalling motifs. Instead, it forms associations with the CD3 complex which is pivotal in the propagation of a downstream signal *via* the phosphorylation of its cytoplasmic ITAMs by a Src kinase named lymphocyte-specific protein tyrosine kinase (Lck) [53, 55]. TCR expression at the cell surface is dependent upon the assembly of the TCR/CD3 complex. This is seemingly facilitated by interactions between the extracellular domains and transmembrane regions of the polypeptide chains [63, 71-73]. Although the stoichiometry of the TCR/CD3 complex has been solved, the exact mechanism with which the αβTCR associates with the CD3 chains is not clear, nor is the spatial organisation of the subunits with respect to each other [63]. Disputes over the valency of the TCR prevails. Some investigations have indicated

that αβTCR/CD3 complexes are monovalent in the resting state [74, 75], whilst alternative studies indicate the that oligomeric forms exist. Yet others have proposed that both monovalent and multivalent forms co-exist [76]. Likewise, a similar controversy exists concerning the valency of pMHC ligands [77, 78].

V.B. TCR downstream signalling

Lck is able to phosphorylate the ITAMs in the CD3 cytoplasmic tails. This activates the cellular signalling machinery [79]. Subsequently, the kinase zeta-chain associated protein of 70 kDa (ZAP-70) is recruited to the phosphorylated ITAMs. This generates a stable interaction helping to protect the tyrosine residues from dephosphorylation by phosphatases like CD45. This is a critical step in the cascade which determines whether a T-cell response is activated or not. It helps to control whether a T cell response is established or whether signalling remains below the threshold [79-81]. ZAP-70 then phosphorylates downstream signalling proteins and this in turn culminates in various responses. These include calcium signalling, cytoskeletal rearrangements and polarisation, an arrest in cellular migration and adhesion. Ultimately, gene transcription is mobilised which affects cellular proliferation, differentiation and cytokine secretion [79, 82].

V.C. Models of T cell activation

Metazoan receptors that depend on tyrosine phosphorylation can possess either inherent tyrosine kinase activity, for example, dimerizing growth factor receptors, or they are dependent on extrinsic tyrosine kinases as is the case for TCR [83, 84]. Currently, three main types of models have been proposed for T cell activation/triggering (Figure 1.1). The TCR complex is comprised of a highly variable TCRα/β heterodimer which engages with peptide-MHC and a non variable signal transduction complex of CD3 that is composed of CD3γ, CD3δ, CD3ε and TCRζ [85]. TCR antigen recognition is unlike other cell membrane receptor ligand interactions. Firstly, the TCR is able to highly sensitively recognise the agonist peptide-MHC located on the membranes of target cells or APCs at a rather low

density; even a single peptide-MHC could induce TCR triggering [86]. Moreover, the TCR can clearly discriminate between the agonist peptide-MHC complexes and self peptide-MHC complexes. Despite the fact that the TCR of a self-tolerant T cell clone shows recognition for self peptide-MHCs with a relatively low affinity, it is however not that different to the binding affinity for foreign peptide-MHCs [85]. Consequently, a robust sensing mechanism has evolved to help discriminate between self and foreign peptides. This is possibly linked to the unique durations involved in the interactions between the TCR and its ligands [87]. Importantly, the interaction of the TCR with peptide-MHC is able to generate varying outcomes, ranging from activation and proliferation upon binding to agonist peptides versus anergy, as in the case of partial agonists.

The TCR is unique in that it has an enormous structural diversity which is the result of genetic recombination and editing of germline encoded segments as the T cells develop [88, 89]. TCR triggering is induced when TCR-peptide-MHC interaction causes molecular changes in the cytoplasmic region of the CD3 complex. This phenomenon has been extensively studied over the years, but its mechanism remains elusive. There are three main models explaining TCR triggering: receptor aggregation, conformational change and segregation or redistribution (Figure 1.1).

V.D. The aggregation model

Soluble multimeric peptide-MHC complexes as well as soluble antibodies are able to cause TCR aggregation on the T cell surface, which culminates in TCR triggering [90, 91]. This activation is believed to be due to the accumulation of Lck molecules in the vicinity of the receptors, leading to net phosphorylation of the TCRs [92]. However, this observation does not help to elucidate on the mechanisms of how a single peptide MHC can activate TCR signalling. Various aggregation models have been put forward to help answer this.

The coreceptor heterodimerization model suggests that CD4 or CD8 coreceptors

bind to the same agonist peptide-MHC whilst the coreceptor associated Lck allows for the ITAMs of CD3 to be phosphorylated [93-95] (Figure 1.1a). But, this model is unable to explain why the majority of the experiments using soluble agonist MHC monomers fail to induce TCR triggering and does not explain how TCR triggering occurs in coreceptor deficient mice [85, 96]. Importantly, affinity of a coreceptor for peptide-MHC is very low compared with that of the TCR, which implies that coreceptor engagement alone would be unable to allow TCR-peptide-MHC complex stabilisation [97]. Additionally, molecular analyses have shown that TCR signalling boosts coreceptor binding to MHC and it seems that TCR phosphorylation precedes coreceptor engagement [98, 99]. In light of these findings, it seems that coreceptor dependent phosphorylation is not sufficient in explaining the central TCR triggering mechanism although it is likely that coreceptors can contribute towards the enhancement of the TCR signal through the recruitment of the Lck kinase [100].

The pseudodimer model proposes that the TCR which interacts with a self peptide-MHC is able to generate dimers with another TCR that engages with an agonist peptide (Figure 1.1b). The underlying principle of this model is that a single coreceptor can intracellularly associate with a TCR which is specific for self peptide-MHC as well as associating with another foreign peptide-MHC *via* its extracellular domain. Consequently, TCR activation occurs because the coreceptor associated Lck is able to phosphorylate the ITAMs [85]. Therefore, spatial localization of Lck in the signalling complexes helps certain self peptide-MHC complexes to simultaneously activate many different TCRs. CD4 is a key molecule, purported to play a significant role in this model. Despite the fact that soluble peptide-MHC monomers are unable to cause TCR activation, studies that have demonstrated that T cells which express CD4 can respond to a single peptide-MHC which is expressed on APCs, support the model. Moreover, when CD4 blockade was induced using antibodies, it was shown that T cells were capable of recognising only approximately 30 ligands. Additionally, findings suggested that the angle between the TCR and its associated CD4 is unlikely to permit any interaction with the same peptide-MHC [101]. Other investigations

have highlighted that in a CD4 dependent mechanism, T cells could be stimulated by bivalent soluble recombinant agonist/self peptide-MHC heterodimers [102]. No clear evidence has been obtained for $CD8^+$ T cells, but it is feasible that the pseudodimer model could help explain how low density agonist peptide-MHC aggregates increase TCR triggering [85]. Nonetheless, just like the coreceptor heterodimerization model, the pseudodimerization model does not give insights into TCR triggering by coreceptor independent Lck or activation of cell surface receptors that lack coreceptors.

There have been uncertainties with regards to the "resting" valency of the TCR [103]. However, it is apparent that TCR ligation with peptide-MHC either precedes or leads to TCR aggregation, generating microclusters which are comprised of 10-100 TCRs [85]. A recent study revealed that, upon interaction with the agonist peptide-MHC displayed on a mouse B cell line, TCR activation could be induced in 293T-HEK cells. These cells have been artificially reconstituted with a transgenic TCR and CD3 complex. Such an artificial TCR triggering model whereby the TCR/self peptide-MHC interaction does not play a role, again, puts the pseudodimerization model under question. It has been posited that at high densities of agonist, pairs of agonists may be generating pseudodimers [104].

V.E. Conformational change models

Some studies have indicated that subtle conformational changes occur in the TCR ectodomain upon peptide-MHC binding, which eventuates in TCR activation [85] (Figure 1.1c). It is believed that the membrane proximal AB loop of the TCRα constant domain allows the stabilization of TCR-CD3 interactions [85, 105]. According to the observation that mutations in the AB loop affect TCR dimerisation, the notion of conformational change induced TCR clustering was put forward as a TCR triggering mechanism [106]. Nevertheless, this model does not explain how this conformational change is transduced to the AB loop from the ligand-binding region and these speculations are hindered by the quality of the TCRα

AB loop resolution in crystals of TCR-peptide-MHC that have been generated [85]. The ectodomains of CD3 have also been investigated for possible conformational changes. The majority of the models supporting conformational changes are incomplete, however, because there has not been any direct structural evidence that shed light on the organisation of the extracellular domains of TCR and CD3 [64, 107]. Kuhns *et al.* revealed that only one side of the TCR was occupied by the CD3 heterodimers. Such observation lead to the proposed notion that conformational changes in the AB loop of TCRα constant domain, which is not in contact with CD3 heterodimers, helps to control the dimerisation of the TCR. As a result, binding induced conformational changes could induce TCR clusters to signal [108] (Figure 1.1d). In contrast, Dong *et al.* recently showed using cryo-electron microscopy that the AB loop of TCRα constant domain is partially buried by the TCRα connecting peptide and adopts a conformation akin to that in the unliganded TCR α constant domain [109]. Additionally, the AB loop is likely to form salt bridges with CD3 [109]. In different studies wherein mutations were generated in the extracellular stalk of CD3ε, it was shown that intracellular signal transmission was impaired but receptor clustering remained unperturbed [110, 111]. This implies that receptor clustering is not adequate for receptor phosphorylation induction, but the absence of the signal in this case could be caused by abrogated CD3ε conformation change.

Various studies have also suggested that CD3 cytoplasmic regions undergo conformational alterations following TCR-peptide-MHC binding [112, 113]. Some investigations suggested that a basic residue-rich sequence in CD3ε, and possibly in TCRζ, could allow binding of the cytoplasmic domains to the negatively charged phospholipids at the cell surface [114, 115]. A nuclear magnetic resonance-based investigation revealed that the CD3ε ITAMs were concealed in lipid bilayers [114]. Taken as a whole, these studies were suggestive that there is possibly a "safety catch" mechanism that stops TCR activation in the resting mode [116]. Yet, alternative studies have offered counter evidence for this notion, since other groups were able to show that a mutant form of CD3ε that couldn't associate with the membrane was

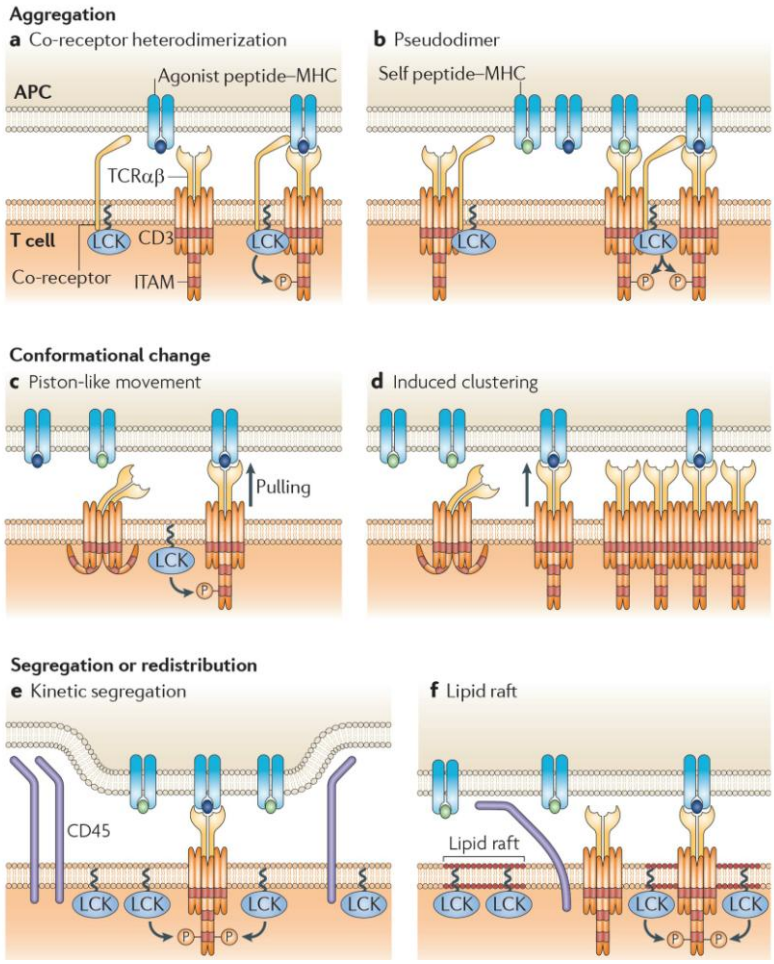


Figure 1.1: Mechanism of T cell receptor triggering adapted from [85]. Models are divided into 3 primary mechanisms: aggregation, conformational change or segregation. (**a**) In the coreceptor heterodimerization model, coreceptor binding to the same peptide MHC complex as the TCR causes coreceptor associated Lck to come into proximity with ITAMs. (**b**) The pseudodimer model proposes that two TCRs are brought together by binding to low affinity self (green) or high affinity agonist (blue) peptide–MHC ligand. The coreceptor further engages with the agonist peptide–MHC complex, generating a dimer. (c) A piston-like displacement of the TCR–CD3 complex is produced by peptide–MHC binding to the TCR. This causes conformation changes in the CD3 cytoplasmic domains, permitting ITAMs to be phosphorylated. (d) Clustering occurs following conformational change in TCR–CD3 complex. (e) The kinetic-segregation model postulates that TCR binding to peptide–MHC keeps the TCR–CD3 complex in close-contact zones. This allows segregation from inhibitory tyrosine phosphatase such as CD45, allowing Lck to phosphorylate ITAMs. (f) The lipid raft model propose that peptide–MHC engagement causes partitioning of the TCR–CD3 complex into areas of the cell surface enriched in LCK and deficient in CD45.

also unphosphorylated in resting cells, but both mutant and wild-type receptors were phosphorylated when exposed to pervanadate, a phosphatase inhibitor [117-120]. This implied that the cytoplasmic domain of wt CD3ε is still accessible to the kinases even when CD3ε forms associations with the cell membrane [120].

V.F. Kinetic segregation and redistribution-based models

The kinetic segregation (KS) model was postulated by Davis and van der Merwe in 1996 [84]. In 1991 Springer had noted that TCR-peptide-MHC complex generation needed the TCR to be segregated from glycocalyx components [121]. These glycocalyx elements include CD45 and CD148 (receptor tyrosine phosphatases), in addition to cellular adhesion molecules such as ICAM-1 and LFA-1. These adhesion molecules contain bulky glycosylated ectodomains and have a much greater size in comparison to the signalling complexes. Springer suggested that size exclusion of the phosphates from the signalling molecules could have signalling consequences [121]. The observation leading to the KS model was that pervanadate treatment of T cells produced strong tyrosine phosphorylation [118]. This implied that the TCR is constitutively phosphorylated and dephosphorylated in resting cells. This therefore helps to maintain a low net phosphorylation level and that receptor triggering could result equally from increasing kinase activity, or from decreasing phosphatase activity.

The KS model proposes that all cell membrane proteins associate transiently and randomly in a resting T cell by diffusing in the membrane. This leads to phosphorylation of the TCR by membrane or coreceptor associated Src kinases, in addition to dephosphorylation of the resulting phosphotyrosines by phosphatases. As a result, net phosphorylation is insufficient for T cell activation (Figure 1.1e). Upon ligation of TCR and the peptide-MHC, a close contact zone is generated and the large phosphatases are subsequently excluded by size. This results in net phosphorylation increasing, leading to triggering of T cell activation. TCRs which do not engage with the correct peptide-MHC would be expected to diffuse out of the

contact zone and in this way are rendered incapable of contributing to downstream T cell signalling. Thus, importantly, the half lives of TCR phosphorylation are dependent on the half lives of the TCR-peptide-MHC interactions.

Various studies have supported the KS model by examining the role of the size exclusion of receptor tyrosine phosphatase. Irles *et al.* and Lin *et al.* revealed that TCR signalling is suppressed when a small, chimeric CD45 is introduced into T cells deficient in CD45 [122] or when CD148 is truncated [123]. Irles *et al.* also demonstrated that a CD45 chimera that possessed a large, unrelated ectodomain of CD43 could also restore activation of the TCR [122]. Another study by Choudhuri *et al.* tried to validate the KS model by approaching it from another angle. They elongated the peptide-MHC ectodomain, such that the inter-membrane distance upon TCR/pMHC engagement was increased. This in turn significantly reduced TCR triggering but left TCR/pMHC ligation intact [124].

Other observations which support this model include: (1) imaging visualisation of the exclusion of CD45 and CD148 from signalling receptors, in microclusters [125], "close-contacts" [126], immunological synapse [123, 127], and a reconstituted giant unilamellar vesicle system [128]; (2) the resistance of the plasma membrane against bending is believed to promote the steric exclusion of glycocalyx proteins energetically [128]; (3) sterically-driven exclusion of CD45 at "close contacts" that are generated between T cells and artificial surfaces is sufficient for the induction of ligand-independent calcium signalling [126]; (4) mathematical modelling predicts that a single TCR/pMHC interaction suffices for passive size-based segregation because these passive rearrangements are not dependent on receptor diffusion [129]; (5) phosphorylation of CD3ζ is influenced to a greater degree by local phosphatase density compared to kinase availability [130]; (6) adhesion molecules such as CD2 which span similar dimensions to TCR/pMHC complexes when bound to their ligands, promote the generation of close-contacts between T cells and APCs [84]; (7) chimeric TCRs induce activity most potently when engaging a membrane-proximal

epitope on their target cell [85, 123]; and (8) surface-immobilised ligands are more active than soluble ones [131]. Nevertheless, more studies are necessary to prove that the KS principle alone is adequate for TCR activation.

V.G. B-cell activation

B-cell activation is triggered by antigen binding to the B-cell receptor (BCR) which initiates a cascade of intracellular signalling that results in the internalization of antigens for processing and presentation to T cells. The early molecular events triggered by ligand binding to BCR have been well characterised both biochemically and using optical microscopy to visualise B cell activation as it occurs. However, there is a lack of clarity for the organisation of the BCR before activation, and several models have been proposed for the initiation of B cell activation. The conformation induced oligomerization model proposes that binding of antigen to single BCRs generates a pulling or twisting force which induces conformational unmasking of a clustering interface in the Cμ4 domain. In contrast, the dissociation activation model suggests that BCRs exist as auto-inhibitory oligomers on the resting B cell surface. Antigen binding is claimed to induce BCR oligomers to dissociate, thus allowing the exposure of phosphorylation residues within Igα/Igβ. Lastly, the collision coupling model suggests that BCRs are segregated from kinases or activating coreceptors and that activation is linked with BCR mobility alterations on the cell membrane. This thus permits the functional interactions of these signalling elements [47]. The possibility that the BCR is triggered by phosphatase segregation according to the principles of the KS model has not been addressed, even though B cells express a large receptor (the BCR) and correspondingly very large phosphatases.

V.H. Superagonistic antibody signalling

Some antibodies can induce signalling in lymphocytes. Antibodies known as 'superagonists' induce high levels of signalling activity and insights into how such superagonists cause signalling have derived from exploring antibodies that bind to the receptor CD28 [132]. The study by Evans and colleagues revealed that the

position of binding of the antibodies, *i.e.* their epitopes, is related to their ability to induce signalling. Importantly, the mechanism underlying the KS model for TCR triggering proposed by Davis and van der Merwe is based on the spatial reorganization of signalling proteins. Based on the KS model, a hypothesis arose: that the greater potency of superagonistic antibodies arises from their ability to more effectively exclude large phosphatases e.g. CD45 from the vicinity of CD28, favouring its phosphorylation (Figure 1.2). This hypothesis can be further extrapolated so that any immobilized antibody binding to a membrane-proximal epitope on a receptor with tyrosine phosphorylation motifs should induce signalling by that receptor. Thus, immobilized antibodies that bind to membrane proximal regions of PD-1 could potentially induce superagonistic downstream signalling and inhibit immune reactions.

VI. Costimulatory pathway

The paradigm of costimulation suggests that two signals are necessary for T cells to become activated [133]. The initial signal is generated when ligation of the TCR with peptide-MHC complex occurs. This is subsequently modified by the second signal generated by the CD28 family of costimulatory receptors [134]. Strikingly, costimulatory receptors can either enhance the first signal to promote T cell activation, as demonstrated for ICOS and CD28, or alternatively, they can cause signal attenuation, as exemplified by PD-1, BTLA-4 and CTLA-4 [135]. Consequently, biological agents that can specifically trigger costimulatory molecules are potentially highly therapeutic, especially in autoimmune settings.

VI.A. CD28

a. Structure/ligands

CD28 is a homodimeric stimulatory cell surface receptor belonging to the Ig superfamily covalently linked by a disulphide bond in the stalk region of its extra cellular domain [136, 137], that plays a critical role in T-cell activation. It is constitutively expressed on cell membranes of almost all rodent T cells and on the

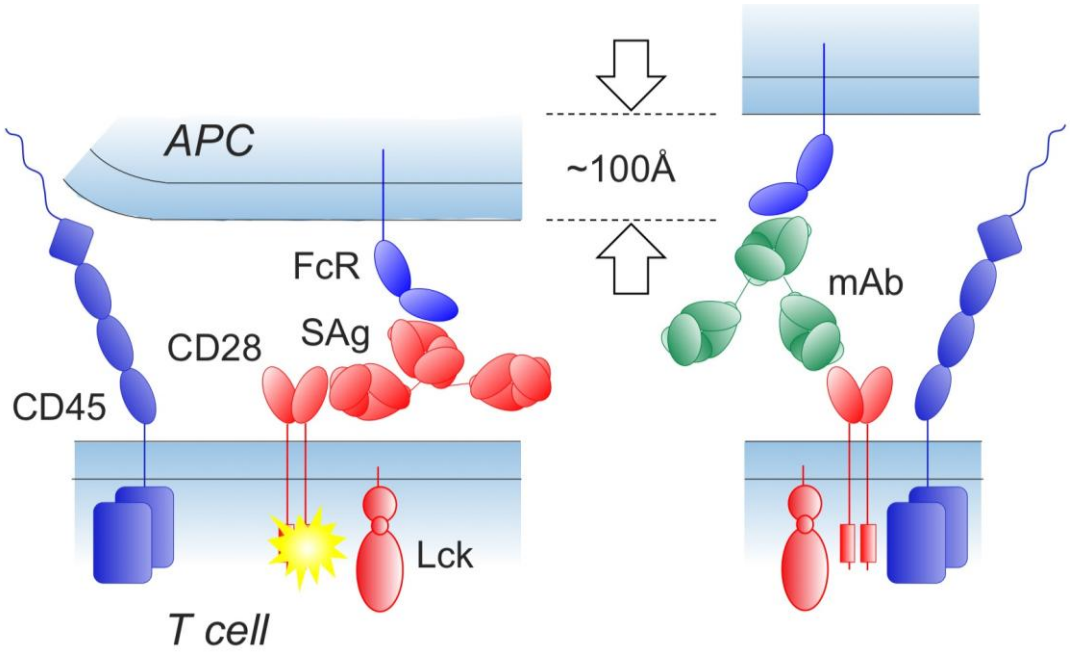


Figure 1.2: Mechanism of superagonistic antibody signalling. Binding of the superagonist (SAg) to CD28 and Fc receptor bridges the membranes of 2 cells, sterically excluding the phosphatase, CD45. Lck, a kinase retains access to CD28, permitting net phosphorylation of the receptor. Conventional antibody gives weaker signalling since the ~100Å larger complex less efficiently excludes CD45 from the receptor, leading to less net phosphorylation.

great majority of $CD4^+$ T cells, but on only approximately half of all circulating human $CD8^+$ T cells [138]. CD28 signals play a vital role in numerous T-cell processes. These include production of cytokines, survival, and differentiation as well cytoskeletal remodelling. CD28 ligation causes unique epigenetic, transcriptional and post-translational alterations in T cells which cannot be recapitulated by TCR ligation alone. CD28 is critical for nTreg survival and for maintaining immune homeostasis [139].

Each CD28 chain contains one V-set immunoglobulin superfamily (IgSF) domain along with a cytoplasmic tail that has multiple key tyrosine residues which can be phosphorylated [140]. Signalling is principally facilitated by the recruitment of Src homology 2 (SH2) and Src homology 3 (SH3) domain-containing signalling molecules to the phosphorylated tyrosine motifs and the proline-rich motifs in the cytoplasmic tail, respectively [132]. CD28 along with a co-stimulatory receptor CTLA-4 are able to bind the same ligands expressed on APCs, *i.e.* CD80 (B7-1) and CD86 (B7-2). This is *via* a conserved hexapeptide (MYPPPY) binding motif in the ligand binding domains of each receptor [141]. CD80 and CD86 have similar structures: they are both comprised of two IgSF domains, *i.e.* a receptor binding V-set domain and a membrane-proximal C1-set (constant domain-like) domain which is linked to a single transmembrane domain and a short cytoplasmic domain [142].

Interestingly, CD80 is expressed on the cell membrane as a combination of non-covalent dimers and monomers whereas CD86 is only presented in the monomeric form [143, 144]. The affinity of CD80 for CTLA-4 is twenty times stronger than that for CD28 whereas the affinity of CD86 for CTLA-4 is 8 times stronger than that for CD28. CD28 binds monovalently to CD80 and CD86 despite being a dimer, owing to steric effects [143, 144], whilst CTLA-4 engages in bivalent interactions. Unlike CD28 which is constitutively expressed on T cells, CTLA-4 cell surface expression usually peaks 24 h after T cell stimulation. Taken as a whole, in silico simulations have suggested that CD86 chiefly binds CD28 whereas CTLA-4 principally binds to

CD80 [140, 145, 146]. CD28 has both pro- and anti-inflammatory effects since its signalling induces the survival, differentiation, proliferation and activity of effector T cells and regulatory T cells, therefore it has been deemed to be a somewhat complicated therapeutic target [143, 147-150].

VI.A.b. Signalling

CD28 was the earliest identified co-stimulatory receptor in T cells. It is of great importance in helping to promote T cell activation, proliferation and survival. Rather than the provision of a qualitatively distinct second signal which leads to a different transcriptional profile, CD28 signalling provides amplification of the transcriptional effects of TCR triggering [151]. CD28 signalling is able to reduce the activation threshold for T cell activation; this permits triggering of the TCR by low affinity ligands. This also means that there is a decrease in the number of TCRs that need to be triggered for T cell activation. When there is a lack of CD28 signalling, the immune cells become anergic and non-responsive and can undergo subsequent apoptosis [152]. Investigations have revealed that T cells derived from CD28-deficient mice manifest attenuated responses to lectins and that helper T cell function is impaired [153]. Nevertheless, the lack of CD28 costimulation did not cause an absolute blockade of T cell function. This is an indication that alternative co-stimulatory pathways may be able partially to compensate for the lack of CD28 activity.

Downstream signalling is initiated when Lck kinase phosphorylates the tyrosine residues in the motifs of the cytoplasmic domain of CD28 [143, 154-156]. Intriguingly, some downstream effectors can also be recruited when the tyrosine motifs have not been phosphorylated [143, 157]. This might be the putative reason why tyrosine motif mutations do not lead to absolute CD28 signalling abrogation, or then again, additional undiscovered motifs could enhance CD28 downstream signalling activity [143, 158]. The likely key effect of CD28 signalling is an enhancement of IL-2 generation. This is brought about by the upregulation of IL-2

transcription *via* nuclear factor of activated T-cells (NFAT) and nuclear factor kappa-light-chain-enhancer of activated B cells (NFκB) in addition to IL-2 messenger RNA stabilisation [159, 160]. However, CD28 has also been implicated in the stabilisation and compartmentalisation of the immunological synapse [81, 161, 162] as well as the recruitment of Vav1, resulting in actin remodelling [163, 164]. Moreover, CD28 induces glycolysis which is needed for cellular growth and proliferation [165], and helps to maintain cellular survival by upregulating an inhibitor of apoptosis, Bcl-x_L [166].

VI.B. CTLA-4

a. Structure/ligands

The T cell protein, cytotoxic T lymphocyte antigen 4 (CTLA-4), is an inhibitory member of the CD28 family of costimulatory receptors. The levels of CTLA-4 expression in most resting T cells are very low. However, upon T cell activation and CD28 engagement, CTLA-4 is quickly upregulated on T cells [167]. CTLA-4 (CD152) contains a single immunoglobulin V-like domain possessing a MYPPPY motif which is essential for ligand binding, a transmembrane domain, and a cytoplasmic tail. In contrast to the surface receptor CD28, CTLA-4 is highly endocytic, and is found in intracellular vesicles [168]. It is constitutively present as a homodimer [169]. Following ligand binding, it does not appear to undergo conformational change [170]. Compared to CD28, CTLA-4 is the higher affinity receptor for the ligands, CD80 and CD86 [171].

VI.B.b. Signalling

CTLA-4 engagement generates an inhibitory signal which suppresses TCR- and CD28-mediated signal transduction [171]. As a result, IL-2 synthesis, progression through the cell cycle and T cell responses are terminated [172]. The importance of this inhibitory protein as a negative regulator of T cell responses was highlighted by the development of fatal lymphoproliferative disease in *Ctla-4*$^{-/-}$ mice, owing to the uncontrolled CD80/CD86 co-stimulation [173]. CTLA-4 has an important role in

the regulation of peripheral T cell tolerance [171].

VI.C. BTLA

a. Structure/ligands

B and T cell lymphocyte attenuator (BTLA) is a coinhibitory receptor of the CD28 family. BTLA is not expressed by naive T cells, but it is induced following T cell activation. It remains expressed on Th1 cells but not Th2 cells [174]. BTLA is unique because it binds to Herpes virus entry mediator (HVEM), a TNF receptor superfamily protein, rather than to an IgSF protein [175]. HVEM plays an important role in controlling both innate and adaptive immunity. It is able to suppress NK cells and T cells following engagement with BTLA and a second IgSF protein that produces inhibitory signals, CD160 [176].

BTLA is a type I transmembrane glycoprotein. It contains a single extracellular IgV-like domain, a transmembrane region and a cytoplasmic tail [177]. Its cytoplasmic region contains three tyrosine residues, which are contained within sequence motifs including, an immunoreceptor tyrosine inhibitory motif (ITIM), a Grb2 potential binding site and an immunoreceptor tyrosine based switch motif (ITSM). Such motifs are conserved in the human and murine orthologs [178].

VI.C.b. Signalling

BTLA engagement leads to the inhibition of T cell proliferation and cytokine production [179]. Strikingly, BTLA deficient mice develop liver inflammation in old age and they also generate autoantibodies [180]. Furthermore, these mice become susceptible to allergic airway inflammation and EAE [135, 181]. Autoimmunity ensues from a lack of HVEM, which implies that coinhibitory signalling through HVEM/BTLA and HVEM/CD160 could play a more prominent role than the positive signals that are generated by LIGHT/HVEM engagement [182]. Additionally, an increased susceptibility to rheumatoid arthritis has been linked to polymorphism in the human BTLA gene [183]. Interestingly, some studies have demonstrated strong costimulatory effects following BTLA-HVEM ligation. This

manifests in the enhancement of NF-Kβ activation and survival signals downstream of HVEM but not BTLA. HVEM can also bind LIGHT (homologous to lymphotoxin, exhibits inducible expression and competes with HSV glycoprotein D for binding to HVEM, a receptor expressed on T lymphocytes), in which case positive costimulatory signals are induced through HVEM, that enhance inflammation and T cell activation [184, 185]. This suggests that therapeutic strategies for enhancing signalling *via* HVEM may not be ideal, because they would not always allow inhibition of immune responses, if this was the desired goal [186]. A more effective immunomodulatory strategy would be, perhaps, to directly target BTLA using agonistic antibodies.

VI.D. ICOS

a. Structure/ligands

The inducible costimulator (ICOS) is a positive costimulatory molecule belonging to the CD28 family, initially discovered in 1994. Unlike CD28, ICOS (CD278) is inducibly expressed on T cells upon activation [187]. ICOS contains a single extracellular IgV-like domain with a FDPPPF motif, which is believed to be important for ligand binding, a transmembrane domain, and a cytoplasmic tail [187]. ICOS forms binding with inducible costimulator-ligand (ICOS-L). In contrast to CD80 and CD86, ICOS-L is not only expressed on hematopoietic cells but also on other cell types [188].

VI.D.b. Signalling

Similar to CD28, ICOS is able to enhance basic T cell responses such as proliferation, CD40 ligand upregulation, effective help for antibody secretion by B cells and secretion of IL-10 [187, 189]. Moreover, such co-stimulation can produce low levels of IL-2 that are required for initiation of T cell proliferation, but are not sufficient for sustained proliferation [190]. ICOS deficiency does not impair naive T cell activation, however, it causes defective germinal centre formation and hypogammaglobulinemia in both humans and mice [191, 192]. Several investigations

have indicated that ICOS plays a role in the maintenance of effector memory T cells [193]. This suggests that ICOS is involved in prolonging ongoing immune reactions.

VII. PD-1

A. PD-1 structure

Programmed death-1 or PD-1 (CD279) is an inhibitory receptor from the CD28 family. It is a type I transmembrane glycoprotein comprised of an V-set IgSF extracellular domain, with a molecular weight of 50-55 kDa. PD-1 shares approximately 30% sequence homology with CD28, CTLA-4, and ICOS. PD-1 lacks a membrane proximal cysteine residue therefore it exists as a monomer both at the cell surface and in solution [194]. Unlike CD28 and CTLA-4, PD-1 lacks the MYPPPY motif in the IgV-like domain, which is integral for binding to CD80 and CD86 [194]. Such underlying structural differences between these molecules suggest that there are prominent differences in their signalling mechanisms and the mode of ligand recognition [195].

The cytoplasmic region of PD-1 contains two important tyrosine resides. The membrane proximal region consists of an immunoreceptor tyrosine based inhibitory motif (ITIM) and an immunoreceptor tyrosine based switch motif (ITSM) [194]. Interestingly, immunoinhibitory receptors such as CD72, killer cell immunoglobulin like receptors (KIR) and FcγRIIB widely contain ITIMs, and thus it was thought that the membrane proximal tyrosine residue was responsible for the inhibitory action of PD-1. Yet, it has been shown through mutagenesis studies utilising a murine B cell line that in fact, it is the tyrosine within the ITSM that is essential for PD-1 signalling and thus its immunosuppressive effects on T cells [196].

VII.B. Regulation of PD-1 expression

PD-1 is expressed on activated T cells, B cells, natural killer (NK) cells, and both mature and immature thymocytes. Compared to the other CD28 family proteins expressed by T cells, PD-1 has a much broader expression, which implies that a

greater range of immune responses are being regulated by PD-1 [197].

PD-1 is upregulated on T cells following TCR engagement [198]. PD-1 expression can additionally be upregulated by cytokine signalling in T cells, the common gamma chain cytokines, IL-7, IL-2, IL-15 and IL-21, being prime examples [199]. IL-12 and IL-6, which use STAT4 and STAT3, respectively, can further induce PD-1 in activated T cells *via* interactions with the PD-1 promoter through its distal regulatory elements [200]. A variety of other, more direct transcriptional elements have been discovered which can control PD-1 expression. These include the transcription factor, T-bet, which actively inhibits PD-1 expression [201]. Following repeated antigenic stimulation, T-bet is downregulated, allowing enhanced PD-1 expression, resulting ultimately in T cell exhaustion. NFATc1, another transcription factor can directly upregulate PD-1 expression [202]. Blimp-1 suppression of PD-1 expression in viral infections results from the production of suppressive chromatin changes in the PD-1 locus along with NFATc1 repression [203]. FoxO1 also serves to reinforce an exhausted cytotoxic T cell profile and therefore causes PD-1 to be upregulated [204].

Alternative epigenetic modifications have been reported to regulate PD-1, for example through DNA methylation. Viral infections cause reductions in DNA methylation in $CD8^+$ T cells, which then enhance PD-1 transcription. There is a direct correlation between the strength and duration of TCR signalling and levels of demethylation [205, 206]. In addition to local cytokines and general T cell activation which upregulate PD-1 expression, reports have indicated that vascular endothelial growth factor A (VEGF-A) can also enhance PD-1 expression on $CD8^+$ T cells *via* VEGF receptors present on these cells [207]. From all these investigations, it is clear that there is a highly complicated network of distinct mechanisms through which PD-1 expression can be altered.

VII.C. PD-1 ligands

a. Structure

PD-1 and its ligands are involved in modulating both peripheral and central tolerance. [208]. PD-L1 (B7-H1, CD274) and PD-L2 (B7-DC, CD273) are both B7 family members. They are currently the only known ligands of PD-1 [209]. Their effects are not exclusively mediated through PD-1, however. PD-L1 is able to interact with CD80 whilst PD-L2 is able to bind to another receptor named RGMb [210, 211]. Both PD-L1 and PD-L2 are type 1 transmembrane glycoproteins comprised of IgV- and IgC-like domains. They share 40 % amino acid identity with one another and 20 % with B7 molecules [212]. Crystal structure studies have highlighted that, unlike the CTLA-4 molecule which utilises the hydrophobic MYPPPY sequence located in the FG loop as the B7 binding site, in order to bind to equivalent faces of PD-Ls, PD-1 uses its AGFCC' β-sheet [213, 214]. Consequently, such face-to-face interaction allows for greater contact area between PD-1 and PD-Ls. Moreover, it provides for a more compact structure to the complex.

VII.C.b. Expression

Although both PD-L1 and PD-L2 bind to PD-1 and allow the delivery of coinhibitory signalling to T cells, they show marked differences in their expression patterns. PD-L1 expression is very diverse, its expression can be observed on macrophages, DCs, monocytes, T cells, B cells and is usually upregulated with activation whilst PD-L2 expression is only expressed in relatively few cells and tissues. Unlike the traditional B7 family members, CD80 and CD86, which show limited expression on APCs only, PD-L1 is expressed in a wide array of non hematopoietic tissues such as lung, liver, skin, placenta, vascular endothelium, pancreas and the heart [215, 216]. This tissue expression has an essential role in the regulation of immune responses in the periphery [217, 218]. Besides these normal tissues, PD-L1 is frequently overexpressed on cancers as a means of immune evasion for the cancerous cells. PD-L2 upregulation occurs on activated antigen presenting cells such as DCs, monocytes and macrophages [219]. Maturing thymocytes express

PD-1 and PD-L1 during the central tolerance induction. PDL-1 is expressed on the thymus whilst PDL-2 expression is limited to the thymic medulla [194].

VII.D. PD-1 Signalling

Commencing with the marked observation that PD-1 knockout mice developed spontaneous autoimmunity, it has since been revealed through many investigations that the PD-1/PD-L1/PD-L2 pathway is important for T cell regulation in numerous mouse models of autoimmunity, cancer and infection [220]. Such findings suggest a vital role for these molecules in terms of T cell response regulation, which is the basis for the development of new strategies for targeted immunotherapies against PD-1 and its ligands.

PD-1 signalling is triggered through engagement with its ligands PD-L1 and PD-L2. Intriguingly, despite the name of this receptor, programmed cell death is not the main consequence of receptor engagement. Rather, the predominant effect of PD-1 signalling is the inhibition of TCR and important costimulatory signals [209]. PD-1 forms clusters and localises to the TCR complex upon engagement [221]. PD-1 signalling leads to the inhibition of the phosphorylation of TCR CD3ζ chains and Zap-70. [221-223]. Additionally, PD-1 is able to suppress the downstream activation of Ras, an enhancer of proliferation and survival as well as repressing the activation of the phosphatidylinositol 3-kinase (PI3K)/Akt pathway through directly blocking of PI3K activation [222, 224]. This action is initiated by the phosphorylation of the intracellular ITSM and ITIM. Consistent with it being the more important motif [196], the phosphorylated ITSM can recruit SHP-2, a tyrosine phosphatase [222]. It is this phosphatase that causes PI3K to be inactivated and hence downstream suppression of the Akt pathway. PD-1 signalling is accompanied by an upregulation of phosphatase and tensin homolog (PTEN) expression and downregulation of phospho-Akt, Erk2, S6, the mechanistic target of rapamycin (mTOR) [225].

Recent studies have suggested that PD-1 also plays a role in the metabolism of T

cells. PD-1 signalling is able to suppress the metabolism of amino acids and glycolysis as well as inducing the promotion of fatty acid oxidation [226]. Although both CTLA-4 and PD-1 can suppress T cells, the mechanisms of inhibition are inherently distinct [222]. There are various downstream signalling effects of PD-1. Like the other coinhibitory receptors, PD-1 is able to inhibit the production of inflammatory cytokines such as tumour necrosis factor α (TNF-α), interleukin 2 (IL-2) and interferon γ (IFN-γ) in addition to T cell proliferation [216, 227, 228]. It seems that PD-1 signalling is self-reinforcing, when PD-1 is activated, this leads to the protection of the transcription factor, FoxO1, from degradation, resulting in more PD-1 expression [204]. Furthermore, more global effects on T cells are induced following PD-1 signalling. Both *in vitro* and *in vivo* studies have demonstrated that PD-L1 functions to aid the differentiation of inducible regulatory T cells (iTregs). This was not restricted to only APCs but also other non hematopoietic cells appeared to be capable of such induction [225].

PD-1 plays a vital role in exhausted T cells. This was first shown for chronic viral infections, whereby PD-1 was found to be selectively upregulated on exhausted $CD8^+$ T cells [227]. This phenomenon has since been observed in many other chronic viral infections in both humans and mice [201, 203, 206, 227, 229, 230]. PD-1 expression by T cells in the tumour microenvironment is also linked to a dysfunctional and exhausted phenotype [231]. Blocking PD-1 signalling is able to reverse the function of exhausted $CD8^+$ T cells, allowing them to restore their cytotoxic capabilities [232]. Experiments in several animal models have used PD-1 blockade treatment to control viral infection [233]. By manipulating PD-1 signalling, such treatments could conceivably help treat infectious diseases and therefore this approach holds considerable therapeutic potential.

VII.E. PD-1 polymorphisms

The *PDCD1* gene which encodes PD-1 is found at chromosome 2q37. It has been shown to have various single nucleotide polymorphisms [194]. Downregulation of

PDCD1 results from a polymorphism in intron 4 which disrupts the binding of the runt-related transcription factor 1 (RUNX1), culminating in impaired PD-1 induction. Studies have demonstrated that a single nucleotide polymorphism (SNP) on the RUNX1-binding site leads to enhanced susceptibility to psoriasis and rheumatoid arthritis (RA) [212, 234]. Other investigations have shown that PD-1 SNPs can lead to diseases such as SLE, multiple sclerosis and allergic bronchial asthma [235, 236].

VIII. Costimulation and therapy

A. Non PD-1 costimulatory pathways

Presently, there are various methods for the treatment of human autoimmunity involving biological agents. They comprise strategies targeting the inflammatory cytokines, depleting cell populations, and modalities for altering cell signalling [237]. Obvious targets for the third strategy are members of the CD28/B7 family, which are closely related molecules that are likely to be triggered in a similar fashion. The following section describes various non PD-1 costimulatory pathways which have been studied for immunotherapy.

Findings have suggested that CD28 deficiency or the blockade of the CD28/B7 axis causes a reduction in disease severity in different mouse models of lupus, multiple sclerosis, myocarditis, arthritis, thyroiditis and myasthenia gravis [238-243]. It is also able to confer resistance to EAE induction and disease progression in NOD mice [244]. Strikingly, administering the blocking agent late in the disease process had no impact on the development of ongoing autoimmunity in NOD mice [245]. In light of this evidence, it has been postulated that the beneficial effect of CD28 blockade in mouse models of autoimmunity could perhaps be restricted to the suppression of the primary autoreactive responses. Therefore, the CD28 pathway may play a less important role if memory cells are the cause of autoimmunity and antigen expression is sustained [246, 247]. Because prevalent features of many autoimmune responses include continual antigen exposure and they are associated with a memory phenotype

in the autoreactive cells, this suggests that CD28 might not be an ideal target for immunotherapy.

Studies have also attempted to stimulate the CD28 pathway for autoimmune disorder treatment. It was demonstrated that a unique class of monoclonal antibodies which targeted CD28 specifically, could specifically promote Treg expansion and consequently inhibit immunopathology in mouse models of autoimmunity [248]. They were named CD28 superagonists [248]. Further investigations in non-human primate models elicited findings consistent with the mouse data. Unfortunately, during a phase I clinical trial of the antibody superagonist, healthy human subjects developed "cytokine storms" following CD28 activation, hence the study was terminated [249]. The underlying reason for this may be that human effector memory $CD4^+$ T cells, which express abundant CD28 became activated, creating the cytokine storm. Such an aberrant response might not have been anticipated because preclinical trials in mice and non-human primates indicated that the $CD4^+$ T cell subset did not express CD28 [250].

Strategies for CD80 and CD86 blockade have been studied in diabetes and EAE models. Interestingly, anti-CD80 monoclonal antibody (mAb) treatment suppressed clinical symptoms of EAE; conversely, anti-CD86 mAb administration caused disease exacerbation [251]. By utilizing a different mouse strain that provided a relapsing-remitting EAE model, it was revealed that anti-CD80 mAb led to relapse and exacerbation whilst anti-CD86 treatment had no effect on relapses. This study also showed that administration of the Fab fragment of anti-CD80 antibody led to clinical remission [252]. Unlike the EAE studies where CD86 blockade did not elicit any effect, in NOD mice models, anti-CD86 treatment was shown to prevent clinical disease if it was administered early in disease progression [253]. Overall, these findings indicate that B7 molecules are perhaps not generalizable targets for autoimmune therapy because of the dual effects of anti-CD80/86 blockade, which will likely be highly disease and model-specific. Moreover, the suppressive effects of

the possible bidirectional signalling between CD80 and PD-L1 needs also to be accounted for when CD80 is targeted *via* blocking agents [254].

In order to block CD80 and CD86, a CTLA-4Ig fusion protein has been generated by Alegra *et al.* CTLA-4Ig is able to prevent CD80 and CD86 interacting with CD28 and can further help suppress DC function [255]. However, CTLA-4Ig has also produced deleterious effects in transplant models whereby reductions in nTreg numbers were observed [256, 257]. On the other hand, other studies showed that this effect could potentially be countered by improved regulatory function [258], in addition to an increase in peripheral iTreg formation [259]. More investigations are required to elucidate the effects of CTLA-4Ig treatment on Tregs. CTLA-4Ig has been shown to have good therapeutic effects in numerous animal models of human diseases such as EAE, allergic contact dermatitis and lupus [238, 260, 261]. In addition, it has been reported that that CTLA-4Ig can allow the prevention of rat cardiac allograft rejection, enhance graft survival, forestall autoimmune glomerulonephritis and inhibit both clinical disease in NOD mice and collagen-induced arthritis [261-263]. Despite the fact that CTLA-4Ig administration has been generally acknowledged as a potential beneficial form of immunotherapy, an EAE study encompassing multiple CTLA-4Ig injections demonstrated disease exacerbating effects [264]. This study further revealed that blocking CD86, but not CD80, helped to augment actively induced EAE. The interaction of CD86 with CD28 and CTLA-4 in EAE therefore appears to have an inhibitory role. An important factor underpinning this mode of treatment may involve the proper timing of such interventions. Finally, clinical trials for rheumatoid arthritis using CTLA-4Ig have shown profound ameliorative effects with enhancements of remission rates in patients [265]. This Ig form of CTLA is currently in use in the clinic. Recent approval has been given by the United States Food and Drug Administration for a second generation CTLA-4Ig to help prevent acute renal transplant rejection [266].

Targeting CTLA-4 *via* agonising antibodies may provide an alternative strategy for

the suppression of immune responses, yet this approach has not been fully explored. Hwang *et al.* showed in mouse models that allogeneic T cell responses could be suppressed when recipients were transferred with allogeneic tumour cells which expressed membrane-bound single chain anti-CTLA-4 antibodies [267]. They also created a transgenic mouse model that expressed a CTLA-4 specific scFv on B cells and demonstrated that expression of this CTLA-4 agonist helped to reduce autoreactive T cell responses as well as preventing NOD mice from developing spontaneous diabetes [268]. It could be envisaged that the membrane bound CTLA-4 scFV constructs would induce strong exclusion of phosphatases from CTLA-4, consequently allowing the delivery of strong inhibitory signals.

An agonistic BTLA antibody showed great therapeutic potential in a human graft versus host disease (GVHD) model. Treatment with these anti-BTLA antibodies prevented GVHD and allowed immunity against viral and bacterial pathogens, *via* the expansion of nTregs and direct inhibition of effector T cells [269]. This suggests that BTLA agonists could be utilised for the prevention of aberrant immune activity without triggering excessive immunoinhibition.

An important strategy for treating autoimmunity involves the elimination of memory immune responses, therefore by blocking the ICOS pathway, this could generate a potential way for treating autoimmune diseases such as rheumatoid arthritis. Studies involving the use of anti-ICOS blocking antibodies in mouse models of GVHD have suggested that blocking ICOS signalling could ameliorate disease [270, 271]. Currently, there are clinical trials involving agonising humanized monoclonal antibodies against ICOS, with aims of targeting tumours [272].

VIII.B. PD-1

PD-1 plays a vital role in chronic viral infections, transplantation immunity, anti-tumour immunity and autoimmunity. The following sections will discuss the importance of PD-1 in such settings in greater depth.

VIII.B.a. Chronic viral infections

Chronic infections generate repeating and high levels of antigen exposure. This can lead to T cell exhaustion [273]. In a mouse model of chronic lymphocytic choriomeningitis virus infection, the blockade of lymphocyte activation gene (LAG-3) and PD-1 helped to reverse the exhausted phenotype and eventually helped to clear the viral infection [274]. Other chronic infections such as hepatitis B and C virus infections in humans as well as HIV can induce T cell exhaustion [275-277]. Nivolumab, an anti-PD-1 monoclonal antibody was tested in interferon refractory and naive patients that were chronically infected with hepatitis C virus (HCV). These patients experienced a significant reduction in HCV RNA following anti-PD-1 antibody treatment, suggesting that reversing T cell exhaustion can be a potentially effective strategy to control viral infections [278].

VIII.B.b. Transplantation immunity

PD-1 plays a critical role in transplantation immunity. A study by Ozkaynak *et al.* has demonstrated that through potentiating PD-1 dependent inhibition *via* PD-L1Fc, the survival of cardiac allografts could be enhanced. They also showed that CC chemokine receptor 2 (CCR2) blockade combined with rapamycin induced permanent survival of islet allografts, and this relied on the PD-1/PD-L1 pathway [279]. It would appear that constitutive and inducible expression of PD-L1 on somatic tissues and the enhanced PD-1 and PD-L1 expression on alloreactive T cells regulate alloreactive responses [279-281]. Alloreactivity is also postulated to be controlled by PD-L2 engagement, which can induce a reduction in the proliferation of $CD8^+$ T cells [282]. It has been observed in cardiac transplant models that following transplantation, PD-L1 is upregulated on both the allograft and the recipient tissues. Studies of PD-L1 deficient allografts and recipients indicated that PD-L1 expression on the recipient tissue plays an essential role in regulating acute alloreactive responses whilst its expression on the allograft is involved in controlling the chronic alloreactive responses along with enabling graft tissue survival [283].

Administration of blocking antibodies against PD-1 can generate different outcomes. In MHC-I and MHC-II mismatched cardiac allografts, alloreactive T cells show enhanced PD-1 expression. Blocking the PD-1 pathway greatly advanced acute graft rejection [284]. In contrast, in single mismatched (MHC-I or MHC-II) allografts, PD-1 and PD-L1 expression was only slightly upregulated. Furthermore, chronic rejection in the form of graft vasculopathy took place and blocking the PD-1 pathway did not have any effect on graft rejection [281, 285]. It is thought that the PD-1 pathway facilitates transplant tolerance by coordinating regulatory and effector T cell homeostasis. Analysis of a cardiac allograft model and the effects of PD-L1 blocking antibodies revealed that graft rejection became accelerated and this was combined with a marked decrease in the number of Tregs and an elevation of infiltrating lymphocytes [286]. Conversely, skin allograft and GVHD models have shown that the blockade of PD-L1 does not lead to acceleration in the alloresponse after $CD4^+CD25^+$ T cells were depleted [287]. Moreover, reductions in PD-1 and PD-L1 expression increased cytokine production and effector T cell numbers. These results suggest that the PD-1 pathway is responsible for curbing alloreactive T cell activity by acting on Tregs [281, 287, 288].

It is believed that PD-L1 may employ a PD-1 independent mechanism to control alloresponses, *via* alloreactive T cell apoptosis. A study that involved a skin transplant model using adoptively transferred allospecific TCR transgenic $CD4^+$ T cells, showed that by blocking PD-L1 but not PD-1, *in vivo* apoptosis of the transferred T cells could be suppressed [280]. Additionally, treatment with an antibody that exclusively blocked the CD80-PD-L1 interaction, caused greater chronic allograft vasculopathy, which was concurrent with a reduction in the number of splenic Treg cells and an upregulation of proinflammatory cytokines [289]. Hence, the CD80-PD-L1 interaction may also have a vital role in controlling alloreactive responses. In the light of all these results, however, it seems plausible that agonizing the PD-1 pathway could potentially be a valuable mode of immunotherapy, helping to reduce graft rejection.

VIII.B.c. Anti-tumour immunity

The success of the inhibition of CTLA-4, a central immune checkpoint regulator, in melanoma paved the way to the development of immune checkpoint inhibitors that target the PD-1/PD-L1 pathway [278, 290]. Indeed, in terms of immunotherapy for the treatment of cancers, many investigations have demonstrated that PD-1 expression on T cells in the tumour microenvironment is of extreme importance: PD-1 expression on T cells is in fact a predictive factor for response to immunotherapies that target this signalling pathway [291]. PD-1 inhibitors prevent interaction with PD-L1 and PD-L2 and can enhance T cell effector function and proliferation [292].

Accumulating evidence shows that both PD-L1 and PD-L2 are expressed on a broad spectrum of hematologic malignancies and solid tumours [293]. Tumour infiltrating lymphocytes manifest exhausted phenotypes, with high PD-1 expression, suggesting that in many cases they are highly immunogenic. This implies that tumours are able to generate suppressive signals which hinder immunosurveillance, thereby providing a tolerogenic microenvironment for tumours to grow through immune evasion [294]. A strong correlation has been identified for the expression of PD-Ls and unfavourable prognosis in melanoma and gastric, pancreatic, renal, oesophageal, ovarian, bladder cancers [293]. The PD-1 pathway has consequently been targeted by a diverse variety of blockade strategies. These include blocking monoclonal antibodies against PD-1 and its ligands, recombinant proteins composed of extracellular segments of PD-1 and PD-L1, genetic ablation of the *PDCD1* gene, RNA interference and DNA vaccination with the extracellular portion of PD-1 [295-300].

Clinical studies using PD-1 pathway inhibitors against treatment resistant tumours were initiated in the United States in 2006 [301]. To date, over 200 such clinical studies have been conducted utilising nine types of antibody in more than 20 types of cancer. These include both solid and haematological tumours [302]. Swift

advancement is being demonstrated in the treatment of different tumour types, and this has resulted in the FDA approval of anti-PD-1 antibody nivolumab for the treatment of melanoma in 2014 and squamous lung cancer treatment in 2015 [303]. Similarly, in 2016, pembrolizumab obtained FDA approval for the treatment of metastatic non-small cell lung cancer [304]. Pembrolizumab and nivolumab are 'humanised' IgG4 and fully human IgG4 monoclonal antibodies, respectively. Importantly, IgG4 manifests low levels of antibody dependent cell mediated cytotoxicity (ADCC) compared to IgG1 and IgG3 subtypes, as well as decreased complement dependent cytotoxicity (CDC) activity. This likely prevents activated T cells from being depleted [197].

VIII.B.d. Autoimmunity

The immune system needs to protect the host from invading pathogens. However, it is also paramount that the scope of the immune response is regulated so that excessive damage to healthy tissue is prevented. This is a very selective process and is controlled by several processes. These include central as well as peripheral tolerance. Central tolerance helps to delete most of the autoreactive immune cells. Unfortunately, this process is not perfect and thus cells that react to self are able to escape into the periphery [305]. As a consequence, various peripheral mechanisms have evolved to help regulate the potentially autoreactive cells that cause autoimmunity. Peripheral deletion, regulation *via* inhibitory receptors, anergy, ignorance, along with the activity of regulatory T cells all contribute in preventing autoimmune diseases [306]. Inhibitory receptors such as PD-1 are essential for T cell regulation during tolerance and immunity, allowing a balance between the two [307].

VIII.B.d.(i) Type I diabetes

Type I diabetes (TID) is an autoimmune disease that results from the destruction of insulin producing β cells in the Langerhan islets of the pancreas [308]. The non-obese diabetic (NOD) mouse is a spontaneous model of TID. It has both pathophysiological and genetic specifications which are also found in the human

disease. In such mice, expansion of autoreactive $CD4^+$ and $CD8^+$ T cells and activation of innate immunity, in addition to the activities of autoantibody producing B lymphocytes leads to deficits in immune tolerance. It is thought that PD-1 signalling is at least partly responsible for the initiation and progression of TID through multiple checkpoints [194]. Intravital microscopy studies have shown that upon PD-1 ligation, TCR signalling in lymph nodes is truncated, whilst prolonged cell-cell interactions during PD-L1 blockade caused an increase in IFN-γ production and a loss of immunological tolerance, leading to TID induction [309, 310].

VIII.B.d.(ii) Experimental autoimmune encephalomyelitis

Experimental autoimmune encephalomyelitis (EAE) is an animal model of multiple sclerosis [311]. The manifestation of this disease is the invasion of self-reactive T cells beyond the blood brain barrier, which results eventually in the destruction of myelin and axons of the central nervous system (CNS) [312]. A mixture of different cells in the CNS exhibit PD-1, PD-L1 and PD-L2 expression. In naive mice, PD-1 is expressed constitutively in retinal neurons, whilst PD-L1 and PD-L2 are expressed under inflammatory conditions in these cells [313]. Immune tolerance regulation *via* PD-1 signalling in EAE has been investigated. During active EAE, in the brain, infiltrating mononuclear cells express PD-1 and PD-1 ligands. This suggests that the PD-1 pathway is important in controlling CNS inflammatory responses [314]. Utilising neutralising monoclonal antibodies to PD-1 or PD-L2, Salma *et al.*, showed that the blockade of PD-L1 or PD-L2 results in an expansion of myelin oligodendrocyte glycoprotein (MOG)-reactive T cells, elevating the number of infiltrating lymphocytes to the CNS. This in turn accelerated the onset and the severity of EAE, therefore, supporting the idea that PD-1 and PD-L2 play pivotal roles in the pathogenesis of EAE [315].

Other studies have demonstrated that neurons which expressed PD-L1 and PD-L2 during inflammation can convert autoreactive T cells to TGF-β producing iTregs, alleviating EAE severity [316]. A study by Kohm *et al.* showed that Tregs play an

ameliorative role in MS. Adoptive transfer of $CD4^+CD25^+$Tregs reduced the inflammatory responses in the CNS and provided significant protection from EAE [317]. It is believed that PD-L1 expressing regulatory cells may be directly converting or inhibiting effector $CD4^+$ T cells through PD-1 ligation, because Tregs have high PD-1 and PD-L1 expression [318, 319]. Furthermore, host cells that express PD-L1 may play an important role in the peripheral conversion of transferred T cells to an iTreg phenotype. This notion is supported by the observation that murine vascular endothelium which expressed PD-L1, was able to activate and induce the generation of allogeneic Tregs [320]. These experiments emphasise the fact that proper regulation of inflammation within the CNS depends strongly on the interaction between the PD-1/PD-L1/PD-L2 pathways and Tregs.

VIII.B.d.(iii) Inflammatory bowel disease

Inflammatory bowel disease (IBD) is a group of inflammatory conditions that affect the colon and small intestine [194]. Chronic autoimmune responses affecting the gastrointestinal tract and colon give rise to Crohn's disease (CD) and ulcerative colitis (UC), respectively [321]. Commensal gut bacteria may generate chronic inflammatory responses in the intestinal mucosa. Under normal circumstances, the intestinal microenvironment is tightly monitored along with meticulous regulation of immune responses. This ensures tolerance towards intestinal flora whilst providing protection against invading pathogens [322]. However, when autoimmunity arises, activation of T cells and macrophages in the lamina propria leads to chronic inflammation in the intestine. This is augmented with the generation and secretion of proinflamatory cytokines including TNF-α and IL-1β [323]. To confront the inflammation in the intestines, one of the fundamental strategies adopted by the host is immune suppression through the utilisation of Tregs, helping to restore tolerance.

Experiments in a murine T cell transfer model of colitis suggested that $CD4^+CD25^+Foxp3^+$ cells can infiltrate the colon and secondary lymphoid organs. The colon samples from either UC or CD patients showed an increase in the number

of $Foxp3^+$ cells [324]. This could indicate that either site-developed or infiltrated Tregs have a compensatory role in order to inhibit the intestinal inflammatory response. Reports have shown that IBD patients' intestinal epithelial cells express higher levels of PD-L1 compared to healthy subjects. This indicates that PD-1/PD-L1 interaction could be key in establishing gut mucosal tolerance [325]. The PD-1 expressing non colitogenic T cells taken from murine spleens of naive cells were shown to be capable of recognising PD-L1. This culminated in the production of a subpopulation of Tregs. Remarkably, a study by Totsuka *et al.* showed that the $CD4^+CD25^-PD\text{-}1^+$ T cells could suppress the development of colitis induced by adoptive transfer of $CD4^+CD45RB^{high}$ T cells into mice with severe combined immunodeficiency (SCID) [326]. Another study demonstrated that treatment with an adenovirus expressing Fc conjugated PD-L1 (PD-L1Fc) significantly improved dextran sulfate soldium (DSS) induced colitis. This was accompanied by a reduction in IL-17A producing CD4 T cells in the colons of the DSS administered mice [327]. The findings further showed that the anti-colitic effect of PD-L1Fc treatment could also be manifested in DSS treated Rag1 knockout mice, suggesting lymphoid independency. Modulation of cytokine production by colonic DCs was induced by PD-L1Fc, which was dependent on PD-1 expression. Disease severity could also be significantly reduced in disease induced by $CD4CD45^{high}$ T cell transfer to Rag-1 knockout mice. Based on the potent protective effects shown by PD-L1Fc it seems that PD-1 mediated suppressive signalling could play an critical role in limiting the development of colonic inflammation. Therefore, agonising the PD-1/PD-L1 pathway could provide a novel therapeutic approach to treat IBD.

VIII.B.d.(iv) Rheumatoid arthritis

Rheumatoid arthritis (RA) is a systemic inflammatory condition that affects approximately 0.5~1% of the general population. It is defined by immune mediated inflammatory responses against the synovium [328-330]. Symptoms of RA include pain and swelling of joints due to synovial inflammation, fatigue, anaemia, osteoporosis, high risk for cardiovascular disease, and small joint involvement with

functional limitation. A human anti-tumour necrosis factor monoclonal antibody, adalimumab, has demonstrated therapeutic effects. It is able to slow the progression of structural joint damage, mitigate the symptoms and ameliorate physical function in active RA recipients [331]. In addition, treatment with anti-TNF-α in RA patients culminated in an enhancement of a specific subpopulation of Tregs, $CD4^{+}CD25^{high}Foxp3^{+}CD62L^{-}$T cells [332].

The inhibitory pathway generated *via* PD-1/PD-L1 signalling is over-activated in synovial T cells and macrophages [333]. RA synovial fluid is enriched with $PD1^{+}$ T cells and anergic T cells [334]. Collagen II (CII) induced arthritis (CIA) is a murine model of human RA and this has been extensively studied, to help investigate the pathogenesis of RA in order to discover novel therapeutics. Intradermal administration of collagen II causes joint swelling which is proceeded by ankylosis of the joints [335]. Studies have suggested that PD-L1 is able to regulate the CII-reactive T cells and thus, joint destruction. PD-L1-Ig given intraperitoneally to mice has been shown to reduce the rate of CIA development and help improve clinical symptoms [336]. Another study indicated that PD-L1-Ig treatment helped to suppress the CII-specific proliferation of splenocytes and reduce proinflammatory cytokines IL-23 and IL-17 [327].

VIII.B.d.(v) Systemic lupus erythematosus

Systemic lupus erythematosus (SLE) is a systemic autoimmune condition, predominantly characterised by the generation of a broad range of autoantibodies [194]. Murine and human SLE involves aberrant T cells, which have abnormal alterations in their gene transcription, receptor and signalling physiology, phenotype, and dysfunctional suppressor activities of regulatory lymphocytes. Such abnormal functioning of T cells leads to dysregulated B cell activity and therefore autoantibody production [337]. C57BL/6 mice with PD-1 deficiency develop lupus like autoimmune proliferative arthritis as well as glomerulonephritis. This is concurrent with C3 complement and IgG3 deposition on the glomeruli [213, 338].

PD-1 expression on a variety of immune cells of SLE patients has been investigated. PD-1 is upregulated on T cells and B cells, PD-L1 on B cells, and PD-L2 on monocytes, but there is no inherent defect in the functioning of PD-1 and PD-Ls on the peripheral blood mononuclear cells (PBMCs) of SLE patients [339]. An increase in circulating follicular T helper cells is linked to increased autoantibody production and subsequent organ damage in SLE patients [340]. PD-1 expression is significantly lower on the $CD25^{high}$ Tregs in SLE patients compared to healthy individuals [341].

IX. Work preceding the project

Three IgG1 anti-human PD-1 antibody clones were generated and initial characterization studies were performed by Sara Morgan and Claire Jessup (Davis laboratory; unpublished observations). IgG1 antibodies bind with high affinity to FcγRs [342]. These anti-PD-1 IgG1 antibodies were designed so as to bind preferentially to FcγRIIB, which is able to induce inhibitory signalling. Constructs which encoded the human extracellular region of PD-1, the transmembrane and intracellular regions of murine CD28, were cloned into a vector named pGFP2-n2 which encoded GFP (Figure 1.3a). Single residue mutant forms of the extracellular region of human PD-1 were produced in order to map the epitopes of these antibodies (Figure 1.3a). It was shown that Clone 19 (Cl19) binds to a membrane proximal epitope on PD-1 whilst Clone 2 (Cl2) and Clone 10 (Cl10) bind to a membrane distal epitope (Figure 1.3b). It is likely that Cl2 and Cl10 antibodies would compete with one another for binding to PD-1 based on the epitope mapping data. Surface plasmon resonance based binding assays for the characterization of the binding kinetics of these three clones were also undertaken. The findings revealed that Cl10 had the highest off-rate (lowest affinity) whilst Cl19 and Cl2 antibodies gave much lower off-rates (Figure 1.3c).

In order to study the scale of the signal-generating activities of these 3 clones, a dimeric form of PD-1 was generated using the extracellular domain of human PD-1 spliced to the transmembrane region of CD3ζ and the cytoplasmic region of mouse

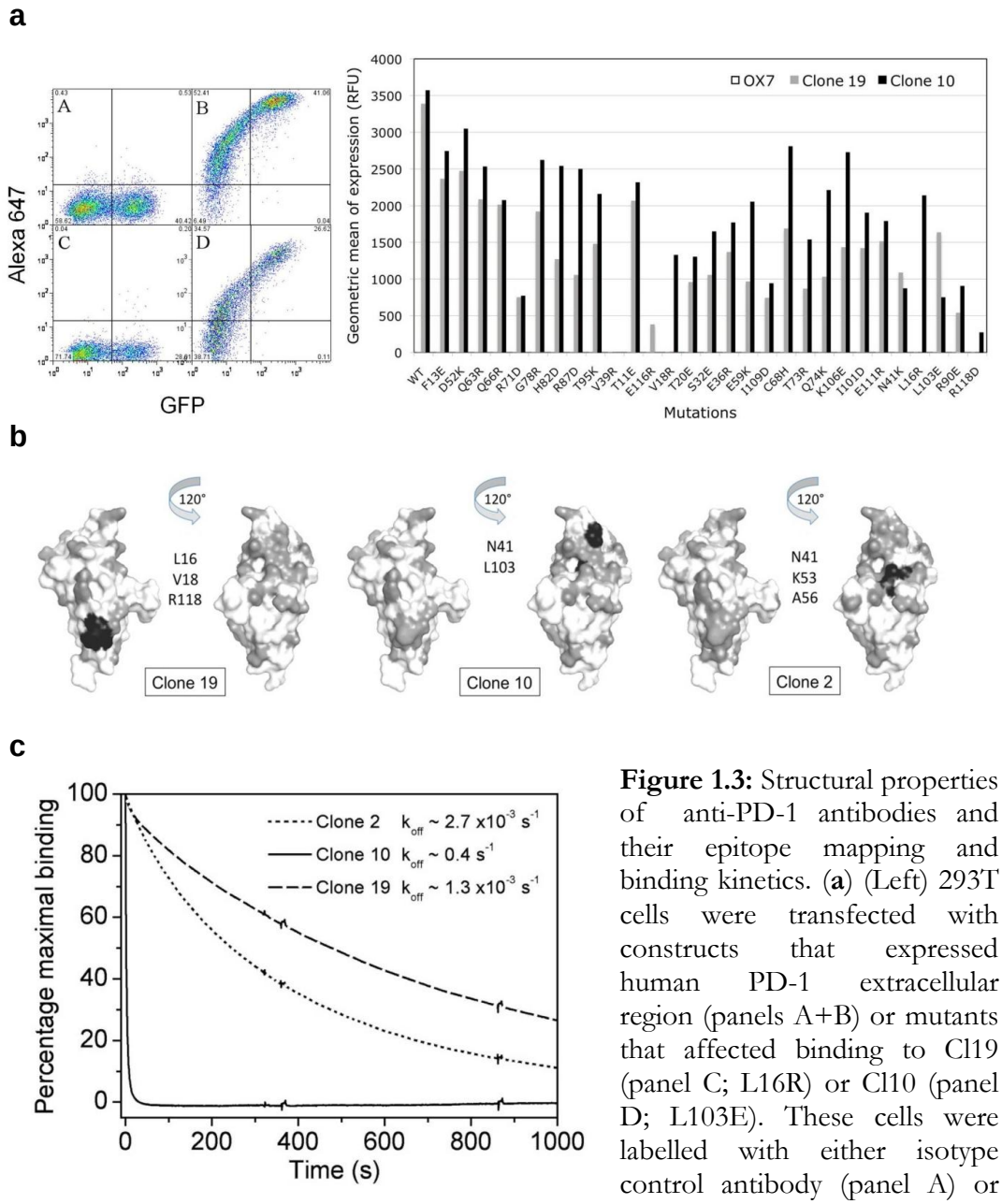


Figure 1.3: Structural properties of anti-PD-1 antibodies and their epitope mapping and binding kinetics. (**a**) (Left) 293T cells were transfected with constructs that expressed human PD-1 extracellular region (panels A+B) or mutants that affected binding to Cl19 (panel C; L16R) or Cl10 (panel D; L103E). These cells were labelled with either isotype control antibody (panel A) or with Cl19 (panels B+C) or Cl10 (panel D) antibody, proceeded with Alexa647 secondary antibody labelling. Antibody binding is shown on the y axis whilst the transfected cells were eGFP positive (x-axis). Geometric means of the Alexa647 fluorescence expression for the GFP^+ cells is shown for all the mutants of PD-1. (**b**) Crystal structures of mouse PD-1 are presented. Residues equivalent to human PD-1 residues which have no effects on binding to Clones 2, 10, 19 are shown in grey and residues when mutated partially or fully that prevent the binding of to these 3 anti-PD-1 antibodies are coloured black. (**c**) Kinetics of PD-1 binding by the three different anti-PD-1 antibodies were measured using the Biacore.

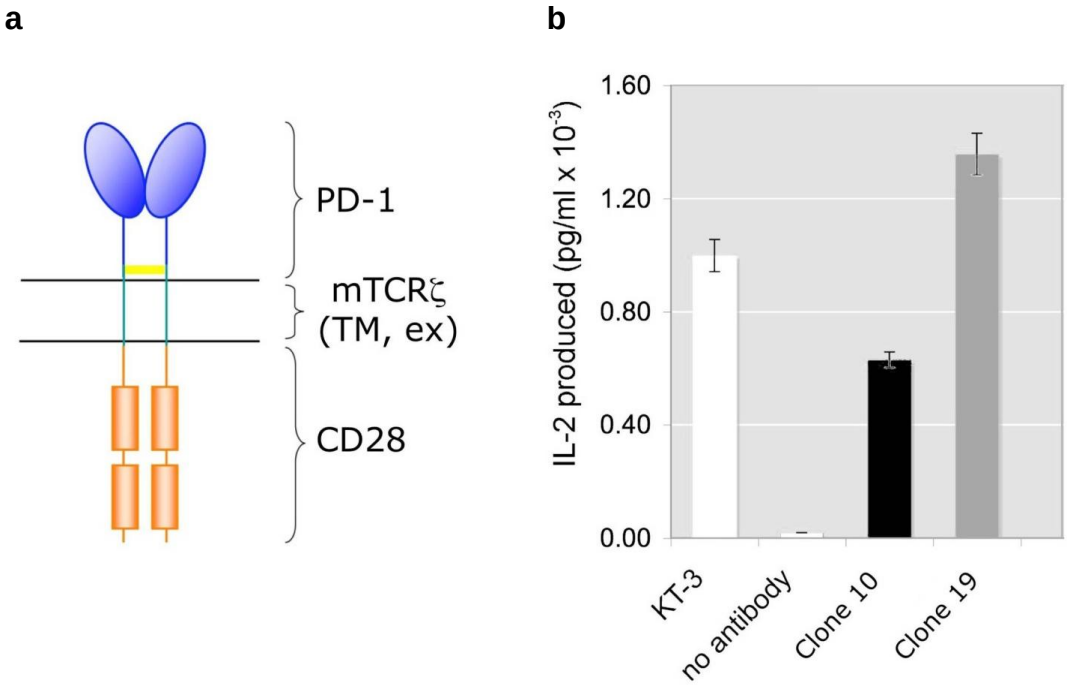


Figure 1.4: IL-2 secretion as a result of anti-PD-1 antibodies engagement to a hPD-1/mTCRζWT/mCD28 chimera. (**a**) A chimera composed of human PD-1 extracellular region fused to mouse TCRζ transmembrane and cytoplasmic regions along with mouse CD28 was expressed in DO11.10 cells. (**b**) The DO11.10 cells were given anti-CD3 (KT-3) or anti-PD-1 antibody treatments, and subsequent IL-2 secretion was recorded.

CD28 (Figure 1.4a). The interleukin-2 (IL-2) secretion was measured. Cl19 was able to induce far greater amounts of IL-2 production than Cl10 by the hPD-1/mTCRζWT/mCD28 chimera (Figure 1.4b). Importantly, this suggested that the topology of the antibody complex formed is what determines the agonistic signalling levels. This study also indicated that the degree of agonistic signalling could be altered with the choice of antibody.

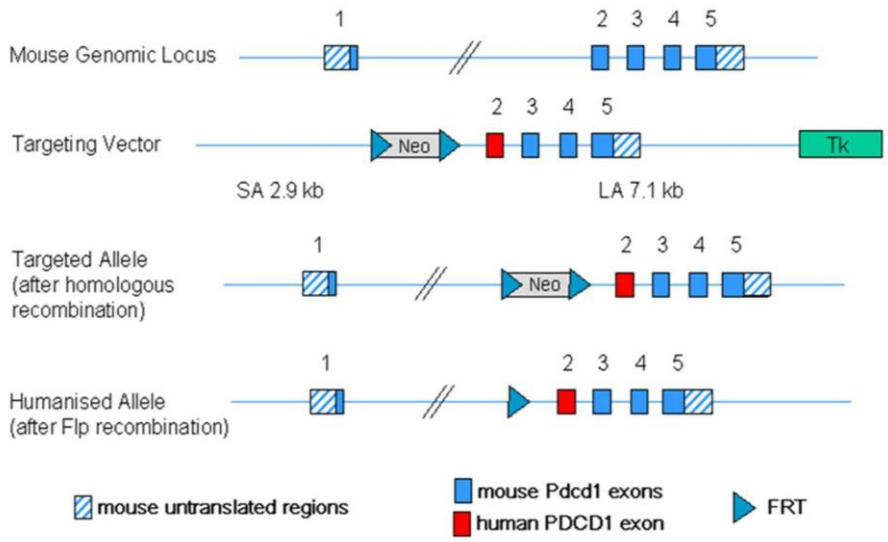
The production of a mouse model in which the ligand- and antibody-binding human PD-1 extracellular domain replaced that of the mouse was undertaken using a constitutive knock-in strategy (Figure 1.5). This humanised homozygous PD-1 knock-in mouse (hPD-1KI) was then characterised by Billur Akkaya (Davis and Cornall laboratories; unpublished observations). Analysis of the expression of the humanized PD-1 protein on T cells which were activated *in vitro* showed that swapping exon 2 of the intrinsic mouse PD-1 gene with exon 2 of the human PD-1 gene did not perturb PD-1 protein folding, as evidenced by antibody binding as well as PD-1 cell membrane expression on activated T cells. Further confirmation that the targeted PD-1 gene expressed normally was shown by the normal upregulation of the humanized PD-1 protein on T cells activated *in vivo*. Furthermore, the resting immune systems of hPD-KI and WT C57BL/6 mice were investigated to see if any abnormalities had arisen through humanized PD-1 gene insertion. There were no significant differences between the splenic and thymic parameters of WT and humanized mice, therefore proving that humanized PD-1 gene insertion does not lead to developmental abnormalities in the adaptive immune system. Both the WT C57BL/6 and hPD-KI mice were thus able to respond to an immunogen with similar strengths using a T dependent immune response assay. Human PD-1 is able to bind to mouse PD-L1/L2 with same affinities as human PD-L1/L2 [343]. These experiments confirmed that the hPD-1KI mouse is a robust and reasonable model for testing the effects of anti-human PD-1 antibodies *in vivo*.

In order to examine the inhibitory actions of these anti-PD-1 antibodies *in vitro,*

inhibition of OKT3 (anti-CD3) antibody induced peripheral blood mononuclear cell proliferation by these three clones was studied (Figure 1.6). OKT3 and anti-PD-1 antibodies were coattached to tosyl-activated Dynalbeads. At lower OKT3 doses, significant reductions in cell proliferation were induced. Surprisingly, Cl10 generally agonized PD-1 more effectively over a broader range of OKT3 stimulation in comparison to Cl19. This seemed likely to be due to the fast binding kinetics of Cl10; Cl10 may be able to target more PD-1 molecules than Cl19 in a given time period, which culminates in greater overall signalling. In this proliferation assay, despite the fact that Clones 2 and 19 have similar slow off-rates, only Cl19 demonstrated suppressive effects. From such observations, it is believed that binding to a more membrane proximal epitope compensates for the disadvantageous slow off-rate.

Having shown Treg inducing effects *in vitro* as well as modulatory effects of the anti-PD-1 antibodies in models of normal immunity *in vivo*, it was hypothesised that the PD-1 antibodies could be potentially therapeutic. To test this hypothesis, Cl19 antibodies were administered in a myelin oligodendrocyte glycoprotein and complete Freund's adjuvant (MOG/CFA) induced EAE mouse model of autoimmunity. However, the initial EAE studies showed a disease exacerbating role for Cl19. This effect was possibly due to the Cl19 treatment immediately down-modulating the cell surface expression of PD-1, as shown for the TCR previously [344], and thus the inhibitory signal was abrogated. However, a second EAE trial showed that by allowing some time for PD-1 upregulation, this helped to limit the disease-exacerbating effect of Cl19 to a certain degree. Importantly, when down-modulation was studied, it turned out that Cl10 treatment induced far less PD-1 cell surface downregulation compared to Cl19. This implied that the degree of PD-1 internalization may be linked to the strength of antibody binding. It was hypothesised that by modifying Cl19 for lower affinity, disease exacerbating potential of this antibody may be removed, thus enhancing its inhibitory and therapeutic effects.

a



b

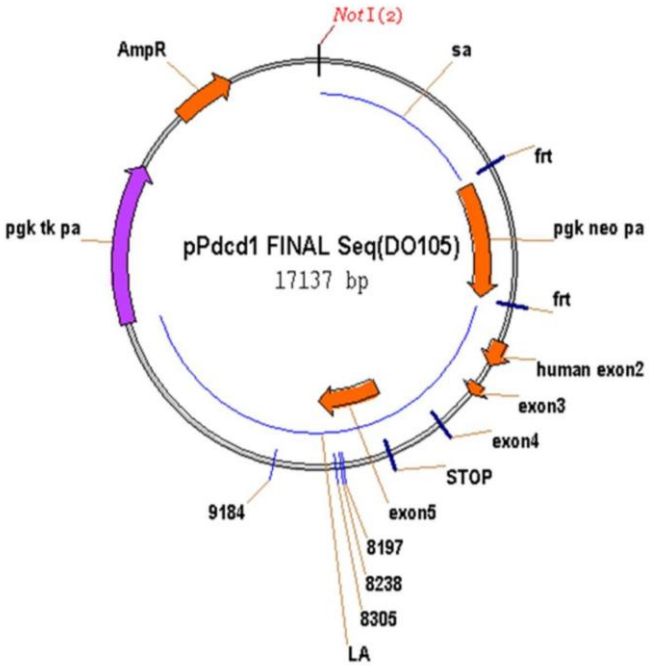


Figure 1.5: Generation of humanized PD-1 knock-in mice. (**a**) Human PDCD1 exon 2 which encode PD-1 extracellular region was PCR amplified from human genomic DNA. Mouse Pdcd1 exon 2 was replaced with the human equivalent. Frt sites flanked the selection marker. The humanised allele was created following *in vivo* Flp mediated removal of selection marker. (**b**) Map showing the targeting vector.

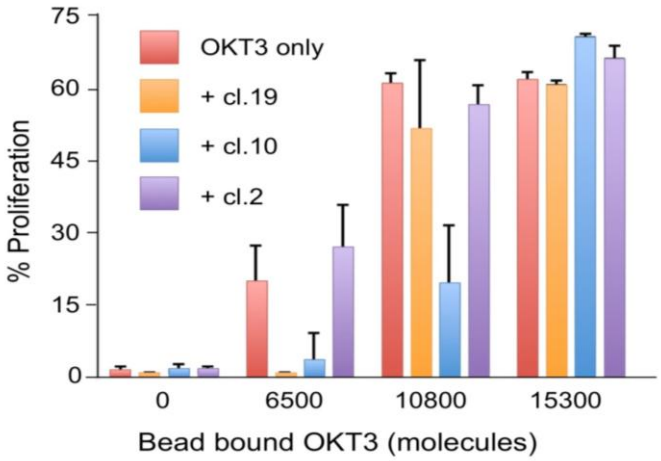


Figure 1.6: *In vitro* inhibition of OKT3 antibody induced PBMC cell proliferation by anti-PD-1 antibodies. The OKT3 and anti-PD-1 antibodies were co-attached to tosyl-activated Dynalbeads. OKT3 levels are shown on the abscissa. At lower OKT3 doses, significant reductions in cell proliferation were induced. The largest inhibitory effects were observed for Cl10 *in vitro*.

X. Objectives of this thesis

Work in the Davis and Cornall laboratories showed that strong inhibitory signalling could be induced by anti-PD-1 antibodies that bind close to the membrane with high affinity, or antibodies binding away from the membrane with very low affinity. This possibly indicates that it may be advantageous for anti-PD-1 superagonists to have much faster off-rates than would normally be expected to be useful, in order to be active. Thus, the aim of the new study comprising this thesis was to combine the apparently advantageous features of the binding properties of both sets of antibodies into a single 2nd generation antibody, *i.e.* by generating variants of a membrane proximally-binding antibody that had a significantly faster off-rate than the present superagonist, Cl19. Such antibodies with altered kinetics and increased off-rates could be expected to potentially induce less PD-1 cell surface downregulation and generate stronger superagonistic receptor triggering, leading to enhanced inhibitory effects and therapeutic potential. We also set out to test the suppressive effects of the 1st generation (original three clones) as well as modified 2nd generation anti-PD-1 antibodies in various *in vitro* and *in vivo* assays.

Chapter 2

Materials and methods

I. Molecular cloning techniques

I.A. Overview of cloning method

Standard molecular cloning procedures were implemented to express the proteins of interest either transiently or stably in various appropriate cell lines. Genes of interest were amplified from vector templates or appropriate cDNA using oligonucleotide primers which incorporated specific restriction enzymes sites at both the 5' - and 3'-ends. Once polymerase chain reaction amplification was performed, the gene of interest along with the destination vector plasmid were digested with the corresponding digestion enzymes. Following the purification of the correct DNA fragments, a ligase reaction was conducted to generate a contiguous plasmid which were subsequently used to transform *E. Coli.* bacteria which were cultured in antibiotics treated culture plates. Once the size and orientation of the DNA insert was confirmed, greater preparations of DNA plasmid were generated using miniprep kits and DNA sequencing was performed to check for sequence accuracy.

I.B. Polymerase chain reaction (PCR)

PCR was used to amplify genes of interest. The following reaction mixture was utilised:

	Company	Conc.	Volume (µl)
Polymerase buffer	NEB	10 x	8.0
dNTP	Bioline	10 mM	2.0
5'-oligo	Sigma-Aldrich	10 µM	2.0
3'-oligo	Sigma-Aldrich	10 µM	2.0

Template	-	100 ng/µl	1.0
Phusion DNA Polymerase	NEB	5 U/µl	0.5
ddH_2O			24.5

With the majority of the cloning strategies, oligonucleotide primers with appropriate restriction sites at the 5'- and 3'-ends were implemented. To allow for sequence integrity for cloning, a Phusion DNA polymerase (NEB) with a robust proofreading capacity was used. This allowed minimal sequence amplification error to incur. The PCR was performed on a DNA Engine Tetrad (MJ Research) with the following steps:

	Step	Temp. (°C)	Time
1	Enzyme activation	95	2 min
2	Denaturing	94	30 s
3	Annealing	58	30 s
4	Extension	72	35 s/kb
5	Repeat 2-4		29 x
6	Final Extension	72	7 min
7	Cooling	4	∞

In order to screen bacterial colonies for the detection of the presence of inserted DNA sequence and correct plasmid, an alternative PCR reaction mixture was utilised:

	Company	Conc.	Volume (µl)
Polymerase buffer	NEB	10 x	3.0
dNTP	Bioline	10 mM	1.0
5'-oligo	Sigma-Aldrich	10 µM	1.5
3'-oligo	Sigma-Aldrich	10 µM	1.5
Colony Stab	-	-	-

DNA Polymerase	Taq NEB	10 U/µl	0.2
ddH_2O			21.8

Modifications to the PCR reaction cycle were made to ensure lysis of bacterial cells prior to amplification:

	Step	Temp. (°C)	Time
1	Lyse bacteria	95	7 min
2	Denaturing	95	30 s
3	Annealing	58	30 s
4	Extension	72	70 s/kb
5	Repeat 2-4		30 x
6	Final extension	72	75 s
7	Cooling	4	∞

In order to generate mutations, a chimeric PCR protocol was implemented. Oligonucleotide primers were generated to incorporate overlapping internal DNA sequences (approximately 20 nucleotides) at the point of mutation. Two separate PCR products were then amplified using the conventional PCR strategy. The two overlapped amplicons of the right size were gel purified using a DNA gel extraction kit (Qiagen). These were subsequently used as templates in a second round of PCR according to the original protocol, albeit reducing the number of cycles (step 4) to 15.

I.C. Agarose gel electrophoresis

Agarose gels were made to help resolve the size and purity of PCR products or plasmids. High-quality agarose (SeaKem LE agarose, BioWhitakker) was dissolved in Tris-borate EDTA (TBE) buffer (Sigma-Aldrich) at 1% (w/v). The gel was heated in the microwave for 90s and then ethidium bromide was added at a final concentration of 0.5 µg/ml. The gel was allowed to set and was cast with specific combs for 20

min. The DNA samples were then mixed with the loading buffer (40% (w/v) sucrose, bromophenol blue, xylene cyanol) and loaded into the gel. Electrophoresis was conducted at 90 mA for 60 minutes using a PowerPac 300 (BioRad). DNA bands were detected using a ultra-violet (UV) irradiation in a GelDoc (BioRad). If excision of specific bands was necessary for subsequent cloning, such DNA-embedded gel bands were cut with a scalpel blade under low power UV light. According to the manufacturer's instructions, a gel extraction kit (Qiagen) was used to help extract and purify the DNA from the agarose gels.

I.D. Restriction enzyme digestion of DNA

Purified DNA samples containing specific restriction sites were digested with the corresponding restriction enzymes (NEB), usually at 10 U/µl, in a reaction mixture as follows:

	Company	Conc.	Volume (µl)
Digestion Buffer	NEB	10 x	10.0
BSA	NEB	100 x	1.0
PCR product or Vector DNA (1 µg)	-	-	50.0
Restriction Enzyme(s)	Sigma-Aldrich	10 U/µl	5.0
ddH_2O			34.0

For double digestions, whereby two restriction enzymes were used simultaneously, only 2.5 µl of each enzyme was applied. This was to allow the glycerol concentration of the reaction mixture to be maintained at a minimum level so as to prevent any possible interference with enzyme activity. Sequential enzyme digestion was performed when no compatible buffer could be utilised for simultaneous digestion of two different enzymes. In order to purify DNA between each digestion step, a PCR Purification Kit (Qiagen) was applied. Samples were digested at relevant temperatures for 60 minutes.

I.E. Ligation of inserts into vectors

Restriction enzyme digested DNA products were cloned into the desired vectors using this reaction mix at 16 °C for 2 hours:

	Company	Conc.	Volume (µl)
T4 Ligase Buffer	NEB	10 x	2.0
Insert DNA	-	varying	10.0
Vector DNA	-	100 ng	5.0
T4 DNA Ligase	NEB	400 U/µl	1.0
ddH_2O		-	2.0

For blunt-ended ligations, the ligation mixes were incubated at 16 °C overnight.

I.F. Competent bacterial cell transformation

Competent *E.coli* bacterial cells were used to transform the ligation products and supercoiled purified plasmids. One ml of an overnight culture of *E.coli* grown at 37 °C was used to inoculate 30 ml Luria-Bertani (LB) Broth in a 75 cm^2 sterile tissue culture flask. This was incubated at 37 °C with the orbital shaking at 200 rpm until the optical density at 600 nm reached between 0.3-0.6. Next, the bacterial cells were centrifuged at 2000 rpm for 14 minutes in the Heraeus Megafuge, and the pellet underwent resuspension in ice-cold 2.5 ml TSS buffer. The TSS buffer was prepared with the following ingredients:

	Company	Conc.	Volume (ml)
DMSO	Sigma	100 %	5 ml
Polyethylene Glycol 600	Sigma	-	10 g
$MgCl_2$	Sigma	1 M	5 ml
LB Broth	Sigma	-	90 ml

For transformation, 10 µl of supercoiled DNA plasmids were added to 100 µl of competent cells and incubated on ice for 20 minutes. They were then heat-shocked at 37 °C for 4 minutes and 30 seconds before immediately returning on ice for 1 min.

400 µl of LB Broth was gently added to the bacteria cells and incubated at 37 °C for 1 hour. Agar was made using LB agar tablets (Sigma) and autoclaved. Antibiotics such as ampicillin were added at the correct concentration to the agar while still molten. These were then poured in 90 mm petri dishes (Sterilin), cooled, set and dried in a 37 °C incubator for 1 hour. The transformed bacteria (400 µl) were pipetted onto the agar plates and spread using an ethanol-sterilized glass spreader. These plates were finally incubated overnight at 37 °C. The next day, bacterial colonies tested for correct insert and orientation by the use of colony PCR.

I.G. Vector production and purification

In order to generate enough quantities of plasmid DNA suitable for sequencing and downstream applications, DNA was extracted from overnight transformed 10 ml bacterial cultures and grown at 37 °C with appropriate antibiotics. PureLink™ HiPure Miniprep kit (Invitrogen) was applied according to manufacturers' instructions. To generate greater stocks of plasmid DNA, Qiafilter™ Midi kits (Qiagen) were used with 100 ml of bacterial cell culture. All the DNA pellets were resuspended appropriate concentrations with TE buffer (10 mM Tris-HCL, 1 mM EDTA, pH 8.0). DNA concentration was measured spectrophotometrically at 260 nm on the Nanodrop spectrophotometer (Thermo Fisher Scientific). The DNA purity was kept by ensuring the 260 nm/280 nm ratio reached 1.8.

I.H. DNA sequencing and analysis

DNA sequencing was performed by the dideoxy termination method in house with suitable primers (Sequencing Unit of the Weatherall Institute of Molecular Medicine, University of Oxford). The DNA sequences were read automatically with the 4Peaks software. For the confirmation of sequence identity and accuracy, automatically called base pairs from sequencing traces were analyzed with both the 4Peaks software and the online nucleotide Basic Local Alignment Search Tool (BLAST) software available at: https://blast.ncbi.nlm.nih.gov/Blast.cgi?PROGRAM=blastn&PAGE_TYPE=BlastSearch&LINK_LOC=blasthome

I.I. Glycerol stocks of transformed bacteria

In order to store transformed bacteria with the desired plasmid DNA vector, 200 µl 80 % (v/v) filter-sterilised glycerol was added to 800 µl of an overnight bacterial culture and frozen at -80 °C. This allowed convenient and quick growth of transformed bacteria for desired plasmid production. In order to grow bacteria from glycerol stocks, a pipette tip was used to retrieve a small portion of the frozen bacteria culture. This was then inoculated with a 5 ml LB Broth solution along with the desired selective antibiotic such as ampicillin at 100 µg/mL. The bacterial culture was subsequently incubated at 37 °C overnight with the orbital shaking at 200 rpm.

I.J. Colony PCR

Typically, ten colonies were picked for colony PCR. Colony PCR was performed to assess the presence of the desired insert. See the relevant programme in the PCR section mentioned previously for PCR settings. A colony was picked with a sterile plastic tip which has been immersed in the PCR mix. This was then streaked on a reference agar plate containing 100 µg/mL ampicillin. The agar plate was incubated at 37 ºC for 4 hours. The extension time were modified accordingly for very big DNA inserts. PCR amplicons were ran on an agarose gel as described above. Normally, two colonies which gave a PCR product of the correct size were typically chosen to be grown up for DNA sequencing.

I.K. Generating Cl19BirAHis WT and mutant Fabs

The strategy for making Cl19 Fab mutants with decreased affinities to PD-1 is as follows. Initially, we mapped the binding surface with drastic mutations in the Fab complementarity determining regions (CDRs), and then re-mutated binding residues with more subtle changes to alter the kinetics. In order to investigate such mutant Cl19 Fabs on the Biacore, a BirAHis tag was added to the Fabs. Thus anti-PD-1 variable heavy chain Fab with BirAHis attached was cloned into the pOPINVH (Figure 2.1) vector and then transiently co-transfected along with anti-PD1 Cl19 Fab light chain pOPINVL vector (Figure 2.2) into 293T cells. The anti-PD-1 antibodies

were cloned from mouse hybridoma cells. Pymol software was utilised to determine which CDR residues of the Fab to mutate based on a model of the Cl19 Fab prepared for us by Prof Shinji Ikemizu of Kumamoto University. In total, in the first round of screening, we made 18 'drastic' mutations using the chimeric PCR approach: 3 mutations per CDR, 9 mutations on both light and heavy chains. A second round of screening followed where a further 6 individual mutations were performed on the variable region of the heavy chain of Cl19. All the amino acid residues selected for mutation were chosen on the basis that they were outward facing and not buried within the CDR; making access to PD-1 more favourable. The residues selected were mutated to arginine apart from basic amino acids lysine, histidine and arginine; instead, these residues were mutated to aspartic acid. Once the 24 constructs were made, the new antibody Fab variants were transiently expressed in 293T cells using pOPINVH and pOPINVL vectors and affinity purification was conducted using Nickel NTA beads.

pOPINVL vector was used to clone the variable region light chain of Fab fragments whilst the pOPINVH vector was utilized for cloning in the variable heavy chain region of the Fabs. The pOPINVL and pOPINVH vectors already contain the corresponding constant regions of the Fabs. The variable region of the light chain was cloned in between the phosphatase secretion leader and the constant region using KpnI and HpaI. A TAT mutation was performed after mutating the CDRs in the light chain in order to get rid of an existing KpnI site within the light chain Fab. TSS transformation using TOP10 *E. Coli* cells were carried out for the cloning of the Fab fragments into the pOPINVH and pOPINVL vectors. The heavy chain construct contained a Histidine tag needed for purification. With 19pVmγ1 pOPINVH Cl43 vector, enzyme digest with KpnI and SfoI removed the variable Fab region and a tiny portion of the constant region. New Fab insert containing variable and constant FabBirAHis was then made, digested with KpnI and AfeI and then ligated to the cut vector. AfeI is compatible with SfoI thus allowing this subsequent ligation. This construct named 19pVmγ1BirAHis pOPINVH Cl16 was

the WT Cl19 heavy chain construct used to make both Cl19 BirAHis Fab as well as the mutant Fabs. Mutated light chain Fab pOPINVL vectors were then co-transfected together with the heavy chain pOPINVH vector for transient expression of the different Fab fragments in T175 flasks *via* the PEI transfection method. Western blots were performed to check for protein expression.

II. Mammalian cell culture

II.A. General techniques

In order to maintain sterility, experiments involving eukaryotic cells were performed in HEPA-filter microbiology safety cabinets. Cells were grown in 37 °C incubators supplemented with 5% CO_2.

II.B. Cell culture media

293T HEK cell line was grown in DMEM (Sigma) supplemented with 10% heat inactivated fetal calf serum (FCS) (Biosera), 100 U penicillin (PAA), 2mM LGlutamine and 100 μg/ml streptomycin (PAA). Mouse splenocytes were grown in RPMI-1640 (Sigma) supplemented with 10% heat inactivated FCS (Biosera), 2 mM L-glutamine (Invitrogen), 100 U penicillin (PAA), 100 μg/ml streptomycin (PAA), 50 μM β-mercaptoethanol (Gibco), 10 mM HEPES (PAA) 100 μM non-essential amino acids solution (Gibco) and 100 μM sodium pyruvate (PAA).

CHOK1 cells were initially grown in DMEM (Gibco) supplemented with 10% fetal calf serum (Sigma), 2 % nucleoside and amino acid supplement (0.35 mg/mL adenosine, 0.35 mg/mL cytidine, 0.35 mg/mL guanosine, 0.35 mg/mL uridine, 0.12 mg/mL thymidine, 0.1 mg/mL asparagine, 0.1 mg/mL glutamic acid), 1 mM sodium pyruvate, antibiotics (50 units penicillin, 50 μg streptomycin and 100 μg neomycin per mL) and 2 mM L-glutamine. On the day of stable transfection, the media was changed to DMEM (Gibco) supplemented with 10% heat inactivated dialyzed FCS (Biosera), 2 % nucleoside and amino acid supplement, 100 μM sodium pyruvate (PAA) and antibiotics (50 units penicillin, 50 μg streptomycin and 100 μg

neomycin per mL) along with varying concentrations of l-methionine sulfoximine (MXS).

Humanized PD-1 k.i. mouse splenocytes were separated using ficoll. They were then cultured in RPMI medium (Sigma) supplemented with 10 % fetal calf serum (Sigma), 2 mM L-glutamine, 2 % none essential amino acids (Gibco), 1 mM sodium pyruvate (PAA), antibiotics (50 units penicillin, 50 μg streptomycin and 100 μg neomycin per ml), and 0.05 mM 2-*Mercaptoethanol.*

II.C. Thawing of cells

Cells were thawed carefully by immersing the frozen cryovials in a 37 °C water bath for approximately 1 min. They were then diluted in 30 ml of pre-warmed appropriate medium and centrifuged at 1300 rpm in a standard microfuge for 3 minutes. Lastly, they were resuspended in fresh growth medium. Cell viability was then monitored after 24-72 hours and cells were grown to full confluence and subsequently passaged.

II.D. Cell freezing

In order to freeze cells for long-term storage, 6-10 x 10^5 cells in the growth phase were harvested. They were then centrifuged at 1300 rpm in a standard microfuge for 3 minutes, resuspended in 1ml of freezing solution (10% (v/v) dimethyl sulfoxide in foetal calf serum) and transferred to a cryovial (Nunc) and put inside an isopropanol containing freezing chamber in the -80 °C freezer. This permitted gradual decrease in temperature which helps to guarantee adequate cell viability upon thawing. Cryovials were transferred to liquid nitrogen for long-term storage.

II.E. Cell counting

In order to count cells, an equal volume of Trypan blue and cells were mixed together, a glass slip was placed over the haemocytometer, and the cell dye mix was pipetted onto a haemocytometer and examined by light microscopy. This helped us

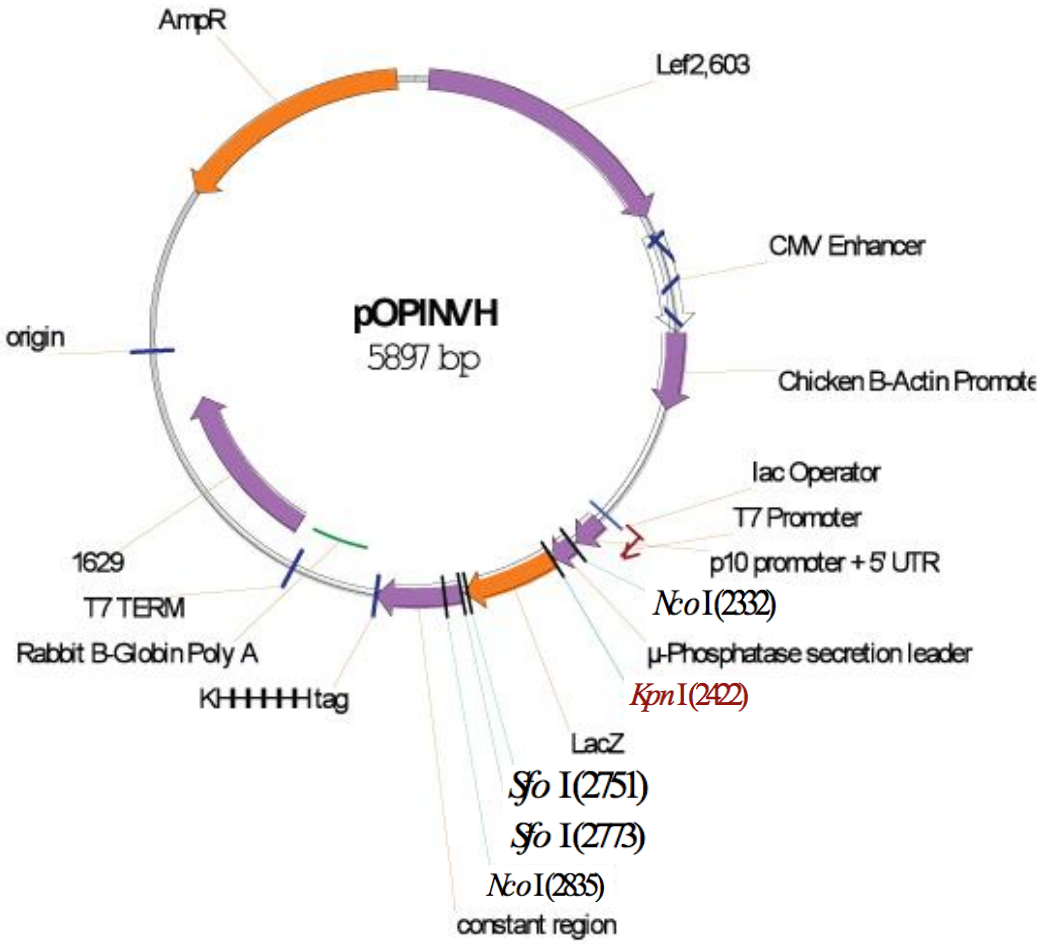


Figure 2.1: pOPINVH vector map containing relevant restriction sites for cloning.

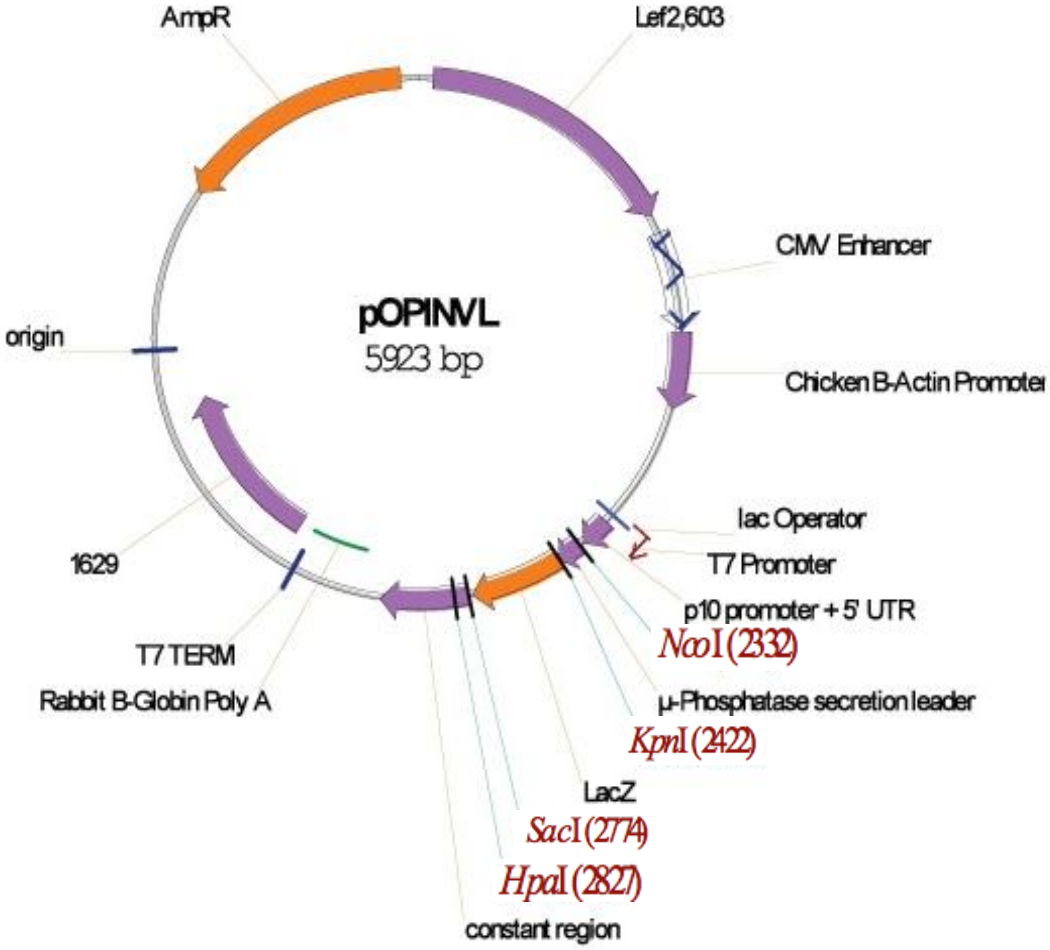


Figure 2.2: pOPINVL vector map containing relevant restriction sites for cloning.

to assess cell density and cell viability of growing culture. Trypan blue staining allowed us to quantify the number of viable cells (shown as white) and dead or dying cells with compromised cell membranes (cells with blue staining). The number of cells in one 4x4 square = $x10^4$ cells/ml.

II.F. Sub-culturing of cells

For the adherent HEK 293T cell line and CHOK1 cell line, the media were removed and cells were washed in sterile cold phosphate-buffered saline (PBS) solution. 5 ml of trypsin diluted in PBS was applied to the cells for 3 minutes. Gentle shaking was then applied which caused cell detachment from the flasks. 10 ml fresh medium was quickly added to inactivate trypsin activity. The cell suspensions were harvested, centrifuged at 1300 rpm in a standard microfuge for 3 min and resuspended in the appropriate volume. Cell densities were counted using a haemocytometer, this helped to determine the suitable cell suspension volume to add to a new flask so as to permit optimal cell growth.

II.G. Plating of cells for transient transfection

In order to plate out adherent cells for transfection in 6-well plates (Nunc), cells were detached from flask and resuspended in medium as described above. Following cell counting, a suitable density was prepared and added to desired plates. The cells were then left in the incubator overnight to allow them to reattach. Cells were plated at a density which would lead to a 60-80% confluence level on the day of transfection.

II.H. PEI Co-transfection of HEK 293T cells for Cl19 Fab production

293 HEK T cells were grown in T175 flasks with DMEM media and supplements. *Polyethylenimine (*PEI) co-transfection with 20 µg of Cl19Fab light chain pOPINVL and 20 µg of Cl19FabBirAHis heavy chain pOPINVH was conducted. 20 µg DNA with 60 µl GeneJuice transfection reagent (Merck) and 1ml DMEM used for each reaction mix. Cells were harvested after 72 hours and the Fabs were purified using NiNTA beads. Protein expression was checked by western blots before biotinylation

was performed.

II.I. Production of soluble His-tagged protein in mammalian cell lines

To produce soluble forms of PD-1FcHis, a mammalian expression system was used to ensure correct folding and glycosylation. Chinese hamster ovary K1 cells (CHOK1) were selected because they are able to generate great amounts of protein. Although a stable transfection system is more laborious and time-consuming compared to transient systems, better yields can be achieved through it. Another advantage is that once created, the cell line can be stored long-term in liquid nitrogen should future experiments require further protein usage. In order to create a soluble, His-tagged form of the desired protein, a short DNA sequence encoding a His-tag followed by a STOP codon was inserted at the C-terminal. To allow for proper secretion of the protein, the N-terminal signal peptide was maintained. Stable transfection of CHOK1 cells using the glutamine synthetase selection system was used to generate PD-1FcHis protein. This allowed for selection of a single high-expressing clone. Once a stably transfected cell line was generated, desired protein secretion and expression into the cell culture supernatant was validated by running Western blots. Typically, two Corning HYPER*Flask* cell culture vessels were seeded with approximately 2 x 10^7 transfected CHOK1 cells in 500 mL medium. Protein harvesting and purification was conducted after 3 weeks.

II.J. Stable cloning and large scale soluble protein production with CHOK1 cells

In order for the selection of CHOK1 clones which express great amounts of protein to be realized, a glutamine synthetase selection system was employed. Importantly, glutamine is a pivotal essential amino acid. CHOK1 cells endogenously express glutamine synthetase which helps to convert glutamate to glutamine. In order to enhance the selective pressure, CHOK1 cells are grown in glutamine-free medium in the presence of a glutamine synthetase inhibitor, methionine sulphoximine (MSX). Ultimately, a single high expressing clone is isolated for generating great amounts of

the protein of interest.

II.K. pEE14 expression vector for stable transfections

For PD-1FcHis stable expression, the protein of interest were inserted into an expression vector named pEE14 (Lonza Biologics) (Figure 2.3). This vector contains a glutamine synthetase minigene under the same promoter that drives expression of the gene of interest. Consequently, transfected CHOK1 cells which are able to show high protein expression for the gene of interest have an advantage over untransfected or low-expressing cells and thus are specifically selected for.

II.L. Stable transfection of CHOK1 cells for the production of first generation and second generation whole anti-PD-1 antibodies

In order to generate whole Cl19, FoR1 and FoR2 antibodies, the heavy chain regions were cloned into pEE6.4 vector (Figure 2.4) whilst the light chain regions were cloned into the pEE12.4 vector (Figure 2.5). The cassettes containing hCMV-ME promoter, heavy chain and PolyA chain from pEE6.4 were subsequently removed and cloned into the pEE12.4 vector. The subsequent pEE12.4 containing both the light and heavy chain regions were stably transfected into CHOK1 cells.

Initially, two T75 Greiner flasks (Sigma) were inoculated with $4*10^6$ CHO-K1 cells in DMEM medium (Gibco) with supplements that contained L-glutamine. The next day, these cells were transfected with the pEE12.4 plasmid containing the tagged genes of interest. The CHO-K1 medium was replaced with glutamine-free CHO-K1 medium. The plasmid was sterilized by being added to an equal volume of ether into an Eppendorf tube. This was then centrifuged at 1100 rpm in a standard microfuge for one minute at room temperature. In the tissue culture hood, the organic layer was discarded using a pipette, and the residual ether was left to evaporate for several minutes. 10 μg of the sterilised plasmid was mixed with 1 ml of unsupplemented glutamine-free DMEM medium (Gibco). This was followed by a further addition of 30 μL GeneJuice transfection reagent (Merck). Once the solution was mixed together

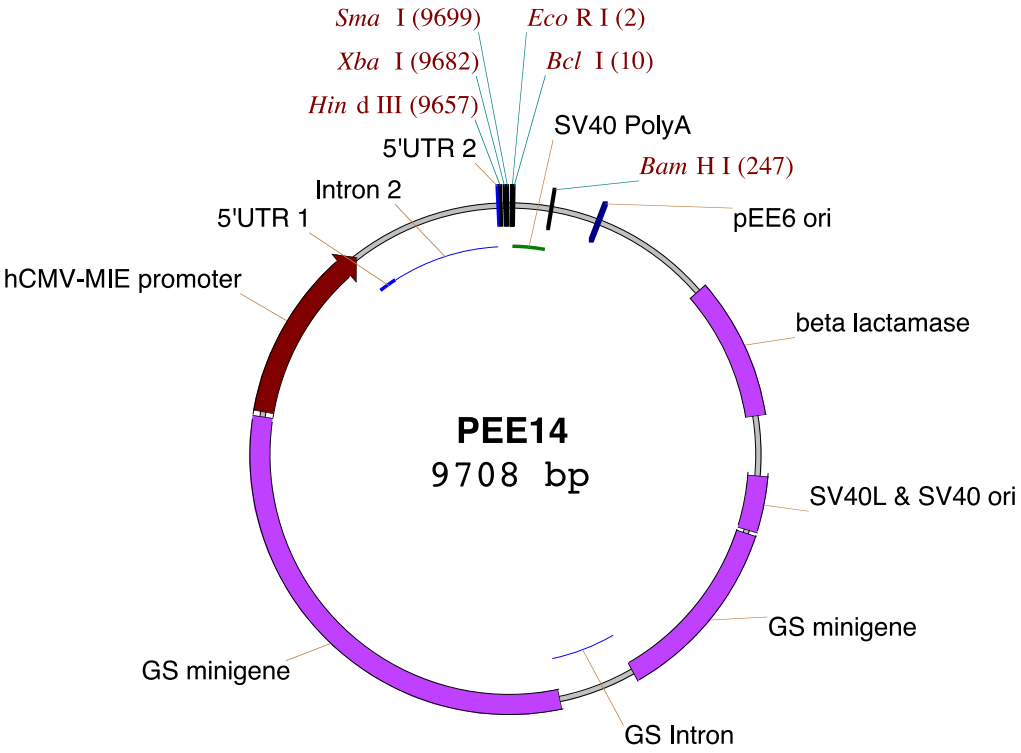


Figure 2.3: pEE14 vector map (Lonza Biologics) containing various critical restriction enzyme sites and glutamine synthetase (GS) minigene.

and incubated at room temperature for 20 minutes, it was next added to one of the CHO-K1 flasks. One ml of unsupplemented glutamine-free DMEM medium (Gibco) was added to the other CHO-K1 flask to used as a mock transfection control. 48 hours later, the cells were trypsinised and the supernatants were removed, the flasks were washed with 10 ml PBS. 5 mL 1x trypsin in PBS (from trypsin solution 10x, Sigma) was added to the cells and incubated at 37 ºC for 3 minutes. The cells were centrifuged at 1300 rpm in the Heraeus Megafuge. The transfected cells were plated out in nine 96-well flat bottom plates (Nunc), 100 µl/well at $1*10^5$ cells/ml in glutamine-free DMEM medium supplemented as described previously. The mock control cells were plated out in three 96-well plates (Nunc) as described. The seeding density was chosen so that ideally, the resultant wells would contain only one cell per well in order to separate single clones. These cells were cultured for a day at 37 ºC 5% CO_2.

II.M. Methionine sulfoxamine (MSX) Selection

The next day, MSX, the glutamine synthetase inhibitor, was added to the plates to select for transfected and highly expressing clones. Three different concentrations of MSX were utilized (30, 35 and 40 µM). The reasoning behind this is that the optimal concentration for the growth of transfected cells and prevention of growth of untransfected clones can somewhat vary, therefore having a range of different selective pressures could maximize the chance of getting more single high expression clones. For the transfected cells, three 96-well plates (Nunc) were applied at each MSX concentration; one plate was used per concentration for the mock control. 100 µl MSX in glutamine-free CHOK1 medium was added per well. Following cell culture for a week, 100 µl of supernatant was removed from each well and replaced with 100 µl fresh glutamine-free CHO-K1 medium containing one-half the original MSX concentration (*i.e.* 15, 17.5, 20 µM). These CHOK1 cells were cultured for a further three weeks. Screening of the wells was conducted to check for clones which had proliferated. Counts of positive wells were compared between MSX concentrations and between transfected cells and mock controls. Subsequently, a dot

blot was performed to screen for the protein production using the clones from the most suitable MSX concentration (*i.e.* making the greatest number of positive wells).

II.N. Dot blot for highly expressing clone identification

100 µl of supernatant from each well to be screened was transferred to a new flat bottom 96-well plate (Nunc). With the use of a grid, 5 µl of each was pipetted onto a nitrocellulose membrane. The membrane was blocked in 1 % skim milk in PBS overnight. Similar to the Western blot procedure, the membrane was probed with a horse radish peroxidase-coupled anti-mouse Fc secondary antibody (Sigma), 1/2000 in 1 % skim milk PBS. The membrane development was achieved using the Pierce ECL Western blotting substrate (Thermo Fisher Scientific) and exposed to an X-ray film. Strong signals on the dot blot indicated clones which gave strong protein expression. Typically, 4 clones were selected for further growth and characterisation. Wells corresponding to the selected clones were washed with PBS, treated with trypsin (50 µl 1x trypsin), then 100 µl glutamine-free CHOK1 medium with the respective MSX concentration were added to the wells, the cell suspensions were pipetted and transferred to 12-well plate (Nunc). They were then cultured in glutamine-free CHOK1 medium with the respective MSX concentration. Once confluent, these clones were trypsinised and transferred to a 6- well plate (Nunc). Once confluence was reached in the 6 well plate, the supernatants were used to check for protein expression *via* a Western blot. This enabled the confirmation that a protein of the correct size was secreted and helped to determine which clone expressed the highest levels of protein. For further sub-culturing, the cells were seeded into T25 Greiner flasks (Sigma).

II.O. Large-scale cell culture of the chosen clone for protein generation

The best expressing clone was expanded by culturing in the presence of MSX, trypsinising and seeding into a larger flask as above. Once the cells reached confluence in a T175 flask (Sigma), they were trypsinised and cells were harvested and froze down for long-term liquid nitrogen storage. A second T175 flask of the

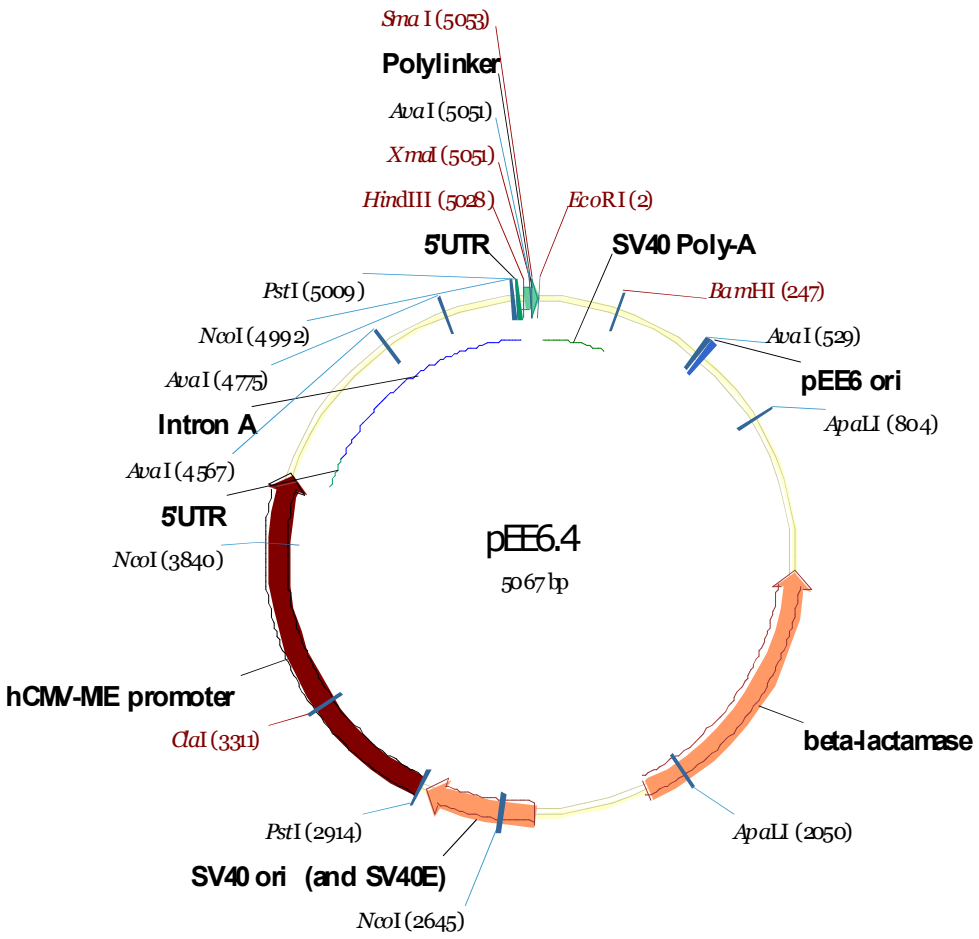


Figure 2.4: pEE6.4 vector map containing relevant restriction enzyme sites for cloning.

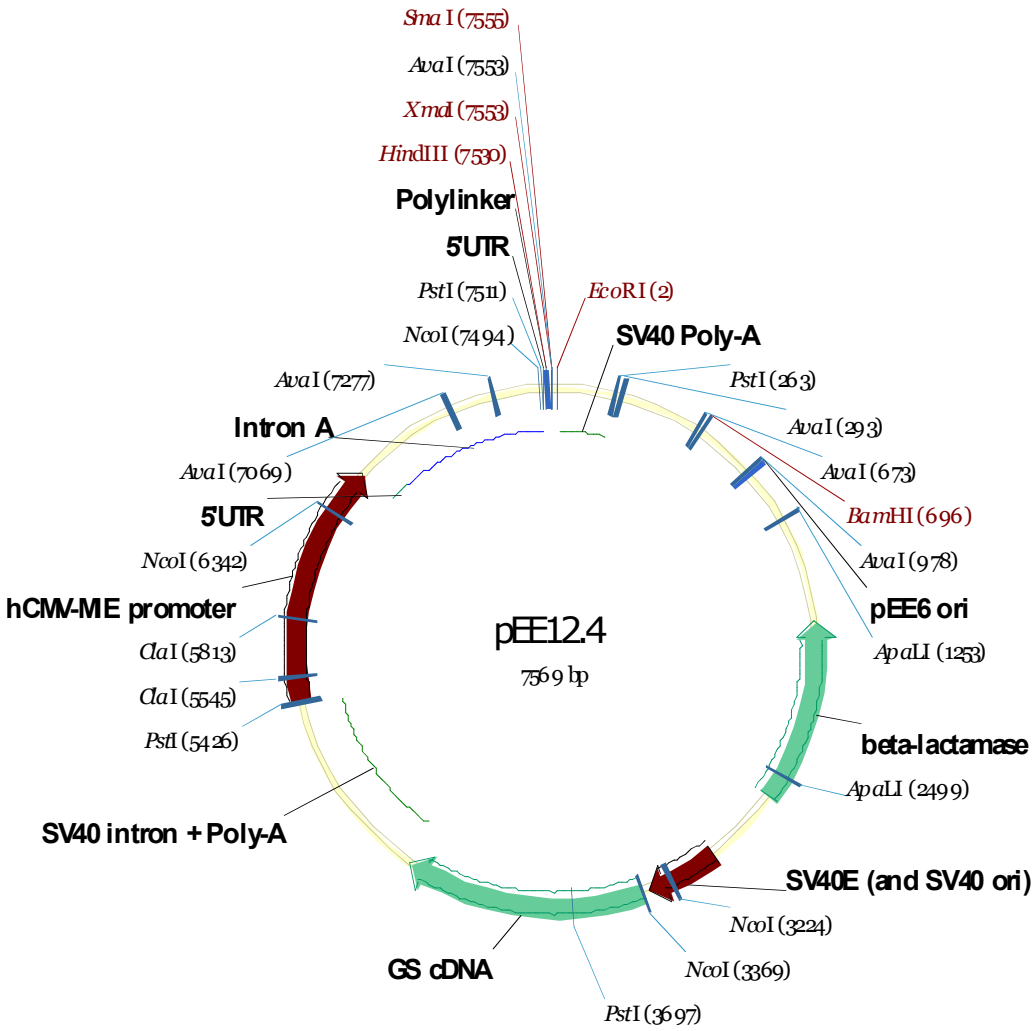


Figure 2.5: pEE12.4 vector map containing relevant restriction enzyme sites for cloning.

best clone was utilized for the inoculation of a Corning HYPER*Flask* cell culture vessel. The cells were finally trypsinised and transferred into cell factories (Nunc) for further culturing and protein production for approximately 3 weeks before harvesting and protein purification using protein G beads.

III. Protein techniques

III.A. Extraction of His tagged protein from tissue culture supernatant

Affinity chromatography was applied for the purification of Histidine-tagged proteins. This made use of the high affinity interaction between histidine residues and bivalent metal ions. 'Nickelated' Sepharaose beads helped with the capturing of secreted proteins *via* its His-tag. Imidazole which has a greater affinity for nickel was then applied to the beads to replace the His-tag, consequently this allowed the His tagged protein of interest to be released from the beads.

In order to remove cells and debris, the tissue culture supernatant (TCS) was centrifuged at 4000 rpm in the Heraeus Megafuge for 15 minutes at 4 ºC. In a large conical flask, the supernatant was diluted in an equal volume of PBS-sodium azide 0.05%, 0.5 M sodium chloride, pH 8.0. Two ml of nickel-charged resin (Ni-NTA agarose, QIAGEN), equilibrated with PBS, was added to the supernatant. The beads were left to slowly stir overnight at 4 ºC. Before the beads were reused each time, they were washed with 5 column volumes of 250 mM imidazole, 5 column volumes of MilliQ water, and 5 column volumes 100 mM EDTA pH 8.0. Recharging of the beads was conducted with 2 column volumes of 100 mM nickel sulphate and subsequently washed with 5 column volumes of MilliQ and then 5 column volumes of PBS for equilibration.

In order to harvest the resin, the diluted supernatant was centrifuged at 1000 rpm in the Heraeus Megafuge for 5 minutes at 4 ºC. The majority of the supernatant was siphoned into a flask and kept for further extractions if required. The remaining 500 ml which contained the resin beads was passed through a small column. This

allowed residual supernatant to flow through but it allowed the beads to be packed and retrained inside the column. Next, the column was washed with 20 ml of PBS. For removing unspecifically bound contaminant proteins, the captured protein was pre-eluted with 10 mM imidazole, pH 8.0. Usually, ten 1.5 ml fractions were collected and protein concentration was measured using spectrophotometry, determined by UV absorbance at 280 nm (Nanodrop, Thermo Fisher Scientific). If the last fraction still contained measurable amounts of protein, further fractions were collected to remove unwanted unspecific proteins. Elution with 250 mM imidazole, pH 8.0 was then applied for the purification of the His-tagged protein of interest. Normally, ten to fifteen 1 ml fractions were collected. Likewise, the protein concentrations were determined as above. Protein-containing fractions of from pre-elution and elution were separated on 12 % acrylamide gels. Gel filtration *via* FPLC was conducted to further purify these His- tagged proteins. PD-1FcHis pEE14 was expressed stably in CHOK1 cells using two cell factories and the proteins were purified using nickel nitrilotriacetic acid (NiNTA) beads as described above.

III.B. Extraction of antibodies from tissue culture supernatant using protein G

The stably transfected CHOK1 suspensions were centrifuged at 4000 rpm in the Heraeus Megafuge for 15 minutes at 4 °C. TCS was collected and diluted with 2 fold volume of PBS pH 7.4. 0.05% sodium azide was then added to prevent bacterial growth. The solution was either stored at 4 °C or subjected directly to protein G purification. Since 1 ml of protein G bead can bind approximately 20 g of human IgG, for the majority of the purification processes, 1 ml protein G beads (GE Healthcare) were utilized. Protein G beads were added to the beaker flasks containing the supernatant diluted with PBS and a magnetic stirrer was added to stir the beads overnight at 4 °C. The next day, the beaker was brought to room temperature and the beads were allowed to settle to the bottom of the flask for two hours. The top of the supernatant was siphoned off using tubing. The rest of the supernatant with beads were loaded into a washed column When packed, the column

was washed with 10 times column volume of cold PBS 0.5 M NaCl pH7.4. Using 0.1 M Glycine/HCl solution at pH 2.5, bound IgG antibodies were eluted into tubes containing enough 2.75 M Tris pH 8.5 needed to neutralize the pH. Approximately twelve 2 ml fractions were collected and their optical densities were measured at 280 nm. Immediately after fraction collections, the column was neutralized using PBS in order to prevent damage to the beads. 10 µl of each fraction from the elute which gave optical densities (ODs) of more than 0.1 mg/ml were run on both non reducing and reducing 12% acrylamide gels. The fractions containing antibody were then pooled and concentrated in Vivaspin concentration tubes (Sartorius) into approximately 500 µl. The final volume was adjusted therefore helping to keep the final antibody concentration below 20 mg/ml for subsequent gel filtration.

III.C. Protein purification by gel filtration

The pooled and concentrated fractions from protein G purification underwent another step of purification *via* gel filtration. This is a form of fast protein liquid chromatography (FPLC). Gel filtration Superdex 200 column (GE Life Sciences) was set up as outlined in the manual. The column was washed with two column volumes of HBS pH 7.4 prior to usage. The 500 µl loop was washed with HBS pH 7.4. The 500 µl pooled and concentrated antibody was then loaded into the loop. I ensured that the concentration of the antibody did not exceed 10 optical density (OD) in order to prevent impairment of the selection process. OD measurements of the peak fractions were quantified by absorbance at 280 nm using the Nanodrop 2000 machine (Thermo Scientific). 10 µl of each fraction were run on both non-reducing and reducing 12 % acrylamide gels. Fractions which possessed more than 0.1 mg/ml IgG were pooled, sterile filtered and subsequently stored in the -80 °C freezer.

III.D. Sodium dodecyl sulphate polyacrylamide gel electrophoresis (SDS-PAGE) for detecting the purity of antibodies

12 % acrylamide gels and stacking gels were prepared. Acrylamide gels were made with 25 % Tris/HCl pH 8.8/ SDS, 35 % dH_2O, 40 % acrylamide, 0.5 % freshly

prepared 10 % (w/v) ammonium persulphate and 0.2 % TEMED whilst stacking gels were made with 25 % Tris/HCl pH 6.8/ SDS, 62 % H_2O, 13 % acrylamide, 0.2 % TEMED and 0.5 % freshly prepared 10% (w/v) ammonium persulphate. Samples, markers and controls were mixed with 2x non reducing and reducing sample buffer. They were then heated to 90 °C for 5 minutes in the DNA Engine Tetrad cycler. They were then loaded onto the gels. The gels were run at 150 V until the bromphenol blue band reached the base of the glass plates. For the visualization of the bands, the gels were stained with Coomassie blue for 20 minutes and the excess stain was removed using de-staining solution along with soaking of the stain using a piece of clean tissue.

III.E. Western blotting

Western blots are highly sensitive at detecting protein expression and thus they implemented to check for the level of protein expression from both transient and stable transfections. Proteins were separated by 12 % SDS-PAGE under both non reducing and reducing conditions. They were then transferred to Hybond-C-extra membranes by electroblotting with ice-cold transfer buffer. The membranes were blocked in TBS, 0.1% (v/v) Tween 20 (TBS-T), containing 5% (w/v) BSA (Sigma). Primary antibody was incubated with the membranes for 1 hour on shaker and then washed with TBS- Tween. A second antibody, usually a HRP-conjugated goat anti-mouse or goat anti-rabbit IgG (Sigma) was then added to membranes and incubated for another hour. Membranes were washed thoroughly with TBS-Tween. The immunoblots were developed using ECL (Amersham Biosciences) and exposure was *via* CL-XPosure films (Pierce). An exposure time of usually 1-5 min was needed for the detection of antibodies.

III.F. Biotinylation of proteins

Cl19 Fabs proteins were concentrated to 500 µl and buffer exchanged with 10mM Tris-HCl pH8. 1/8 volume of Biomix A and 1/8 volume of Biomix B were added. This was topped up with 2 µl BirA (Sigma) at 1 mg/ml and subsequently, incubation

at 30 °C for 2 hours was performed. FPLC was used to remove ATP and purify the biotinylated protein.

IV. Surface Plasmon Resonance (SPR) using Biacore

Surface plasmon resonance as implemented in the Biacore™ T200 (GE Healthcare) was used for kinetic characterization of the interaction between anti-PD-1 antibodies and PD-1 monomer. The purity of the ligands and analyte were confirmed using SDS-PAGE and size exclusion chromatography. They were buffer-exchanged into HBS with 0.05% sodium azide during gel filtration so as to match the running buffer used in the Biacore. Prior to testing on the Biacore, they were centrifuged at 1100 rpm in the standard microfuge for 5 minutes at 4 °C for the removal of any aggregate. The analyte concentration was measured spectrophotometrically via absorbance at 280 nm and subsequently, a dilution series was prepared. Likewise, the samples for testing i.e. anti-PD-1 antibodies and Fabs were centrifuged for the prevention of any air bubbles. Experiments were performed at 37 °C in HBS-EP buffer (25 mM HEPES pH 7.4, 150 mM NaCl, 0.05% sodium azide, 3 mM EDTA, 0.005% v/v Surfactant P20). The matrix surface of the CM5 sensor chip was firstly activated through amine coupling with 75 mg/ml 1-Ethyl-3-(3-dimethylaminopropyl) carbodiimide hydrochloride and 11.5 mg/ml N-Hydroxysuccinimide (EDC/NHS) mixed in a 1:1 ratio (GE Healthcare), with an activation time of 6 min. Such amine coupling allowed the ligands to be directly immobilised onto the CM5 sensor chip. The ligands were diluted to 5 μg/ml in 10 mM sodium acetate pH 5.0 (GE Healthcare). To characterize the ligands: full-length anti-PD-1 antibodies (Cl10 and Cl19), IgG1 (serving as the negative control), the anti-PD-1 antibodies were injected in the appropriate flow cells at 10 μg/ml in 10 mM sodium acetate, pH 5.0, and directly immobilised onto the matrix surface, resulting in final immobilization levels of 800-1200 response units (RU). To achieve this, a small volume of ligand was injected in order to obtain a low level of ligand immobilization of approximately 100 RU. Inactivation of the chip followed using ethanol amine chloride for the prevention of unspecific analyte binding. Using a reference chamber on the chip, the

negative control ligand was immobilised so that a control sensorgram could be created to measure the background response. This was subtracted from the sample sensorgrams to create background-corrected sensorgrams.

To characterize the anti-PD-1 Cl19 antibody Fab mutants (FoR1 and FoR2), the same technique of amine coupling using CM5 chip described above was used in addition to the usage of the Biotin CAPture chip. To do so, 0.25 mg/ml streptavidin (Sigma) in 10 mM sodium acetate, pH 5.0, was firstly injected over the flow cells to achieve an immobilization level of approximately 4000 RU. The biotinylated Fab mutants were then indirectly immobilised in Fc_2 or Fc_4 (Fc_1 or Fc_3 was left blank as negative control) through being injected at 10 μg/ml, resulting in immobilization levels of 300-400 RU. The matrix surface of the sensor chip was inactivated by an injection of 1.0 M ethanolamine-HCl pH 8.5 for 5 min. Soluble and monomeric human PD-1 was injected into the appropriate flow cells (Fc_1 and 2 or Fc_3 and 4) using serial dilutions from 0.28 mg/ml. In case of fast kinetics (complete dissociation occurs within 30 s), each injection was of 80 s duration at a buffer flow-rate of 20 μl/min.

In case of slow kinetics, each injection was of 30 s duration at a buffer flow-rate of 30 μl/min, followed by a dissociation period of 60 s. In order to regenerate the sensor chip surface, an injection of Glycine-HCl pH 2.5 for 30 s was performed between each cycle. In case of fast kinetics, the binding data was analysed using the curve fitting tools of Prism 6 (GraphPad Software) in order to derive the affinities and dissociation rates. The association rates were then calculated using these determined parameters. In case of slow kinetics, the binding data were fitted with the multi-cycle kinetics model using Biacore T200 evaluation software (GE Healthcare) in order to directly derive kinetic parameters.

V. Flow cytometry

Flow cytometry was utilized to assess expression levels of different cell surface

proteins. This analysis provided useful information on single cells as well as statistical information across large groups of cells. Essentially, the flow cytometer generates a current of cells which pass through the analyzer one at a time. The fluorescence of each cell is recorded. Cells can show fluorescence either because they were transfected with a fusion protein with a fluorescent protein, or it could be due to the fact that they were stained with fluorophore coupled-antibodies against a surface receptor. In the first case, general expression in the cytoplasm as well as at the cell surface is measured, whilst the latter scenario only focuses on expression at the cell membrane. Since fluorescence can be detected in multiple channels simultaneously, two or more different receptors were able to be stained in varying colours in one experiment.

Cultured cells were transferred from flat bottomed 96 well plates to round bottom 96 well plates. The plates were then centrifuged at 2000 rpm in the Heraeus Megafuge for 2 min. The supernatant was subsequently discarded. 150 µl of PBS-sodium azide 0.05% was added to the cells and centrifuged at 2000 rpm in the Heraeus Megafuge for 3 min. The supernatant was discarded. The staining cocktail of desired fluorochromes containing various monoclonal antibodies specific for the receptors of interest, were added at 20 µl per well. Staining was performed for 25 min in the dark at 4 ºC. 180 µl of PBS-sodium azide 0.05% was added to the wells for washing; the cells were centrifuged at 2000 rpm in the Heraeus Megafuge for 3 min and supernatant was discarded. Finally, 180 µl of PBS-sodium azide 0.05% was added to the cells and flow cytometry was conducted. Stained cells were analyzed on a BD FACSCanto flow cytometer. Compensation was applied when more than one channel was analyzed simultaneously. This helped to correct for bleed-through between the channels. The FlowJo software was used for data analysis.

VI. Mouse Model: humanized PD-1 knock-in (hPD-1 k.i.) mice

The *in vivo* experiments conducted used humanized PD-1 knock-in mice which expressed human PD-1 extracellular and mouse PD-1 transmembrane and

intracellular domains. These mice were made by implementing a constitutive knock-in strategy.

VII. Cell purification: ficoll stratification of mouse splenocytes

hPD-1 k.i. mouse spleens are crushed in petri dish with the tips of a syringe. The cells were then spun at 1200 rpm in the Heraeus Megafuge for 7 min. Supernatant was removed and 10 ml RPMI (Sigma) media was added. Cells were then spun again at 1200 rpm in the Heraeus Megafuge for 7 min and TCS was removed. The pellet was resuspended in 10 ml of RPMI media. Next, 5 ml of ficoll (Sigma) was added and the cells were centrifuged at 2000 rpm in the Heraeus Megafuge for 25 min. A 4 ml layer of splenocytes was harvested and topped up with 10 ml RPMI media and spun at 1500 rpm in the Heraeus Megafuge for 15 min. Supernatant was removed, 10 ml RPMI media was added and cells were centrifuged in the Heraeus Megafuge for another 10 min at 1200 rpm. TCS was removed and 10 ml of RPMI media was added. The cells were then counted using a haemocytometer and Trypan blue exclusion.

VIII. *In vitro* assays

VIII.A. CFSE cell proliferation assay

hPD-1 k.i. mouse splenocytes were separated using ficoll accordingly. These cells were then washed with D-PBS 0.1 % FCS. CFSE was diluted in D-PBS to 2.5 μM and then 2 ml of this mixture was added to the cells and incubated at room temperature for 8 min covered in foil. 2 ml of RPMI media was added and cells were centrifuged at 1200 rpm in the Heraeus Megafuge for 5 min. A further two more rounds of washes with RPMI media was performed. The cells were then resuspended in the appropriately supplemented RPMI media and left in the incubator to recover for 30 min. They were then plated out, stimulated with anti-CD3 (0.5 μg/ml) and anti-CD28 (2 μg/ml) antibodies and then incubated with anti-PD-1 antibodies (30 μg/ml) for 72 h and subsequent flow cytometry was conducted to check for inhibitory effects on cell proliferation.

VIII.B. Sheep red blood cell specific enzyme-linked immunosorbent assays (ELISAs)

ELISA is a highly specific and sensitive quantitative tool which can used for the detection of the presence of a soluble substance *via* the application of specific antibodies. The read-out is provided with a colour reaction. In a sandwich ELISA, an antibody specific to the substance of interest is immobilised on a surface prior to sample application. A second antibody specific to the substance of interest is then added, this is coupled to an enzyme which causes the catalysis of a colour change once the substrate is applied.

Sheep red blood cells (SRBCs) were washed and resuspended with PBS at $5x10^7$ cells/ml. ELISA plates were coated by adding 100 µl of this SRBC suspension to each well. The plates were incubated overnight at 4 °C. The next day, 20 µl 1.8% glutaraldehyde solution (Sigma) was added to each well to fix the SRBCs. The plates were then incubated at room temperature for 30 min and then were washed with PBS for five times. This was followed by blocking with 1% skimmed milk in PBS for 1.5 hours at 37 °C. All the mouse samples were diluted in PBS. The dilutions were as follows: 1/16-1/64-1/256-1/1024-1/16384. After washing, the diluted mouse sera were added to the wells and incubated for 1.5 hours at 37 °C. The plates were washed again and alkaline phosphatase (ALP) conjugated goat anti-mouse IgM (1/30000, Sigma) or goat anti-mouse IgG (1/1000, Sigma) was added to the wells and incubated for 1 hour at 37 °C. Following the final wash, ALP substrate was dissolved in p-nitrophenyl phosphate (p-NPP) buffer at 2 mg/ml and added to the wells for a further room temperature incubation for 1 hour. The plates were read with a Biorad plate reader at 405 nm. A pool of serum from mice that were injected with SRBCs was used as the standard. An internal standard, set at 1000 arbitrary units (AU) was used. The levels of IgM and IgG relative to the standard were calculated. In contrast, serum from naive mice was applied as the negative control. All the samples, standard and negative control were serially diluted starting from 1/16.

VIII.C. Anti-mouse IL-2, TNF-α, IFN-γ ELISAs

The TCS of hPD-1 k.i. cells that were stimulated with anti-CD3 antibody, anti-CD28 antibody and various anti-PD-1 antibodies were collected after 48-72 h incubation. Several cytokine based ELISAs including anti-mouse IL-2, TNF-α, IFN-γ (eBioscience) were performed to test for suppressive effects of the anti-PD-1 antibodies.

Costar flat-bottom 96-well EIA-RIA ELISA plates were coated with 25 µl capture antibody in Coating Buffer (for 2 half-area plates, 24 µl detection antibody mixed with 6 ml 1x Assay Diluent). The plates were sealed and incubated overnight at 4 °C. The next day, wells were aspirated wells and washed 3 times with Wash Buffer (PBS 0.05% Tween-20). Allowing time for soaking (~1 min) during each wash step increases the effectiveness of the washes. The plates were blotted onto absorbent paper to remove any residual buffer. 5x Assay Diluent was diluted to 1x with deionized water (40 ml total for 2 half-area plates). The plates were then blocked with 50 µl 1x Assay Diluent in each well, sealed with cling film and incubated at room temperature for 1 hour. Following this, aspirate of the wells and 3 rounds of washing with the Wash Buffer was performed. 25 µl of the TCS was applied into each sample well. The standard was diluted and added in the plate (in duplicate). Four wells were left which we used as blanks by only adding 25 µl Assay Diluent to the plate. After adding the samples and standard, the plates were incubated at room temperature for 2 hours. They were then aspirated and washed 5 times with Wash Buffer. For detection, 25 µl of detection antibody was diluted in 1x Assay Diluent per well and added to the plates. Incubation at room temperature for 1 hour ensued and aspiration and another 5 rounds of plate washing with Wash Buffer was conducted. Finally, 25 µl Avidin-HRP diluted in 1X Assay Diluent per well were added to the plates and incubated at room temperature for 30 minutes. The wells were aspirated and washed 7 times with Wash Buffer. 25 µl of substrate solution per well was added and the plates were incubated at room temperature for 15 min. 12.5

µl H_2SO_4 (1 M) per well was added to stop the reaction. The plates were read at 450 nm and 570 nm on the ELISA plate reader. The values of 570 nm from those of 450 nm were subtracted.

VIII.D. NP5-BSA and NP25-BSA ELISAs

NP5-BSA or NP25-BSA were diluted to a final concentration of 5 µg/ml in bicarbonate buffer. A total of 2.5 ml diluted NP-BSA was needed for each 96 well flat bottom plate. 25 µl of diluted NP-BSA was pipetted into each well. The plates were incubated at room temperature for 2 hours or at 4 °C overnight. Plates were washed with PBS, 100 µl per well. Repeat wash 2 more times for a total of 3 washes. The plates were then blocked. For each plate, a preparation containing 5 ml of 5% milk in PBS (2.5 g dehydrated fat-free milk per 50 ml PBS) was made. 50 µl of 5% milk PBS were pipetted per well. The plates were then wrapped in Saran wrap and incubated at 37 °C for 2 hours. During the blocking step, serum dilutions were prepared. Day 7 – 1/75, day 14 – 1/300, day 28 – 1/1000, day 42 – 1/10000. Mouse serum were diluted in Eppendorf tubes; thawed serum was vortexed and 1 µl of serum per Eppendorf tube containing the appropriate volume of 1% milk were pipetted. The dilutions for the standards were also prepared in Eppendorf tubes. The samples, blanks and standards were transferred to a 96-well ELISA plates. 25 µl of each serum sample (in 1% milk) were added per well. The plates were incubated at 37 °C for exactly 1 hour and then washed with PBS supplemented with 0.05 % Tween-20. The wash was repeated 5 more times for a total of 6 washes. Secondary antibody was added by diluting AP (alkaline phosphatase)-conjugated goat anti-mouse IgG1 1:2000 in 1 % milk. A total of 2.5 ml of diluted anti-IgG was needed for each plate. 25 µl of diluted anti-IgG per well was added for each plate. The plates were wrapped in Saran film and incubated at 37 °C for 1 hour. The plates were washed with PBS 0.05% Tween-20 a total of 6 repeats. Finally, the plates were developed. The substrate was prepared by adding 1 tablet of phosphatase substrate per 5 ml p-NPP buffer. 80 µl of the prepared substrate was added per well. This was

followed by incubation at room temperature, in the dark, for approximately 10 min. The absorbance at 405 nm was read on the ELISA plate reader.

Chapter 3
PD-1 and Cl19 Fab production for binding analysis

I. Introduction

To start with, we established methods for producing PD-1 and Cl19 Fab in order to probe their interaction. This was intended to form the basis for generating mutated Cl19 Fabs, with altered binding kinetics. The goal was to then produce and test such second generation Cl19 whole antibodies with faster off-rates and lower binding affinity to PD-1. The expectation was that the new antibodies could hold the potential to enhance agonistic antibody triggering against PD-1, allowing for greater immune suppression through reduced PD-1 receptor downregulation.

Recombinant protein expression was utilised to prepare PD-1FcHis and Cl19 Fab. This required the cloning of the genes of interest into an expression vector and then protein production in a heterologous expression system. There is a broad range of expression systems available for the production of proteins. Chinese hamster ovary (CHO) cells produce high yields and high quality recombinant proteins which are widely used in structural and functional studies, as well as for the industrial production of, e.g., cytokines and therapeutic antibodies [347]. The glutamine synthetase (GS)-based protein expression system, which has been extensively used in our laboratory for more than 20 years, was developed by Lonza Biologics. This relies on a robust viral promoter and selection *via* glutamine metabolism, which leads to high-yielding and stable cell lines derived from CHO cells. The GS system uses the plasmid vector pEE14, which encodes a GS mini-gene and carries the gene of interest. Transfected cells are subsequently selected in the presence of graded amounts of the competitive GS inhibitor methionine sulphoximine (MSX). As a consequence, the isolation of cells possessing notably high plasmid copy numbers (>

2000/cell) can be produced [348].

In this chapter, PD-1FcHis was produced and subsequently cleaved to produce soluble PD-1 for Biacore analysis of the interaction of the extracellular region of PD-1 with Cl19 antibody and derivatives thereof with faster kinetics. In addition, Cl19 Fab constructs were generated and tested for expression transiently, as a prelude to detailed mutational analysis of the interaction, and also for complexing with soluble PD-1 for possible structural (*i.e.* crystallographic) work.

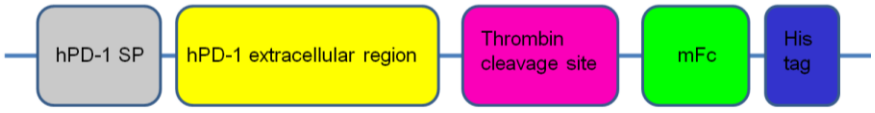
II. Results

II.A. PD-1FcHis expression and purification

Initially, DNA sequence encoding the human PD-1 signal peptide and extracellular region, fused with sequence encoding a thrombin cleavage-site (Leu-Val-Pro-Arg-Gly-Ser), mouse IgG1 Fc and a His tag (giving PD-1FcHis), was cloned into the pEE14 vector (Figure 3.1). Thrombin is able to recognise the consensus LVPRGS sequence, cleaving the peptide bond between Arg and Gly. A Kozak sequence was also added as it can act as an enhancer for translation. This construct was subsequently expressed stably in the Chinese hamster ovary (CHO) cells in a large-scale (2 litres) culture, following which protein purification was performed *via* affinity chromatography using nickel nitrilotriacetic acid (Ni-NTA) beads which bound to the histidine tag. Further purification of the 10 mM- and 250 mM imidazole-eluted fractions was undertaken *via* gel filtration/size exclusion chromatography using an AKTA fast protein liquid chromatography (FPLC) system fitted with a Superdex 200 column. The preparations from the affinity chromatography stage and from further purification using the FPLC were run on SDS-PAGE gels to analyse the size and purity of the soluble proteins.

The SDS-PAGE gel of the purified FPLC elutions of PD-1FcHis, indicated that the protein was relatively clean, running at 66 kDa under non-reducing conditions. The top band observed in the SDS-PAGE gel was most likely due to an electrophoresis

a



b

SmaI Kozak START hPD-1 signal peptide hPD-1 extracellular region Thrombin cleavage site mFc 6xHistidine tag STOP BamHI

```
TAG TAG CCC GGG CTC AAG CAG GCC ACC atg cag atc cca cag gcg ccc tgg cca gtc gtc
*   *   P   G   L   K   Q   A   T   M   Q   I   P   Q   A   P   W   P   V   V
tgg gcg gtg cta caa ctg ggc tgg cgg cca gga tgg ttc tta gac tcc cca gac agg ccc
W   A   V   L   Q   L   G   W   R   P   G   W   F   L   D   S   P   D   R   P
tgg aac ccc ccc acc ttc tcc cca gcc ctg ctc gtg gtg acc gaa ggg gac aac gcc acc
W   N   P   P   T   F   S   P   A   L   L   V   V   T   E   G   D   N   A   T
ttc acc tgc agc ttc tcc aac aca tcg gag agc ttc gtg cta aac tgg tac cgc atg agc
F   T   C   S   F   S   N   T   S   E   S   F   V   L   N   W   Y   R   M   S
ccc agc aac cag acg gac aag ctg gcc gcc ttc ccc gag gac cgc agc cag ccc ggc cag
P   S   N   Q   T   D   K   L   A   A   F   P   E   D   R   S   Q   P   G   Q
gac tgc cgc ttc cgt gtc aca caa ctg ccc aac ggg cgt gac ttc cac atg agc gtg gtc
D   C   R   F   R   V   T   Q   L   P   N   G   R   D   F   H   M   S   V   V
agg gcc cgg cgc aat gac agc ggc acc tac ctc tgt ggg gcc atc tcc ctg gcc ccc aag
R   A   R   R   N   D   S   G   T   Y   L   C   G   A   I   S   L   A   P   K
gcg cag atc aaa gag agc ctg cgg gca gag ctc agg gtg aca gag aga agg gca gaa gtg
A   Q   I   K   E   S   L   R   A   E   L   R   V   T   E   R   R   A   E   V
ccc aca gcc cac ccc agc ccc tca ccc agg cca gcc ggc cag ttc caa ctg gta ccc cgg
P   T   A   H   P   S   P   S   P   R   P   A   G   Q   F   Q   L   V   P   R
ggt agt gga tca aag cct agc ata agt aca gtc cca gaa gta tca tct gtc ttc atc ttc
G   S   G   S   K   P   S   I   S   T   V   P   E   V   S   S   V   F   I   F
ccc cca aag ccc aag gat gtg ctc acc att act ctg act cct aag gtc acg tgt gtt gtg
P   P   K   P   K   D   V   L   T   I   T   L   T   P   K   V   T   C   V   V
gta gac atc agc aag gat gat ccc gag gtc cag ttc agc tgg ttt gta gat gat gtg gag
V   D   I   S   K   D   D   P   E   V   Q   F   S   W   F   V   D   D   V   E
gtg cac aca gct cag acg caa ccc cgg gag gag cag ttc aac agc act ttc cgc tca gtc
V   H   T   A   Q   T   Q   P   R   E   E   Q   F   N   S   T   F   R   S   V
agt gaa ctt ccc atc atg cac cag gac tgg ctc aat ggc aag gag ttc aaa tgc agg gtc
S   E   L   P   I   M   H   Q   D   W   L   N   G   K   E   F   K   C   R   V
aac agt gca gct ttc cct gcc ccc atc gag aaa acc atc tcc aaa acc aaa ggc aga ccg
N   S   A   A   F   P   A   P   I   E   K   T   I   S   K   T   K   G   R   P
aag gct cca cag gtg tac acc att cca cct ccc aag gag cag atg gcc aag gat aaa gtc
K   A   P   Q   V   Y   T   I   P   P   P   K   E   Q   M   A   K   D   K   V
agt ctg acc tgc atg ata aca gac ttc ttc cct gaa gac att act gtg gag tgg cag tgg
S   L   T   C   M   I   T   D   F   F   P   E   D   I   T   V   E   W   Q   W
aat ggg cag cca gcg gag aac tac aag aac act cag ccc atc atg gac aca gat ggc tct
N   G   Q   P   A   E   N   Y   K   N   T   Q   P   I   M   D   T   D   G   S
tac ttc gtc tac agc aag ctc aat gtg cag aag agc aac tgg gag gca gga aat act ttc
Y   F   V   Y   S   K   L   N   V   Q   K   S   N   W   E   A   G   N   T   F
acc tgc tct gtg tta cat gag ggc ctg cac aac cac cat act gag aag agc ctc tcc cac
T   C   S   V   L   H   E   G   L   H   N   H   H   T   E   K   S   L   S   H
tct cct ggt aaa CAT CAC CAT CAC CAT CAC TAA GGA TCC
S   P   G   K   H   H   H   H   H   H   *   G   S
```

Figure 3.1: Human PD-1 mouse Fc His construct. (**a**) Schematic diagram of hPD-1mFcHis construct (**b**) Sequence of hPD-1mFcHis construct.

artefact (Figure 3.2a), perhaps arising from transient disulphide bonding and dimer formation as the protein begins to unfold in the denaturant detergent. The dimers were evidently not present prior to denaturation because there was no hint of size separation of the two forms of protein on the FPLC column itself (the ratio of the two bands does not vary across the fractions). The presence of disulphide bonds in the folded protein was evidenced by the reduction in the size of the dominant monomeric band (~50 kDa) in reducing conditions (Figure 3.2b). Some small amount of contaminating protein was noted as smaller fragments separable under reducing conditions. In total, approximately 20 mg of hPD-1FcHis was purified from the two-litre culture.

II.B. PD-1FcHis cleavage and deglycosylation

Thrombin cleavage of 10 mg of purified PD-1FcHis and subsequent deglycosylation using endoglycosidase H (Endo H) were used to generate ~2 mg of PD-1 protein suitable for eventual structural studies (Figure 3.3). Thrombin is a trypsin-like member of the chymotrypsin family of serine proteases [349]. The thrombin cleavage site (Leu-Val-Pro-Arg-Gly-Ser) had been included in the linker region of the PD-1FcHis fusion protein construct to allow release of the PD-1 portion. Following histidine tag-based Ni-NTA protein purification, thrombin was utilised to selectively cleave between the arginine and glycine residues of the cleavage site. This efficiently removed the FcHis tag from hPD-1FcHis with a high degree of specificity. Endo H is a recombinant glycosidase cloned from *Streptomyces plicatus* that is overexpressed in *E. coli*. It is able to cleave the chitobiose core of oligo-mannose oligosaccharides in addition to some hybrid oligosaccharides from N-glycosylated glycoproteins. Following enzymatic deglycosylation, the protein was passed through a lectin column comprised of equal parts of lentil lectin, concanavalin A and wheat germ agglutinin to remove non-deglycosylated material. α-D mannose elution from the lectin column was then used to recover the remaining glycosylated hPD-1 for reuse (~20 kDa non-reducing; Figure 3.3a).

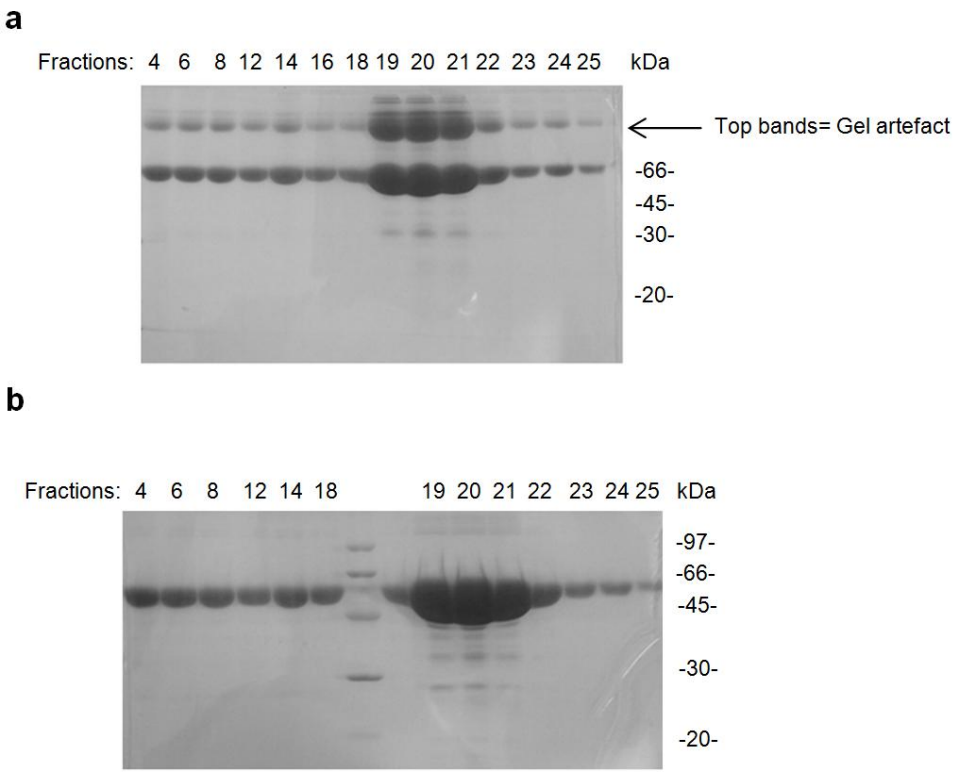


Figure 3.2: SDS-PAGE of FPLC fractions of purified and soluble PD-1FcHis protein (from stably transfected CHOK1 cells). Samples were separated on a 12 % acrylamide gel. 10 µl of each FPLC elution fraction was loaded, under either (**a**) non-reducing or (**b**) reducing conditions.

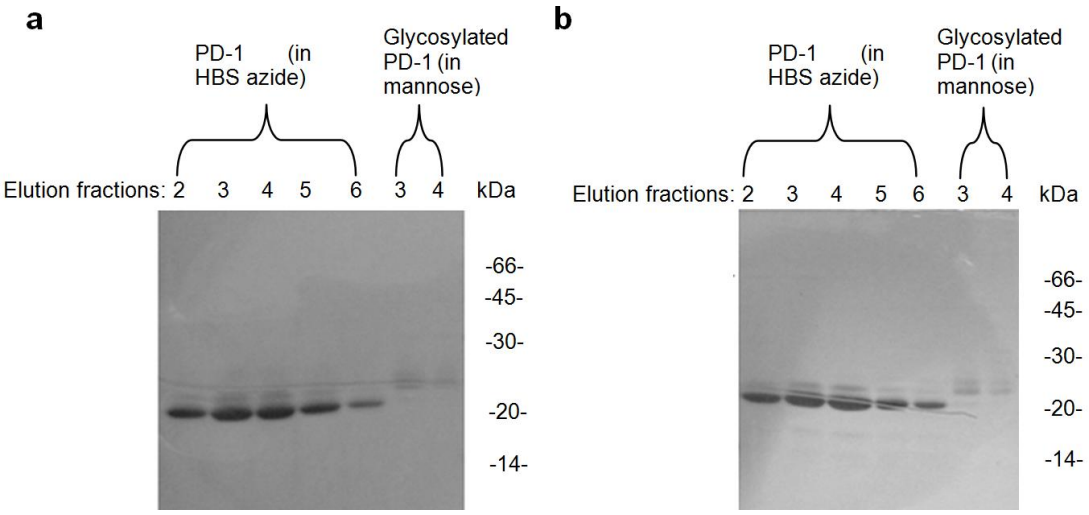


Figure 3.3: SDS-PAGE of FPLC fractions of thrombin cleaved PD-1FcHis. 10 mg of PD-1FcHis thrombin was cleaved to remove FcHis and deglycosylated using Endo H. PD-1 was eluted in HBS with 0.05% sodium azide from a lectin column. Remaining glycosylated PD-1 was eluted with α-D-mannose. Samples were separated on a 12 % acrylamide gel. 10 µl of each elution fraction was loaded, under either (**a**) non-reducing or (**b**) reducing conditions.

II.C. Anti-PD-1 Cl19 Fab transient expression and purification

The variable segments of Cl19 light chain and Cl19 heavy chain were cloned into vectors that already contained Fab constant regions: *i.e.* the pOPINVL and pOPINVH vectors, respectively. A histidine tag was attached to the heavy chain sequence to facilitate purification. The Cl19 light chain Fab pOPINVL and Cl19 heavy chain Fab pOPINVH vectors were then co-transfected into 293T cells at 1:1, 1:2 and 2:1 (μg) ratios of light to heavy chain constructs. 293T cells are adherent cells, a variant of transformed human embryonic kidney cells (HEK). These cells are an attractive heterologous system for glycoprotein expression because they have post-translational modification machineries needed for the optimal biological activity and proper folding of target proteins. Furthermore, they can produce good protein yields [350].

The Cl19 Fab expressed well in small-scale, trial transfections. The Western blot indicated that a 1:1 ratio of light to heavy chain Fab vector constructs gave the highest overall protein expression; thus for future Fab expression, a 1:1 ratio was used. The Fab ran at ~45 kDa on the non-reducing blot and ~26 kDa in reducing conditions (Figure 3.4). Following this, Cl19 Fab expression was scaled-up into 40 x T175 flasks (1.6 litre in total) of transiently transfected 293T cells. The Fab was purified using Ni-NTA beads and FPLC. For the large-scale transfections, for economic reasons, DNA was introduced into the host cells *via* polyethylenimine (PEI) transfection. PEI is a stable cationic polymer which condenses DNA into positively charged particles that bind to anionic cell surfaces; subsequently, the DNA:PEI complex undergoes endocytosis and the DNA is released into the cytoplasm [351].

In accordance with previous small-scale expression tests, following large-scale transfections, the purified anti-PD-1 Cl19 Fab ran similarly at ~45 kDa (non-reducing) and ~27 kDa on SDS-PAGE gels respectively (Figure 3.5 & 3.6). The total amount of Fab purified from the large-scale cultures of transiently transfected 293T

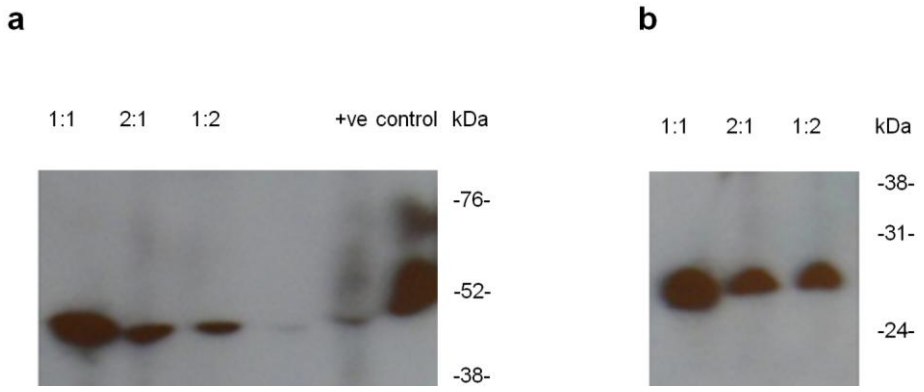


Figure 3.4: Western blot confirms expression of anti-PD-1 Cl19 Fab. Tissue culture supernatant (TCS) containing Cl19 Fab from 293T cells co-transfected with 1:1, 1:2, 2:1 (μg) ratios of light chain Fab to heavy chain Fab constructs was used for blotting. Heavy chain Fab contains histidine tag used for detection. Positive control used was CD5His protein (5 mg/L). Samples were separated on a 12 % acrylamide gel. 7.5 μl of TCS was loaded, under either (**a**) non-reducing or (**b**) reducing conditions. The proteins were transferred onto a nitrocellulose membrane and probed with an anti-penta-His antibody (Qiagen) and then an HRP-conjugated anti-mouse Fc antibody (Sigma-Aldrich). Incubation with Pierce ECL Western blotting substrate ensued and final detection was *via* luminescence on an x-ray film.

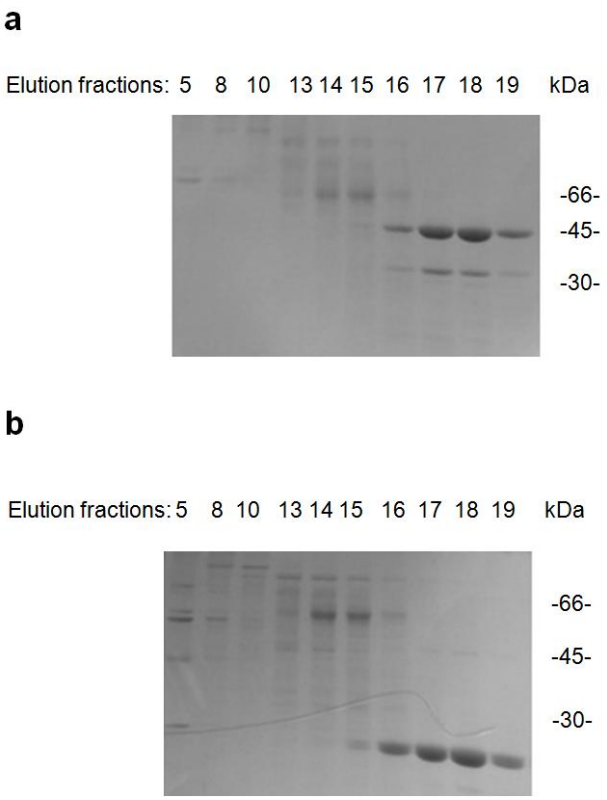


Figure 3.5: SDS-PAGE of purified and soluble FPLC size exclusion fractions of Cl19 Fab protein eluted from Ni-NTA beads using 10 mM imidazole (from transiently transfected 293T cells). Samples were separated on a 12 % acrylamide gel. 10 µl of each FPLC elution fraction was loaded, under either (**a**) non-reducing or (**b**) reducing conditions.

.



Figure 3.6: SDS-PAGE of purified and soluble FPLC fractions of Cl19 Fab protein eluted from Ni-NTA beads using 250 mM imidazole (from transiently transfected 293T cells). Samples were separated on a 12 % acrylamide gel. 10 µl of each FPLC elution fraction was loaded, under either (**a**) non-reducing or (**b**) reducing conditions.

cells was ~0.7 mg.

II.D. Test for PD-1FcHis and Cl19 Fab complex formation and binding using FPLC

To undertake a simple test of whether the purified Cl19 Fab and the PD-1FcHis were correctly folded and could bind to one another, the purified Cl19 Fab (from large scale transient expression in 293T cells) was mixed with uncleaved PD-1FcHis at a 1:5 ratio (molar concentration) and loaded into the S200 column of an Akta FPLC system (Figure 3.7). Separate FPLC runs with only anti-PD-1 Fab or PD-1FcHis only were also performed (Figure 3.7). A slight shift to the left was seen for the PD-1FcHis peak in the chromatogram when PD-1FcHis was mixed with the Cl19 Fab compared to just the PD-1FcHis only FPLC run (Figure 3.7). This was assumed to be due to the increase in mass of the bound complex. Also, a decrease in the Fab peak on the PD1FcHis and Fab chromatogram was seen as compared to just the Fab FPLC peak on its own. Together, these chromatograms suggested that PD-1FcHis was able to bind Cl19 Fab and form a stable complex.

II.E. Stable expression and purification of Cl19 Fab

Following successful expression in 293T cells and having been satisfied that the protein was well-folded and active, the Cl19 Fab pOPINVH and Cl19 Fab pOPINVL constructs along with pEE14 (to allow for selection) were stably co-expressed in large-scale (4 litre) cultures of CHOK1 cells using the GS based gene expression system. Large amounts of Fab were produced in case structural analysis of the PD-1/Fab complex was needed to guide mutation of the Fab. Approximately 50 mg of Cl19 Fab protein was purified *via* Ni-NTA affinity chromatography and gel filtration (Figures 3.8 & 3.9). Somewhat surprisingly, the Fab purified from 10 mM imidazole Ni-NTA column elutions gave very clean FPLC fractions, with only a single band of correctly folded protein at ~45 kDa (non-reducing; Figure 3.8), whereas the Fab FPLC fractions from 250 mM imidazole elutions gave strong bands at ~45 kDa but also several other smaller bands of ~30 kDa (Figure 3.9). These

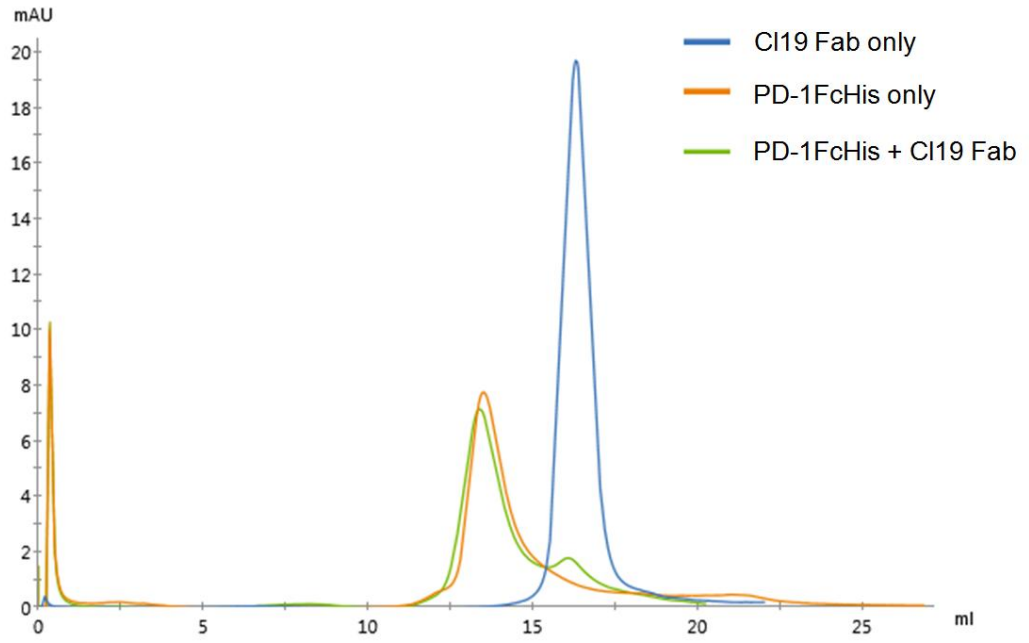


Figure 3.7: Chromatogram of FPLC (gel filtration) runs of various mixtures (all at 0.15 mg/ml): anti-PD-1 Cl19 Fab only (blue), PD-1FcHis only (orange), PD1-FcHis and anti-PD1 Cl19 Fab complex (5:1) (green). Anti-PD1: Cl19 Fab bound complex gives a peak that shifts to the left (increase in mass, thus elutes earlier in column) compared to PD-1FcHis alone.

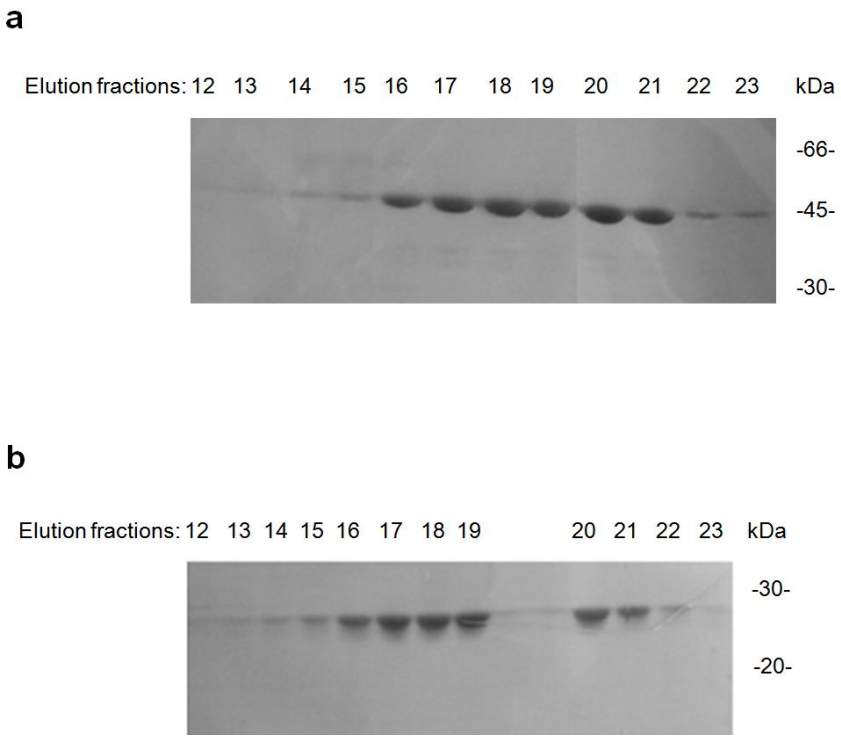
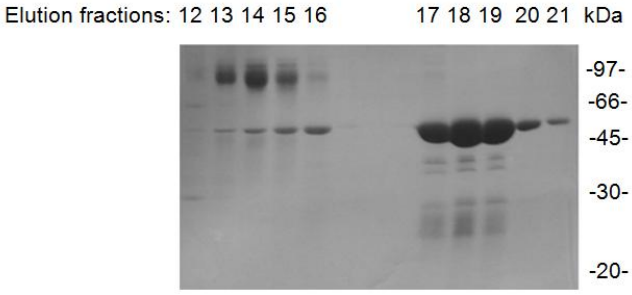


Figure 3.8: SDS-PAGE of purified and soluble FPLC fractions of Cl19 Fab protein eluted from Ni-NTA beads using 10 mM imidazole (from stably transfected CHOK1). Samples were separated on a 12 % acrylamide gel. 10 µl of each FPLC elution fraction was loaded, under either (**a**) non-reducing or (**b**) reducing conditions.

a



b

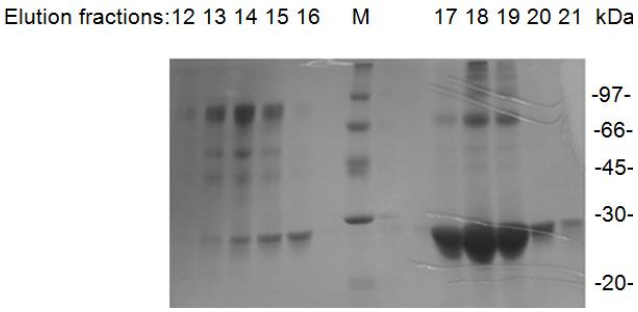


Figure 3.9: SDS-PAGE of purified and soluble FPLC fractions of Cl19 Fab protein eluted from Ni-NTA beads using 250 mM imidazole (from stably transfected CHOK1). Samples were separated on a 12 % acrylamide gel. 10 µl of each FPLC elution fraction was loaded, under either (**a**) non-reducing or (**b**) reducing conditions.

lower bands could conceivably be fragmented Fabs but were estimated to comprise < 10 % of the protein. The level of protein expression overall was extremely high (> 25 mg/L).

II.F. Analysis of the kinetics of binding of PD-1 to Cl19 Fab using a surface plasmon resonance-based assay

Kinetic analysis of the binding of PD-1 to Cl19 Fab was performed to further confirm that the Cl19 Fab was well folded and could interact properly with the receptor using the Biacore (GE Healthcare), which is based on surface plasmon resonance (SPR). SPR provides detailed kinetic information to be obtained across a wide range of molecular weights, without the need to utilise labelling or wash steps [352]. An equilibrium measurement is usually used to determine the affinity of the protein-protein interaction. For this, the analyte is injected at various concentrations covering several orders of magnitude. A mathematical fit with a 1:1 binding model is used for calculation of the dissociation constant (K_D). This is because any statements regarding the affinity quantitative measurements on the Biacore are only valid for molecules that interact with a 1:1 binding stoichiometry. The binding affinity (K_D), which is defined as the quotient of the dissociation rate constant (k_{off}) and association rate constant (k_{on}), indicated a strong interaction with slow dissociation between PD-1 and Cl19 Fab. The K_D was 0.041 μM (Figure 3.10).

III. Discussion

We were able to successfully express and purify PD-1FcHis and Cl19 Fab *via* stable transfection of CHOK1 cells and transient transfection in 293T cells using affinity chromatography *via* Ni-NTA Sepharose beads and subsequent gel filtration. Approximately 20 mg of PD1FcHis (stable transfection), and 50 mg and 0.7 mg of Cl19 Fab (obtained *via* stable and transient transfections, respectively) were purified. Thrombin cleavage and subsequent deglycosylation *via* Endo H were used to generate ~2 mg of hPD-1 protein from 10 mg of purified hPD-1FcHis recombinant protein. This protein was prepared in case it was required for eventual structural

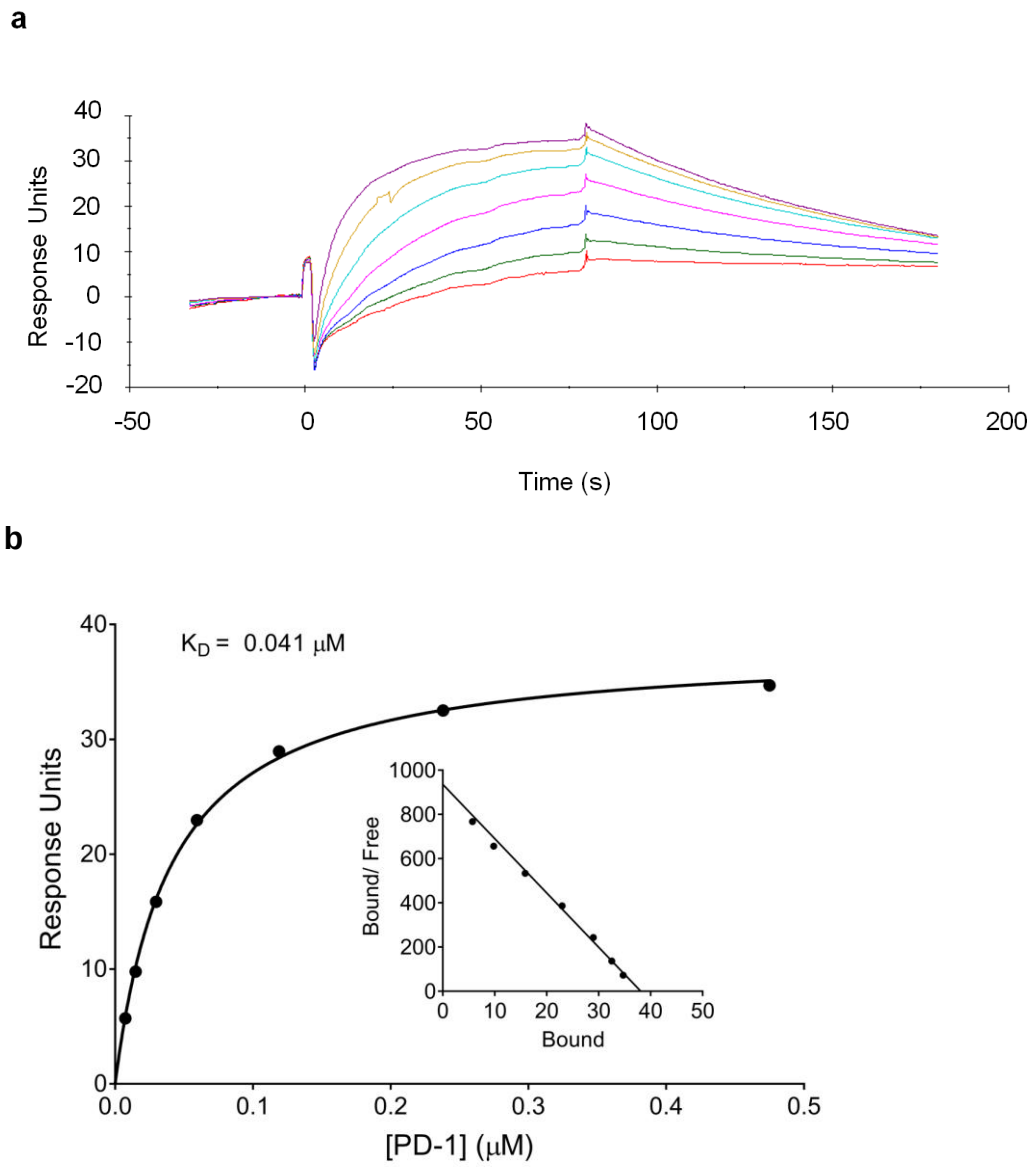


Figure 3.10: Binding of PD-1 to Cl19 Fab using CM5 Chip on the Biacore. Equilibrium along with kinetics-based measurement of the affinity of Cl19 Fab for PD-1 were performed at 37 ºC. Cl19 Fab binds to PD-1 with somewhat high affinity. (**a**) Sensorgram displaying binding of Cl19 Fab to PD-1. (**b**) Equilibrium binding data are plotted. Nonlinear regression analysis with a 1:1 Langmuir binding model, along with a Scatchard plot are shown. The derived K_D value is displayed.

studies that would be used to guide the mutational analysis of Cl19. The advantages of using affinity chromatography to purify the proteins were that it has relatively high specificity, therefore high degrees of purity can be obtained, and the process is very robust. Substantially greater yields of Cl19 Fab were expressed and purified through stable transfection using CHOK1 system compared to the transient transfection and expression in 293T cells. The drawbacks of stable transfection are that it is more labour intensive and costly, and it takes a longer time for proteins to be expressed and purified.

To test initially whether the Cl19 Fab was well folded, it was mixed with PD-1FcHis and passed over the FPLC and compared to just PD-1FcHis or Cl19 Fab run alone. Since a slight shift to the left for the elution peak was shown on the chromatogram for the Cl19 Fab and PD-1FcHis mixture, this suggested that a complex had formed, indicating that the Cl19 Fab was correctly folded, to the extent that it allowed for stable binding to the PD-1 receptor. It was also very encouraging that the levels of expression of the proteins was relatively high. In our collective experience, poorly folded proteins express poorly. To examine the binding kinetics, Cl19 Fab was tested for binding with PD-1 on the Biacore using a CM5 chip. From such measurements, strong binding was observed and a K_D of 0.041 μM was obtained. This offered further confirmation that the Fab was well folded. Lastly, establishing the transient transfection strategy for Fab expression in 293T cells provided the basis for undertaking a subsequent mutational analysis of Cl19 Fabs, as discussed in the next chapter.

Chapter 4
Production and characterisation of new fast off-rate Cl19 antibody derivatives

I. Introduction

The aim of this chapter was to produce anti-PD-1 antibodies with altered kinetics: *i.e.* to generate Cl19-derived, PD-1 proximally binding anti-PD-1 antibodies that have increased off-rates comparable to the existing Cl10 antibody, which is agonistic *in vitro* but is less prone to inducing PD-1 down-modulation *in vivo*. These second-generation antibodies could potentially induce stronger superagonistic receptor triggering and therefore hold enhanced therapeutic capabilities. We also aimed to create a novel isotype control anti-PD-1 antibody which would still be able to bind to the Fc receptors but would not bind the PD-1 receptor, and would not induce downstream PD-1 signalling.

In this chapter, we prepared new constructs for making anti-PD-1 Cl19 Fabs with altered kinetics. The strategy for making Cl19 Fab mutants with decreased affinities for PD-1 for screening on the Biacore, was as follows. Initially, we wanted to map the binding surface with drastic mutations in the Fab complementarity determining regions (CDRs) in order to delineate the PD-1 binding region on the antibody. It was our intention then to re-mutate the thus-identified binding-site residues with more subtle changes to alter the kinetics of binding. A variable domain of an antigen receptor contains three complementarity determining regions (CDRs): CDR1, CDR2, CDR3. These hyper-variable regions are crucial to the diversity of antigen specificities generated by lymphocytes. In order to investigate the mutant Cl19 Fabs on the Biacore, a BirAHis tag was added to the mutated Fabs to allow for

biotinylation and immobilization on a CAPture Chip. The histidine tag was included in the construct to allow for affinity chromatography purification using Ni-NTA beads.

In total, a set of 24 Cl19 Fab mutants was characterized. The generation of a Cl19 isotype control protein was also undertaken, for which PD-1 binding was expected to be completely eliminated.

II. Results

II.A. Production of anti-PD-1 Cl19 FabBirAHis

DNA encoding the anti-PD-1 heavy chain variable region, with BirAHis sequence attached was cloned into the pOPINVH vector and then co-transfected, along with anti-PD1 Cl19 light chain variable region encoded in the pOPINVL vector, into 293T cells. BirA is a 35-kD DNA-binding biotin protein ligase from *Escherichia coli* which is normally involved in the biotinylation of a subunit of acetyl-CoA carboxylase. It functions as a transcriptional repressor for the biotin biosynthetic operon [353]. A Western blot performed using the TCS following expression suggested that this construct expressed well transiently in 293T cells, forming slightly heavier bands in both non-reducing (~38 kDa) and reducing conditions (~24 kDa) compared to the anti-PD-1 Cl19 Fab protein lacking the BirA sequence that was expressed in parallel (Figure 4.1).

The wildtype Cl19 FabBirAHis Fab was biotinylated and then attached to a Biotin CAPture Chip on the Biacore, for measurements of binding to PD-1 at 37 ºC. The Biotin CAPture chip has an advantage over the CM5 chip in that it can be regenerated and thus be reused. This method gave comparably similar results to the CM5 chip binding data previously obtained for the non-biotinylated protein (Chapter 3). Strong binding and slow dissociation between PD-1 and Cl19 FabBirAHis, with a K_D of 0.051 μM, was observed (Figure 4.2).

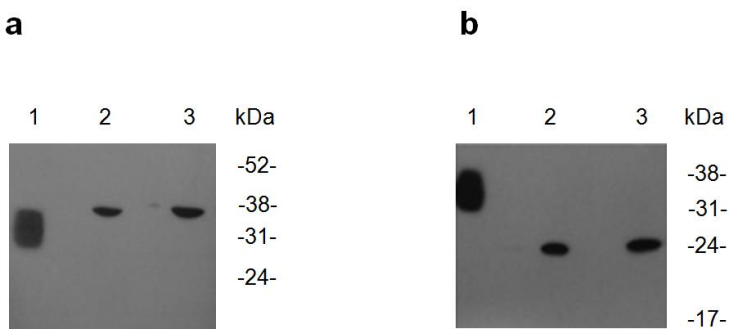
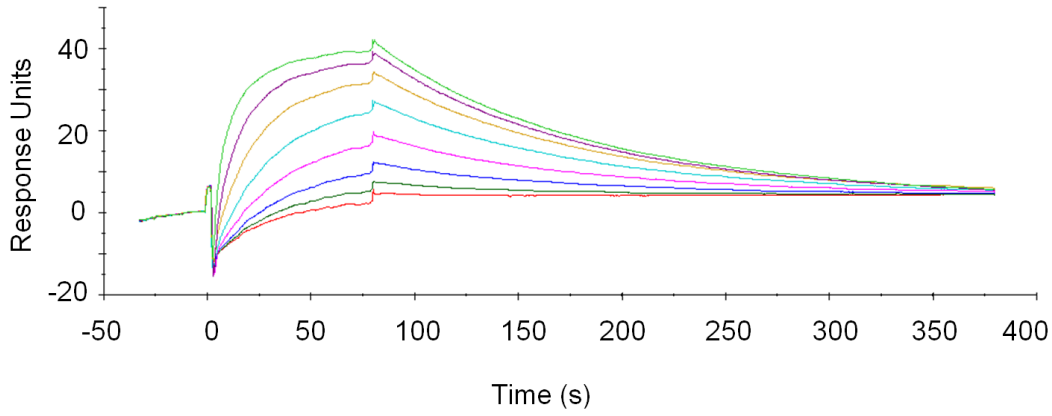


Figure 4.1: Western blotting confirms expression of Cl19 Fab BirAHis. Tissue culture supernatant (TCS) was taken from 293T cells that were transiently transfected with the following vectors: Lane 1, Positive control (rmIL10RBHis-pEE14); Lane 2, Cl19 Fab light chain pOPINVL and Cl19 Fab heavy chain pOPINVH; Lane 3, Cl19 Fab light chain pOPINVL and Cl19 Fab BirAHis heavy chain pOPINVH. Samples were separated on a 12 % acrylamide gel. 7.5 µl of TCS, or rmIL10RBHis protein as a positive control, was loaded, under (**a**) non-reducing or (**b**) reducing conditions. The proteins were transferred onto a nitrocellulose membrane and probed with an anti-penta-His antibody, followed by an HRP-conjugated secondary antibody. Chemi-luminescence was detected on x-ray film.

a



b

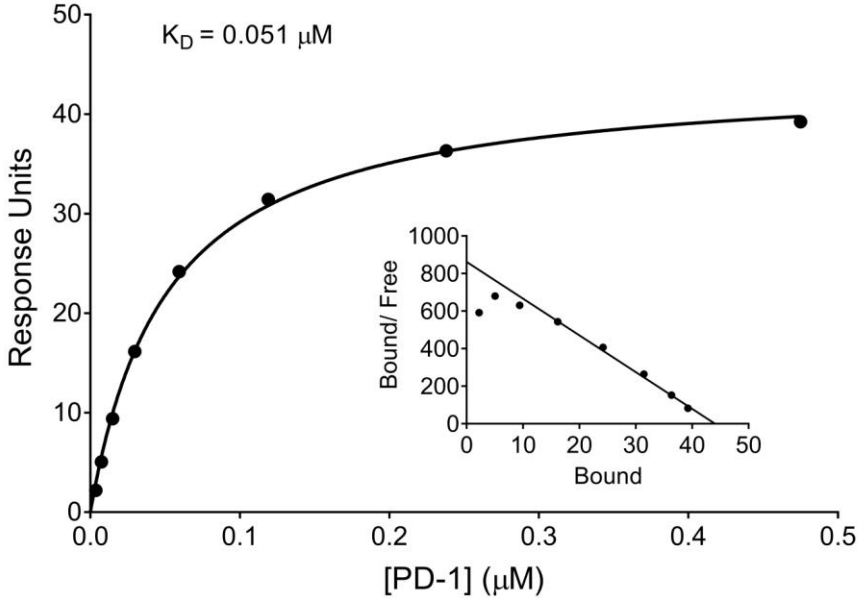


Figure 4.2: Binding of PD-1 to Cl19 FabBirAHis using the Biotin CAPture Chip on the Biacore. Equilibrium along with kinetics-based measurement of the affinity of Cl19 Fab for PD-1 were performed at 37 ºC. Cl19 FabBirAHis binds to PD-1 with somewhat high affinity. (**a**) Sensorgram showing binding between Cl19 FabBirAHis and PD-1, (**b**) Equilibrium binding data are plotted. Nonlinear regression analysis with a 1:1 Langmuir binding model, along with a Scatchard plot. The derived K_D value is displayed.

II.B. Mutant anti-PD-1 Cl19BirAHis Fabs

Having established that anti-PD-1 Cl19 Fab BirAHis could be expressed transiently in 293T cells, mutated forms of the Fab were made with the objective of reducing the binding affinity and increasing the dissociation properties of the Cl19 antibody. Pymol software was utilised to determine which residues of the Fab created the CDR regions so that they could be mutated. For this purpose, a model of the Cl19 Fab was prepared for us by Prof Shinji Ikemizu of Kumamoto University. This was based on the Fab structure whose sequence best matched the sequence of Cl19 in the variable regions.

In the first round of screening, 18 'drastic' mutations which mostly covered the three CDRs of both chains of the Cl19 antibody variable region were made using a PCR-based approach: three mutations per CDR, nine mutations on both light and heavy chains, respectively (Table 4.1, Figure 4.3). This involved using a similar mutagenesis-based approach previously adopted by Fernandes and colleagues [354]. All the amino acid residues selected for mutation were chosen on the basis that they were outward-*i.e.* solvent-facing and not buried within the CDR, making access to PD-1 more favourable. The residues selected were all mutated to arginine apart from basic amino acids lysine, histidine and arginine; instead, these residues were mutated to aspartic acid. This was to ensure maximum disruption of the antibody epitopes. By mutating selected residues drastically, if any residues critical in the structural stability of Cl19 Fab were chosen, their drastic mutation would mean that the resultant protein would not be successfully expressed, therefore this helped to reduce the amount of false negatives. These initial 18 constructs were produced and the new antibody Fab variants were transiently expressed in 293T cells using pOPINVH and pOPINVL vectors as described above and in Chapter 3. They were then biotinylated and characterized on the Biacore using the CAPture chip at 37 ºC, in order to test the binding kinetics to PD-1.

Table 4.1: Amino acid residues mutated in CDRs (underlined) of anti-PD-1 Cl19 heavy chain FabBirAHis pOPINVH and anti-PD-1 Cl19 Fab light chain pOPINVL constructs in the first round of screening for binding to PD-1 (a total of 18 mutations).

	CDR1	CDR2	CDR3
Cl19 Vκ (light chain)	RASSSVISSYLH	STSNLAS	QQYNGYPLT
Cl19 VH (heavy chain)	GYTFTTYPIE	NFHPYNDDTKYNE KFKG	ENYGSHGGFVY

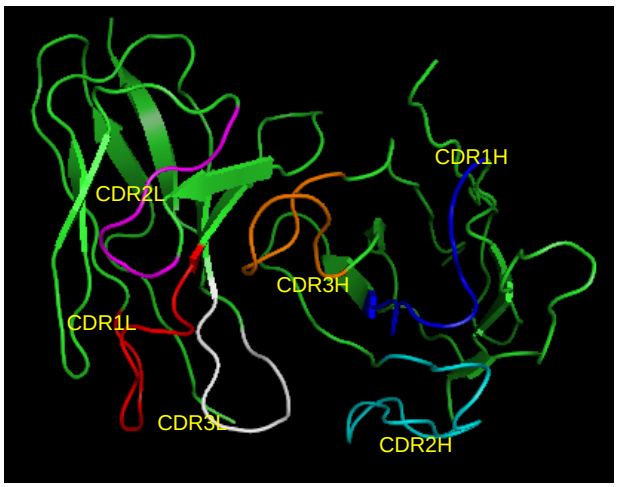


Figure 4.3: Pymol ribbon diagram showing the CDRs of anti-PD-1 Cl19 heavy chain FabBirAHis pOPINVH and anti-PD-1 Cl19 Fab light chain pOPINVL constructs to be mutated in first round of screening for binding to PD-1 on the Biacore. Cl19 light chain: red, magenta, grey (CDR1, CDR2, CDR3). Cl19 heavy chain: navy, light blue, orange (CDR1, CDR2, CDR3).

II.C. First set of mutant anti-PD-1 Cl19 Fabs and their binding kinetics

The first-round screening of the 18 mutants immediately suggested that two mutations in CDR3 in the light chain (residues N92 and Y94) reduced binding to PD-1 but did not completely eliminate it, and increased the off-rate compared to the 1st generation Cl19 Fab (Figure 4.4, Figure 4.5, Table 4.2). For naming the mutants, R refers to the CDR, M to the mutant number, and L or H to the light and heavy chains. CDR3 mutation 2 in the light chain is therefore called R3M2L, and CDR3 mutation 3 in the light chain is called R3M3L. Five other mutations, some in the light chain and some in the heavy chain, completely eradicated binding to PD-1: R2M3L, R3M1L, R1M2H, R2M1H and R3M3H (Figure 4.4, Table 4.2). The complete elimination of binding by these five mutations suggested that these key residues in the CDR regions formed the essential interactions with the PD-1 receptor. Surprisingly however, these mutations were widely distributed across the surface created by the CDRs in the model whereas it would be expected that the mutations would be clustered in a contiguous surface (Figure 4.5). It is possible that the model of the Fab has some inaccuracies or that the mutations have substantial indirect effects. Nevertheless, these complete 'knockout' mutations were good potential residues for the generation of an anti-PD-1 Cl19 isotype control antibody which could be used in further *in vitro* and *in vivo* experiments for testing the suppressive capacities of the second-generation anti-PD-1 antibodies.

II.D. Kinetic analysis of the Cl19 R3M2L and R3M3L mutants

In order to characterise the binding of Cl19 R3M2L and R3M3L mutants to PD-1, additional binding kinetics tests following the initial equilibrium measurements were carried out using both the Biotin CAPture Chip and CM5 chips (Table 4.3 and Table 4.4, respectively). The binding analysis showed that the mutants had a relatively fast off-rate (Table 4.3, Table 4.4, Figure 4.6). Although binding was very weak, the reproducibility of the measurements was good, as indicated by the low standard deviations. R3M2L showed weak binding to PD-1 demonstrated by the large K_D value of 2.2 μM and high dissociation rate (large k_{off} of $0.58s^{-1}$) on the Biotin

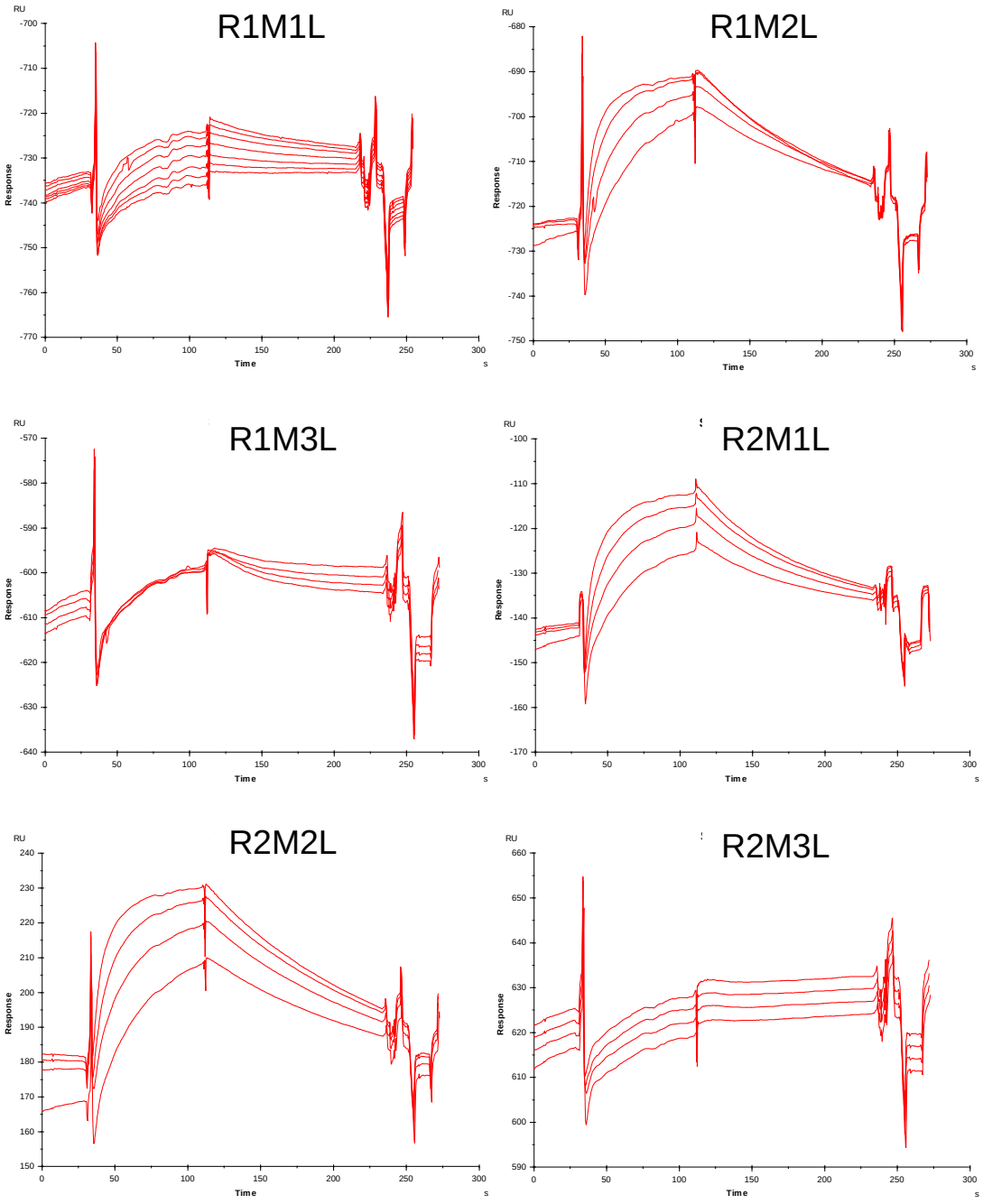


Figure 4.4 (a): Sensorgrams showing equilibrium measurements and binding of the first set of 18 mutant Cl19 FabBirAHis to PD-1 on the Biacore *via* the Biotin CAPture chip at 37 ºC. Out of the initial screening, mutation 2 and 3 in the CDR3 of the light chain (R3M2L and R3M3L) reduced binding to PD-1 and did not completely knock out binding. Five other mutations completely eradicated binding to PD-1: R2M3L, R3M1L, R1M2H, R2M1H and R3M3H. X axis displaying time and Y axis displaying response units.

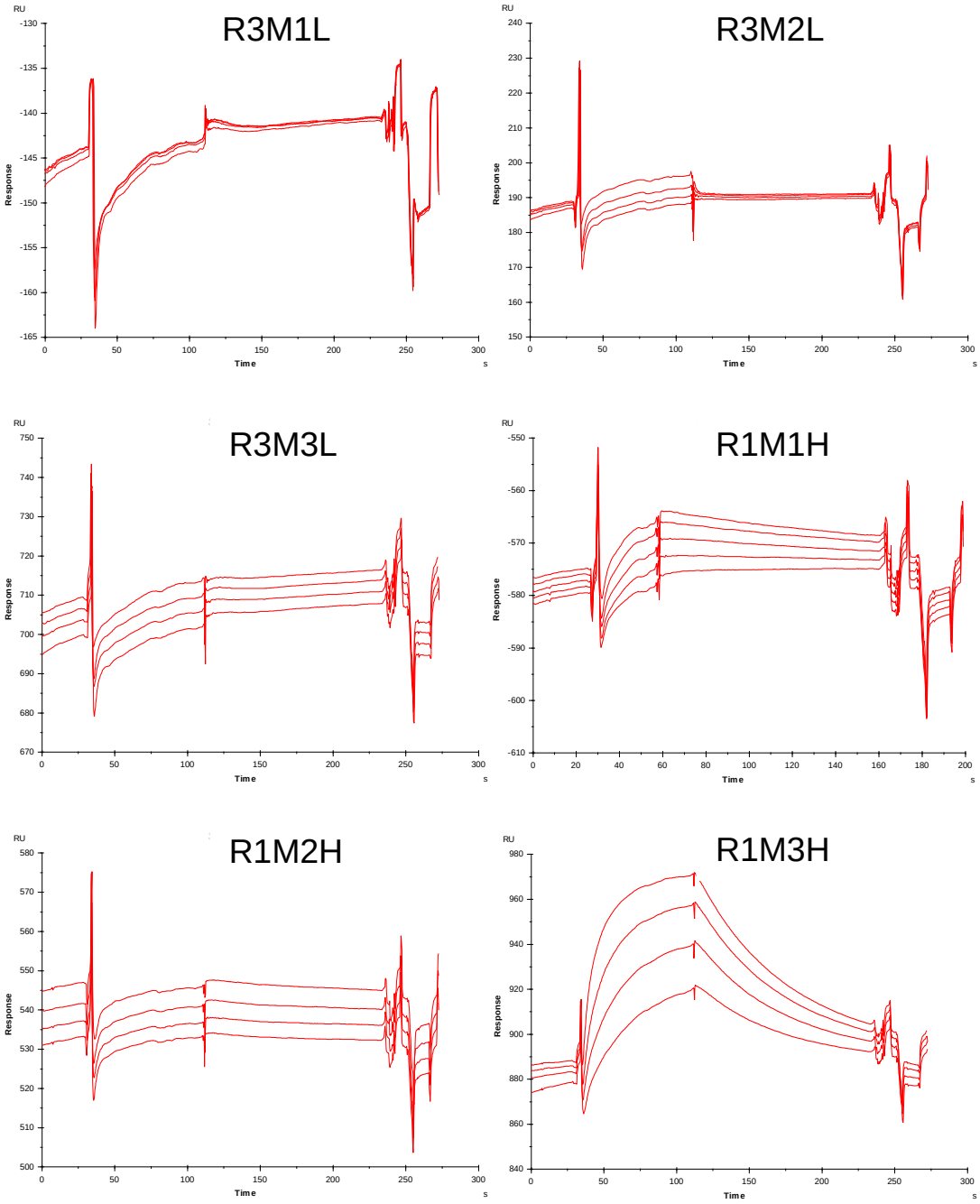


Figure 4.4 (b): Sensorgrams showing equilibrium measurements and binding of the first set of 18 mutant Cl19 FabBirAHis to PD-1 on the Biacore *via* the Biotin CAPture chip at 37 ºC. Out of the initial screening, mutation 2 and 3 in the CDR3 of the light chain reduced binding to PD-1 and did not completely knock out binding. Five other mutations completely eradicated binding to PD-1: R2M3L, R3M1L, R1M2H, R2M1H and R3M3H.

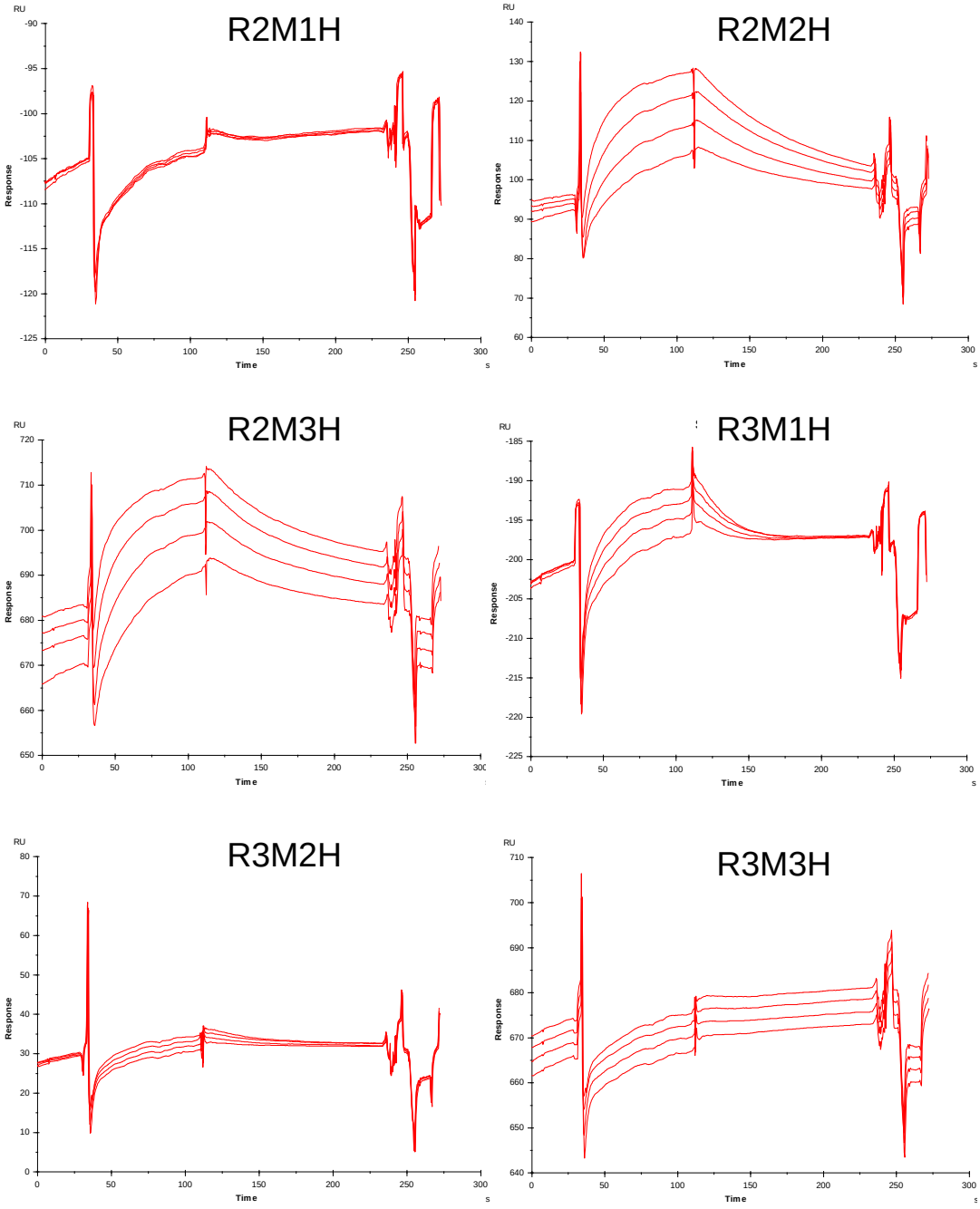


Figure 4.4 (c): Sensorgrams showing equilibrium measurements and binding of the first set of 18 mutant Cl19 FabBirAHis to PD-1 on the Biacore *via* the Biotin CAPture chip at 37 ºC. Out of the initial screening, mutation 2 and 3 in the CDR3 of the light chain reduced binding to PD-1 and did not completely knock out binding. Five other mutations completely eradicated binding to PD-1: R2M3L, R3M1L, R1M2H, R2M1H and R3M3H.

Table 4.2 : Table showing binding kinetics of first set of mutant Cl19 FabBirAHis to PD-1 *via* the Biacore at 37 ºC. Biotin CAPture chip was used. Out of the initial first round screening of 18 mutations, mutation 2 and 3 in CDR3 in the light chain (R3M2L and R3M3L) reduced binding to PD-1 and did not completely abolish binding. This is shown by the relatively high K_D values and increased off-rates compared to 1st generation Cl19 Fab. Five other mutants completely knocked out binding to PD-1: R2M3L, R3M1L, R1M2H, R2M1H and R3M3H.

	K_D (10^{-8} M)	K_D (10^{-7} M)	K_D (10^{-6} M)	K_D (10^{-5} M)	Non-measurable binding
R1M1L	3.24				
R1M2L		2			
R1M3L		3.5			
R2M1L	8.6				
R2M2L		2.6			
R2M3L					✓
R3M1L					✓
R3M2L			1.5		
R3M3L				5.2	
R1M1H		1.66			
R1M2H					✓
R1M3H		1.1			
R2M1H					✓
R2M2H		1.52			
R2M3H		1.7			
R3M1H		2			
R3M2H		1.1			
R3M3H					✓

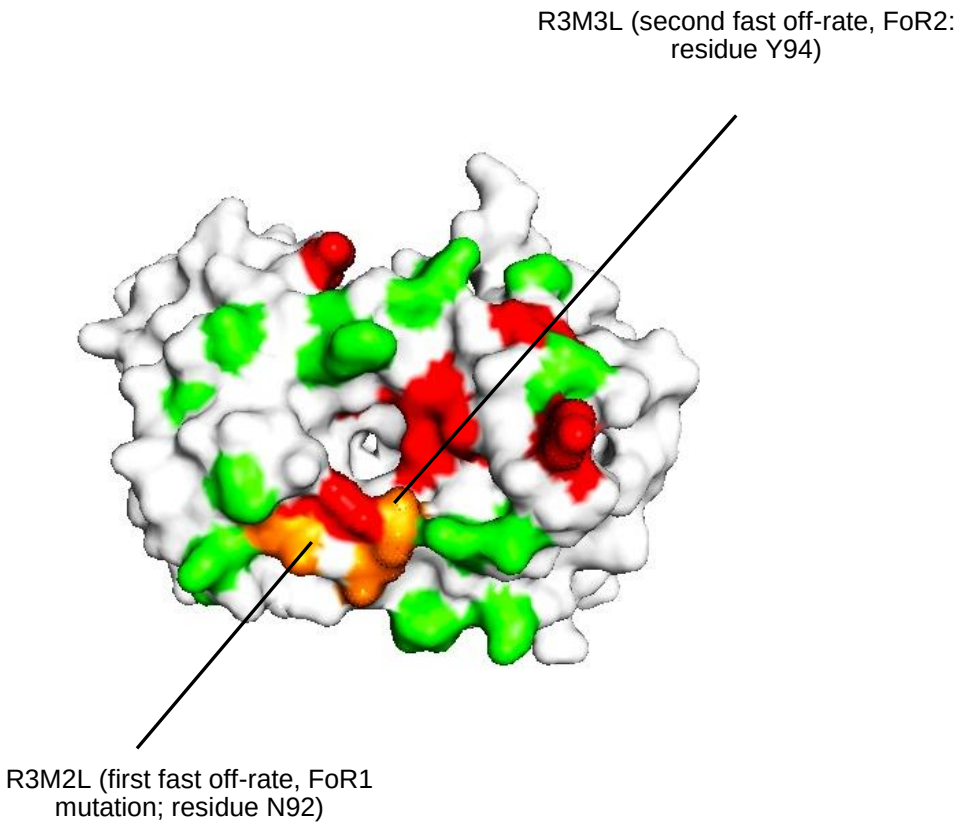


Figure 4.5: Pymol diagram showing binding kinetics of first set of 18 mutant Cl19 FabBirAHis to PD-1 using Biacore data. Green= strong binding, orange= weak binding, red= no binding to PD-1. R3M2L (FoR1) and R3M3L (FoR2) both gave fast off-rates compared with 1st generation Cl19 (see pg. 118). These mutations were subsequently made into whole Cl19 antibodies to generate 2nd generation antibodies with altered binding kinetics with the potential to induce greater inhibitory suppression *via* PD-1 signalling.

CAPture chip (Table 4.3). Similarly, the R3M3L mutant had a large off-rate and slightly higher affinity compared to the R3M2L Fab (Figure 4.7, Table 4.4).

Comparisons were also made to the binding kinetics of the 1st generation anti-PD-1 antibodies Cl10, Cl19 versus the new Cl19 fast off-rate mutant Fabs. The mutant forms of Cl19, R3M2L and R3M3L, which bind in the same position as Cl19 exhibited similar binding kinetics to Cl10. The off-rates were increased by approximately 70-fold in the 2nd generation Cl19 Fabs compared with the 1st generation Cl19 antibody. The off-rates were similar between R3M2L and R3M3L, but R3M3L manifested a slightly faster on-rate compared with R3M2L (Table 4.4). Hereafter, CDR3 mutation 2 in the light chain (R3M2L) became known as first fast off-rate antibody (FoR1) and CDR3 mutation 3 in light chain (R3M3L) was called second fast off-rate antibody (FoR2).

II.E. Second-round mutations of anti-PD-1 Cl19 FabBirAHis

In order to determine whether we could generate additional Cl19 antibody mutants that manifested reduced affinity to PD-1, a second set of six mutant anti-PD-1 Cl19 FabBirAHis constructs with mutations in only the CDRs of the heavy chain were generated and cloned into the pOPINVH vector. The mutant heavy-chain constructs were then co-expressed with the light chain and subsequently purified and biotinylated as before. These mutant Fabs were tested for binding with PD-1 on the Biacore using the Biotin CAPture chip (Table 4.5). Heavy chain mutant (HM) 1, HM2, and HM5 completely eliminated binding to PD-1 (Figure 4.8), and no additional fast off-rate Cl19 mutations were discovered through this new round of screening for binding to PD-1. Altogether, the data indicate that the combining site of Cl19 is centred on a small contiguous region created by Y91 of the light chain (CDR3), and P145 (CDR1), E147 (CDR1) and E211 (CDR3) of the heavy chain (Figure 4.9b). Tyrosine, proline, glutamic acid were the residues which we found to form part of the binding interface on Cl19 Fab to PD-1. Glutamic acid is charged and its side chains are able to form salt bridges, whilst tyrosine is polar, hydrophilic,

and able to form hydrogen bonds as proton donors or acceptors, these residues are typical of antibody-antigen interactions [355]. On the other hand, proline is non-polar, hydrophobic and is normally buried inside the protein core, hence it was somewhat surprising to find that this type of residue was involved in the Cl19 antibody binding interface [355]. The mutations generating the fast off-rate kinetics, N92 and Y94, lie at the side of this region, perhaps explaining their partial effects on binding (Figure 4.9c).

II.F. Expression of intact forms of the 1st generation Cl19 antibody and 2nd generation anti-PD-1 antibodies

In order to make whole 1st generation Cl19, FoR1, FoR2 and Cl19 isotype control antibodies, the heavy chain regions were cloned into the pEE6.4 expression vector whilst the light chain regions were cloned into the pEE12.4 vector. The cassettes comprising the hCMV-ME promoter, heavy chain-encoding region and poly A chain from pEE6.4 were then moved into the pEE12.4 vector. Stable transfection into CHOK1 cells using the GS selection system allowed co-expression of both chains of the antibodies. The stable transfection system was chosen because, although it is more time-consuming and labour intensive, better yields can be achieved compared to transient transfection systems. Additionally, the transfected cell lines could be stored long-term should future experiments require freshly purified protein.

Following expression, Protein G beads were used initially to purify the antibodies from the TCS. The antibodies were eluted with 0.1 M Glycine-HCl pH 2.0 and neutralised with 2.75 M Tris-HCl pH 8.0. Gel filtration using the AKTA FPLC protein purification system fitted with a Superdex 200 column, helped to further purify and buffer exchange the antibodies into PBS (Figure 4.10). The purities of the protein G and subsequent gel filtration antibody fractions were confirmed by SDS-PAGE. The FPLC chromatograms for all four anti-PD-1 antibodies were similar to the example shown in Figure 4.11. They exhibited a single major elution peak indicative of pure unaggregated antibody along with a small peak at the start of the

Table 4.3: Binding kinetics of Cl19 R3M2L mutant Fab (FoR1) to PD-1 using Biotin CAPture chip in 3 separate runs on the Biacore performed at 37 ºC.

	1	2	3	Average	StDev
K_D (M)	2.3×10^{-6}	2.3×10^{-6}	1.9×10^{-6}	2.2×10^{-6}	0.23×10^{-6}
k_{on} ($M^{-1} s^{-1}$)	2.7×10^{5}	2.4×10^{5}	3.1×10^{5}	2.9×10^{5}	0.36×10^{5}
k_{off} (s^{-1})	6.1×10^{-1}	5.5×10^{-1}	5.9×10^{-1}	5.8×10^{-1}	0.31×10^{-1}

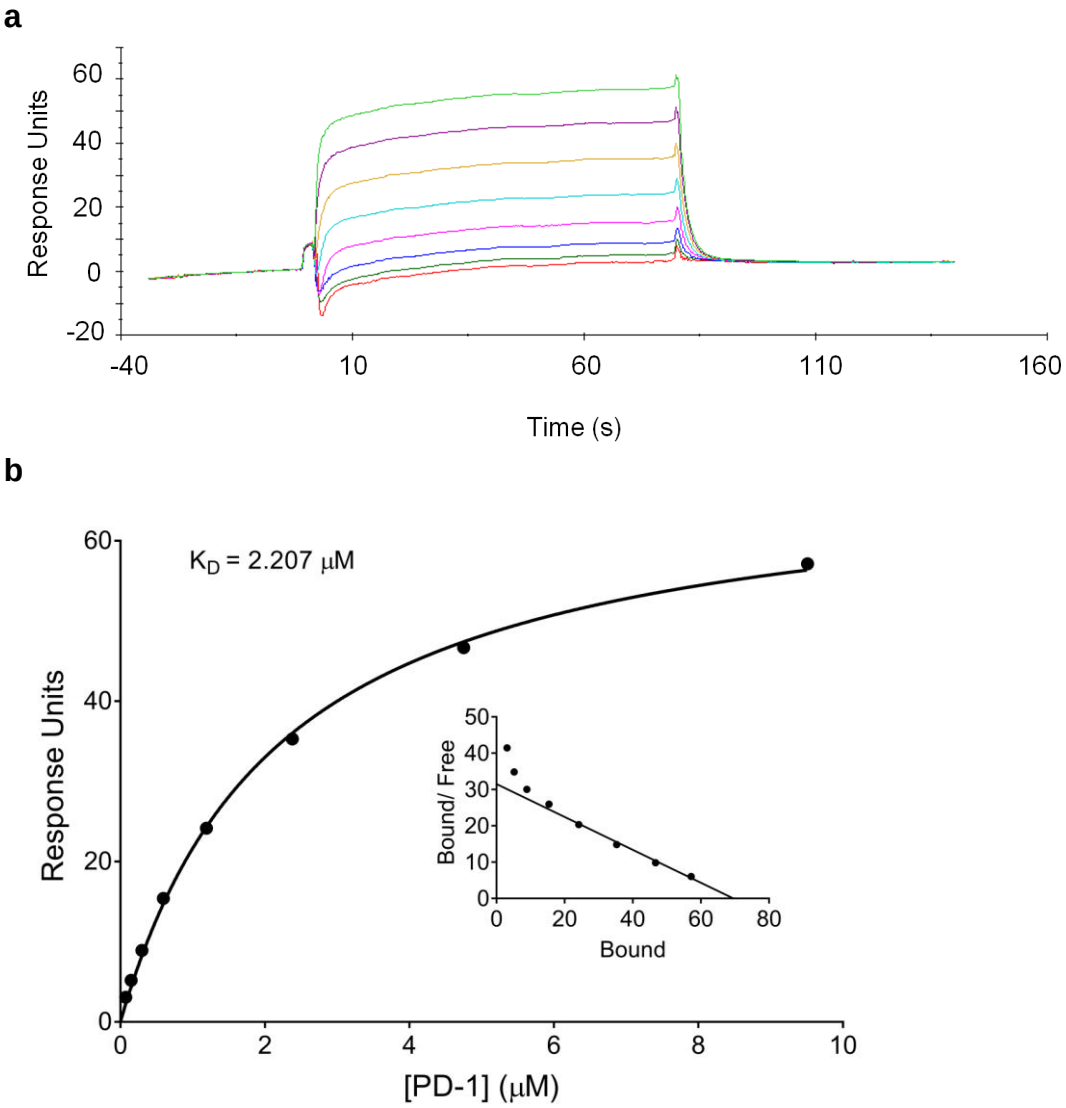


Figure 4.6: Binding kinetics of Cl19 R3M2L mutant (FoR1) Fab to PD-1 using the CM5 Chip *via* the Biacore. Kinetics-based measurements of the affinity for FoR1 Fab with monomeric hPD-1 were carried out at 37 ºC. FoR1 Fab binds PD-1 with low affinity. (**a**) Equilibrium measurements shown on sensorgram. (**b**) Equilibrium binding data are plotted. Nonlinear regression analysis with a 1:1 Langmuir binding model, along with a Scatchard plot are shown. The derived K_D value is displayed.

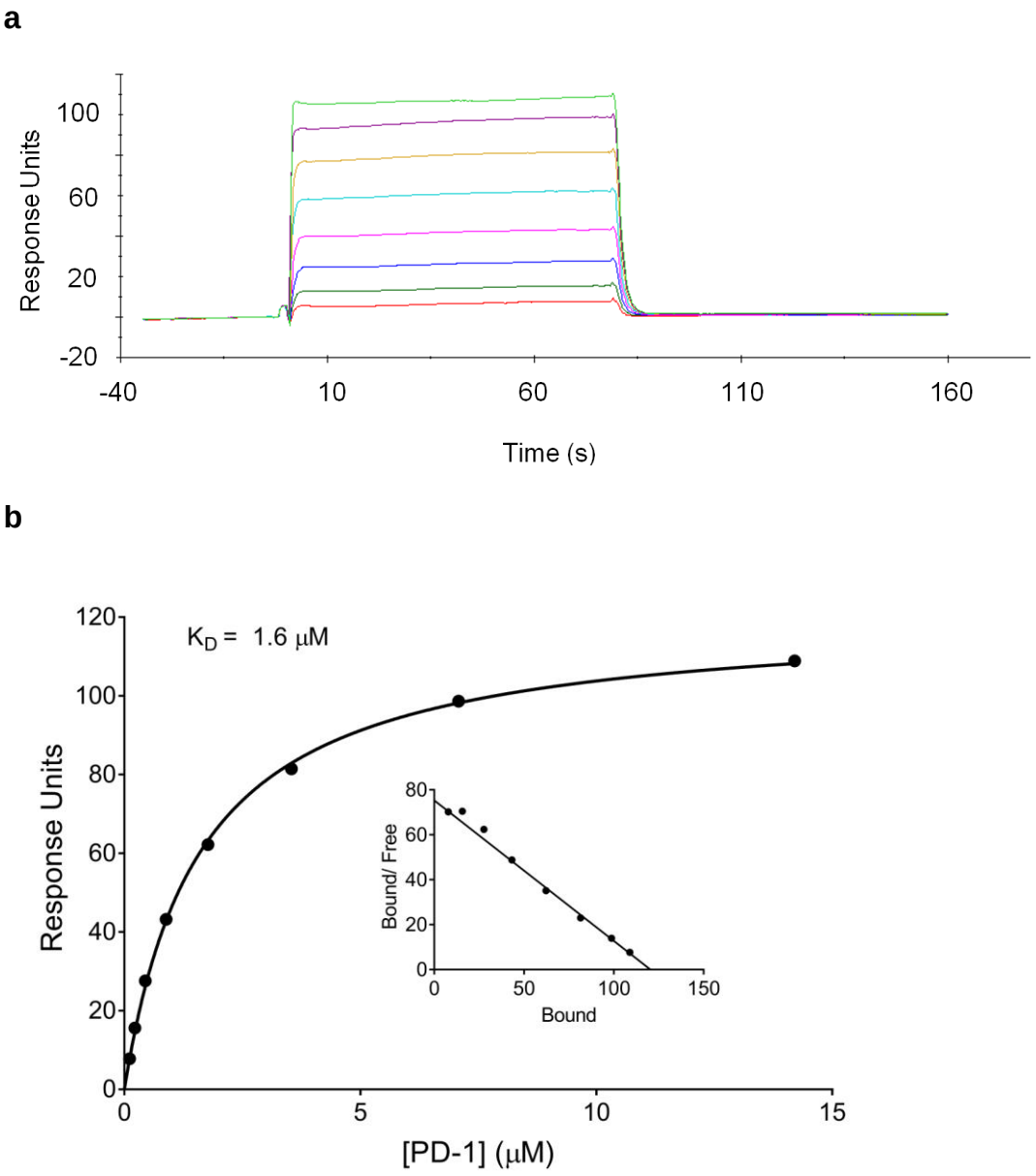


Figure 4.7: Binding kinetics of Cl19 R3M3L (FoR2) mutant Fab to PD-1 using the CM5 chip on the Biacore. Kinetics-based measurements of the affinity for FoR2 Fab with monomeric hPD-1 were carried at 37 ºC. FoR2 Fab binds PD-1 with low affinity relative to Cl19 Fab and exhibited slightly higher affinity compared to FoR1 Fab. (**a**) Equilibrium measurements shown on sensorgram. (**b**) Equilibrium binding data are plotted. Nonlinear regression analysis with a 1:1 Langmuir binding model, along with a Scatchard plot are presented. The derived K_D value is displayed.

Table 4.4: Binding kinetics of Cl10, Cl19, FoR1 (R3M2L) Fab, and FoR2 (R3M3L) Fab were compared on the Biacore using a CM5 chip. Experiments were carried out at 37 ºC. Two new antibodies with fast off-rates: FoR1 and FoR2 that bind in the same position as Cl19 but have very similar kinetics to Cl10 were made. These second generation antibodies' off-rates increased by ~70 fold compared to the 1st generation Cl19 antibody. FoR2 showed a slightly faster on-rate compared to FoR1.

	Agonist Cl10	Superagonist Cl19	FoR1 (R3M2L)	FoR2 (R3M3L)
Analyte	PD-1	PD-1	PD-1	PD-1
n	5	5	5	5
K_D (μM)	3.66 ± 0.2	0.06 ± 0.02	2.4 ± 0.25	1.59 ± 0.2
k_{on} ($M^{-1} s^{-1}$)	3.19×10^5	1.99×10^5	3.24×10^5	5.05×10^5
k_{off} (s^{-1})	1.14	0.011	0.73	0.74

Table 4.5: Amino acid residues mutated in CDRs (underlined) of anti-PD-1 Cl19 heavy chain FabBirAHis pOPINVH in the second round of screening for generating mutations which either completely knocks out binding or partially reduces binding to PD-1.

	CDR1	CDR2	CDR3
Clone 19 VH (heavy chain)	GYTFTTYPIE	NFHPYNDDTKYNEKFKG	ENYGSHGGFVY

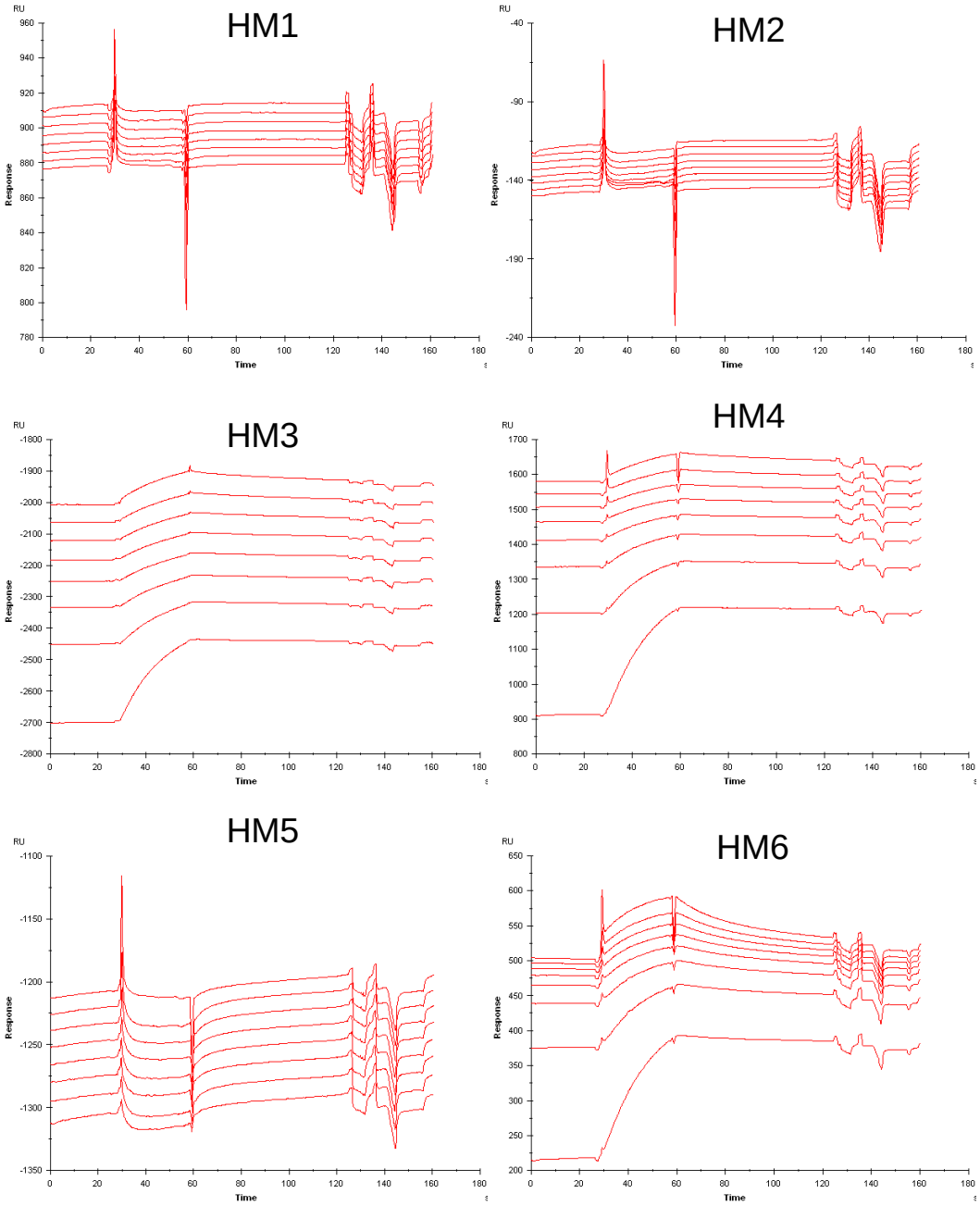


Figure 4.8: Sensorgrams showing equilibrium measurements to test binding of the second round of Cl19 heavy chain mutant Fabs to PD-1 on the Biacore using Biotin CAPture chip. Second round of heavy chain mutants 1, 2, and 5 (HM1, HM2, and HM5) completely knocked out binding to PD-1.

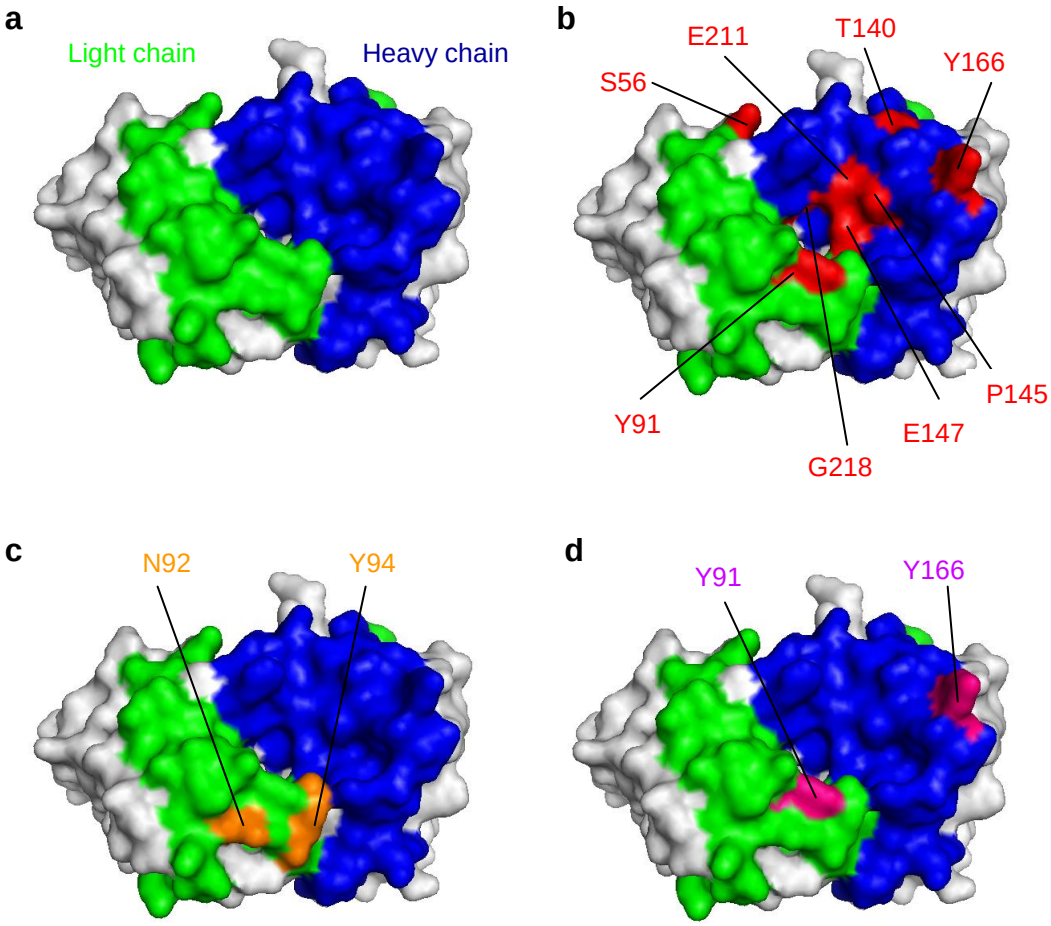


Figure 4.9: Pymol diagram showing mutations in both light and heavy chain CDR regions of Cl19 Fab from two rounds of Biacore screening experiments. (**a**) Light chain and heavy chain CDR regions of Cl19. Light chain in green, heavy chain in blue. (**b**) Mutations that gave no binding to PD-1 shown in red. (**c**) Fast off-rate mutations in light chain (FoR1 and FoR2) shown in orange. (**d**) Cl19 isotype control antibody made with mutations in Y91 (light chain) and Y166 (heavy chain) shown in magenta.

elution which suggested the presence of a small amount of protein aggregation. After confirming by SDS PAGE gels for the right size and purity of the proteins, *i.e.* that there was a single band above 97 kDa in the non-reducing condition, and bands of ~50 kDa and ~25 kDa under reducing conditions, the fractions from the single major elution peak were pooled and concentrated to ~2 mg/ml for storage. The protein yields and expression were high for all four whole antibodies: 40 mg, 20 mg, 15 mg, 20 mg of 1st generation Cl19, FoR1, FoR2 and Cl19 isotype control antibodies were purified (Figure 4.12). The high levels of expression implied that the proteins had folded well and would be stable.

II.G. Testing of Cl19 isotype control antibody on the Biacore

We generated an anti-PD1 Cl19 isotype control antibody by creating a construct that combined mutations in both the light and heavy chains of Cl19 that each gave no binding to PD-1 monomer in the two rounds of screening (Figure 4.9d). This isotype control antibody comprised drastic mutations in residue Y91 of the light chain and residue Y166 of the heavy chain of Cl19 (Figure 4.9d). Human PD-1 was injected over immobilised C119 or Cl19 isotype control antibody. Unlike the 1st generation Cl19 antibody which bound strongly with an increase of ~400 response units and then dissociated from monomeric soluble PD-1, the Cl19 isotype control antibody exhibited no binding on the Biacore, as shown by a lack of increase in response units following PD-1 injection (Figure 4.13). The new isotype control antibody was prepared for use in subsequent *in vitro* and *in vivo* assays as a control in tests of the suppressive activity of our putative agonising anti-PD-1 antibodies.

III. Discussion

Anti-PD-1 Cl19 FabBirAHis along with mutant versions of this Fab expressed well transiently in 293T cells and could be purified efficiently *via* affinity chromatography using NiNTA beads. It was relatively straightforward to set up this medium-throughput assay for mutant screening. Once all the mutant constructs were generated *via* cloning, it was relatively straight forward to set up multiple transient

transfections simultaneously in T175 tissue culture flasks and then allow for subsequent protein expression. 293T cells grew quickly and, compared to stable transfections in CHOK1 cells, this setup was a much more efficient process in terms of protein production and mutant screening.

The Pymol model helped with the selection of likely CDR regions of Cl19 Fab. Non-CDR mutations would not have interfered with PD-1 binding, of course, hence it was helpful to be able to identify the CDR regions. All the Cl19 Fab mutants expressed at a similar level of approximately 2 mg/L, implying that all the proteins were likely well folded and that the mutations did indeed target surface exposed CDR residues.

Somewhat unexpectedly, in the first round of screening of binding of Cl19 mutant Fabs to PD-1, which was assayed using surface plasmon resonance, two mutants, *i.e.* FoR1 (R3M2L) and FoR2 (R3M3L) showed promising altered kinetics, *i.e.* substantially reduced binding affinities to PD-1 compared to 1st generation Cl19, with a K_D and off-rates that were comparable to the 1st generation antibody, Cl10. Potentially, this indicated that these Cl19 mutants might induce higher overall suppressive PD-1 signalling by engaging with more PD-1 receptors in a shorter period of time compared to 1st generation Cl19 antibody. We determined that the binding kinetics of the new FoRs, FoR1 and FoR2, to PD-1, were more similar to PD-L2, rather than the alternative native ligand of PD-1, PD-L1. FoR1 and FoR2 Fabs showed binding to PD-1 with a K_D of ~2.4 μM and ~1.59 μM respectively, whilst PD-L1 and PD-L2 binding to PD-1 is known to have a K_D of ~8.2 μM and ~2.3 μM respectively [343].

Five other Cl19 antibody mutants exhibited non-measurable binding to PD-1 from the first round of screening with the surface plasmon resonance-based assay. The distribution of the disabling mutations were clustered fairly close together, and as predicted, it suggested that this was the binding site to PD-1 and therefore the Pymol

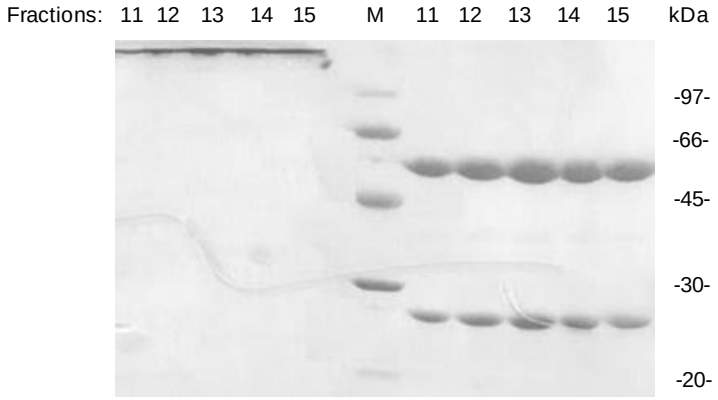


Figure 4.10: SDS-PAGE of purified and soluble FPLC fractions of whole FoR1 antibody eluted from 0.1 M Glycine pH 2.0 neutralised with 2.75 M Tris-HCl pH 8.0 using protein G beads (purified from stably transfected CHOK1 cells). Samples were separated on a 12 % acrylamide gel. 10 µl of each FPLC elution fraction was loaded, under either non-reducing (left hand side of marker lane (M)) or reducing conditions (right hand side of M).

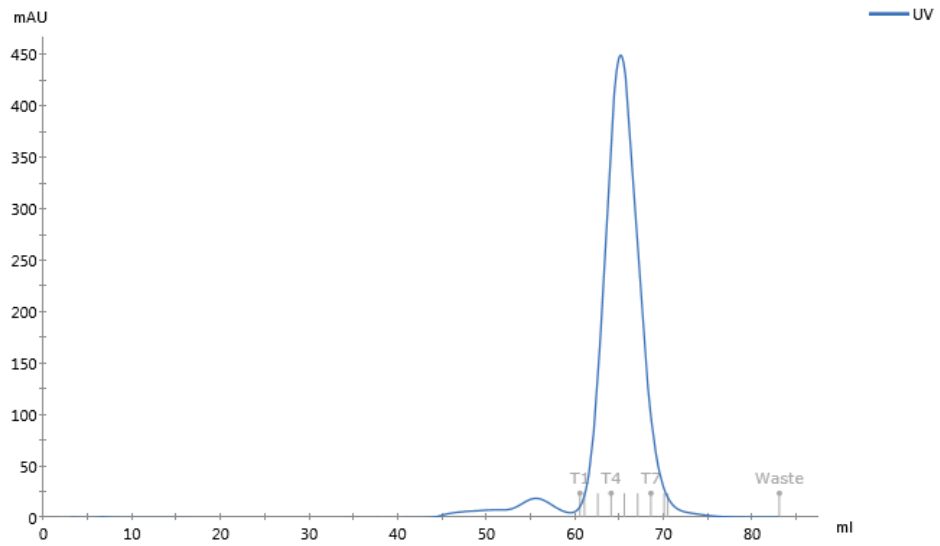


Figure 4.11: Purification of soluble anti-PD-1 FoR1 antibody with size exclusion chromatography. Chromatogram of FPLC (gel filtration) run for purified FoR1 antibody from protein G beads. An Akta FPLC system was utilised, fitted with a Sepharose 200 column of size 10/300. Protein elution was made with PBS and 500 µl fractions were collected and frozen at -20 ºC for subsequent usage.

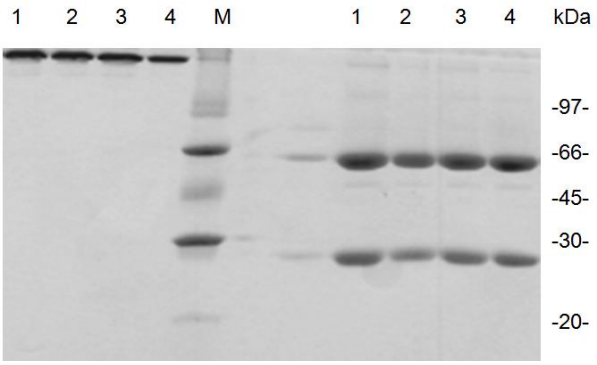


Figure 4.12: SDS-PAGE of purified and soluble FPLC fractions of purified whole anti-PD-1 antibodies. Lane (1) 1st generation Cl19, (2) 2nd generation: FoR1, (3) FoR2, and (4) Cl19 isotype control (left to right). Samples were separated on a 12 % acrylamide gel. 10 µl of each FPLC elution fraction was loaded, under either non-reducing (left hand side of Marker (M)) or reducing conditions (right hand side of M).

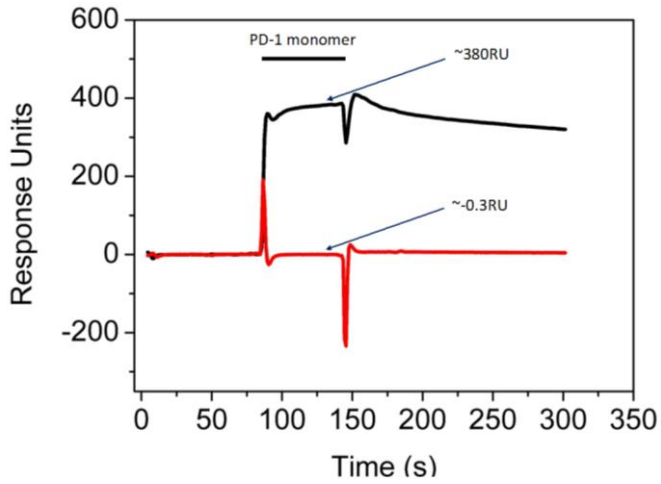


Figure 4.13: Binding of PD-1 to Cl19/Cl19 isotype control antibody on the Biacore at 37 ºC using the CM5 chip. Amine coupling used to directly immobilise Cl19/ Cl19 isotype antibody onto the matrix surface of the CM5 chip. Lack of binding of PD-1 to Cl19 isotype antibody (red line) and binding of PD-1 to Cl19 antibody (black line) displayed.

model of the CDR regions of Cl19 used was apparently reliable and accurate. Some of the drastic mutations led to partial effects on binding, presumably because the mutations were on the edge of the binding site to PD-1 (Figure 4.9).

To determine whether we could generate more mutants that either completely abrogated binding or partially reduced binding, we made a second set of Cl19 FabBirAHis mutants and carried out a second round of screening for binding to PD-1 using the surface plasmon resonance-based binding assay. Three more mutants, HM1, HM2, and HM5, showed complete elimination of binding to PD-1. These results further confirmed that these residues in the heavy-chain variable region of the antibody were important for binding to PD-1. Using this information, we generated a Cl19 isotype control antibody by incorporating a single mutation in both the light chain (Y91) and heavy chain (Y166) which showed no binding to PD-1 as demonstrated in the binding assay.

Through stable transfection of CHOK1 cells, we were able to express and purify high yields of clean and high quality 2nd generation fast off-rate anti-PD-1 whole antibodies along with Cl19 1st generation and Cl19 isotype control antibodies. Instead of using NiNTA beads, protein G beads were used for protein purification. Despite the protein expression being higher for stable transfections compared to transient transfections, several rounds of purification were still carried out in order to obtain enough protein, which made it more labour intensive and time consuming compared to transient transfection based protein expression systems. These newly generated anti-PD-1 antibodies were then subsequently used in both *in vitro* and *in vivo* assays to test for their suppressive activities in various settings.

Chapter 5
Analysis of the inhibitory effects of anti-PD-1 antibodies *in vitro*

I. Introduction

Having produced 2nd generation anti-PD-1 antibodies, we aimed to compare their inhibitory capabilities with those of the 1st generation antibodies using a series of *in vitro* assays. We also wanted to investigate the effects of these antibodies on PD-1 cell surface expression by T cells. To have effective PD-1 signalling, it's important that agonistic antibodies do not induce high levels of receptor downregulation. By maintaining receptors at the cell surface, this can help perpetuate receptor triggering and hence elicit more potent immunosuppressive effects. In fact, rather than being immunosuppressive, antibodies that down-regulate inhibitory receptors would be expected to be potentially immune activating. These new 2nd generation antibodies have fast binding kinetics similar to Cl10, hence, they hold the potential of binding, if only transiently, to a greater number of PD-1 molecules compared with the 1st generation Cl19 antibody in a given time period, and consequently could potentially lead to a better overall signal and, perhaps, avoiding down-regulation. We tried to assess the signalling capacities of the new FoR antibodies in experiments described in this chapter. As readouts for signalling we examined IL-2, TNF-α, and IFN-γ.

In 1975, IL-2 was found to be a growth-promoting activity for T lymphocytes [356]. This was one of the first cytokines that was characterised molecularly. Subsequent studies revealed that IL-2 comprised the soluble activity present in conditioned medium derived from cells stimulated with mitogens. Consequently, its discovery enabled T lymphocytes to be cultured. Interestingly, IL-2 exerts a striking array of

pleiotropic effects on a wide variety of target cells, its effects most prominently observed on T cells. IL-2 is a small, monomeric, secreted glycoprotein with a molecular weight of 15 kDa. One of the most immediate ramifications of T cell activation through its antigen receptor is the *de novo* synthesis of IL-2. This rapidly leads to the expression of a high affinity IL-2 receptor. In turn, this allows selective and swift expansion of effector T cell populations activated by antigen [357]. Accordingly, an essential function of this cytokine is in the proliferation of both $CD4^+$ and $CD8^+$ T cells.

TNF-α is a key regulator of inflammation. Studies have shown that antagonists of TNF-α are useful for treating inflammatory diseases for which the cytokine plays a pivotal pathogenetic role. Suppression of TNF-α effects has been found to be an effective immunotherapy for patients with immunological conditions such as rheumatoid arthritis and other types of inflammatory disorders such as psoriatic arthritis, inflammatory bowel diseases, ankylosing spondylitis and psoriasis [358].

IFN-γ is vital for tumour control and immunity against intracellular pathogens. Investigations have indicated that aberrant IFN-γ expression is linked to several autoimmune and autoinflammatory disorders. This cytokine is secreted predominantly by effector Th1 $CD4^+$ cells and $CD8^+$ CTL once antigen-specific immunity develops as well as by NK cells and NKT cells that play important roles in innate immunity [359].

Previous *in vitro* experiments have revealed that engagement of PD-1 by its native ligands PD-L1 and PD-L2 leads to suppression of T cell proliferation as well as secretion of cytokines such as IL-2, TNF-α and IFN-γ [216, 228]. This suggests that PD-1 downstream signalling is able to induce various forms of immunosuppression. These types of immunosuppression in turn could contribute greatly to helping prevent inflammation, allow for tolerance to occur and prevent autoimmunity and the development of autoimmune disorders. Hence, we wanted to determine if we

could induce inhibition of immune responses using our new anti-PD-1 antibodies that have varying binding kinetics and have either membrane proximal epitopes or membrane distal epitopes which could result in them possessing different signalling capacities according to the KS model, differences which might ultimately affect their therapeutic potential.

II. Results

We first set about characterising the properties of the 1st generation anti-PD-1 antibodies: Cl2 and Cl19 that bind with high affinity, and Cl10 that binds with low affinity (see Figure 1.3). In the first round of experiments the antibodies were used in a soluble form, to mimic the situation of antibody presentation *in vivo*.

II.A. PD-1 cell surface downregulation upon activation *in vitro*

In order to determine the effects of the anti-PD-1 antibodies on PD-1 cell surface expression on T cells *in vitro*, hPD-1 knockin (k.i.) mouse splenocytes were stimulated with anti-CD3 antibody (1 μg/ml) and cultured for 3 days together with 1st generation PD-1 antibodies added either from time zero (T0, same time as anti-CD3 antibody stimulation) or 24 h (T24) later. We wanted to establish whether the timing of the addition of anti-PD-1 antibodies affected the PD-1 cell surface expression or not. Flow cytometry was used to check for PD-1 cell surface expression shown by the median fluorescence intensity (MFI) of staining of these splenocytes. The mouse splenocytes were gated on CD4 or CD8 coreceptors. Both Cl2 and Cl19 antibodies were labelled with an Alexa 647 labelling kit, and these were used to detect PD-1 expression. Alexa-647 is a bright, far-red fluorescent dye with excitation suited for the 594 nm or 633 nm laser lines. Alexa-647 conjugated Cl2 was used to stain hPD-1 splenocytes incubated with Cl19, whilst Cl19 Alexa647 was utilised to stain cells incubated with Cl2 or Cl10 antibodies.

For the $CD4^+$ T cells, out of the three 1st generation antibodies, a dose dependent effect on PD-1 cell surface downregulation was observed only for Cl19 antibodies

and not for Cl2 or Cl10. That is, with higher concentrations of Cl19 PD-1 antibodies, a greater level of downregulation of PD-1 was induced (Figure 5.1a). The loss of staining was most likely real because there was no competition for the staining antibody. For Cl19 treated cells, timing of activation made no difference; PD-1 expression was reduced to lower than that of unstimulated cells. For Cl10 treated cells, the marked initial reduction in staining at all concentrations of antibody is likely due to residual blocking of the staining with the treatment antibodies. Timing in this case also made no difference to the remaining amounts of PD-1 that could be detected, and there was no dose-dependent effect. The similar loss in PD-1 signal in Cl2-treated cells is more difficult to explain, as there was no competition for the Cl19 antibody used for staining.

For the $CD8^+$ T cells, similar data were obtained. A considerably smaller dose dependent increase in PD-1 cell surface downregulation was observed, and again only for the Cl19 antibody and not for Cl2 or Cl10 (Figure 5.1b). For Cl10, staining was probably blocked by residual treatment antibody, and for Cl2, the effects are again difficult to explain. More useful insights into the down-modulating effects of the antibodies might come from *in vivo* experiments. However, the data do suggest that the 1st generation Cl19 antibody is a down-regulator of PD-1 expression, especially in the case of $CD4^+$ T cells.

II.B. Effects of 1st generation antibodies on cytokine production

To test the potential inhibitory effects of these anti-PD-1 antibodies, the 1st generation antibodies were tested with hPD-1 k.i. mouse splenocytes to determine whether suppression of cytokine production following anti-CD3 antibody stimulation *in vitro* could be achieved or not. Enzyme-linked immunosorbent assay (ELISA) was carried out using the TCS to measure cytokine secretion following incubation with the anti-PD-1 antibodies in solution. Initially, the levels of stimulatory anti-CD3 antibody were titrated to assess the optimal levels of activation which could be induced by triggering the TCR alone in the hPD-1 k.i. splenocytes.

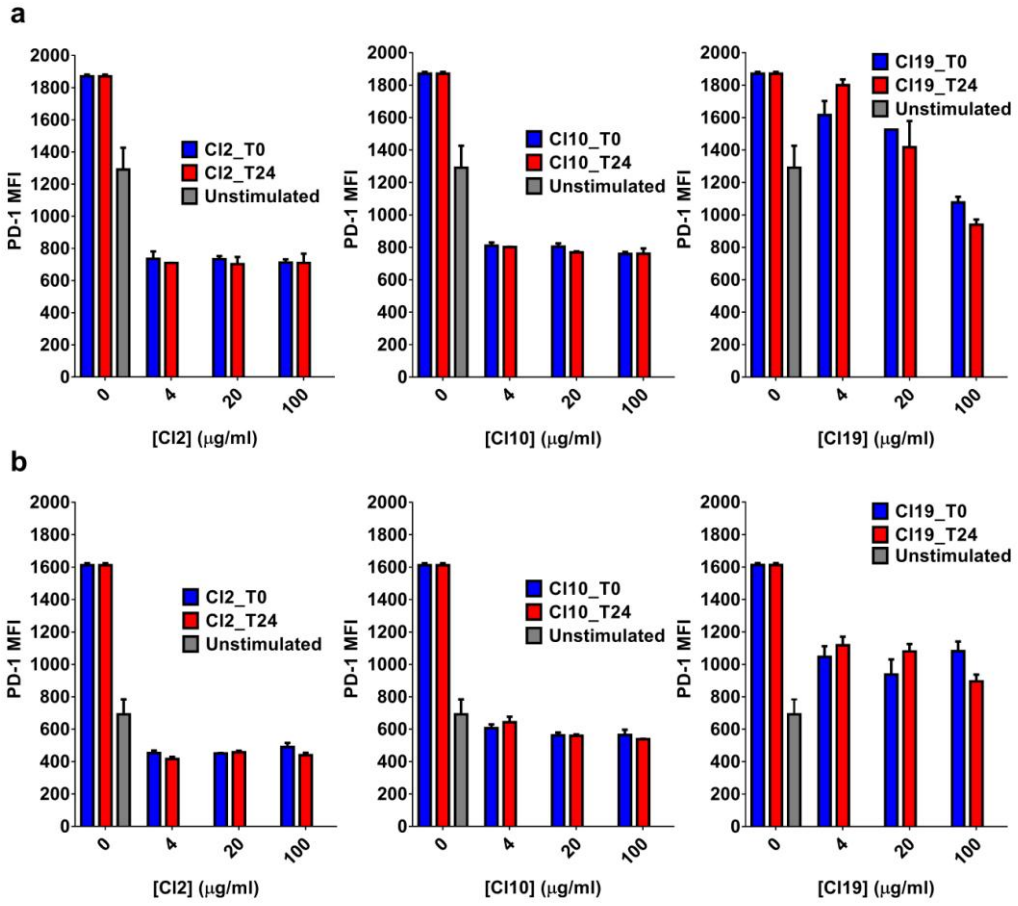


Figure 5.1: (**a**) PD-1 downregulation in $CD4^+$ or (**b**) $CD8^+$ hPD-1 k.i. mouse splenocytes. hPD-1 k.i. mouse splenocytes were stimulated with anti-CD3 antibody (1 μg/ml) and cultured for 3 days together with 1st generation PD-1 antibodies added either from time zero (T0, same time as anti-CD3 antibody stimulation) or 24 h (T24) later. Flow cytometry conducted and cells were gated on $CD4^+$ T cells. PD-1 median fluorescence intensity (MFI) displayed. Conjugated Cl2 Alexa647 was used to stain cells incubated with Cl19 antibodies, whilst conjugated Cl19 Alexa647 was utilised to stain cells incubated with Cl2 or Cl10 antibodies. Data points shown are means of duplicates ± SEM. Data are representative of two independent experiments.

IL-2 ELISA was performed using TCS collected from hPD-1 k.i. splenocytes incubated for various times, *i.e.* 24, 48, 72 h with different levels of anti-CD3 antibody stimulation (Figure 5.2). It was apparent that the cells were activated within 24 h, producing greater amounts of IL-2 with increased levels of anti-CD3 antibody, with the response saturating after reaching 10 μg/ml. Following 48 h of incubation, the levels of IL-2 reduced, indicating that the cells started to consume the IL-2 that was produced or perhaps went into an anergic phase since no co-stimulation was provided. After 72 h, IL-2 production following anti-CD3 stimulation was completely abolished. This suggested that the cells had completely consumed all of the residual IL-2 and stopped producing new IL-2.

This prompted us to try adding costimulation in the form of anti-CD28 antibody stimulation for the activation of the hPD-1 k.i. splenocytes. We titrated in the levels of anti-CD3 antibody along with the anti-CD28 antibody (Figure 5.3). As expected, this led to enhanced levels of overall IL-2 secretion compared to anti-CD3 antibody stimulation alone. For this experiment, we titrated the levels of anti-CD3 antibody and anti-CD28 antibody down from 5 μg/ml. Relatively high levels of IL-2 that were comparable to the levels produced after 24 h (Figure 5.3a), were now detected after 48 h (Figure 5.3b) incubation with the cells. However, as with the anti-CD3 antibody-only stimulation, it seemed that the IL-2 had been completely consumed by the cells at 72 h (Figure 5.3c). The greatest levels of IL-2 production were seen with 1 to 5 μg/ml of both anti-CD3 and anti-CD28 antibody stimulation. Following these experiments, 48 hours was the time point chosen for harvesting the TCS for subsequent ELISAs, and the concentrations of anti-CD3 and anti-CD28 antibodies used was 2 μg/ml.

Cl10 and Cl19 antibody at 25 μg/ml were observed to inhibit IL-2 production by hPD-1 k.i. mouse splenocytes following anti-CD3 and anti-CD28 antibody stimulation (Figure 5.4a); much weaker effects were observed for IFN-γ or TNF-α

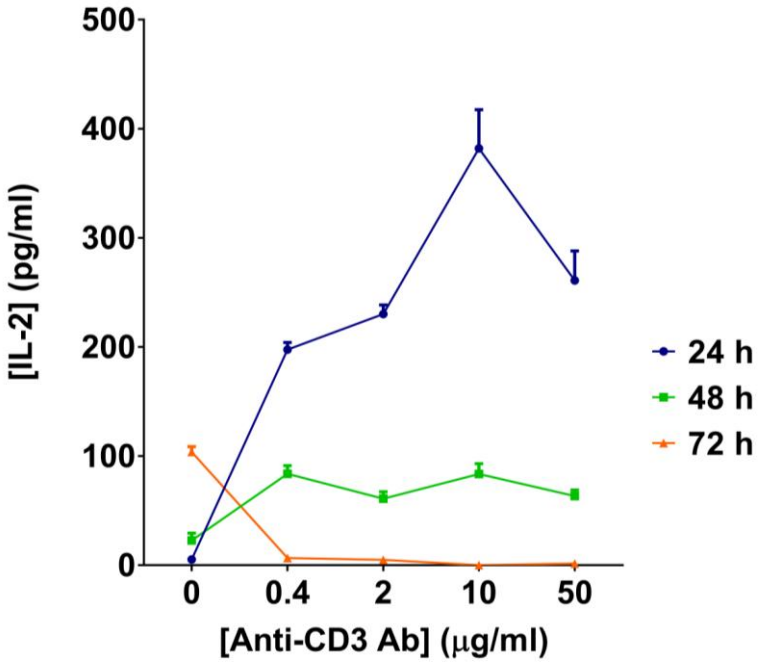


Figure 5.2: Anti-CD3 antibody titration assay. IL-2 ELISA performed with TCS from hPD-1 k.i. mouse splenocytes incubated for various times, 24, 48, 72 h with different levels of anti-CD3 antibody stimulation. Data points shown are means of duplicates ± SEM. Data are representative of two independent experiments.

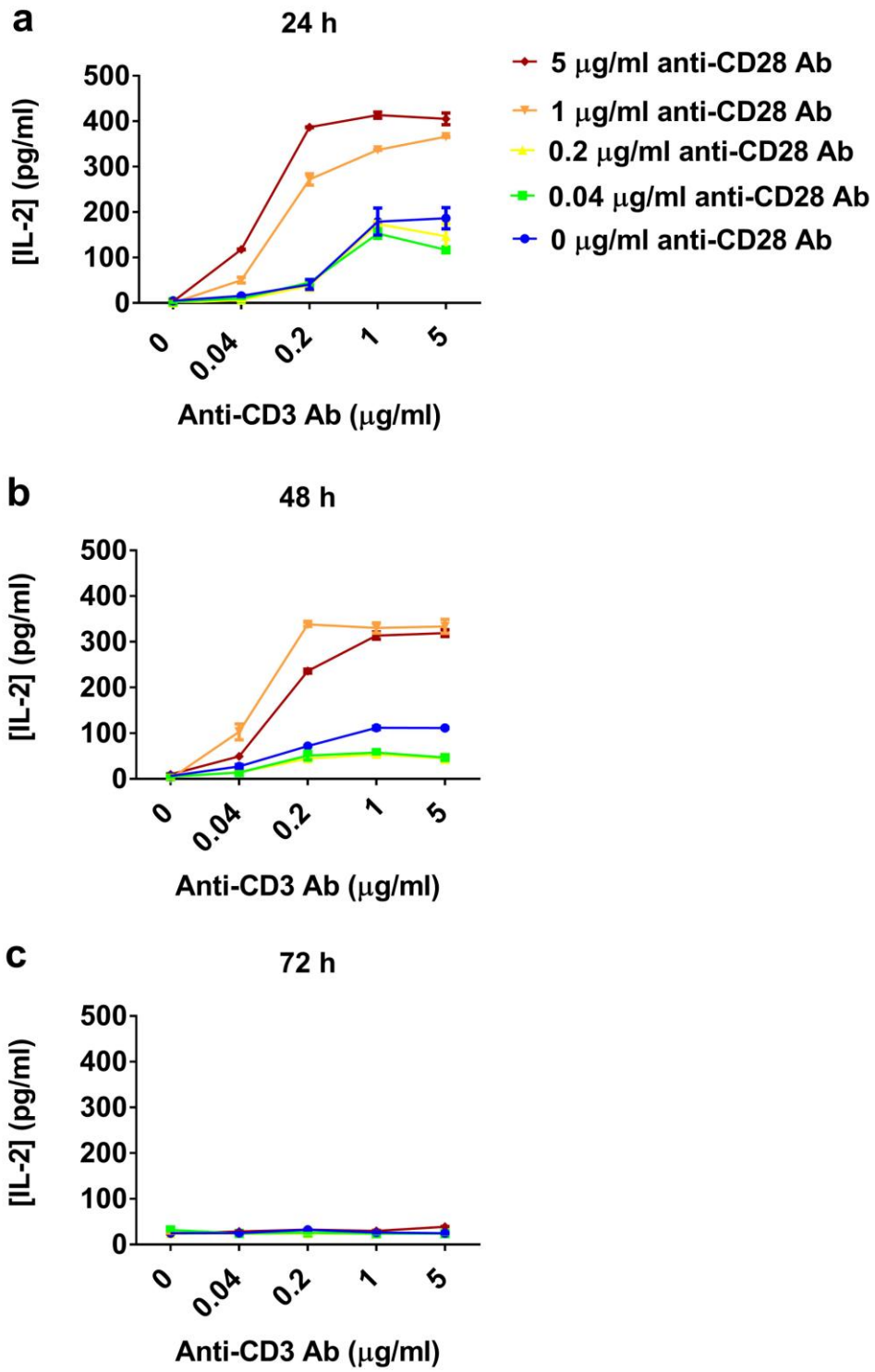


Figure 5.3: IL-2 ELISA performed with TCS from hPD-1 k.i. mouse splenocytes incubated for various times; (**a**) 24 h, (**b**) 48 h, or (**c**) 72 h with different levels of anti-CD3 and anti-CD28 antibody stimulation. Data points shown are means of duplicates ± SEM. Data are representative of two independent experiments.

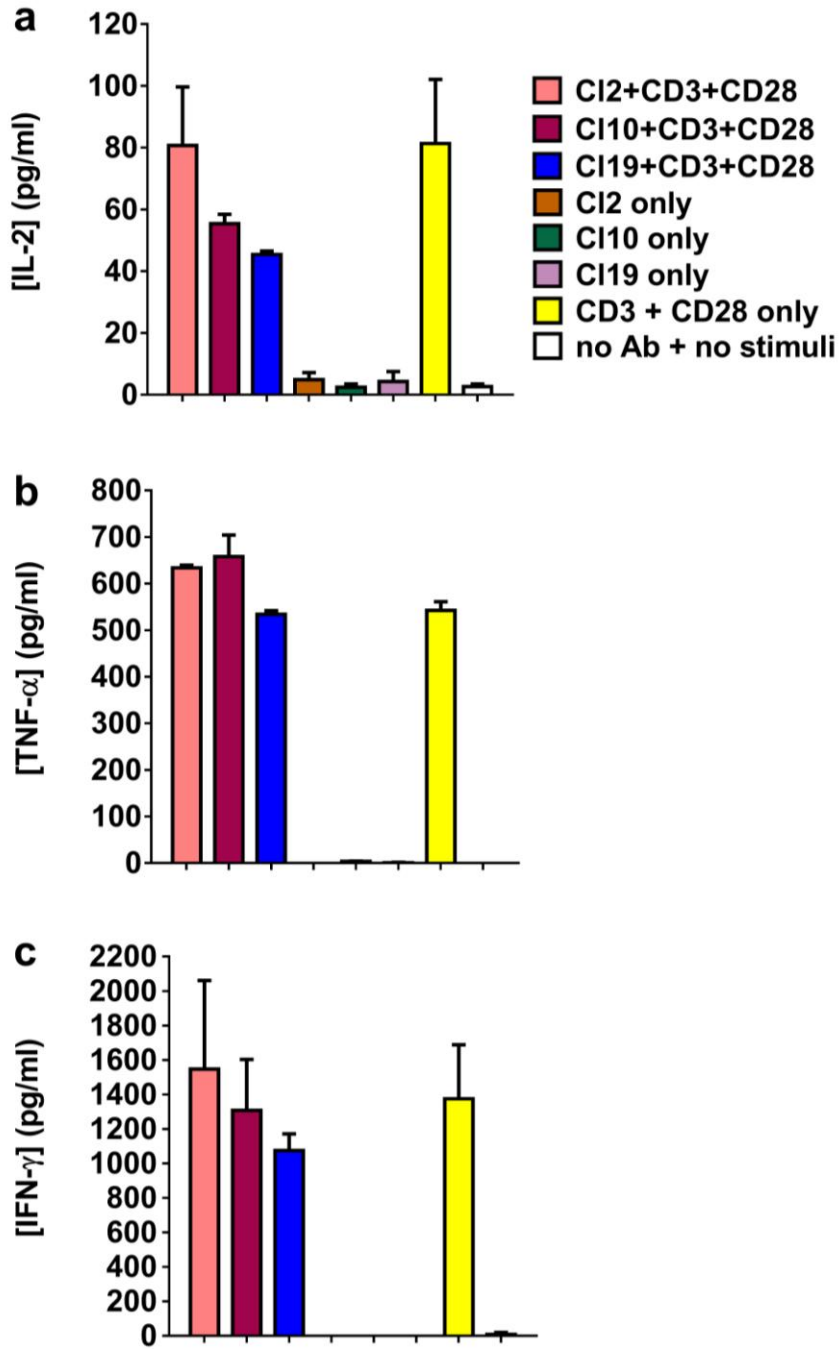


Figure 5.4: Anti-mouse (**a**) IL-2, (**b**) TNF-α or (**c**) IFN-γ ELISAs to test for suppressive effects on cytokine production induced by anti-PD-1 antibodies on hPD-1 k.i. splenocytes *in vitro*. A stimuli combination of anti-CD3 antibody (2 μg/ml) and anti-CD28 antibody (2 μg/ml) were applied for 2 h prior to anti-PD-1 antibody incubation (25 μg/ml). ELISA performed using TCS, following 48 h incubation with anti-PD-1 antibodies. Data points shown are means of duplicates ± SEM. Data are representative of three independent experiments.

production (Figure 5.4b,c). Cl2 did not show suppressive effects on either IL-2, IFN-γ or TNF-α production in this assay.

II.C. Effects of 2nd generation antibodies and antibody combinations on cytokine production

Single antibodies and combinations of anti-PD-1 antibodies were used to test for synergistic effects on cytokine suppression by hPD-1 k.i. mouse splenocytes *in vitro*. The hPD-1 k.i. mouse splenocyte mixtures were employed in suspension with the anti-PD-1 antibodies added in solution to mimic the situation of antibody presentation *in vivo*. Once again, IL-2 ELISA was performed using TCS collected from the hPD-1 k.i. splenocytes incubated with anti-PD-1 antibodies for 48 h (Figure 5.5). A stimuli combination of anti-mouse CD3 and anti-mouse CD28 antibodies were applied for 2 h prior to anti-PD-1 antibody incubation (Figure 5.5). In these experiments, the 1st generation and the Cl19 fast off-rate derivatives were tested (Figure 5.5).

Combinations of anti-PD-1 antibodies were also used to test for synergistic effects on cytokine suppression by hPD-1ki mouse splenocytes. In the IL-2 production assay, the fast off-rate Cl19 antibodies FoR1 ($p<0.01$) and FoR2 (Figure 5.5b) did not induce as much significant IL-2 suppression as 1st generation Cl19 antibodies (all with $p<0.0001$) (Figure 5.5a) compared to the Cl19 isotype control antibody following strong stimulation with anti-CD3 (2 μg/ml) and anti-CD28 antibody (2 μg/ml) (Figure 5.5, Table 5.1). It seemed that the FoR antibodies were not very active on their own *in vitro* following high anti-CD3 and anti-CD28 antibody stimulation. Out of the 1st generation anti-PD-1 antibodies, Cl10 showed the strongest inhibitory effect (Figure 5.5a, Table 5.1). The Cl19+Cl2, Cl2+FoR1 and Cl2+FoR2 combinations (Figure 5.5c) did, however, show some synergy in IL-2 suppression, but only at high anti-PD-1 antibody concentrations. The Cl10+FoR1 ($p<0.0001$) combination gave the strongest inhibitory effects, and the Cl10+FoR2 combination showed some synergy in producing significant effects at intermediate

concentrations ($p<0.0001$) (Figure 5.5d). Statistical significance which corresponded to Figure 5.5 was determined with a two-way ANOVA, performed with Bonferroni correction (Table 5.1).

These experiments were performed using rather high levels of stimulation: 2 μg/ml anti-CD3 mouse antibody along with anti-CD28 antibody at 2 μg/ml. In case the levels of activation provided were too strong and therefore masked the inhibitory effects of our anti-PD-1 antibodies on the hPD-1 k.i. mouse splenocytes, the anti-CD3 antibody concentration was once again titrated out to narrow down the critical level of anti-CD3 antibody stimulation needed to give the best chance of observing a reduction in IL-2 production; IFN-γ cytokine production in the presence of anti-PD-1 antibodies was also tested (Figure 5.6). For these anti-CD3 antibody titration experiments, anti-PD-1 antibodies were applied at 60 μg/ml and the ELISA was performed following 48 h of incubation with anti-PD-1 antibodies. The experiments showed that, overall, the largest suppressive effects of the anti-PD-1 antibodies on IL-2 (Figure 5.6a) or IFN-γ production (Figure 5.6b) occurred at relatively low levels of anti-CD3 antibody stimulation (0.25 and 0.5 μg/ml).

Following from the anti-CD3 antibody titration, a low level of CD3 stimulation of 0.5 μg/ml was subsequently used alongside the anti-CD28 antibody (2 μg/ml; Figure 5.7, Table 5.2). The results obtained from these IL-2 ELISAs were broadly consistent with those obtained at the higher level of anti-CD3 antibody. Generally, larger effects were observed for 0.5 μg/ml compared to 2 μg/ml. A dose dependent effect was seen with Cl19 ($p<0.0001$), FoR1 ($p<0.001$) and FoR2 ($p<0.001$) with respect to significantly inhibiting IL-2 production compared to Cl19 isotype control. Moreover, the 2nd generation Cl19 antibodies and Cl19 seemed to inhibit IL-2 production in a similar manner at the highest concentration of 90 μg/ml. In terms of synergy, Cl19 and Cl2 generated synergistic effects for IL-2 suppression even at low concentrations whilst Cl2+FoR1 and Cl2+FoR2 showed synergy only at high concentrations (Figure 5.7c). Again, consistent with the high-stimulation data, the fast off-rate combination

antibodies, *i.e.* Cl10+FoR1 gave the greatest synergistic effects at reducing IL-2 production, with Cl10+FoR2 also showing some synergy at the highest concentration (Figure 5.7d). Statistical significance which corresponded to Figure 5.7 was determined with a two-way ANOVA, performed with Bonferroni correction (Table 5.2).

II.D. Effects of different types of immobilisation on IL-2 suppression

In order to optimise the IL-2 ELISA assay to further examine the suppressive effects of the anti-PD-1 antibodies *in vitro,* we sought new ways to more effectively present the inhibitory antibodies to the hPD-1 k.i. cells in order to produce enhanced immunosuppression.

In the first approach, the stimulating antibodies were added to the plate for 2 h followed by washing with PBS, and then incubating with anti-PD-1 antibody overnight. In another method, both the stimuli and the inhibitory Cl19 antibody were added all together overnight for binding to the plate. Finally, a secondary antibody, namely donkey anti-mouse IgG (DAM) antibody, which is able to bind to all of the anti-PD-1 antibodies, was added alongside the stimulating antibodies overnight, after which the anti-PD-1 antibody was added for 2 h prior to the assay (the "DAM" method). It seemed that by adsorbing DAM antibody to the plate prior to adding Cl19, greater deliverance of PD-1 signalling could be produced, causing a greater reduction in IL-2 production to be observed (Figure 5.8).

We next compared the effects of the 1st generation anti-PD-1 antibodies and the 2nd generation antibodies in the solid-phase assay using the DAM method. Negative control antibodies included both Cl19 IgG1 isotype control and the commercial MOPC21 antibody. MOPC21 is a mouse IgG1/kappa monoclonal antibody frequently used as an isotype control. A low concentration of anti-PD-1 antibodies was chosen initially (30 μg/ml). At anti-CD3 antibody stimulation of 1 μg/ml, Cl10, Cl19 and FoR1 reduced the IL-2 levels by more than half (Figure 5.9a). At higher

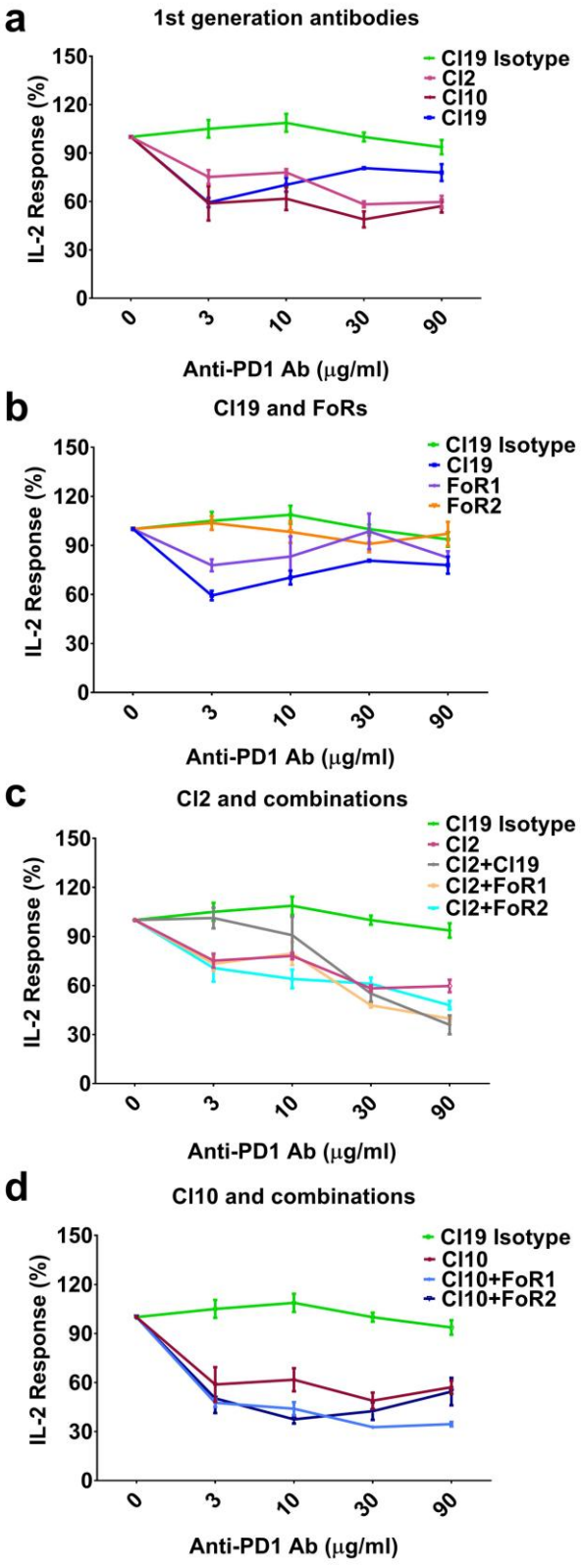


Figure 5.5: Mouse IL-2 suppression with (**a**) & (**b**) single, or (**c**) & (**d**) combinations of anti-PD-1 1st and 2nd generation antibodies *in vitro using* strong stimuli. A stimuli combination of anti-CD3 antibody (2 μg/ml) and anti-CD28 antibody (2 μg/ml) were applied first for 2 h prior to anti-PD-1 antibody incubation with hPD-1 k.i. splenocytes. ELISAs performed using TCS 48 h after incubation with anti-PD-1 antibodies. For the anti-PD-1 antibody combinations, 3, 10, 30, 90 μg/ml of each anti-PD-1 antibody was applied. IL-2 Response (%) displayed are the percentages of IL-2 production compared to stimulation alone. Cl19 isotype antibody used as the control. Data points shown are means of duplicates ± SEM. Data are representative of two independent experiments.

Table 5.1: Statistical analysis for the corresponding Figure 5.5. Statistical significance was determined with a two-way ANOVA, performed with Bonferroni correction.

Comparison with Cl19 isotype	Summary	Adjusted p value
1st generation antibodies		
Cl2	****	<0.0001
Cl10	****	<0.0001
Cl19	****	<0.0001
Cl19 and FoRs		
Cl19	****	<0.0001
FoR1	**	<0.01
FoR2	ns	0.9396
Cl2 and combinations		
Cl2	****	<0.0001
Cl2+Cl19	****	<0.0001
Cl2+FoR1	****	<0.0001
Cl2+FoR2	****	<0.0001
Cl10 and combinations		
Cl10	****	<0.0001
Cl10+FoR1	****	<0.0001
Cl10+FoR2	****	<0.0001

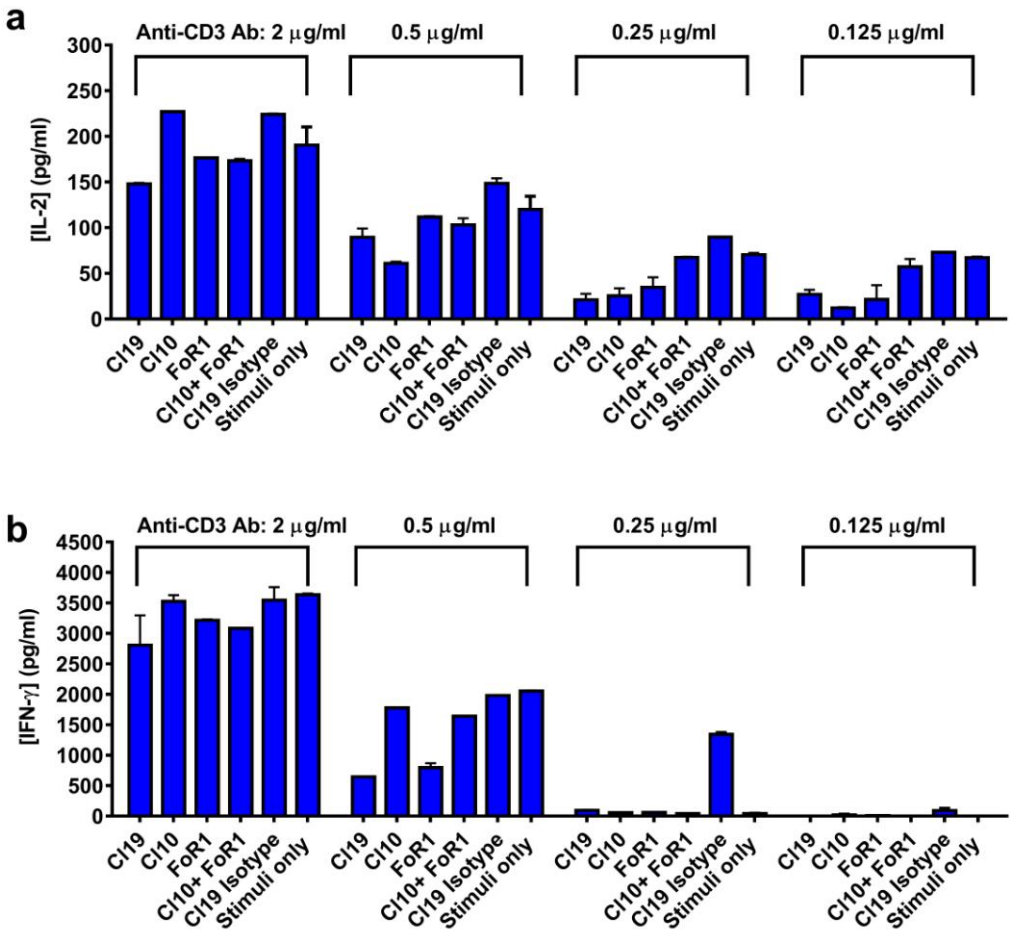


Figure 5.6: Cytokine suppression ELISAs to test for anti-CD3 antibody titration. (**a**) Anti-mouse IL-2 ELISA or (**b**) anti-mouse IFN-γ ELISA performed on hPD-1 k.i. mouse splenocytes stimulated with anti-CD3 and anti-CD28 antibodies. Anti-PD-1 antibodies (60 μg/ml each) were incubated for 48 h to test for immunosuppressive activity. For TCR stimulation, a range of anti-CD3 antibodies were used: 2, 0.5, 0.25, 0.125 μg/ml, alongside costimulation *via* anti-CD28 antibody at 2 μg/ml. Cl19 isotype control antibody at 60 μg/ml was used. Data points shown are means of duplicates ± SEM. Data are representative of two independent experiments.

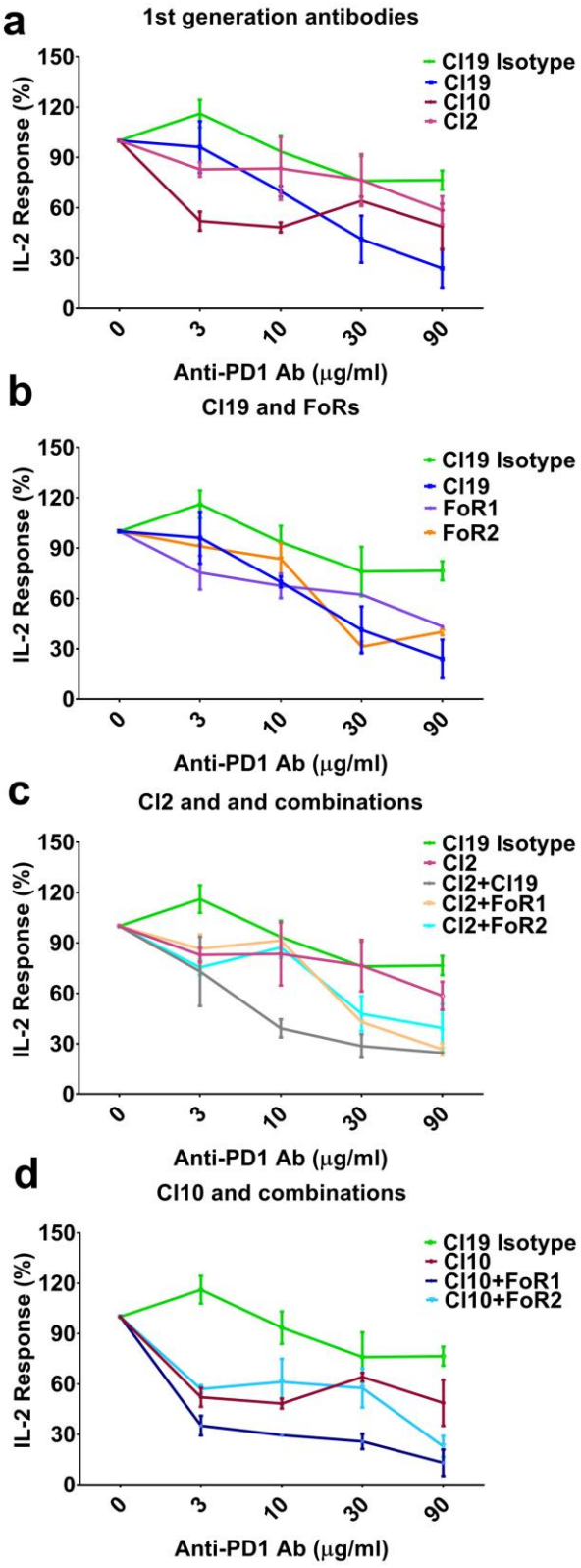


Figure 5.7: Mouse IL-2 suppression with (**a**) & (**b**) single, or (**c**) & (**d**) combinations of anti-PD-1 1st and 2nd generation antibodies *in vitro* with low stimulation of anti-CD3 antibody (0.5 μg/ml) and anti-CD28 antibody (2 μg/ml) stimulation. Anti-CD3 antibody and anti-CD28 antibody were applied first for 2 h prior to anti-PD-1 antibody incubation with hPD-1 k.i. splenocytes. ELISAs performed using TCS from hPD-1 k.i. splenocytes 48 h after incubation with anti-PD-1 antibodies. For the anti-PD-1 antibody combinations, 3, 10, 30, 90 μg/ml of each anti-PD-1 antibody was applied. IL-2 Response (%) displayed are the percentages of IL-2 production compared to stimulation alone. Cl19 isotype antibody used as the control. Data points shown are means of duplicates ± SEM. Data are representative of two independent experiments.

Table 5.2: Statistical analysis for the corresponding Figure 5.7. Statistical significance was determined with a two-way ANOVA, performed with Bonferroni correction.

Comparison with Cl19 isotype	Summary	Adjusted p value
1st generation antibodies		
Cl2	ns	0.1639
Cl10	****	<0.0001
Cl19	***	0.0004
Cl19 and FoRs		
Cl19	****	<0.0001
FoR1	***	<0.001
FoR2	***	<0.001
Cl2 and combinations		
Cl2	ns	0.1545
Cl2+Cl19	****	<0.0001
Cl2+FoR1	***	0.0008
Cl2+FoR2	**	0.0011
Cl10 and combinations		
Cl10	****	<0.0001
Cl10+FoR1	****	<0.0001
Cl10+FoR2	****	<0.0001

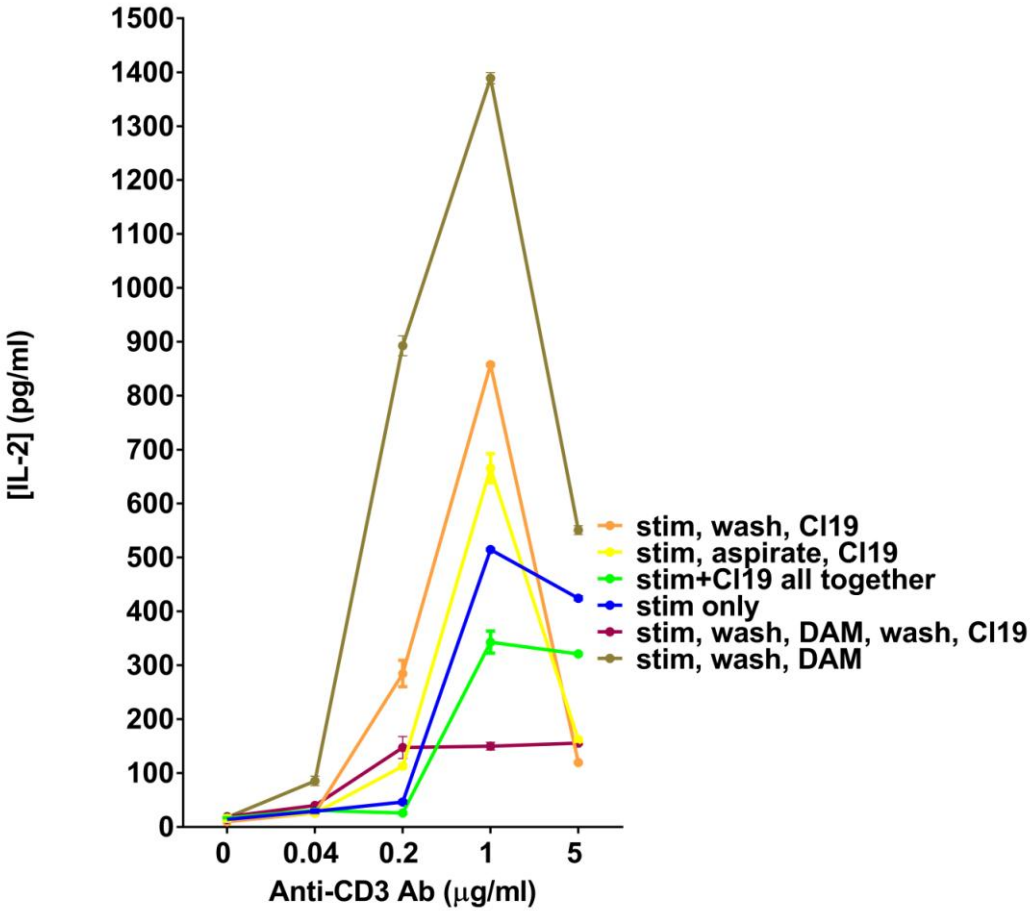


Figure 5.8: IL-2 immunosuppression with different forms of antibody immobilisation. IL-2 ELISAs performed with TCS from hPD-1 k.i. mouse splenocytes incubated for 48 h, following 2 h stimulation using varying levels of anti-CD3 and constant level of anti-CD28 antibody stimulation (1 μg/ml). Cl19 antibody at 100 μg/ml and DAM antibody at 500 μg/ml were utilised. Data points shown are means of duplicates ± SEM. Data are representative of two independent experiments.

levels of anti-CD3 antibody, *i.e.* 5 μg/ml, the suppressive effects of the anti-PD-1 antibodies were not as prominent, with Cl10 and CL19 appearing to be strongest at suppressing IL-2 production (Figure 5.9a). When we increased the concentration of the anti-PD-1 antibodies from 30 μg/ml to 100 μg/ml, a greater level of IL-2 suppression could be achieved (Figure 5.9b). The greatest reduction in IL-2 suppression compared to stimulation alone was observed for 1 μg/ml of anti-CD3 stimulation with Cl10 and Cl19 being the most potent at reducing IL-2 production (Figure 5.9b). Importantly, FoR1 gave similar levels of inhibition of IL-2 production at the higher levels of anti-PD-1 antibody immobilization.

II.E. Suppression of proliferation with single immobilised anti-PD-1 antibodies

Several assays exist for monitoring lymphocyte division. These include [(3)H]thymidine incorporation and carboxyfluorescein succinimidyl ester (CFSE) dilution. The disadvantages of using [(3)H]thymidine include difficulties in differentiating between different populations of cells as well as labelled and unlabelled cells in co-culture experiments. In contrast, because it is a fluorescein-based dye, CFSE allows for the use of multi-colour flow cytometry, therefore simultaneous analysis of different T-cell subsets can be performed [360]. CFSE is able to covalently label long-lived intracellular molecules with its fluorescent moiety, carboxyfluorescein. Therefore, when a CFSE-labelled cell undergoes cell division, its progeny carry with them half the number of carboxyfluorescein-tagged molecules. It is an ideal dye to measure cell division because CFSE has low cell toxicity and can label lymphocyte populations with a high fluorescent intensity with extremely low variance [361].

Anti-PD-1 k.i. mouse splenocytes were harvested and incubated with plate bound anti-CD3 (0.5 μg/ml) and anti-CD28 (2 μg/ml) antibodies in solution, and then CFSE labelled. Anti-PD-1 antibodies were added together at T0 (immediately after CFSE labelling) or 18 h (T18) later, to test for CFSE-based cell proliferation

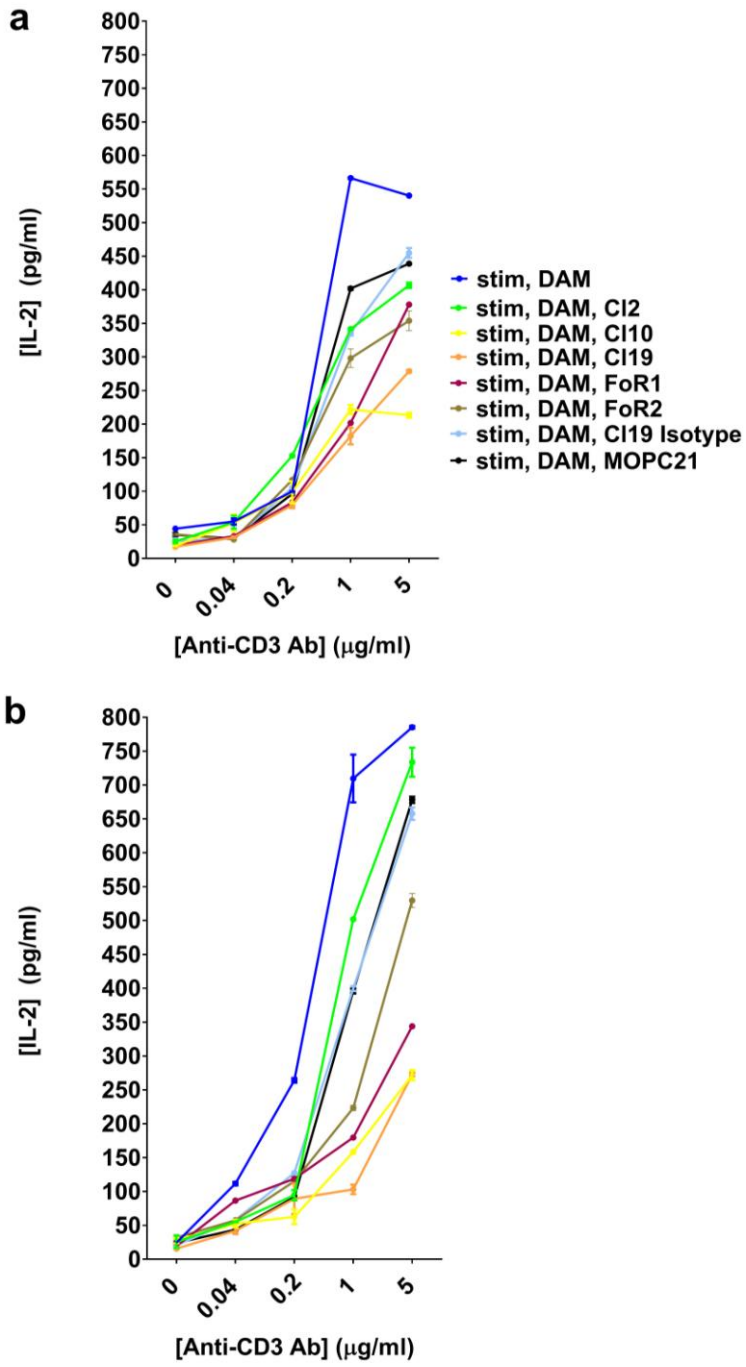


Figure 5.9: IL-2 immunosuppression in hPD-1 k.i. splenocytes stimulated with anti-CD3 (0, 0.04, 0.2, 1, 5 μg/ml) and anti-CD28 antibody (1 μg/ml) for 2 h, DAM (500 μg/ml) treated overnight and then 2 h incubation with anti-PD-1 antibodies (**a**) (30 μg/ml) or (**b**) (100 μg/ml) the next day. IL-2 ELISAs performed with TCS 48 h post stimulation. Cl19 isotype antibody and MOPC21 antibody were used as controls. Data points shown are means of duplicates ± SEM. Data are representative of two independent experiments.

suppression *in vitro*. After 72 h incubation of antibodies with the hPD-1 k.i. splenocytes, analysis by flow cytometry was conducted by gating on $CD4^+$ and $CD8^+$ T cells. Although the levels of proliferation were relatively low overall, of the single PD-1 antibodies, FoR2 gave the most reduction in '>5' and '5 rounds' of proliferation as well as having the largest fraction of 'non-proliferated' $CD4^+$ T cells at T0 and T18 compared to all other anti-PD-1 antibodies (Figure 5.10). Similarly, FoR2 seemed to have the largest fraction of 'non-proliferated' cells at both T0 and T18 time points for $CD8^+$ T cells assayed in this way, for which the overall levels of proliferation were much higher (Figure 5.11). These data further indicate that the FoR2 antibody had activity inhibiting T cell proliferation. However, the results also show that the effects of the antibodies on proliferation are relatively small.

II.F. Suppression of proliferation with combinations of immobilised anti-PD-1 antibodies

Combinations of anti-PD-1 antibodies were also added to hPD-1 k.i. splenocytes to test for suppression of cell proliferation. Flow cytometry was conducted and the T cells were gated on $CD8^+$ T cells. With respect to the Cl2 antibody combinations, some slight synergistic effects were observed compared to Cl2 antibody alone, since there were slight increases in the fraction of $CD8^+$ T cells that had not proliferated (Figure 5.12a). However, with the Cl10 combinations, only the Cl10+FoR1 combination increased the fraction of $CD8^+$ T cells that had not proliferated (Figure 5.12b). This was consistent with the synergistic inhibitory effects of the soluble Cl10+FoR1 (Figures 5.7d).

II.G. IL-2 production in the solid-phase assay

To understand why the limited cell proliferation inhibition may have occurred, mouse cytokine ELISAs were performed on the TCS from the proliferation assay (Figure 5.13). The ELISAs suggested that FoR2 ($p<0.01$, at T0) and FoR1 individually suppressed IL-2 production the most compared to the other single 1st generation antibodies (Figure 5.13a). Cl2 combinations surprisingly increased IL-2

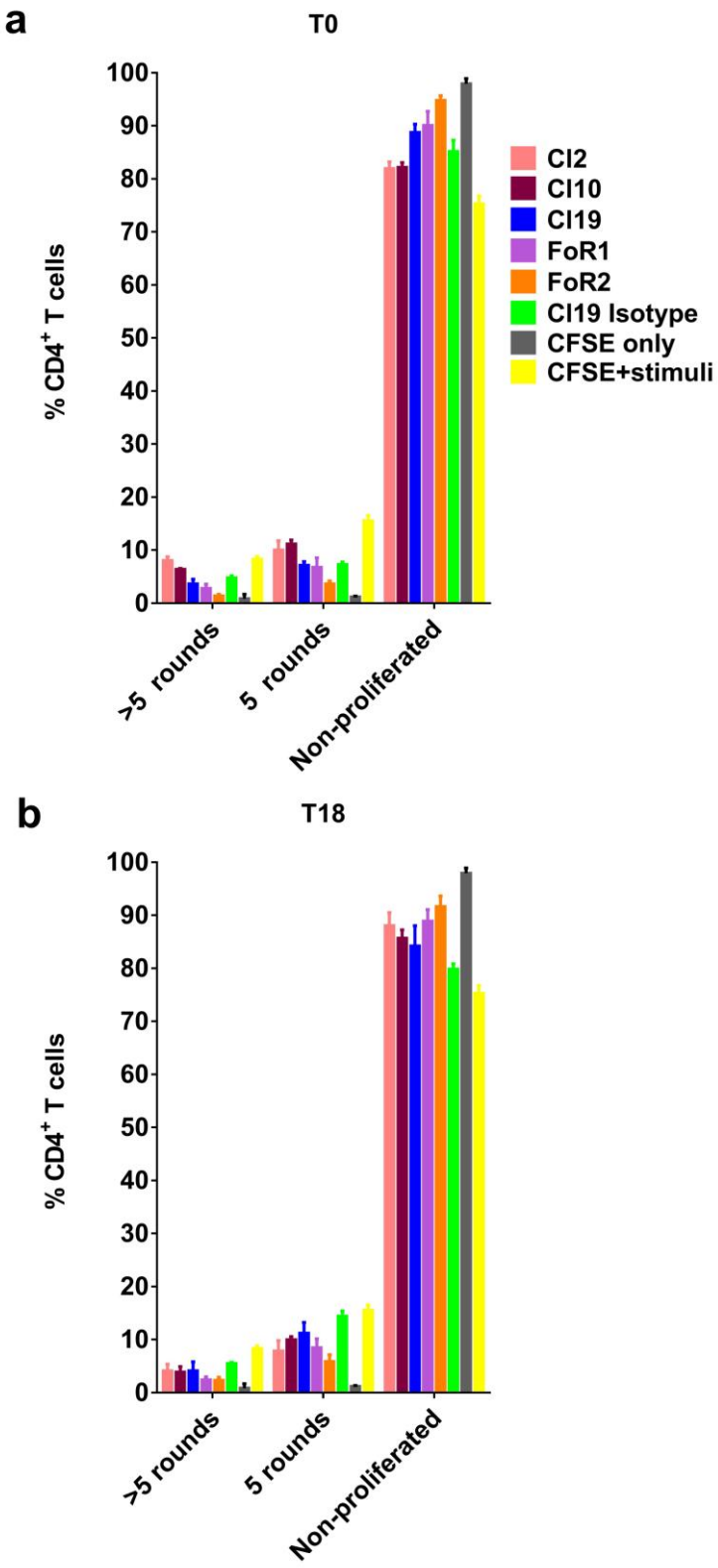


Figure 5.10: Suppression of CFSE-based cell proliferation with single 1st and 2nd generation anti-PD-1 antibodies *in vitro*. Flow cytometry was conducted. hPD-1 k.i. mouse splenocytes were gated on $CD4^+$ T cells. Cells were categorised into non-proliferated, 5 rounds and >5 rounds of proliferation depending on the CFSE levels. Anti-PD-1 antibodies (30 µg/ml) were added together at (**a**) T0 (immediately after CFSE labelling) or (**b**) 18 h (T18) later. Cl19 isotype antibody was used as the control (30 µg/ml). Data points shown are means of duplicates ± SEM. Data are representative of two independent experiments.

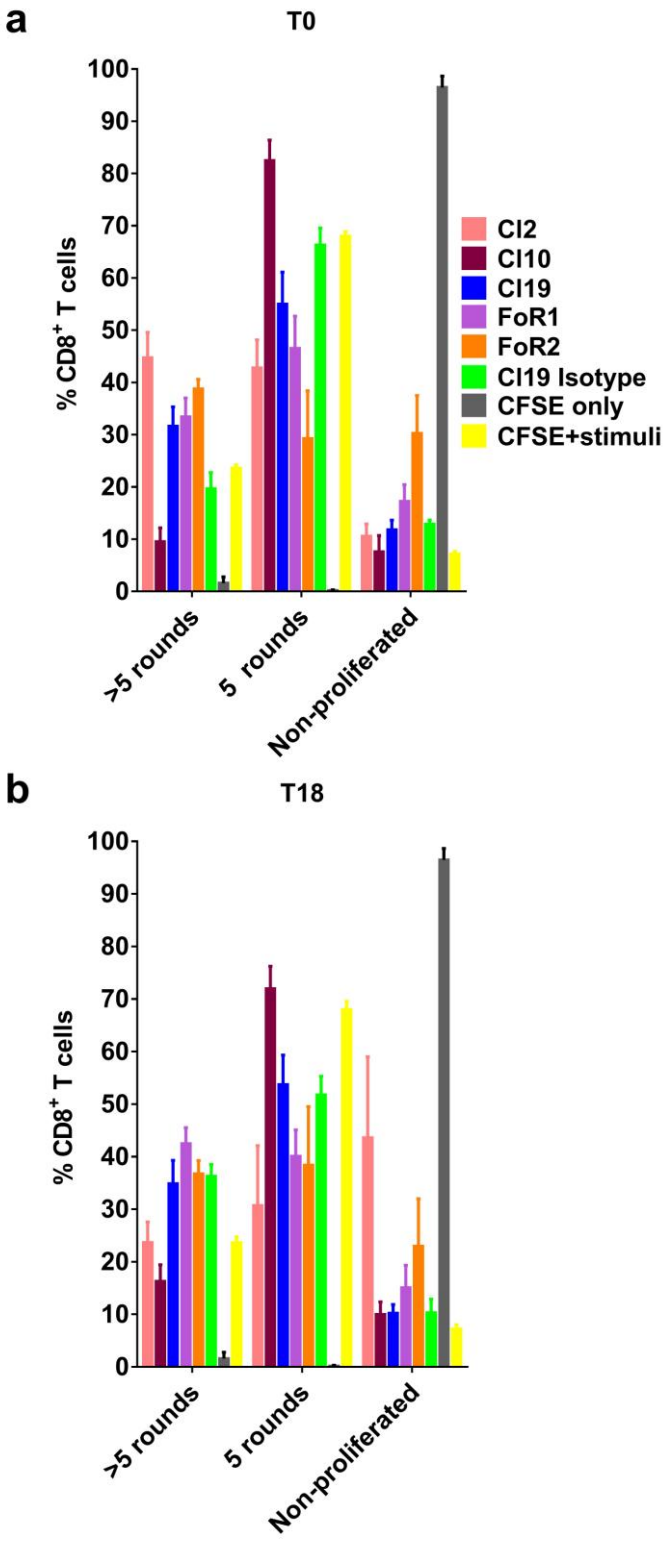


Figure 5.11: Suppression of CFSE-based cell proliferation with single 1st and 2nd generation anti-PD-1 antibodies *in vitro*. Flow cytometry was conducted. hPD-1 k.i. mouse splenocytes were gated on $CD8^+$ T cells. Cells were categorised into non-proliferated, 5 rounds, and >5 rounds of proliferation depending on the CFSE levels. Anti-PD-1 antibodies (30 µg/ml) were added together at (**a**) T0 (immediately after CFSE labelling) or (**b**) 18 h (T18) later. Cl19 isotype antibody was used as the control (30 µg/ml). Data points shown are means of duplicates ± SEM. Data are representative of two independent experiments.

production (Figure 5.13b) whilst Cl10 and both fast off-rate antibody combinations decreased IL-2 production (Figure 5.13c). Cl10 and FoR1 (T0) combination ($p<0.01$) was able to significantly reduce the IL-2 production when compared to Cl19 isotype control (Figure 5.13c). However, this latter effect was not due to synergism as the levels of IL-2 production were not lower than in the presence of FoR1 and FoR2 (Figure 5.13a).

III. Discussion

The work described in this chapter aimed to elucidate the inhibitory potential of anti-PD-1 agonist antibodies *in vitro* using several different approaches. From the anti-CD3 antibody titration experiments, it was clear that suppression of cytokine production by the anti-PD-1 antibodies was most observable at lower levels of anti-CD3 antibody stimulation (0.5 μg/ml). These data are in agreement with a previous study of PD-1/PD-L1 interactions [228] which revealed that the PD-1 pathway is more effective at low levels of TCR stimulation. Like the natural ligands of PD-1, anti-PD-1 agonists seem to exert their activity when relatively weak TCR signalling is delivered, as is probably the case *in vivo*. In order to fully activate the T cells, we found that it was necessary for costimulation using anti-CD28 antibodies to be included in the inhibition assays. Interestingly, a recent study by Hui *et al.* has revealed that perhaps, rather than suppressing signalling through the TCR, in fact, it may be that the co-receptor CD28 is strongly preferred over the TCR as a target for dephosphorylation by PD-1-recruited SHP-2 phosphatase [362]. Thus, PD-1 may suppress T cell function predominantly by the inactivation of CD28 signalling. Therefore, this indicates that the costimulatory pathways could play vital roles in controlling effector T cell function and responses to anti-PD-1/PD-L1 immunotherapy.

Using anti-PD-1 antibodies, we were able to demonstrate considerable suppression of cytokine production using mixtures of hPD-1 k.i. mouse splenocytes. Compared to TNF-α and IFN-γ ELISAs, IL-2 ELISAs exhibited greater reproducibility and

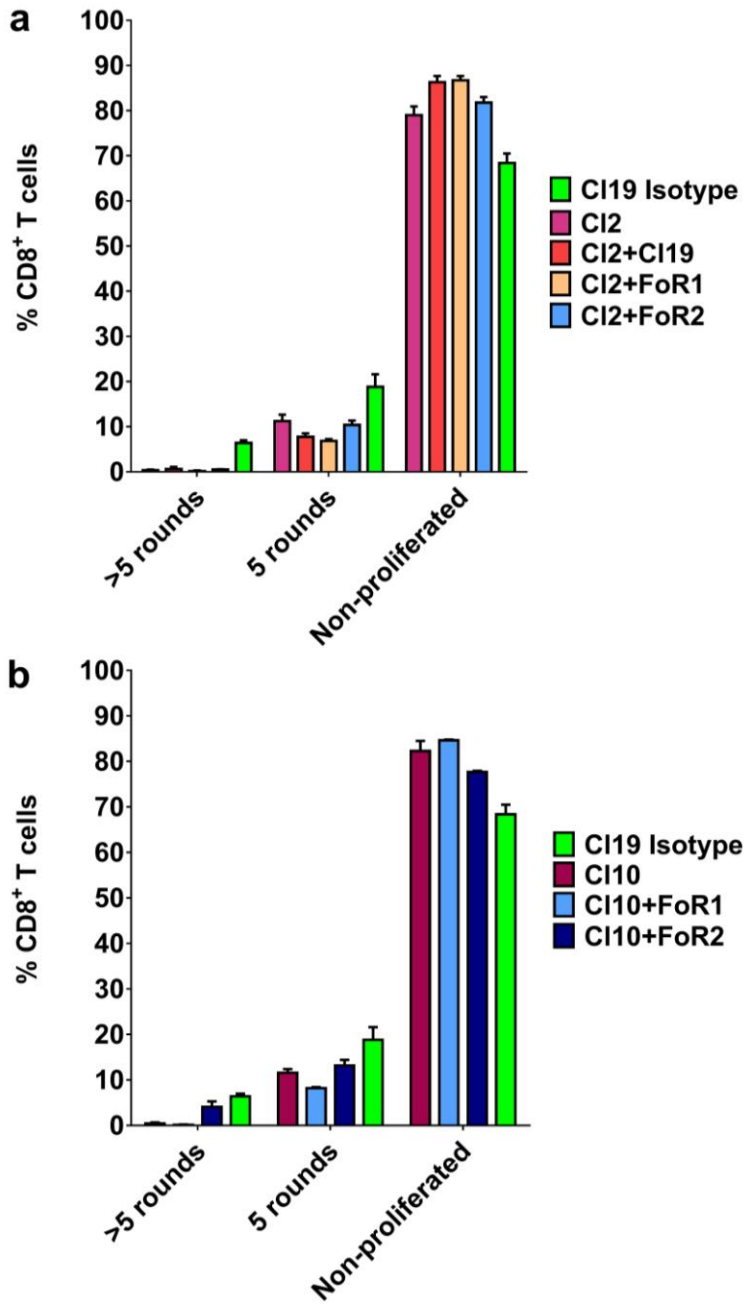


Figure 5.12: Suppression of CFSE proliferation with combinations of anti-PD-1 antibodies (30 μg/ml each) conducted using flow cytometry. hPD-1 k.i. mouse splenocytes were gated on $CD8^+$ T cells. Cells were categorised into non-proliferated, 5 rounds, and >5 rounds of proliferation depending on the CFSE levels. (**a**) Effects on suppression using Cl2 and combinations or (**b**) Cl10 and combinations, after 72 incubation are shown. Cl19 isotype antibody was used as the control (30 μg/ml). Data points shown are means of duplicates ± SEM. Data are representative of two independent experiments.

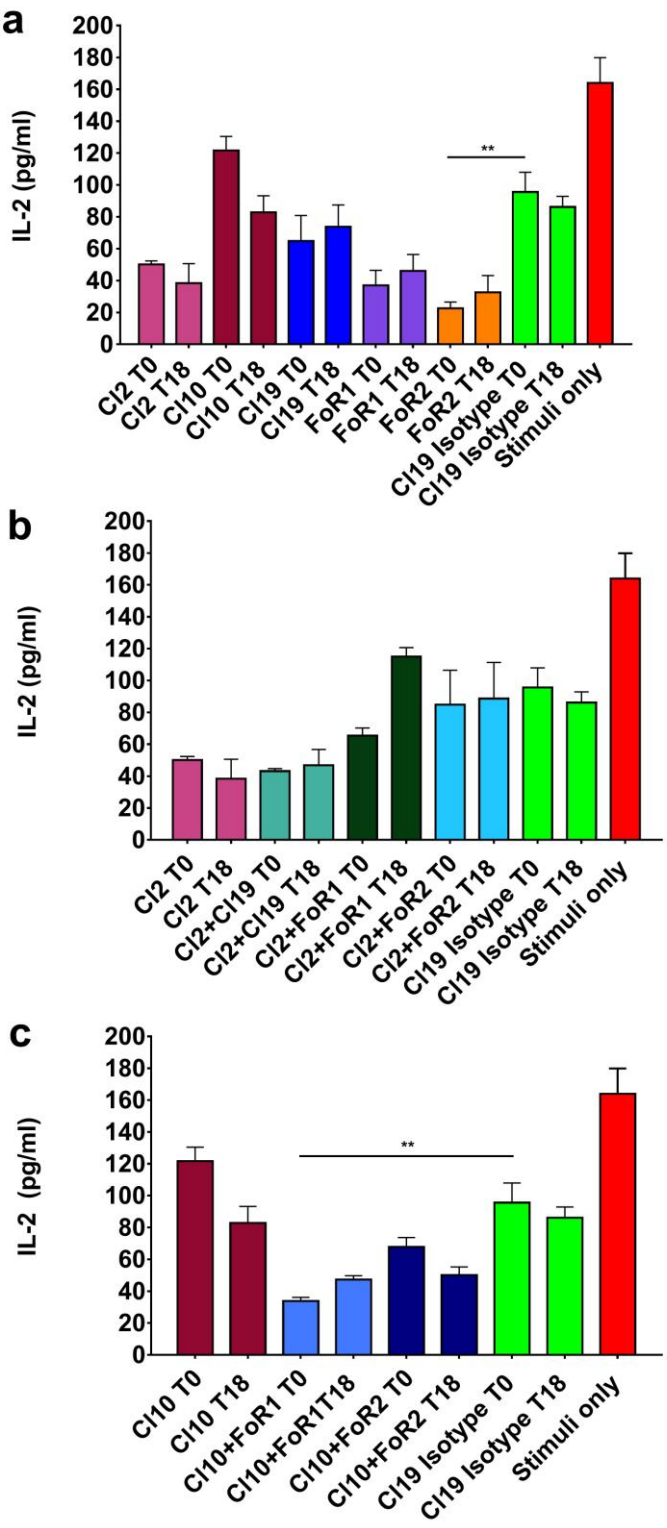


Figure 5.13: Suppressive effects of anti-PD-1 antibodies alone or in combination on IL-2 production by hPD-1 k.i. mouse splenocytes. IL-2 ELISAs performed using TCS from CFSE labelled hPD-1 k.i. mouse splenocytes following anti-CD3 antibody (0.5 µg/ml) and anti-CD28 antibody (2 µg/ml) stimulation, and single/combinations of anti-PD-1 antibody suppressive treatments at 30 µg/ml each: (**a**) single antibodies, (**b**) Cl2 and combinations, (**c**) Cl10 and combinations. Cl19 isotype control antibody at 30 µg/ml applied. Data points shown are means of duplicates ± SEM. Data are representative of two independent experiments. Statistical significance was determined with a one-way ANOVA, performed with Bonferroni correction (**$p<0.01$).

higher levels of suppression, hence we decided to mainly focus on this particular cytokine for further testing. IL-2 generation was also suitable as the principal read-out for superagonistic signalling since it is indicative of full T cell activation instead of sub-threshold signalling [363]. IL-2 is known to be one of the cytokines sensitive to effects produced through TCR triggering, CD28 costimulation and PD-1 cell surface receptor triggering [364].

Several different *in vitro* systems were set up to examine the effects of anti-PD-1 antibodies on cytokine production. Initially, hPD-1 k.i. mouse splenocyte mixtures were employed in suspension with the antibodies in a soluble form, to mimic the situation of antibody presentation *in vivo*. We also altered the way of presenting the agonising antibodies by immobilising them to a plate using secondary antibodies, since this could potentially cross-link more anti-PD-1 antibodies and therefore enhance downstream receptor triggering. Thus, suppression of T cell activation *via* the KS model of phosphatase exclusion from the PD-1 receptors could lead to prolonged phosphorylation of PD-1 and overall greater immune inhibition. Generally, we found that by adding greater levels of inhibitory anti-PD-1 antibodies, greater IL-2 suppression was observed, regardless of how the antibodies were presented, either in solution or plate bound. Moreover, the greatest synergistic effects were observed for the antibody combinations, also used at the highest concentrations. This suggested that synergy is greater when more anti-PD-1 antibodies were present, to ensure greater levels of PD-1 receptor engagement.

To observe inhibitory effects on cytokine production, suitable isotype control antibodies had to be employed. The Cl19 isotype antibody, which is a derivative of Cl19 mutated to prevent binding, was initially used. In most of the *in vitro* experiments, the Cl19 isotype appeared to be inactive, yet for some experiments, at high concentrations, Cl19 isotype showed some agonising activity. To address this issue, the MOPC21 IgG1 isotype antibody was also included as a control in later

experiments. The use of both isotype antibodies did not substantially alter the conclusions of the experiments.

Using the CSFE-based cell proliferation assay, we were also able to show that the anti-PD-1 antibodies were also able to weakly suppress cell proliferation *in vitro*. The inhibitory effects were not as large as those observed in the IL-2 ELISA assays. This may be due to the fact that PD-1 signalling has a greater effect on cytokine suppression, rather than on cell proliferation.

The *in vitro* data in this chapter gave us an insight into whether the new 2nd generation anti-PD-1 antibodies would be active as agonists, and encouraged us to undertake further testing *in vivo*, as will be discussed in Chapter 6.

Chapter 6
Analysis of the inhibitory effects of anti-PD-1 antibodies *in vivo*

I. Introduction

In order for clinical trials of novel immunotherapies to take place, preclinical studies are normally undertaken which involve *in vivo* models for the prediction of the effects of the candidate therapeutics on humans. Due to their ease of maintenance and short generation times, mouse models have been widely utilized in such studies. While human and mouse immune system elements resemble one another, there are however important differences between them. This is due to approximately 100 million years of divergent evolution that has occurred [365]. Therefore, non-human primate models are regarded as the best models for preclinical trials since they are evolutionarily closer to humans [366]. The limitations of non-human primate models are their high costs both financially and ethically, thus they are typically implemented just prior to the introduction of novel therapeutics into clinical trials. Additionally, there are differences between primate proteins and human counterparts, thus imposing another limitation on these models [367]. Ultimately, the need is high for the use of animal models that are robust, sensitive, reproducible, simple and cost-effective.

Mouse models are often created *via* the generation of transgenic mice. The main principle behind the "knock-in" mouse is the insertion of a transgene in a selected locus. This means that murine genes can be swapped with their human counterparts. This approach is highly useful and convenient since it allows the effects of the potential human therapeutics to be investigated directly in mice.

There are many recent examples of studies in which humanized mouse models were used to study the effects of antibodies *in vivo*, including blocking anti-human CTLA-4 antibodies, anti-coagulation tissue factor antibodies, and anti-human CD3ε antibodies [366-368].

In order to characterize the effects of our anti-human PD-1 antibodies *in vivo*, we out-sourced the generation of a humanized PD-1 k.i. mouse model. This mouse stably expresses the human PD-1 extracellular region along with the mouse PD-1 transmembrane and intracellular domains. The experiments described in this chapter have utilised this hPD-1 k.i. mouse for *in vivo* studies. As discussed in the Introduction, PD-1 plays key roles in a broad array of immune responses which include the germinal centre (GC) reaction, antibody responses, responses to acute and chronic infections as well as the allogeneic response [286]. We first used the humanized PD-1 k.i. mouse model and the putative PD-1 agonistic antibodies to examine the effects of the PD-1 pathway in the GC response to sheep red blood cells (SRBC).

Essentially, the GC reaction results in memory B cell formation and high affinity plasma cells that can be either short or long-lived *via* somatic hypermutation and isotype class switching events. These processes need to be tightly regulated since the ongoing mutation and proliferation of GC B cells could potentially lead to the development of autoimmunity if unchecked. PD-1 is a marker for follicular helper T (Tfh) cells [369], which are responsible for regulating high affinity B cell clone production in the GCs. It has been suggested that PD-1 is able to inhibit the TCR derived signals in the Tfh cells and also reduce Tfh cell activity [370].

GCs are structures that are generated transiently within peripheral lymphoid organs in response to T cell-dependent antigen. Within GCs, B cells that express high-affinity antibodies develop and these then differentiate into memory B cells that mediate and sustain protection against invading pathogens, and plasma cells that

secrete antibodies. The importance of the GC reaction is best demonstrated by the immunodeficiency syndromes that are manifested in patients who are incapable of GC formation [371]. Initiation of the GC reaction takes place through a coordinated cascade with various cell types that drive antigen-engaged B cells into the GC. Within the GCs, B cells proliferate at a rate that is otherwise unparalleled in mammalian tissues. Importantly, their immunoglobulin variable region (IgV) genes are diversified by somatic hypermutation [372]. It is indicative of the presence of effective selection processes within the GC that inferior antibody mutants or autoreactive ones are outcompeted by higher affinity antibodies. Usually, antigen-specific plasma cells and memory B cells appear within 1 week after encountering antigen [373].

It has been demonstrated that for chronic viral infections, there is a correlation between virus specific $CD8^+$ T cell exhaustion, increased viral load, and persistently high PD-1 expression [227]. Yet, PD-1's function in acute $CD8^+$ T cell driven responses is less well understood [374]. Investigations have shown that *in vitro* blockade of PD-1 or *in vivo* PD-1 deficiency generates a higher recall response following re-stimulation of effector $CD8^+$ T cells from the primary response using virus-specific peptides, implying that PD-1 signalling has an inhibitory effect on $CD8^+$ T cell memory generation [375, 376]. Using a heat inactivated modified vaccinia Ankara virus (MVA), we studied the suppressive effects of the anti-PD-1 antibodies on the functionality of $CD8^+$ T cells during a primary immune response.

Finally, the results from our *in vitro* experiments presented in Chapter 5 suggested that our anti-PD-1 antibodies induced PD-1 cell surface downregulation following receptor binding, thus we aimed to assess whether down-modulation of PD-1 would occur *in vivo* or not, and if so, how the different forms of the anti-PD-1 antibodies would behave. In particular, we wanted to know whether, by reducing the binding affinities in the 2nd generation antibodies, there might be less PD-1 cell surface receptor downregulation.

II. Results

II.A. Effects of single anti-PD-1 antibody administration on GC B cell formation following SRCB challenge

In order to investigate the effects of anti-PD-1 Cl19 antibody on GC B cell formation following SRBC challenge, homozygous hPD-1 k.i. mice (8-12 weeks of age) were immunized with SRBC intraperitoneally. Twenty-four hours post SRBC administration, the mice were treated intravenously with various doses of Cl19 or MOPC21 isotype control antibody. Seven days after SRBC administration, spleens and mesenteric lymph nodes were removed and blood was collected for measuring the antibody responses. Splenocytes were stained for $CD4^+$ T cells, $CD8^+$ T cells, Tfh cells ($CD4^+CD44^{hi}CXCR5^+$), GC B cells ($B220^+GL7^+CD95^+$), and total B cells ($B220^+$). Flow cytometry was conducted to investigate the ratio of GC B cells over total B cells in both the spleens and mesenteric lymph nodes of these hPD-1 k.i. mice (Figure 6.1). As we increased the amount of Cl19 administered to 20 mg/kg, compared to the PBS treated mice, the percentage of GC B cells over total B cells decreased significantly in the spleen ($p<0.05$), whilst in the mesenteric lymph nodes, there was no significant difference with differing levels of Cl19 antibody treatment (Figure 6.1).

II.B. SRBC challenge and inhibitory effects of anti-PD-1 antibodies on the GC response with a combination of anti-PD-1 antibodies

Since anti-PD-1 antibodies in combination showed some synergistic agonising effects *in vitro*, a combination of anti-PD-1 antibodies at 1 mg/kg was used to determine whether there were synergistic effects on the GC response following the SRBC challenge *in vivo* as measured by GC B cells as a percentage of total B cells (Figure 6.2a) and Tfh cell numbers (Figure 6.2b). Cl19 and Cl2 antibodies bind to different epitopes on PD-1. We predicted that the combination of these antibodies could allow for antibody cross-linking and thus enhance overall PD-1 signalling *in vivo*. However, we observed that the combination of Cl19 and Cl2 did not give an additive suppressive effect on the GC response after SRBC challenge compared to

the Cl19 isotype control antibody (Figure 6.2a). This was perhaps in part due to the fact that, overall, the dose of 1 mg/kg of intravenously administered anti-PD-1 antibodies was not high enough to induce substantial inhibition of the GC response.

Moreover, we wanted to confirm that the anti-PD-1 antibodies were not cytotoxic and determine whether any cytotoxic effects had ensued. The absolute Tfh cell numbers were measured and the results suggested that these antibodies were not cytotoxic. This was reflected by the similar Tfh cell numbers measured for the Cl19 isotype control, PBS, and anti-PD-1 antibody treated mice (Figure 6.2b).

II.C. The effects of anti-PD-1 Cl19 antibodies on the primary antibody response following SRBC challenge

The effects of intravenously administered Cl19 antibodies on the primary antibody response following intraperitoneal SRBC challenge in hPD-1 k.i. mouse was also examined. Nine days post SRBC immunization, sera was collected and anti-SRBC IgG and anti-SRBC IgM ELISA-based assays were conducted (Figure 6.3). These were performed using ELISA plates coated with glutaraldehyde fixed whole SRBC.

With increasing concentrations of Cl19 antibodies, the levels of anti-SRBC IgG antibodies (Figure 6.3a) did not reduce in a dose dependent manner whilst anti-SRBC IgM antibodies (Figure 6.3b) were suppressed slightly more at the higher levels of Cl19 antibody administration, although this did not reach statistical significance. This suggested that IgM antibody formation, a SRBC-specific primary antibody response, was perhaps inhibited *via* agonising the PD-1 signalling pathway using Cl19 antibodies. This would be consistent with the suppression of the GC B cells in the GC response (Figure 6.1).

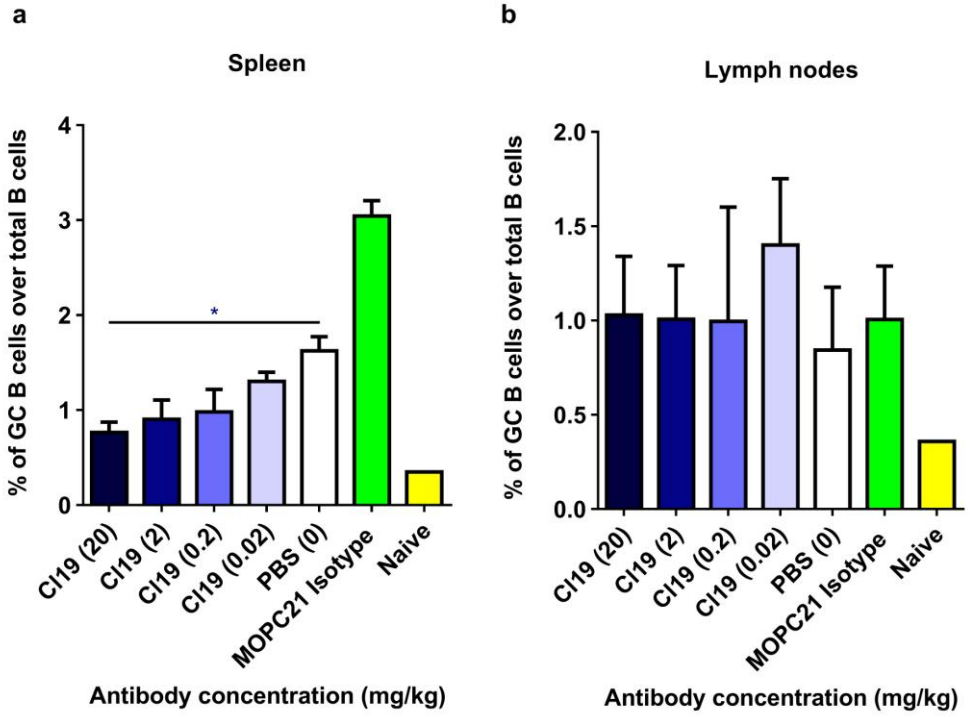


Figure 6.1: Effects of anti-PD-1 Cl19 antibody on GC response in hPD-1 k.i. mouse following SRBC challenge. Homozygous hPD-1 k.i. mice were immunised with SRBC intraperitoneally, and treated intravenously with varying concentrations of Cl19 antibodies (20, 2, 0.2, 0.02 mg/kg) or MOPC21 IgG1 isotype control antibody (20 mg/kg), 24 h after the SRBC injection. Seven days after SRBC injection, the GC response in the spleen and mesenteric lymph nodes was analysed using flow cytometry. Percentage of GC B cell numbers over total B cells in (**a**) spleen and (**b**) lymph nodes are shown. Data points presented are mean ± SEM. Statistical significance was determined with a one-way ANOVA, performed with Bonferroni correction (*$p<0.05$). Four mice were used per treatment group.

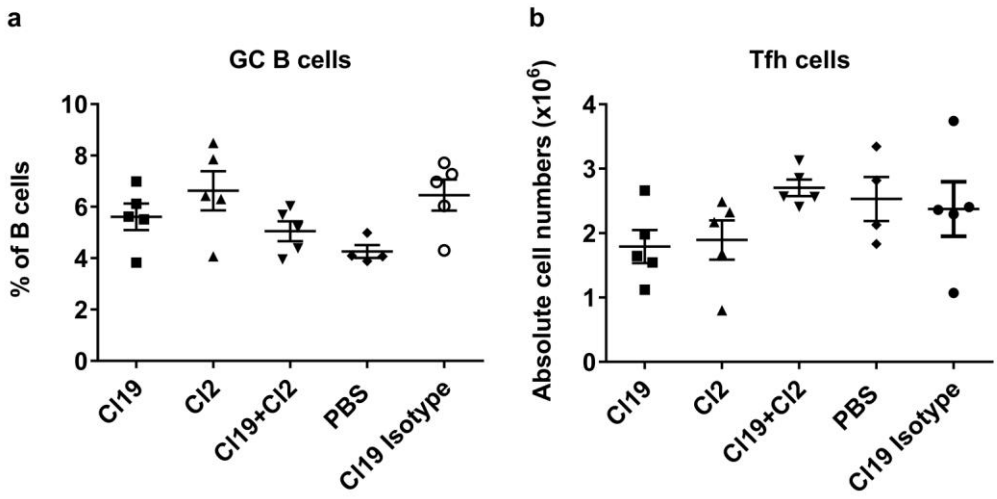


Figure 6.2: Effects of anti-PD-1 antibody combination on GC response in hPD-1 k.i. mouse following SRBC challenge. Homozygous hPD-1 k.i. mice were immunised with SRBC intraperitoneally, and treated intravenously with 1 mg/kg each of Cl19, Cl2, Cl2+Cl19 antibodies or Cl19 isotype control antibody, 24 h after the SRBC injection. Seven days post SRBC injection, the GC response in the spleen was analysed using flow cytometry. (**a**) Percentage of GC B cells over total B cells and (**b**) absolute numbers of Tfh cells are shown. Data points presented are mean ± SEM. Each symbol represents one mouse.

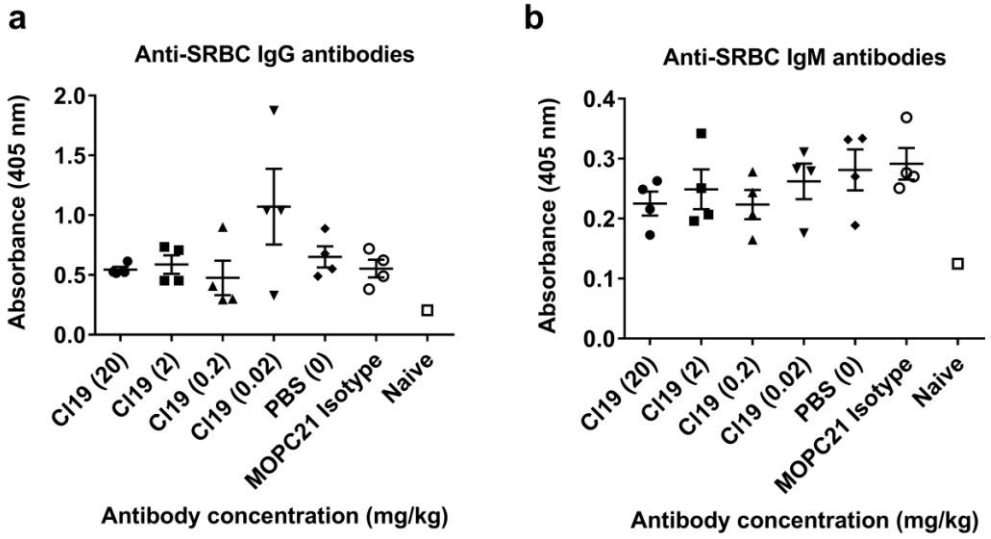


Figure 6.3: The effects of anti-PD-1 Cl19 antibody on the primary antibody response following SRBC challenge in hPD-1 k.i. mouse. (**a**) Anti-SRBC IgG and (**b**) anti-SRBC IgM ELISAs were performed using mouse serum following intraperitoneal SRBC and intravenous anti-PD-1 Cl19 antibody administration. Mouse sera was collected on day 9 post SRBC immunization. Production of the IgG and IgM class antibodies were detected using the appropriate secondary antibodies. Data points shown are mean ± SEM. Each symbol represents one mouse.

II.D. NP-CGG challenge and effects of anti-PD-1 antibodies on antibody affinity maturation

NP-conjugated chicken γ-globulin (NP-CGG) immunization of PD-1 k.i. mice was used to test the effects of anti-PD-1 antibodies on antibody affinity maturation (Figure 6.4, Table 6.1). The percentage of high-affinity (NP5-binding)/total (NP25-binding) IgG antibodies was used as an index for antibody affinity maturation. IgG NP5BSA and NP25BSA ELISAs were conducted at days 7, 14, 21 and 28 following NP-CGG and anti-PD-1 antibody intravenous administration at 1 mg/kg. These experiments were performed to assess the effects of anti-PD-1 antibodies on the primary and secondary immune responses. At day 21, compared to MOPC21, Cl19 appeared to weakly reduce the percentage of NP5 to NP25 IgG antibodies ($p<0.01$), but the effect was not sustained. Indeed, by day 28, Cl19 antibody administration appeared to significantly enhance the ratio of NP5 to NP25 IgG antibodies ($p<0.0001$) suggesting, overall, that Cl19 was unable to effectively suppress affinity maturation in the GC.

IgM NP25BSA ELISA following NP-CGG and anti-PD-1 antibody intravenous administration on hPD-1 k.i mice was also performed (Figure 6.5, Table 6.2). IgM levels peaked at day 7 and then reduced by day 14, returning to base level at day 28. Of the three 1st generation anti-PD-1 antibodies, compared to the MOPC21 isotype control antibody, Cl19 had the greatest effect on inhibiting IgM production at Day 7 ($p<0.001$) (Figure 6.5, Table 6.2).

II.E. Effects of anti-PD-1 antibody administration on cell surface PD-1 downregulation following SRCB challenge

Assays such as the SRBC immunization, which examine antigen specific antibody production, offer relatively comprehensive and sensitive assessment of immune function [377]. As described earlier in section A, following SRBC immunization intraperitoneally and anti-PD-1 Cl19 antibody intravenous treatment, 7 days post SRBC immunisation, blood samples were taken from the hPD-1 k.i. mice. Flow

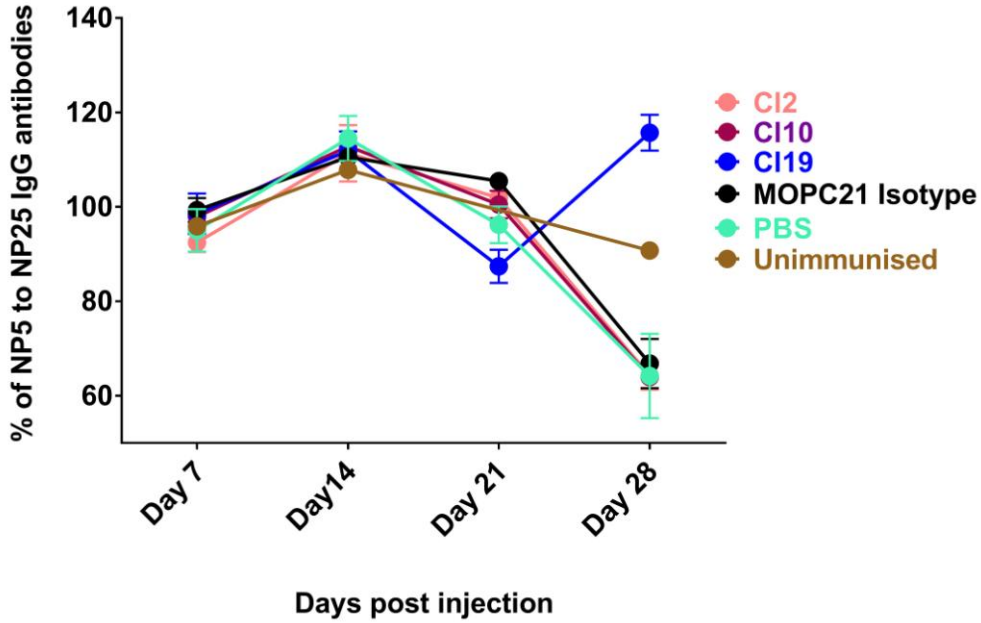


Figure 6.4: Effects of anti-PD-1 antibody administration on antibody affinity maturation. IgG NP5BSA and NP25BSA ELISAs were performed following NP-CGG immunization and anti-PD-1 antibody intravenous administration (1 mg/kg) on hPD-1 k.i. mice. MOPC21 IgG1 antibody used as an isotype control (1 mg/kg). Percentage of NP5 to NP25 IgG antibodies are shown. Data points presented are mean ± SEM. Four mice were used per treatment group.

Table 6.1: Statistical analysis for corresponding Figure 6.4. Statistical significance was determined with a two-way ANOVA, performed with Bonferroni correction.

Comparison with MOPC21 Isotype	Summary	Adjusted p value
Day 21		
Cl19	**	<0.01
Day 28		
Cl19	****	<0.0001

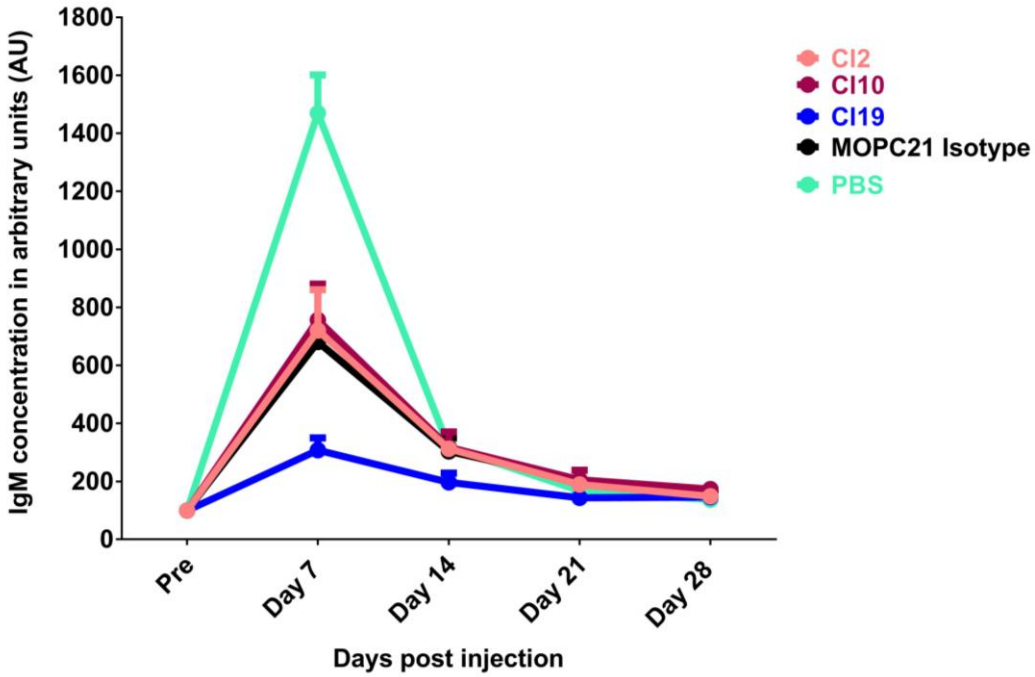


Figure 6.5: Effects of anti-PD-1 antibody administration on antibody affinity maturation. IgM NP25BSA ELISA was performed following NP-CGG and anti-PD-1 antibody intravenous administration on hPD-1 k.i. mice. Production of IgM class antibodies were detected using the appropriate secondary antibodies. At Day 7, Cl19 antibody treatment significantly reduced IgM levels compared to Cl2, Cl10 and MOPC21 isotype control. An internal standard, set at 1000 arbitrary units (AU) was used. The levels of IgM relative to the standard are displayed in AU. Data points shown are mean ± SEM. Four mice were used per treatment group.

Table 6.2: Statistical analysis for the corresponding Figure 6.5. Statistical significance was determined with a two-way ANOVA, performed with Bonferroni correction.

Comparison with MOPC21 Isotype	Summary	Adjusted p value
Day 7		
Cl19	***	<0.001

cytometry was then conducted to examine PD-1 cell surface expression on the B and T cells (Figure 6.6). For examining B cells, we used the B220 marker, whereas for the T cells we used CD4 or CD8 as surface markers.

PD-1 expression by the B cells in the blood was not affected by increasing doses of Cl19 antibody. For both $CD4^+$ and $CD8^+$ T cells, a dose dependent effect was observed, with a higher dose of the Cl19 antibody inducing greater PD-1 downregulation. In particular, a significant reduction in PD-1 MFI compared to MOPC21 isotype control was observed for $CD4^+$ cells treated with 20 mg/kg ($p<0.01$) or 2 mg/kg of Cl19 antibody ($p<0.05$) (Figure 6.6). This suggested that the T cells downregulated more PD-1 at the cell surface *in vivo,* perhaps in response to greater inhibitory PD-1 signalling delivered by the increased amounts of receptor engagement.

PD-1 cell surface expression was also measured for the $CD4^+$ and $CD8^+$ T cells in the spleen of the SRBC immunized hPD-1 k.i. mice using flow cytometry (Figure 6.7). The results indicated that Cl19 had a dose dependent effect at reducing median PD-1 expression in $CD4^+$ T cells (Figure 6.7a) but not for $CD8^+$ T cells (Figure 6.7b). A significant reduction in median PD-1 expression in $CD4^+$ T cells compared to the MOPC21 isotype control was observed at the highest three concentrations (20, 2, 0.2 mg/kg) of Cl19 antibody treatment ($p<0.0001$). This suggested that $CD4^+$ T cells in the spleen could be more sensitive to antibody-based receptor triggering compared to $CD8^+$ T cells, and therefore induced greater PD-1 cell surface downregulation. In addition to the mean expression levels of PD-1 being reduced with increasing doses of Cl19 administration, we also observed a significantly smaller fraction of the $CD4^+$ spleen T cells expressing PD-1^+ following SRBC challenge, at the three highest concentrations of Cl19 ($p<0.0001$) (Figure 6.8). These results confirmed the strength of the down-regulatory effects of the Cl19 agonist antibody.

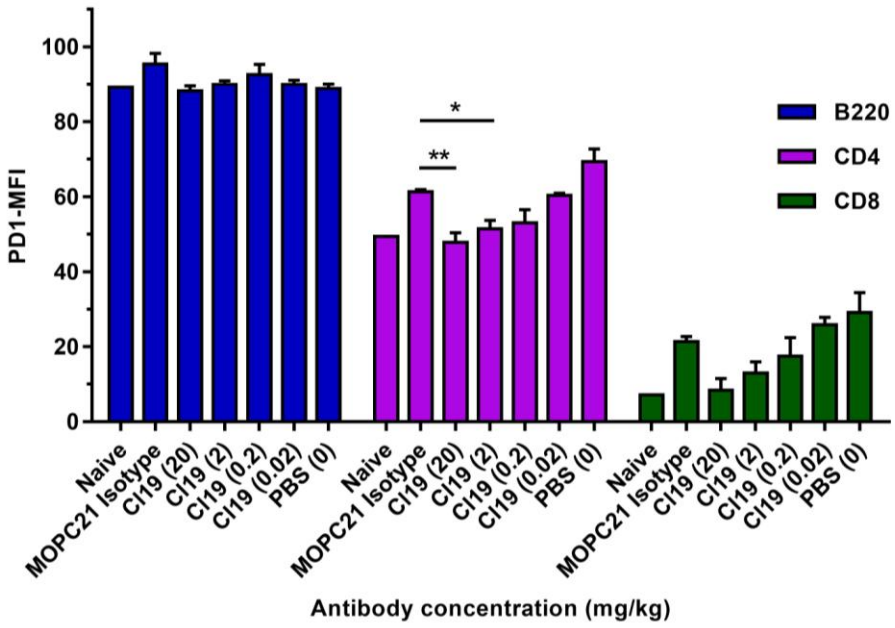


Figure 6.6: PD-1 cell surface expression in blood hPD-1 k.i. mouse $CD4^+$ and $CD8^+$ T and B cells (B220) following intraperitoneally SRBC challenge and intravenous Cl19 antibody administration. PD-1 mean fluorescence intensity (MFI) measured 7 days after SRBC injection using flow cytometry. MOPC21 antibody used as an isotype control antibody (20 mg/kg). Data points shown are mean ± SEM. Statistical significance was determined with a one-way ANOVA, performed with Bonferroni correction (*$p<0.05$, **$p<0.01$). Four mice were used per treatment group.

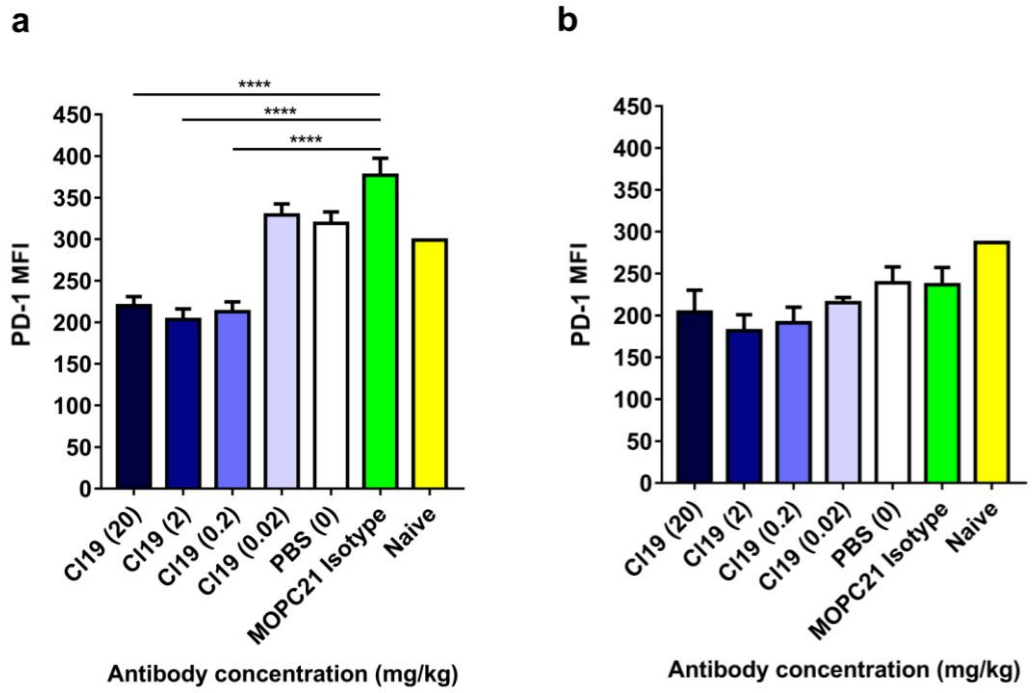


Figure 6.7: Effects of PD-1 antibody on splenic PD-1 cell surface expression in hPD-1 k.i. mice following SRBC challenge and Cl19 administration. PD-1 MFI on (**a**) $CD4^+$ or (**b**) $CD8^+$ splenocytes shown. Data points shown are mean ± SEM. Four mice were used per treatment group. Statistical significance was determined with a one-way ANOVA, performed with Bonferroni correction (****$p<0.0001$).

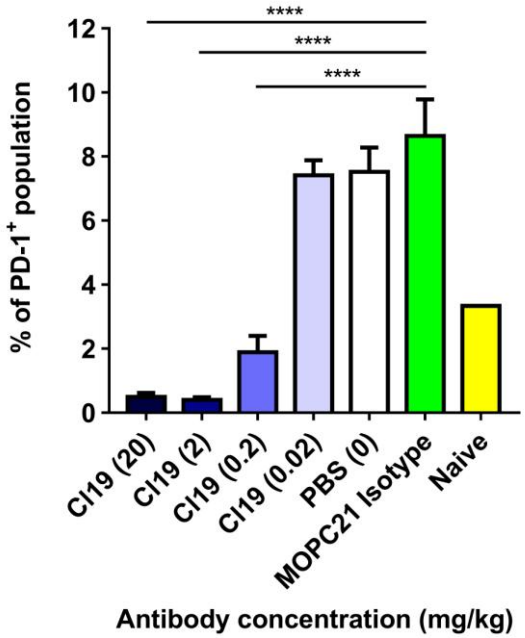


Figure 6.8: Effects of Cl19 antibody on splenic PD-1 cell surface expression following intraperitoneal SRBC challenge and intravenous Cl19 administration. Flow cytometry conducted. Percentage of PD-1$^+$ CD4$^+$ T cells from hPD-1 k.i. mouse spleen are shown. Data points presented are mean ± SEM. Four mice were used per treatment group. Statistical significance was determined with a one-way ANOVA, performed with Bonferroni correction (p****<0.0001).

II.F. The effects of anti-PD-1 antibody administration on the antigen specific $CD8^+$ T cell response

In addition to the SRBC immunization model, for which only polyclonal responses could be studied, we turned to an "adoptive transfer" transgenic model that would allow us to follow more directly the effects of the PD-1 antibodies on T-cell expansion. A transgenic mouse producing MHC class I-restricted, ovalbumin (OVA)-specific, $CD8^+$ T cells (OT-I cells) was crossed with the hPD-1k.i. mice and a GFP reporter mouse that expressed enhanced Green Fluorescent Protein (GFP) under control of the human ubiquitin C promoter (Jax mouse database: 004353, C57BL/6-Tg(UBC-GFP)30Scha/J), providing for humanized PD-1 expressing OT-I mice carrying a GFP reporter.

$CD8^+$ T cells isolated from the spleens of the triple transgenic OT-I-GFP-hPD-1k.i. (CD45.2) mice by magnetic separation were adoptively transferred into naïve C57BL/6-SJL (CD45.1) congenic recipients along with GFP negative $CD8^+$ T cells from transgenic OT-I-C57BL/6 mice (CD45.2) at a 1:1 OT-I-GFP-hPD-1k.i. (hPD-1) to OT-I-C57BL/6 (wildtype/WT) ratio. These recipients were then immunized with 10^6 plaque forming unit (PFU) of heat inactivated MVA-OVA intra-muscularly and 24 hours after immunization, the anti-PD-1 antibodies were administered intravenously (Figure 6.10a). On the day of the peak response (day 9), spleens from the recipients were harvested and the ratio of the OT-I-GFP-hPD-1k.i. (hPD-1) cells to OT-I-C57BL/6 cells (WT) cells analysed using flow cytometry (Figure 6.9) in order to gauge the impact of the antibodies on the expansion of the human PD-1 expressing versus non-expressing cells.

Initially, we only tested Cl19 and FoR1 antibodies and MOPC21 was chosen as an isotype control antibody (Figure 6.10a). The suppression of the $CD8^+$ T cell response was only observed with the Cl19 antibody, evidenced by the significantly reduced hPD-1/WT ratio to ~0.5 ($p<0.001$), whilst the mice administered with FoR1 only showed a similar response to the MOPC21 isotype control antibody

(Figure 6.10a). This was perhaps because the dose of 1 mg/kg may not have been high enough for FoR1 to show strong suppression *in vivo* (Figure 6.10a).

By changing the delivery of the antibody administration to subcutaneous rather than intravenous, and then increasing the dose of the anti-PD-1 antibodies to 20 mg/kg, larger effects could be observed. All three anti-PD-1 antibodies, Cl19 ($p<0.0001$), FoR1 ($p<0.0001$), and FoR2 ($p<0.01$) were able to strongly suppress the $CD8^+$ T cell response, which was evidenced by the significant reduction in the hPD-1/WT cell ratios (Figure 6.10b). This result was confirmed when we repeated the experiment and included both the 1st generation and 2nd generation anti-PD-1 antibodies (Figure 6.10c). The antigen specific $CD8^+$ T cell response of the transferred OT-I-GFP-hPD-1k.i. cells were significantly suppressed by all five anti-PD-1 antibodies. However, the most prominent suppression was observed with Cl19 and also by FoR1, whilst Cl2 and FoR2 showed similar levels of suppression ($p<0.0001$). Despite being able to still induce significant reductions in the hPD-1/WT cell ratio, Cl10 ($p<0.001$) seemed to be the least effective of the five anti-PD-1 antibodies at suppressing reactivity in this assay, which is somewhat unexpected, because Cl10 antibody had exhibited potency in some *in vitro* inhibitory assays.

II.G. Reduced PD-1 downregulation with 2nd generation antibodies and lack of cytotoxicity *in vivo*

Following the SRBC challenge and anti-PD-1 antibody subcutaneous administration (20 mg/kg) in hPD-1 ki mice, we wanted to determine if the 2nd generation antibodies reduced the down-regulation of PD-1, in the manner of Cl19. PD-1 cell surface expression on the Tfh cells was measured using flow cytometry (Figure 6.11). Strikingly, the Cl19 antibody administration lead to significant reductions in the PD-1 expression (MFI) on the Tfh cells ($p<0.001$) whilst the FoR1 and FoR2 antibodies had a much smaller effect on the cell surface expression of PD-1 (Figure 6.11). This is encouraging because it suggested that the 2nd generation antibodies

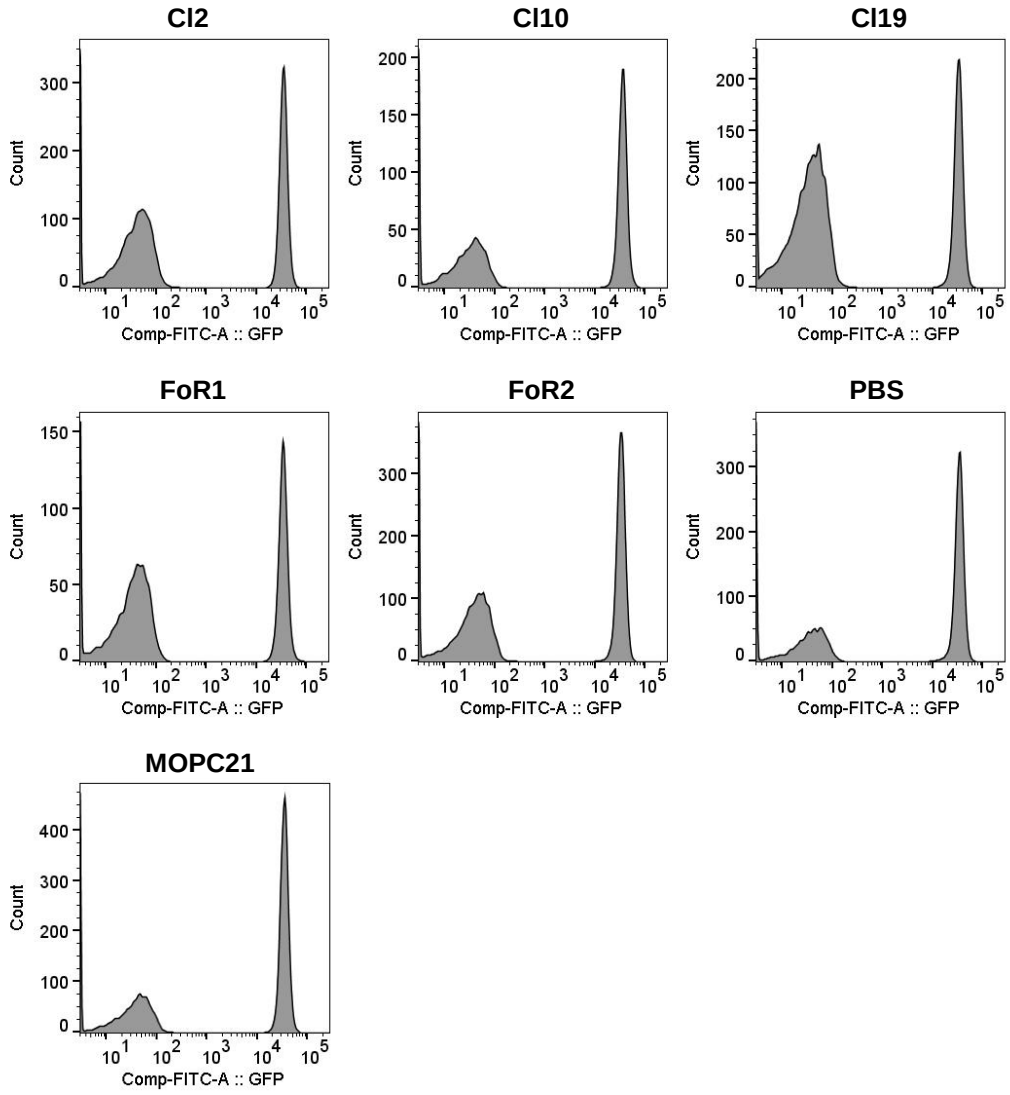


Figure 6.9: Suppression of specific $CD8^+$ T cell response by anti-PD-1 antibody treatment following MVA OVA challenge and adoptive transfer. Example flow cytometry histograms are shown to demonstrate how the CD45.2 GPF^+ (OT-1-hPD-1 k.i.) and CD45.2 GPF^- (OT-I-C57BL/6 WT) populations were detected. The x axis shows the amount of GFP fluorescence. The left peak corresponds to the cells that could not bind the antibodies, and the right peak the cells that could. The ratios of the two peaks were calculated and plotted on Figure 6.10. Flow cytometry was gated on $CD45.2^+$ $CD8^+$ GFP^+ cells. MOPC21 antibody was used as an isotype control.

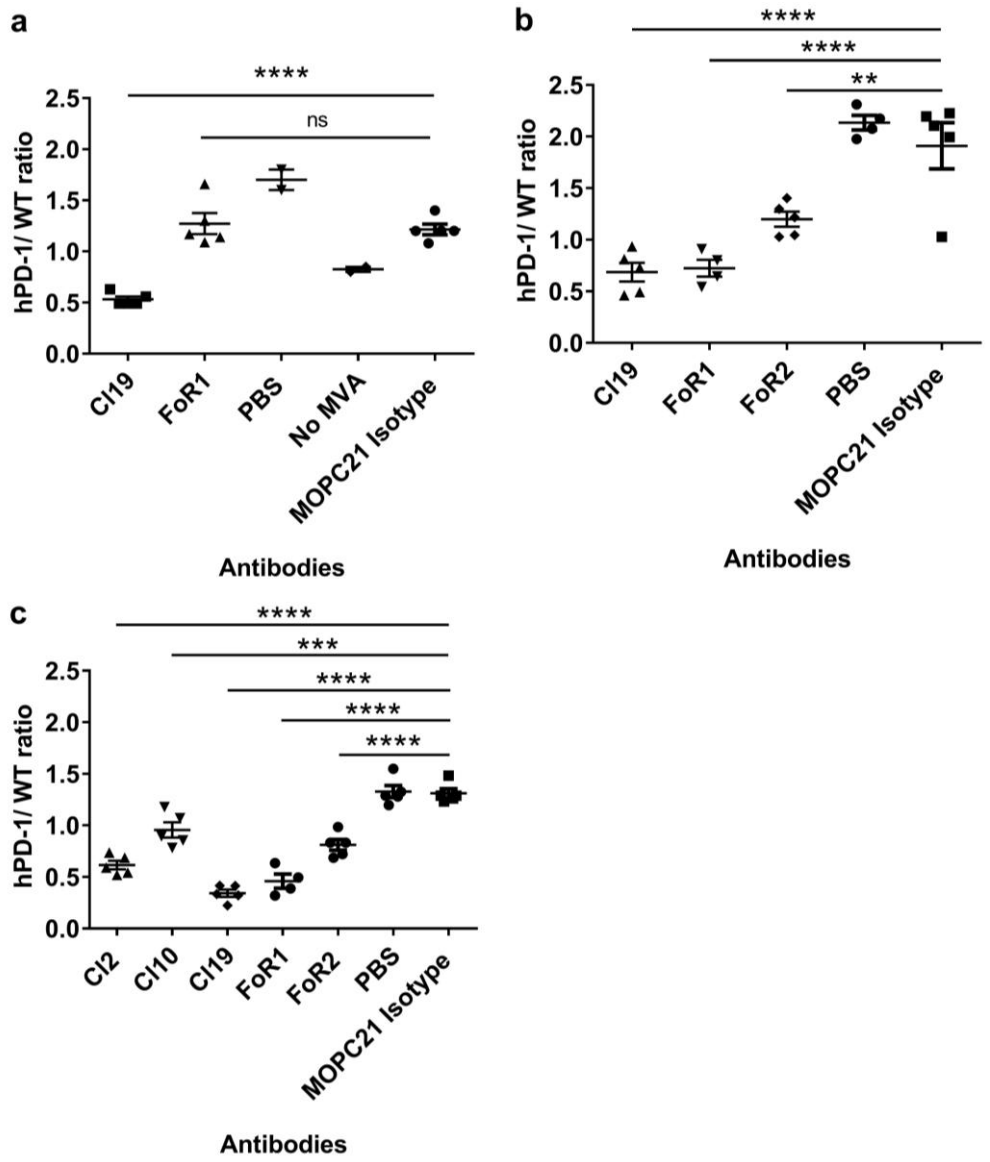


Figure 6.10: Suppression of specific $CD8^+$ T cell response by anti-PD-1 antibody treatment following MVA OVA challenge and adoptive transfer. (**a**) *In vivo* effects of Cl19 and FoR1 mAb at 1 mg/kg adminsitered intravenously. OT-1 cells from heterozygous OT-1-hPD1k.i.-GFP mice and OT-1-C57BL/6 transgenic mice were adoptively transferred into congenic C57BL/6 mice at a 1:1 ratio. Recipient mice were infected with 10^6 plaque forming unit (PFU) of MVA-OVA and treated with MOPC21 isotype control or anti-PD-1 antibodies. Nine days later, the resultant ratio of the hPD-1 cells to WT cells were measured using flow cytometry. (**b+c**) MVA OVA challenge and adoptive transfer with 20 mg/kg subcutaneous administration of anti-PD-1 antibodies. Data points presented are mean ± SEM. Statistical significance was determined with a one-way ANOVA, performed with Bonferroni correction (ns= not significant, p**<0.01, p***<0.001, p****<0.0001).

helped to keep PD-1 at the cell surface by inducing less downregulation, and that they would still augment immunomodulatory signalling.

Finally, it was necessary to confirm that the anti-PD-1 antibodies were not cytotoxic, as this would perhaps explain the loss of PD-1 expressing cells in the presence of Cl119 in the GC. We wanted to determine whether any cytotoxic effects had ensued due, for example to antibody dependent cell mediated cytotoxicity (ADCC). The absolute Tfh cell numbers were measured and the results demonstrated that these antibodies were not cytotoxic since the numbers were similar between the isotype control, PBS and anti-PD-1 antibody treated mice (Figure 6.12).

III. Discussion

Various methods were implemented to test the effects of anti-PD-1 antibodies *in vivo*. The effects on GC B cell formation following SRBC challenge with increasing concentrations of Cl19 antibodies were studied. Surprisingly, a dose dependent effect on the percentage of GC B cells over total B cells was only observed in the spleen and not in the mesenteric lymph nodes. This may be due to the fact that GC B cells were more difficult to detect in the mesenteric lymph nodes.

Antibodies play a major role in preventing viral infection and offer protection against subsequent re-challenge, which is dependent upon the maintenance of protective antibody titres [378]. In mice, such maintenance of long-term protective antibodies following primary antigen exposure is orchestrated by both memory B cells and long-lived plasma cells. Unexpectedly, a dose dependent effect was only seen with anti-SRBC IgM production and not with anti-SRBC IgG antibodies in the primary response. One advantage of this method is that the ELISAs are relatively straight forward.

The inhibitory effects of using a combination of anti-PD-1 antibodies with different epitopes, namely Cl19 and Cl2, on the GC cells following SRBC challenge were also

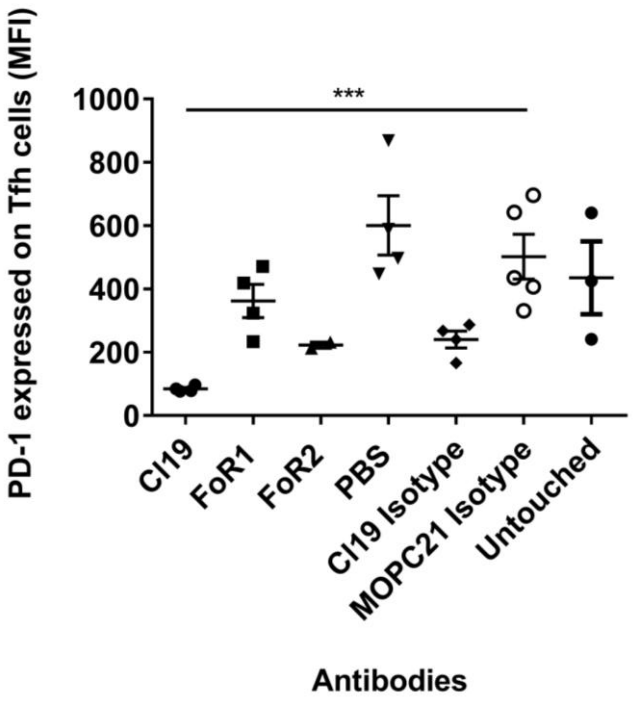


Figure 6.11: Assay for PD-1 downregulation following SRBC challenge and subcutaneous anti-PD-1 antibody treatment (20 mg/kg) in hPD-1 k.i. mouse. Mean fluorescence intensity of PD-1 cell surface expression on Tfh cells measured *via* flow cytometry. Data points presented are mean ± SEM. Statistical significance was determined with a one-way ANOVA, performed with Bonferroni correction (***$p<0.001$). MOPC21/Cl19 isotype antibody (20 mg/kg) was used as a control.

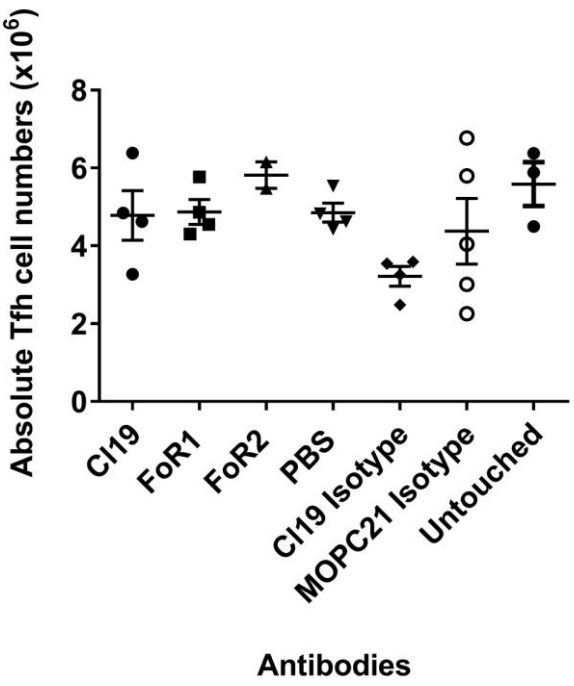


Figure 6.12: Cytotoxicity assessment following SRBC challenge and subcutaneous anti-PD-1 antibody treatment (20 mg/kg) in hPD-1 k.i. mouse. Tfh absolute cell numbers shown. Lack of cytotoxicity is presented by similar Tfh absolute cell numbers. FoR1 and FoR2 antibodies helped to maintain high PD-1 expression compared to Cl19 antibody treated mice. MOPC21/Cl19 isotype antibody (20 mg/kg) was used as a control. Data points presented are mean ± SEM.

examined. However, the Cl19 and Cl2 antibody combination was not able to generate an observable synergistic effect in our experiments. This might be because the concentration of antibodies used was not high enough, or perhaps because strong agonising signals induced PD-1 receptor downregulation, masking the overall inhibitory effects of these antibodies.

Of the three 1st generation anti-PD-1 antibodies, Cl19 showed the greatest effect on antibody affinity maturation in response to NP-CGG challenge by the hPD-1 k.i. mice. Following SRBC challenge and Cl19 antibody administration to the PD-1 k.i. mice, PD-1 cell surface downregulation in a dose dependent manner was confirmed in the spleen and blood, but not in the lymph nodes.

The adoptive transfer MVA OVA challenge was used to test more directly for suppression of the $CD8^+$ T cell response with anti-PD-1 antibodies. Initially, the results using 1 mg/kg intravenous delivery of antibodies showed that only Cl19 and not FoR1 was able to suppress the T cell response. However, additional experiments which utilised subcutaneous delivery of anti-PD-1 antibodies at a higher dose of 20 mg/kg gave more potent suppressive effects relative to the intravenous method. Intravenous drug delivery is usually used for its rapid administration and immediate drug effect whilst medication given *via* subcutaneous injection is commonly absorbed more slowly. Perhaps, the efficacy of the anti-PD-1 antibodies could be further increased *via* subcutaneous delivery since it is slowly released giving reduced, sustained rates of absorption. When all five different anti-PD-1 antibodies, *i.e.* three 1st generation and two 2nd generation were tested together, the most prominent suppression of the $CD8^+$ T cell response was observed with Cl19 and also by FoR1, whilst Cl2 and FoR2 demonstrated similar levels of inhibition. In contrast, surprisingly, Cl10 seemed to be least effective in the inhibition of the antigen specific response. This was unexpected given the high potency exhibited in the *in vitro* inhibitory cytokine assays, but could perhaps be explained by the notion that epitope position and affinity work together to create superagonistic signalling potential *in vivo*.

Reduced PD-1 downregulation was observed with the 2nd generation anti-PD-1 antibodies compared to the 1st generation Cl19 antibody *in vivo*. The lack of cytotoxicity following SRBC challenge was evidenced by the relatively consistent absolute numbers of Tfh cells following antibody administration. This suggested that these anti-PD-1 antibodies were exerting a true inhibitory effect *in vivo* and were not causing cell death, e.g. by ADCC. This is encouraging because it suggests that a greater overall PD-1 signalling can be achieved with FoR1, which could lead to greater suppression of the immune response to the extent that it may be utilised in autoimmune disease settings in the future. FoR2 was able to maintain high PD-1 expression in *vivo* but it did not show strong agonising capacities compared to FoR1.

The results from this chapter seemed to indicate that the dose of suppressive anti-PD-1 antibody is important in delivering potent signals. If the threshold for signalling is not reached, not enough inhibitory signalling created by PD-1 triggering will mean that significant inhibitory effects on the GC response, primary antibody response and $CD8^+$ T cell response will not be achieved. Thus, the dose will generally have to be optimised in a therapeutic setting. Also, the method of antibody delivery can also alter the potency of the inhibitory response. Thus, for maximal and specific therapeutic effects, more work needs to be done to determine the best combination of dose and delivery of these anti-PD-1 antibodies.

Chapter 7
General discussion

The immune system has the daunting challenge of recognising and defending against a wide array of microbial pathogens, whilst preventing self-reactivity simultaneously. Although central tolerance mechanisms lead to the deletion of most self-reactive T cells, some of these T cells do however manage to escape to the periphery. Therefore, to further prevent the development of autoimmunity, several mechanisms of peripheral tolerance have evolved. These comprise of T cell deletion, suppression by Tregs and anergy [220]. However, if these mechanisms fail, this can result in autoimmune disorders. T cell co-inhibitory pathways play pivotal roles in mediating the fine balance between protective immunity and tolerance. Such pathways can prevent effector, memory and regulatory T cell responses. The co-inhibitory pathway involving PD-1, an inhibitory member of the CD28 family of co-receptors, and its native ligands, PD-L1 and PD-L2, permit the deliverance of suppressive signals which help control the balance among T cell activation, tolerance and immune-mediated tissue damage [379]. Furthermore, the PD-1:PD-L pathway is implicated in T cell exhaustion, as well as a lack of viral control, and it helps create an immune-suppressive tumour microenvironment [379].

'Superagonists' are antibodies that induce high levels of receptor signalling. Insights into how superagonists induce signalling have derived from studying anti-CD28 antibodies [132]. An anti-hCD28 superagonist, TGN1412, was utilized in a 'first-in humans' clinical trial with the goal of selective Treg activation [380]. However all six healthy volunteers experienced an unexpected cytokine storm [380]. Pre-clinical *in vitro* experiments did not suggest such detrimental effects, perhaps because the antibodies were not immobilised in the way they probably were *in vivo* [381], and also

because of the species-specific differences in CD28 signalling or expression [382]. Thus, the possible clinical use of superagonistic antibodies against CD28 or other alternative costimulators remain very contentious. In contrast, it may be safer to target checkpoint inhibitors like PD-1 and CTLA-4, as they may offer a potentially safer way of modulating immune reactions using superagonistic antibodies, and could be utilized to inhibit TCR-mediated signalling in autoimmune settings.

Evans *et al.* showed that the location of an antibody's epitope is related to its ability to induce superagonistic signalling [132]. Utilizing the principles of the KS model, it has been suggested that the greater potency of superagonistic antibodies arises from their ability to more effectively exclude large phosphatases like CD45 from the vicinity of CD28, leading to greater phosphorylation [132]. An extension of this hypothesis is that any immobilized antibody binding to a membrane-proximal epitope on a receptor with tyrosine phosphorylation motifs should be able to induce signalling by that receptor. Therefore, immobilized antibodies that bound to membrane proximal regions of PD-1 could potentially generate greater superagonistic downstream signalling and suppress immune activity than membrane-distally binding antibodies. Previous work has further suggested that in addition to the epitope of the anti-PD-1 antibody, the affinity to the receptor could also affect its signalling capacities (S.H. Morgan, unpublished data). Thus, it was hypothesised that it might be advantageous for therapeutic inhibitory antibodies to combine both membrane proximal binding properties with fast binding kinetics, since it might induce a greater overall level of inhibitory receptor signalling through enhanced receptor engagement, therefore allowing control of excessive immune responses. This thesis has therefore sought to extend our understanding of the *in vitro* and *in vivo* effects of a novel class of 2nd generation, low-affinity, membrane-proximally binding anti-PD-1 agonistic antibodies.

I. Results from this thesis

I.A. Mutational analysis of the Cl19 PD-1 binding

In experiments described in Chapter 3, we succeeded in preparing the PD-1 extracellular domain from cleaved PD-1FcHis, and Cl19 Fabs using both stable and transient transfections in CHOK1 and 293T cells, respectively, in order to test for binding. Initially, we confirmed that the purified Cl19 Fab could form a stable protein complex with PD-1FcHis using size-exclusion chromatography. We observed a small decrease in the elution time of the Cl19 Fab and PD-1FcHis mixture, compared to Cl19 Fab or PD-1FcHis alone, which indicated that the antibody Fab was correctly folded, allowing binding to the PD-1 receptor. Once this was established, kinetic analysis of the binding of Cl19 Fab to PD-1 was performed in SPR-based assays. The K_D measured for Cl19 Fab was 0.041 μM, revealing high affinity binding to PD-1. This was in contrast to the binding of PD-1 to its native ligands, PD-L1 and PD-L2, which has much weaker affinities: *i.e.* K_D values of ~8.2 μM and ~2.3 μM respectively [343]. Since low affinity antibody binding seemed to confer agonistic potential to anti-PD-1 antibodies (S.H. Morgan, unpublished), it was thought that faster kinetics may lead to greater serial triggering of PD-1 and hence greater overall agonistic signalling. We therefore set out to make low-affinity forms of Cl19, using site-directed mutagenesis.

I.B. Production and characterisation of new fast off-rate Cl19 derivatives[1]

In experiments described in Chapter 4, we succeeded in generating and characterising new fast off-rate Cl19 antibody derivatives using a medium-throughput assay for mutant screening. Using a similar mutagenesis-based approach previously adopted by Fernandes *et al.* [354], we generated drastic mutations in the predicted CDR loops of Cl19 Fab variable regions. In the initial round of screening of Cl19 mutant Fabs binding to PD-1, which was assayed using SPR-based methods, two CDR3 light chain mutants FoR1 (N92) and FoR2 (Y94) Fabs showed promising

[1] The analysis described in this section was performed with the assistance of Dr Yuan Lui, T-cell Biology Group, University of Oxford.

altered behaviour, *i.e.* substantially reduced binding affinities to PD-1 compared to the 1st generation Cl19 antibody, with K_D and off-rates that were comparable to the 1st generation Cl10 antibody. Consistent with asparagine and tyrosine being abundant in antibody-antigen complex interfaces [383], these were good candidates for markedly weakening antigen binding as observed through our SPR-based assays. We discovered that the binding kinetics of the new FoRs, *i.e.* FoR1 and FoR2, to PD-1, were more similar to those of PD-L2, rather than the alternative native ligand of PD-1, PD-L1 [343]. Our results showed that FoR1 and FoR2 Fabs bound to PD-1 with K_D values of ~2.4 μM and ~1.59 μM, respectively.

I.C. The properties of the Cl19 Fab/PD-1 interaction

Earlier work has suggested that Cl19 antibody binds to the base of the PD-1 molecule using four key residues: L41, V43, R143, T145 (S.H. Morgan, unpublished), whilst studies of FDA-approved cancer drugs, *i.e.* high affinity anti-PD-1 blocking antibodies Pembrolizumab [384] and Nivolumab [385], showed that these antibodies bind to the side of the PD-1 and the N-terminal loop/top of PD-1, respectively. Using PyMOL (The PyMOL Molecular Graphics System, Version v1.7.4.5 Schrödinger, LLC.), the binding interfaces of Cl19 (S.H. Morgan, unpublished), Pembrolizumab (Protein Data Base (PDB) code 5B8C) and Nivolumab (PDB code 5WT9) antibodies on PD-1 can be visualized (Figure 7.1). The more membrane-proximal position of the Cl19 epitope compared to Nivolumab and Pembrolizumab implied that Cl19 would be able to form flatter complexes, that more efficiently exclude large tyrosine phosphatases from PD-1, and hence allow for greater phosphorylation and possibly induce greater agonistic signalling [84].

From the two rounds of mutant screening, mutations of eight residues on the Cl19 Fab were found to produce non-measurable binding to PD-1 in our binding assays, of which four were centred on a small contiguous region. The distribution of these four disabling mutations, *i.e.* that they were clustered fairly close together, suggested that the model of the CDR regions of Cl19 that we used was relatively accurate. The

drastic mutations of FoR1 and FoR2, *i.e.* N92 and Y94, which lead to partial effects on binding to PD-1, is perhaps explained by these residues being on the edge of the PD-1 binding site of Cl19.

Using a combination of PyMOL tools, automatic docking performed by High Ambiguity Driven protein-protein Docking (HADDOCK) [386], previous unpublished mutational data on PD-1 from S.H. Morgan, our drastic mutation data, and finally a Proteins, Interfaces, Structures, and Assemblies (PISA) analysis [387], we were able to build a model of the interfaces formed by Cl19 Fab (green) and PD-1 (red) (Figure 7.2). Interface residues that are >50 % buried when the proteins interact (yellow), and sites that were mutated and eliminated binding (cyan) are shown (Figure 7.2a). Surface diagrams of PD-1 (left) with unpublished mutational data from S.H. Morgan (cyan), and Cl19-Fab (right) with our drastic mutation data (cyan), showing the interfaces, are also presented (Figure 7.2b). PD-1 has a long stalk of ~20 amino acids (grey dotted lines) (Figure 7.2), which would allow for considerable flexibility of the molecule on the cell surface, which makes this model depicting PD-1/Cl19 binding at an angle very feasible.

In total, 17 residues form the chief interface on Cl19 for its interaction with the PD-1 receptor, with all six CDRs on the light and heavy chain being involved. Tyrosine and histidine were the most common amino acid residues likely to be involved in binding, which correlates well with previous studies. Davies *et al.*, for example, have shown that a large percentage (34%) of the antibody-contacting residues generally are aromatic in character (histidine, phenylalanine, tryptophan and tyrosine); of these more than two thirds are tyrosine residues [388]. Conversely, the interface residues in the antigens contain somewhat fewer residues that are aromatic [388]. Again, this was consistent with our model of Cl19, and by the Nivolumab and Pembrolizumab structures, which exhibited a large fraction of aromatic residues in the anti-PD-1 antibody interface, but low numbers of aromatic residues in the PD-1 antigen epitopes (Table 7.1). Unlike Cl19, which appears to bind to PD-1 using all six CDR

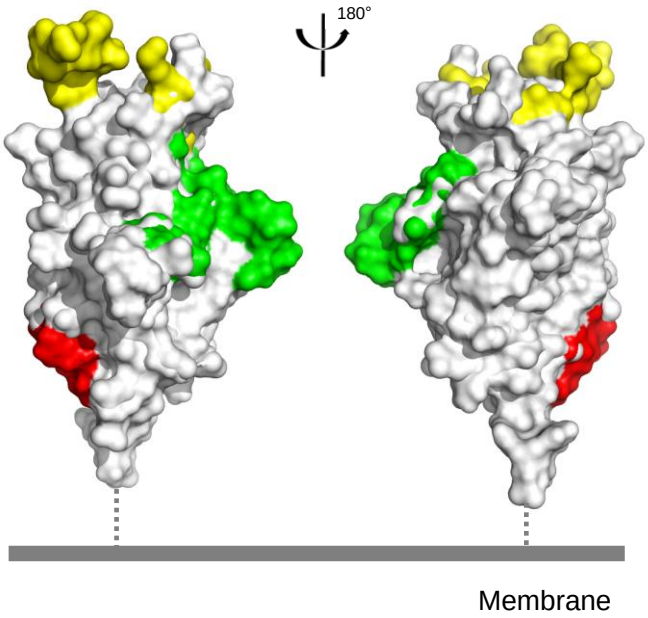


Figure 7.1: Surface diagrams of PD-1 showing the positions of the epitopes of various anti-PD-1 antibodies binding to human PD-1. Interface residues on PD-1 that bind to Cl19 (red), Pembrolizumab (green) and Nivolumab (yellow) are displayed. Grey dotted lines denote the stalk of PD-1.

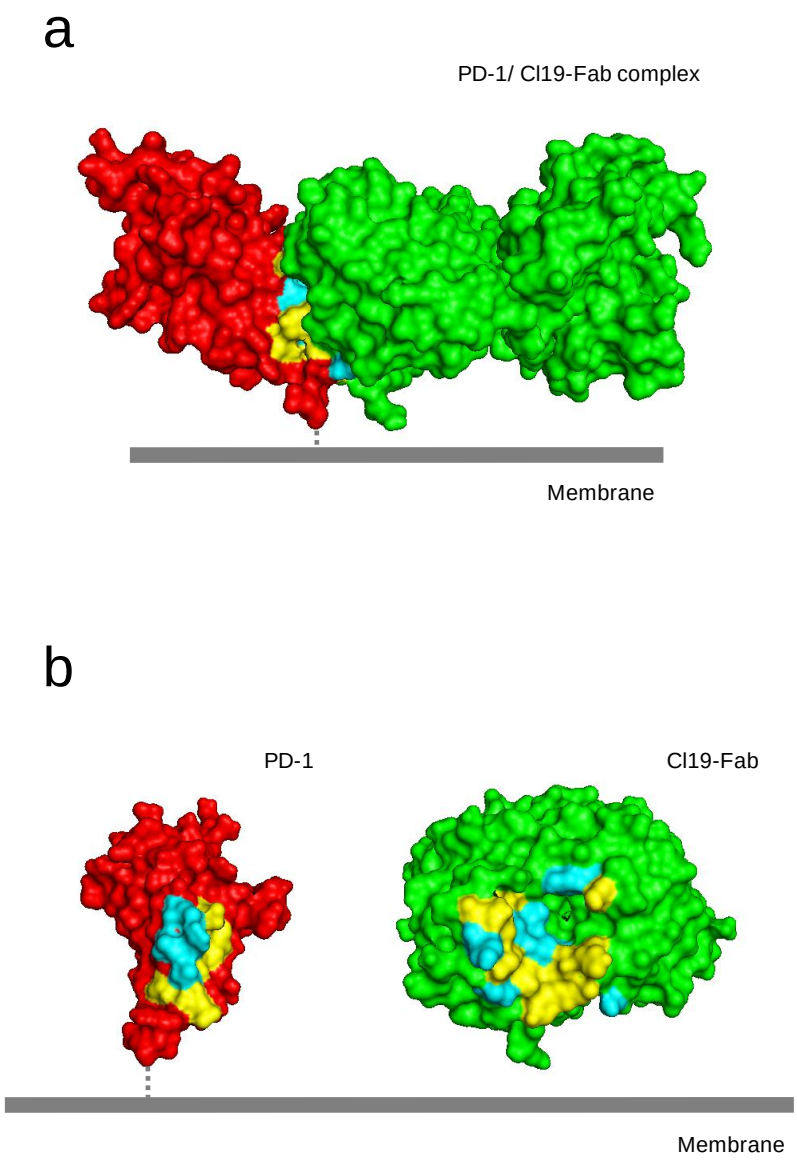


Figure 7.2: Cl19-Fab and human PD-1 complex interface analysis. (**a**) Surface diagram of the PD-1 (red)/Cl19-Fab (green) complex model. Interface residues that are >50 % buried when the proteins interact according to the model are coloured yellow, and sites that were mutated and eliminated binding are shown in cyan. Grey dotted lines denote the ~20 amino acid stalk of PD-1. The position of the membrane is indicated. (**b**) Surface diagrams of PD-1 (left) and Cl19-Fab (right) showing the binding interfaces in the model, with buried interface residues coloured yellow and unpublished mutations of PD-1 from S.H. Morgan and our drastic mutations of Cl19, all of which eliminate binding, coloured cyan. This figure was prepared with the help of Dr Yuan Lui.

Table 7.1: The Anti-PD-1 antibody/antigen interface. Aromatic residues include histidine, phenylalanine, tryptophan and tyrosine. PISA analysis was conducted using Cl19 (our drastic mutation/binding analysis and automatic docking HADDOCK data), PD-1 (S.H. Morgan's unpublished data), Nivolumab (PDB code 5WT9) and Pembrolizumab (PDB code 5B8C) data.

	Buried area (Å^2)			No. of residues			No. of aromatic residues		
Antibody	V_L	V_H	Antigen	V_L	V_H	Antigen	V_L	V_H	Antigen
Clone 19	177.3	778.8	949	6	22	24	3	7	0
Nivolumab	290.6	571.3	926	14	20	17	4	4	0
Pembrolizumab	551.8	662.1	1170.9	15	19	31	4	4	3

loops, Nivolumab uses three CDRs on the heavy chain and only the CDR1 and CDR2 loops of the light chain [385], whilst Pembrolizumab utilises three CDRs on the heavy chain and just CDR3 of the light chain [384]. The buried areas on the PD-1 antigen were similar for Cl19, Nivolumab and Pembrolizumab, with Pembrolizumab being the largest (949, 926, 1170.9 $Å^2$ respectively; Table 7.1). As noted, for all three antibodies the V_H region formed a larger proportion of the interface compared to the V_L region (Table 7.1). According to our model of the superagonistic complex that we generated, therefore, in terms of the total number of binding residues in the binding interface, the number of aromatic residues, as well as the binding interface area, Cl19 exhibited similar features to the therapeutic anti-PD-1 antibodies, Nivolumab and Pembrolizumab. A study by Evans *et al.* also demonstrated that superagonistic and conventional anti-CD28 antibodies have similar properties when it comes to these three elements [132]. However, these antibodies differ in terms of their binding positions on the receptor, with both Cl19 and the superagonistic anti-CD28 antibody binding to a membrane proximal epitope on PD-1 and CD28 respectively. Overall the data indicate that it is the position of the epitope, not the chemistry of binding, that determines whether an antibody is an effective agonist and a blocker of TCR signalling or not.

Using the mutant screening data, we generated a Cl19 'isotype control' antibody by incorporating a single drastic, binding-preventing mutation in both the light chain (Y91) and heavy chain (Y166). The Cl19 isotype control antibody was tested for binding to PD-1 using SPR and, as expected, it did not exhibit measurable binding to PD-1.

I.D. Inhibitory effects of anti-PD-1 antibodies *in vitro*

In experiments described in Chapter 5, we were able to demonstrate the inhibitory potential of anti-PD-1 agonist antibodies *in vitro* using several methods. From the anti-CD3 antibody titration experiments, it was evident that cytokine production was inhibited by the anti-PD-1 antibodies most prominently at lower levels of anti-CD3 antibody stimulation (0.5 μg/ml). These data are in agreement with previous

examination of the effects of PD-1 engagement [196, 216, 220, 228], which revealed that the extent of PD-1 mediated inhibition is dependent upon the strength of the TCR signal, such that more suppression occurs at low levels of TCR stimulation. Like the natural ligands of PD-1, anti-PD-1 agonists seem to exert their activity when relatively weak TCR signalling is delivered, as is probably the case *in vivo*. In order to fully activate the T cells, we found that it was necessary for costimulation to be provided by using anti-CD28 antibodies in the suppression assays. Recently, Hui *et al.* demonstrated that rather than inhibiting signalling through the TCR, CD28 is strongly preferred over the TCR as a target for dephosphorylation by PD-1-recruited SHP-2 phosphatase [362]. Therefore, PD-1 could inhibit T cell function primarily by CD28 signalling inactivation. Consequently, this indicates that the costimulatory pathways could be crucial in controlling effector T cell function and responses to anti-PD-L1/PD-1 immunotherapy.

Using anti-PD-1 antibodies, we were able to demonstrate suppression of cytokine production in assays utilizing mixtures of hPD-1 k.i. mouse splenocytes. Compared to TNF-α and IFN-γ ELISAs, the IL-2 ELISAs exhibited greater reproducibility and higher levels of overall suppression, prompting us to focus on this particular cytokine for further testing. IL-2 generation was also suitable as the principal read-out for superagonistic signalling since it is indicative of full T cell activation instead of sub-threshold signalling [363]. Another reason that it was appropriate for evaluating PD-1 signalling is that IL-2 is known to be one of the cytokines most sensitive to TCR triggering, CD28 costimulation and PD-1 cell surface receptor triggering [364].

We set up several different *in vitro* systems to examine the effects of anti-PD-1 antibodies on cytokine generation. Initially, hPD-1 k.i. mouse splenocyte mixtures were employed in suspension with the antibodies in a soluble form, to some extent mimicking the situation of antibody presentation *in vivo*. We then altered presentation by immobilising the antibodies to a plate using secondary DAM antibodies, since this could potentially cross-link more anti-PD-1 antibodies and thus enhance downstream

receptor signalling. Generally, we discovered that by adding greater levels of inhibitory anti-PD-1 antibodies, greater IL-2 suppression was observed, regardless of the method in which antibody presentation took place, either in solution or plate-bound. Furthermore, the greatest synergistic effects were observed for antibody combinations, *i.e.* Cl19 and Cl2, and Cl10 with FoR1, also used at the highest concentrations. This indicated that synergy is greater when more anti-PD-1 antibodies were present, to allow for higher levels of PD-1 receptor engagement. A combination of signalling antibodies, utilizing binding to two non-overlapping epitopes, allowed cross-linking which is likely to lead to better local concentration of PD-1 and thus stronger overall signalling. However, further studies need to be performed to confirm and extend these findings with antibody combinations.

To observe inhibitory effects on cytokine production, suitable isotype control antibodies had to be employed. The Cl19 isotype antibody, which is a derivative of Cl19 mutated to prevent binding, was initially used. In most of the *in vitro* experiments, the Cl19 isotype control antibody appeared to be inactive. However, for the cytokine suppression experiments conducted at high concentrations, unexpectedly the Cl19 isotype control antibody showed some agonising activity. Perhaps, this antibody was still able to bind very weakly to PD-1, without it being detectable in the SPR assays, and thus could induce some residual PD-1 signalling. To avoid this problem, the MOPC21 isotype antibody was also included as a control in later experiments. Importantly, the use of both isotype control antibodies did not substantially alter the conclusions of the experiments.

A previous study which examined the functional consequences of PD-1:PD-L engagement on murine $CD4^+$ and $CD8^+$ T cells revealed that these interactions result in inhibition of cell proliferation; the CSFE analysis revealed fewer cells cycling and a lower division rate [364]. Likewise, another study showed that PD-1 signalling blocked cell cycle progression in the G1 phase and hence suppressed T cell proliferation [389]. Using the CSFE-based cell proliferation assay, we too were able

to show that the anti-PD-1 antibodies were able to suppress cell proliferation *in vitro,* albeit weakly. The inhibitory effects were not as large as those observed in the IL-2 ELISA assays. Perhaps, this is because PD-1 signalling has a greater effect on cytokine suppression, instead of cell proliferation as previously argued by Sharpe and colleagues [220]. Overall, regardless of the method of antibody presentation, our data suggested that potent inhibitory superagonists can be generated against receptors like PD-1.

I.E. Inhibitory effects of anti-PD-1 antibodies *in vivo*

In experiments described in Chapter 6, the suppressive effects of the anti-PD-1 antibodies *in vivo* were investigated. A role for PD-1 in the regulation of autoimmunity and T cell tolerance was first discovered by the phenotype of PD-$1^{-/-}$ mice [338]. PD-1 deficiency causes the spontaneous development of various features of a late onset lupus-like disease which is characterized by mild glomerulonephritis and autoantibodies in C57BL/6 mice [338]. Utilising PD-1- and PD-L1/2-deficient mice, Good-Jacobson *et al.* showed that PD-1 plays a role in the development and function of Tfh cells, and therefore regulates the GC B cell response and antibody production [390]. In our study, we showed that the primary GC response can be modulated by PD-1 ligation using Cl19 antibody. The effects on GC B cell formation following SRBC challenge with increasing concentrations of Cl19 antibodies were thus examined. Unexpectedly, in the spleen, an inhibitory and dose dependent effect on the fraction of GC B cells over total B cells was detected, but no significant suppressive effects were shown in the mesenteric lymph nodes. This may be because detection of GC B cells was more difficult in the mesenteric lymph nodes since there were fewer total GC B cells available. PD-1 cell surface downregulation was also observed in a dose dependent manner in the spleen and blood, but again, not in the lymph nodes. Anti-SRBC ELISAs were performed to detect the effects of Cl19 antibodies on the primary response. Unexpectedly, a dose dependent effect was only seen with anti-SRBC IgM production and not with anti-SRBC IgG antibodies in the

primary response. Consistent with the findings of Good-Jacobson *et al.,* this suggests that PD-1 negatively regulates IgM production during a primary GC reaction.

The suppressive effects of using a combination of Cl19 and Cl2 antibodies, that bind to different epitopes, on the GC cells following SRBC challenge were also studied. This combination did not result in observable synergistic effect in our experiments. The reason for this could be that the antibody concentration applied was not high enough, or perhaps the strong agonising signals by Cl19 induced PD-1 receptor downregulation. Thus, the overall inhibitory effects of these antibodies might have been masked. [220]. Of the three 1st generation anti-PD-1 antibodies, Cl19 exhibited the largest effect on antibody affinity maturation in response to NP-CGG challenge by the hPD-1 k.i. mice. This supports the general hypothesis that the proximity of the epitope to the membrane may influence the potency of the agonistic activity of antibodies *in vivo* in accordance with the KS model [84].

In order to test more directly for suppression of the $CD8^+$ T cell response with anti-PD-1 antibodies, the adoptive transfer MVA OVA challenge was performed. It has been demonstrated that the PD-1 pathway plays a major role in $CD8^+$ T cell memory reprogramming, following an acute immune response against an inactivated vaccinia virus [376]. Initially, the results using 1 mg/kg intravenous delivery of antibodies indicated that only Cl19 and not FoR1 was able to suppress the T cell response. Further experiments which relied on subcutaneous delivery of anti-PD-1 antibodies at a higher dose of 20 mg/kg elicited more potent suppressive effects relative to the intravenous method. Importantly, intravenous drug delivery is usually chosen for its immediate effect whilst medication given *via* subcutaneous injection is commonly absorbed less quickly. Possibly, the efficacy of the anti-PD-1 antibodies could be further enhanced *via* subcutaneous delivery since it is slowly released, and gives reduced yet sustained rates of absorption. When all five different anti-PD-1 antibodies, *i.e.* three 1st generation and two 2nd generation antibodies were tested together, the most prominent suppression of the $CD8^+$ T cell response was observed

with Cl19 and also by FoR1, whilst Cl2 and FoR2 demonstrated similar levels of inhibition. In contrast, unexpectedly, Cl10 seemed to be least effective in suppressing the antigen specific response *in vivo*. This was surprising given the high potency exhibited in the *in vitro* inhibitory cytokine assays but could perhaps be explained by the notion that epitope position and affinity work synergistically to create superagonistic signalling potential *in vivo*, explaining the activity of FoR1 versus Cl10. As in the *in vitro* cytokine assays, our *in vivo* assays implied that a higher concentration of anti-PD-1 antibody application led to greater suppressive effects, thus dose optimisation will also be key for maximisation of the inhibitory potential of these antibodies.

The lack of cytotoxicity following SRBC challenge was evidenced by the relatively consistent absolute numbers of Tfh cells following antibody administration. This indicated that these anti-PD-1 antibodies were exerting a true inhibitory effect *in vivo* and were not inducing cell death, *e.g.* by ADCC.

I.F. PD-1 receptor downregulation

Endocytosis involves the internalization of cell surface receptors and extracellular material into cells *via* membrane-bound carriers [391]. Clathrin-mediated endocytosis (CME) is the main uptake mechanism used by all known eukaryotic cells [392] and is the best-characterised endocytic pathway [392]. Clathrin-coated vesicle formation comprises of five stages: initiation, cargo selection, coat assembly, scission and uncoating [392]. The CME pathway is versatile since a range of accessory adaptor proteins can help with cargo packaging which is destined for endosomes [392]. Such internalised cargo is sorted either back to the cell surface or into other compartments (multi-vesicular bodies and lysosomes), in order to be degraded [392]. In contrast, several clathrin-independent endocytosis (CIE) routes exist in parallel to CME, as has been reported in both *in vitro* and *in vivo* settings [393, 394]. It has been observed that some CIE processes are speedier than CME and play a role in physiological processes which need faster internalization from the cell surface, e.g.

in response to receptor hyperstimulation [395]. There are three distinct molecular mechanisms by which CIE carriers form. The major mechanism utilised by fast endophilin-mediated endocytosis and IL-2 receptor endocytosis involves cargo capture by cytosolic proteins [391]. Macropinocytosis is driven by acute signalling-induced membrane remodelling whilst cargo/extracellular clustering by the glycolipid-lectin hypothesis facilitates the uptake of receptors by the clathrin-independent carriers/glycosylphosphatidylinositol-anchored protein-enriched endocytic compartments pathway [391].

Antibody targeting of cell surface molecules can result in multiple outcomes such as cell depletion, blockade of ligand/receptor interactions, and induced signalling and/or receptor downregulation [396]. A previous report has shown that *in vivo* administration of anti-BTLA 4G12b antibody was able to induce a profound and lasting BTLA downregulation which led to BTLA receptor internalisation [396]. Because BTLA seems to be vital to T cell survival [397], BTLA downregulation may cause BTLA expressing cells to be more prone to apoptosis, consequently helping inhibit T cell responses against alloantigens [396]. Similarly, in our *in vivo* assays, our anti-PD-1 antibodies also induced PD-1 receptor downregulation. However, reduced PD-1 downregulation was observed with the 2nd generation anti-PD-1 antibodies compared to the 1st generation Cl19 antibody. Indeed, it was this that partly prompted the production of the FoR antibodies, since it was found that Cl10, whilst being agonistic *in vitro*, produced relatively little down-regulation *in vivo* (B. Akkaya, unpublished work). It seems likely that Cl19, because it is able to bind more strongly to PD-1, can cause more PD-1 molecules to be stripped from the cell surface *via* endocytosis either through CME or the CIE pathways. Because of the reduced affinity of FoR1 compared to Cl19, higher overall suppressive PD-1 signalling may be achieved through faster dissociation of FoR1 from PD-1 in the long-term, allowing for greater engagement with more PD-1 molecules in a shorter period of time.

As proposed previously for the antibody agonists developed against tumour necrosis factor receptor superfamily member Fas, our findings indicate that an inverse correlation between the affinity and the potency of agonistic antibodies might exist [398]. The altered antibody binding kinetics of FoR1 therefore could help to retain more PD-1 receptor at the cell surface *via* reduced receptor internalisation and consequently hold greater therapeutic potential. In contrast, FoR2 was also capable of maintaining high PD-1 expression in *vivo,* but unexpectedly, it did not show as strong agonising capacities as FoR1. Our experiments demonstrate, however, that it is possible, in principle, to uncouple signalling and down-regulation by changing the binding kinetics of antibodies to receptors of interest.

I.G. Signalling implications

SHP-2 tyrosine phosphatase is known to interact with PD-1 and is important for PD-1-mediated suppression [399]. The cytoplasmic tail of PD-1 contains an ITIM and an ITSM [399]. Using GST-SHP-2 fusion protein, Bardhan *et al.* showed that PD-1 interacted with SHP-2 after PD-1 ligation with simultaneous TCR/CD3-mediated activation [399]. The phosphorylation of the ITSM was necessary for this interaction and was abrogated when the ITSM tyrosine Y248 was mutated to phenylalanine. However, when mutation was made to the ITIM tyrosine Y223, the interaction between SHP-2 and PD-1 stayed intact [399]. SHPs dephosphorylate effector molecules associated with the TCR, leading to termination of TCR signal transduction [196, 223]. Our finding that PD-1 downregulation can be uncoupled from receptor triggering by altering the affinity could be due to the fact that the tyrosine in the PD-1 tail might have different roles in downregulation. The weak binding elicited by FoR1 may activate signalling *via* the ITSM, whilst with strong binding as in the case with the 1st generation Cl19 antibody, receptor internalisation and subsequent downregulation may occur. Internalization is not required for signal transduction, but it may change the biology of a particular signalling system by removing the receptor from the cell surface [344]. There are varying fates of internalized receptors, many are rapidly recycled to the cell surface while others are

directed to lysosomes for degradation [400]. For receptors like PD-1 that mediate transmembrane signal transduction, internalization may be a way of modulating responsiveness to the particular ligand [344].

FcγRIIB is the only inhibitory Fc receptor [345]. It helps to regulate a variety of immune and inflammatory responses. Variation in the gene encoding this protein is linked to susceptibility to autoimmune disorders such as systemic lupus [345]. Studies have shown that the Fc fragments of IgG plays an important role in inhibiting humoral immunity [346]. Moreover, if FcγRIIB is cross-linked to the BCR, the B cell activation threshold is elevated and antibody production decreases [345]. Since our anti-PD-1 antibodies are the IgG1 isotype, they could potentially bind to FcγRIIBs, become hyper-cross-linked, and enhance their agonistic inhibitory signalling capacity by concentrating PD-1 receptors at the cell surface and causing increased downstream inhibitory signalling. In contrast, FcγRIIB disabled mAbs may have reduced inhibitory signalling capacity, and thus prove to be less effective in autoimmune settings.

Further investigation, perhaps in the form of alternative methods to ascertain PD-1 downstream signalling *via* anti-PD-1 agonising antibodies following T cell activation could be examined. This will help to determine if and in what way the effects of changing receptor binding kinetics could contribute to superagonist-induced signalling. PD-1 alters membrane proximal signalling events in T cells, yet the exact biochemical mechanisms through which PD-1 inhibits T cell activation remain poorly understood. Previous studies have indicated that SHP-2 phosphatase activity is significantly increased by anti-CD3 antibody and PD-L2 stimulation and this caused enhanced levels of SHP-2 associated with the PD-1 receptor [401]. Moreover, other work has shown that PD-1 inhibits the further-downstream induction of phosphatidylinositol-3-kinase (PI3K) activity and downstream Akt activation [222]. Both Akt and PI3K activity play essential roles in glycolysis and glucose transport and so PD-1 mediated inhibition of such signalling molecules

could modulate cell bioenergetics. Bearing this in mind, it would be of interest to use hPD-1 k.i. mouse splenocytes, activate them with anti-CD3 and anti-CD28 antibodies and then assess downstream SHP-2, PI3K and Akt activity and see if inhibitory effects could be generated through PD-1 ligation with our anti-PD-1 antibodies. Phospho-flow cytometry could be utilised to ascertain the levels of SHP-2, PI3K and Akt phosphorylation.

PD-1 ligation further causes inhibition of extracellular signal-regulated kinase 1/2 (ERK1/2) phosphorylation and activation. The ERK cascade is a fundamental signalling pathway needed for regulation of a broad variety of stimulated cellular processes, including proliferation, differentiation, survival, apoptosis and stress response [402]. The effects of our anti-PD-1 antibodies on the ERK pathway, would therefore also be of interest. Both the PD-L pathway and T reg cells are vital in the maintenance of peripheral tolerance. PD-L1 mediated conversion of naive T cells to iTregs have been demonstrated successfully in previous studies [225]. Such PD-L1 signalling allowed elevated and sustained Foxp3 expression and enhanced the suppressive function of iTreg cells. Since Tregs are essential components required for preventing autoimmunity, it would be of interest to analyse the effects of anti-PD-1 antibodies on this type of Treg conversion and also investigate the corresponding Foxp3 expression associated [225].

In addition to cytokine suppression assays that have been performed here, which investigated the inhibition of inflammatory cytokines by our anti-PD1 antibodies, further experiments could investigate the effects of PD-1 signalling in monocytes in terms of increase in production of anti-inflammatory cytokines like IL-10 [403]. Furthermore, different mouse models of autoimmunity for IBD, arthritis, transplant rejection, graft versus host disease, hyperproliferative immune disorders and type I diabetes could be used to test the suppressive effects of the anti-PD-1 antibodies *in vivo*. These will help to reveal if our anti-PD-1 antibodies can help dampen the immune response in order to ameliorate disease symptoms. Song *et al.* have shown

that PD-L1-Fc treatment on intestinal inflammation using a dextran sodium sulfate-induced and a T cell transfer induced mouse model of colitis, is able to generate significant protective effects [327]. This treatment led to a decrease in pathogenic Th17 responses, as well as impaired colonic DC production of various cytokines including TNF-α, IL-6 and IL-1β [327].

The *in vivo* data collected indicated that the dose of suppressive anti-PD-1 antibody is critical in delivering potent signals. If the threshold for signalling is not reached, not enough inhibitory signalling generated by PD-1 triggering will mean that significant inhibitory effects on the GC response, primary antibody response and $CD8^+$ T cell response will not be obtained. Consequently, optimisation of the dose will be important in a therapeutic setting. Moreover, the method of antibody delivery can further affect the potency of the suppressive response. Therefore, for maximal and specific therapeutic effects, more work would be necessary for determining the best combination of dose and delivery of the anti-PD-1 antibodies.

II. Concluding remarks

The association of immune checkpoint receptors with autoimmune disorders in humans, and the autoimmune responses observed when such receptors are inactivated in experimental mice or blocked therapeutically in cancer patients all provide strong evidence for the key role these pathways play in the regulation of immunity [404]. It also suggests that the induction of signalling through these inhibitory receptors may offer a way to turn off adverse immune responses and allow the immune system to return to a state of tolerance after control has been thwarted in autoimmune conditions [404]. Previously, agonistic antibodies, Fc-fusion proteins and other novel compounds which trigger checkpoint receptors have exhibited ameliorative effects in animal models of autoimmunity [327, 336, 405-410]. Although there are a limited number of studies that have investigated agonistic compounds capable of delivering suppressive signals to T cells through checkpoint receptors, their potential importance is apparent since such inhibitory agonists, if they could be

translated into human disease, could act as useful and potent immunosuppressive agents [404].

The work presented in this thesis indicated that by modulating antibody affinity, the agonistic signalling capacities of anti-PD-1 antibodies could be enhanced in certain settings. We showed that PD-1 downregulation can be uncoupled from receptor triggering by altering affinity: FoR1 showed suppressive capacities comparable to Cl19 in both *in vitro* and *in vivo*, and much less down-regulation. Due to the reduced PD-1 receptor downregulation induced by these novel 2nd generation fast off-rate antibodies compared to the 1st generation Cl19 antibody, in the long term, they may have therapeutic value in the setting of delivering sustained inhibitory PD-1 signalling *in vivo*. The experiments embodied in this thesis therefore offer a foundation for developing a novel class of potentially therapeutic antibodies, the inhibitory superagonists.

Bibliography

1. Parkin, J. and B. Cohen, *An overview of the immune system.* Lancet, 2001. **357**(9270): p. 1777-89.
2. Cooper, M.D. and B.R. Herrin, *How did our complex immune system evolve?* Nat Rev Immunol, 2010. **10**(1): p. 2-3.
3. Kimbrell, D.A. and B. Beutler, *The evolution and genetics of innate immunity.* Nat Rev Genet, 2001. **2**(4): p. 256-67.
4. Mushegian, A. and R. Medzhitov, *Evolutionary perspective on innate immune recognition.* J Cell Biol, 2001. **155**(5): p. 705-10.
5. Cooper, M.D. and M.N. Alder, *The evolution of adaptive immune systems.* Cell, 2006. **124**(4): p. 815-22.
6. Witko-Sarsat, V., et al., *Neutrophils: molecules, functions and pathophysiological aspects.* Lab Invest, 2000. **80**(5): p. 617-53.
7. Feldmann, M. and R.N. Maini, *Anti-TNF alpha therapy of rheumatoid arthritis: what have we learned?* Annu Rev Immunol, 2001. **19**: p. 163-96.
8. Mackay, C.R., *Chemokines: immunology's high impact factors.* Nat Immunol, 2001. **2**(2): p. 95-101.
9. Sarma, J.V. and P.A. Ward, *The complement system.* Cell Tissue Res, 2011. **343**(1): p. 227-35.
10. Min, H., E. Montecino-Rodriguez, and K. Dorshkind, *Effects of aging on early B- and T-cell development.* Immunol Rev, 2005. **205**: p. 7-17.
11. Cobb, R.M., et al., *Accessibility control of V(D)J recombination.* Adv Immunol, 2006. **91**: p. 45-109.
12. von Boehmer, H., et al., *Pleiotropic changes controlled by the pre-T-cell receptor.* Curr Opin Immunol, 1999. **11**(2): p. 135-42.
13. Klein, L., et al., *Antigen presentation in the thymus for positive selection and central tolerance induction.* Nat Rev Immunol, 2009. **9**(12): p. 833-44.
14. Miosge, L. and R. Zamoyska, *Signalling in T-cell development: is it all location, location, location?* Curr Opin Immunol, 2007. **19**(2): p. 194-9.
15. Curotto de Lafaille, M.A. and J.J. Lafaille, *Natural and adaptive foxp3+ regulatory T cells: more of the same or a division of labor?* Immunity, 2009. **30**(5): p. 626-35.
16. Zhu, J., H. Yamane, and W.E. Paul, *Differentiation of effector CD4 T cell populations (*).* Annu Rev Immunol, 2010. **28**: p. 445-89.
17. Horwitz, D.A., et al., *Critical role of IL-2 and TGF-beta in generation, function and stabilization of Foxp3+CD4+ Treg.* Eur J Immunol, 2008. **38**(4): p. 912-5.
18. Kidd, P., *Th1/Th2 balance: the hypothesis, its limitations, and implications for health and disease.* Altern Med Rev, 2003. **8**(3): p. 223-46.
19. Romagnani, S., *Th1/Th2 cells.* Inflamm Bowel Dis, 1999. **5**(4): p. 285-94.
20. Romagnani, S., *T-cell subsets (Th1 versus Th2).* Ann Allergy Asthma Immunol, 2000. **85**(1): p. 9-18; quiz 18, 21.
21. Vesosky, B., D.K. Flaherty, and J. Turner, *Th1 cytokines facilitate CD8-T-cell-mediated early resistance to infection with Mycobacterium tuberculosis in old mice.* Infect Immun, 2006. **74**(6): p. 3314-24.

22. Bettelli, E., T. Korn, and V.K. Kuchroo, *Th17: the third member of the effector T cell trilogy.* Curr Opin Immunol, 2007. **19**(6): p. 652-7.
23. DiPaolo, R.J., et al., *Autoantigen-specific TGFbeta-induced Foxp3+ regulatory T cells prevent autoimmunity by inhibiting dendritic cells from activating autoreactive T cells.* J Immunol, 2007. **179**(7): p. 4685-93.
24. Trapani, J.A., *Granzymes: a family of lymphocyte granule serine proteases.* Genome Biol, 2001. **2**(12): p. REVIEWS3014.
25. Gordy, C. and Y.W. He, *Endocytosis by target cells: an essential means for perforin- and granzyme-mediated killing.* Cell Mol Immunol, 2012. **9**(1): p. 5-6.
26. Podack, E.R., *Functional significance of two cytolytic pathways of cytotoxic T lymphocytes.* J Leukoc Biol, 1995. **57**(4): p. 548-52.
27. Berg, R.E. and J. Forman, *The role of CD8 T cells in innate immunity and in antigen non-specific protection.* Curr Opin Immunol, 2006. **18**(3): p. 338-43.
28. Sakaguchi, S., et al., *FOXP3+ regulatory T cells in the human immune system.* Nat Rev Immunol, 2010. **10**(7): p. 490-500.
29. Sojka, D.K., Y.H. Huang, and D.J. Fowell, *Mechanisms of regulatory T-cell suppression - a diverse arsenal for a moving target.* Immunology, 2008. **124**(1): p. 13-22.
30. Liao, C.M., M.I. Zimmer, and C.R. Wang, *The functions of type I and type II natural killer T cells in inflammatory bowel diseases.* Inflamm Bowel Dis, 2013. **19**(6): p. 1330-8.
31. Schluns, K.S. and L. Lefrancois, *Cytokine control of memory T-cell development and survival.* Nat Rev Immunol, 2003. **3**(4): p. 269-79.
32. Weng, N.P., Y. Araki, and K. Subedi, *The molecular basis of the memory T cell response: differential gene expression and its epigenetic regulation.* Nat Rev Immunol, 2012. **12**(4): p. 306-15.
33. Neefjes, J., et al., *Towards a systems understanding of MHC class I and MHC class II antigen presentation.* Nat Rev Immunol, 2011. **11**(12): p. 823-36.
34. Marsh, S.G.E., P. Parham, and L.D. Barber, *The HLA factsbook*. Factsbook series. 2000, San Diego: Academic Press.
35. Dalchau, N., et al., *A peptide filtering relation quantifies MHC class I peptide optimization.* PLoS Computat Biol, 2011. **7**(10).
36. Howe, C., et al., *Calreticulin-dependent recycling in the early secretory pathway mediates optimal peptide loading of MHC class I molecules.* EMBO J, 2009. **28**(23): p. 3730-44.
37. Petersen, J.L., C.R. Morris, and J.C. Solheim, *Virus evasion of MHC class I molecule presentation.* J Immunol, 2003. **171**(9): p. 4473-8.
38. Bessoles, S., et al., *Adaptations of Natural Killer Cells to Self-MHC Class I.* Front Immunol, 2014. **5**: p. 349.
39. Seidel, U.J., P. Schlegel, and P. Lang, *Natural killer cell mediated antibody-dependent cellular cytotoxicity in tumor immunotherapy with therapeutic antibodies.* Front Immunol, 2013. **4**: p. 76.
40. Miller, J.F. and G.F. Mitchell, *Cell to cell interaction in the immune respons: I. Hemolysin-forming cells in neonatally thymectomized mice reconstituted with thymus or thoracic duct lymphocytes.* J Exp Med, 1968. **128**(4): p. 801-20.

41. Mitchell, G.F. and J.F. Miller, *Cell to cell interaction in the immune response: II. The source of hemolysin-forming cells in irradiated mice given bone marrow and thymus or thoracic duct lymphocytes.* J Exp Med, 1968. **128**(4): p. 821-37.
42. Nossal, G.J., et al., *Cell to cell interaction in the immune response: III. Chromosomal marker analysis of single antibody-forming cells in reconstituted, irradiated, or thymectomized mice.* J Exp Med, 1968. **128**(4): p. 839-53.
43. Crotty, S., *A brief history of T cell help to B cells.* Nat Rev Immunol, 2015. **15**(3): p. 185-9.
44. Aguzzi, A., J. Kranich, and N.J. Krautler, *Follicular dendritic cells: origin, phenotype, and function in health and disease.* Trends Immunol, 2014. **35**(3): p. 105-13.
45. Schroeder, H.W., Jr. and L. Cavacini, *Structure and function of immunoglobulins.* J Allergy Clin Immunol, 2010. **125**(2 0 2): p. S41-52.
46. Plomp, R., et al., *Hinge-Region O-Glycosylation of Human Immunoglobulin G3 (IgG3).* Mol Cell Proteomics, 2015. **14**(5): p. 1373-84.
47. Treanor, B., *B-cell receptor: from resting state to activate.* Immunology, 2012. **136**(1): p. 21-7.
48. Raghavan, M. and P.J. Bjorkman, *Fc receptors and their interactions with immunoglobulins.* Annu Rev Cell Dev Biol, 1996. **12**: p. 181-220.
49. Bruhns, P., *Properties of mouse and human IgG receptors and their contribution to disease models.* Blood, 2012. **119**(24): p. 5640-5649.
50. Bruhns, P. and F. Jönsson, *Mouse and human FcR effector functions.* Immunol Rev, 2015. **268**(1): p. 25-51.
51. Sondermann, P., et al., *The 3.2-A crystal structure of the human IgG1 Fc fragment-Fc gammaRIII complex.* Nature, 2000. **406**(6793): p. 267-73.
52. Woof, J.M. and D.R. Burton, *Human antibody-Fc receptor interactions illuminated by crystal structures.* Nat Rev Immunol, 2004. **4**(2): p. 89-99.
53. Dushek, O., J. Goyette, and P.A. van der Merwe, *Non-catalytic tyrosine-phosphorylated receptors.* Immunol Rev, 2012. **250**(1): p. 258-76.
54. Merwe, P.A. and S.J. Davis, *Molecular interactions mediating T cell antigen recognition.* Ann Rev Immunol, 2003. **21**: p. 659-684.
55. Davis, S.J. and P.A. van der Merwe, *The kinetic-segregation model: TCR triggering and beyond.* Nat Immunol, 2006. **7**(8): p. 803-809.
56. Allard, J.F., et al., *Mechanical modulation of receptor-ligand interactions at cell-cell interfaces.* Biophys J, 2012. **102**(6): p. 1265-1273.
57. Daeron, M., et al., *Immunoreceptor tyrosine-based inhibition motifs: a quest in the past and future.* Immunol Rev, 2008. **224**: p. 11-43.
58. Reth, M., *Antigen receptor tail clue.* Nature, 1989. **338**(6214): p. 383-4.
59. Shlapatska, L.M., et al., *CD150 association with either the SH2-containing inositol phosphatase or the SH2-containing protein tyrosine phosphatase is regulated by the adaptor protein SH2D1A.* J Immunol, 2001. **166**(9): p. 5480-7.
60. Billadeau, D.D. and P.J. Leibson, *ITAMs versus ITIMs: striking a balance during cell regulation.* J Clin Invest, 2002. **109**(2): p. 161-8.

61. Rachmilewitz, J. and A. Lanzavecchia, *A temporal and spatial summation model for T-cell activation: signal integration and antigen decoding.* Trends Immunol, 2002. **23**(12): p. 592-5.
62. Gett, A.V. and P.D. Hodgkin, *A cellular calculus for signal integration by T cells.* Nat Immunol, 2000. **1**(3): p. 239-44.
63. Kuhns, M.S., M.M. Davis, and C.K. Garcia, *Deconstructing the Form and Function of the TCR/CD3 Complex.* Immunity, 2006. **24**(2): p. 133-139.
64. Call, M.E. and K.W. Wucherpfennig, *The T cell receptor: critical role of the membrane environment in receptor assembly and function.* Annu Rev Immunol, 2005. **23**: p. 101-25.
65. Garcia, K.C., et al., *Structural basis of plasticity in T cell receptor recognition of a self peptide-MHC antigen.* Science, 1998. **279**(5354): p. 1166-72.
66. Reiser, J.B., et al., *A T cell receptor CDR3beta loop undergoes conformational changes of unprecedented magnitude upon binding to a peptide/MHC class I complex.* Immunity, 2002. **16**(3): p. 345-54.
67. Ding, Y.H., et al., *Four A6-TCR/peptide/HLA-A2 structures that generate very different T cell signals are nearly identical.* Immunity, 1999. **11**(1): p. 45-56.
68. Mason, D., *A very high level of crossreactivity is an essential feature of the T-cell receptor.* Immunol Today, 1998. **19**(9): p. 395-404.
69. Rudolph, M.G. and I.A. Wilson, *The specificity of TCR/pMHC interaction.* Curr Opin Immunol, 2002. **14**(1): p. 52-65.
70. Hennecke, J. and D.C. Wiley, *T cell receptor-MHC interactions up close.* Cell, 2001. **104**(1): p. 1-4.
71. Manolios, N., J.S. Bonifacino, and R.D. Klausner, *Transmembrane helical interactions and the assembly of the T cell receptor complex.* Science, 1990. **249**(4966): p. 274-7.
72. Teixeiro, E., et al., *T cell division and death are segregated by mutation of TCRbeta chain constant domains.* Immunity, 2004. **21**(4): p. 515-26.
73. Call, M.E., et al., *The organizing principle in the formation of the T cell receptor-CD3 complex.* Cell, 2002. **111**(7): p. 967-79.
74. James, J.R., et al., *The T cell receptor triggering apparatus is composed of monovalent or monomeric proteins.* J Biol Chem, 2011. **286**(37): p. 31993-32001.
75. James, J.R., et al., *Single-molecule level analysis of the subunit composition of the T cell receptor on live T cells.* Proc Natl Acad Sci U S A, 2007. **104**(45): p. 17662–17667.
76. Schamel, W., et al., *Coexistence of multivalent and monovalent TCRs explains high sensitivity and wide range of response.* J Exp Med, 2005. **202**(4): p. 493-503.
77. Sigalov, A.B., *"Monovalent" ligands that trigger TLR-4 and TCR are not necessarily truly monovalent.* Mol Immunol, 2012. **51**(3-4): p. 356-362.
78. Dillard, P., et al., *Nano-clustering of ligands on surrogate antigen presenting cells modulates T cell membrane adhesion and organization.* Integr Biol, 2016. **8**(3): p. 287-301.
79. Acuto, O., V. Bartolo, and F. Michel, *Tailoring T-cell receptor signals by proximal negative feedback mechanisms.* Nat Rev Immunol, 2008. **8**(9): p. 699-712.

80. Wang, H., et al., *ZAP-70: An Essential Kinase in T-cell Signaling.* Cold Spring Harb Perspect Biol, 2010. **2**(5): p. a002279.
81. Yokosuka, T. and T. Saito, *The immunological synapse, TCR microclusters, and T cell activation*, in *Immunological Synapse*, T. Saito and F.D. Batista, Editors. 2010, Springer Berlin Heidelberg: Berlin, Heidelberg. p. 81-107.
82. Moreau, H.D.D., et al., *Signal strength regulates antigen-mediated T-cell deceleration by distinct mechanisms to promote local exploration or arrest.* Proc Natl Acad Sci U S A, 2015. **112**(39): p. 12151-12156.
83. Ullrich, A. and J. Schlessinger, *Signal transduction by receptors with tyrosine kinase activity.* Cell, 1990. **61**(2): p. 203-12.
84. Davis, S.J. and P.A. van der Merwe, *The kinetic-segregation model: TCR triggering and beyond.* Nat Immunol, 2006. **7**(8): p. 803-9.
85. van der Merwe, P.A. and O. Dushek, *Mechanisms for T cell receptor triggering.* Nat Rev Immunol, 2011. **11**(1): p. 47-55.
86. Sykulev, Y., et al., *Evidence that a single peptide-MHC complex on a target cell can elicit a cytolytic T cell response.* Immunity, 1996. **4**(6): p. 565-71.
87. Palmer, E. and D. Naeher, *Affinity threshold for thymic selection through a T-cell receptor-co-receptor zipper.* Nat Rev Immunol, 2009. **9**(3): p. 207-13.
88. Arstila, T.P., et al., *A direct estimate of the human alphabeta T cell receptor diversity.* Science, 1999. **286**(5441): p. 958-61.
89. Casrouge, A., et al., *Size estimate of the alpha beta TCR repertoire of naive mouse splenocytes.* J Immunol, 2000. **164**(11): p. 5782-7.
90. Ratcliffe, M.J., et al., *T cell receptor aggregation, but not dimerization, induces increased cytosolic calcium concentrations and reveals a lack of stable association between CD4 and the T cell receptor.* J Immunol, 1992. **148**(6): p. 1643-51.
91. Abastado, J.P., et al., *Dimerization of soluble major histocompatibility complex-peptide complexes is sufficient for activation of T cell hybridoma and induction of unresponsiveness.* J Exp Med, 1995. **182**(2): p. 439-47.
92. Cooper, J.A. and H. Qian, *A mechanism for SRC kinase-dependent signaling by noncatalytic receptors.* Biochemistry, 2008. **47**(21): p. 5681-8.
93. Delon, J., et al., *CD8 expression allows T cell signaling by monomeric peptide-MHC complexes.* Immunity, 1998. **9**(4): p. 467-73.
94. Salter, R.D., et al., *A binding site for the T-cell co-receptor CD8 on the alpha 3 domain of HLA-A2.* Nature, 1990. **345**(6270): p. 41-6.
95. Jameson, S.C. and M.J. Bevan, *T cell receptor antagonists and partial agonists.* Immunity, 1995. **2**(1): p. 1-11.
96. Locksley, R.M., et al., *Helper T cells without CD4: control of leishmaniasis in CD4-deficient mice.* Science, 1993. **261**(5127): p. 1448-51.
97. Davis, S.J., et al., *The nature of molecular recognition by T cells.* Nat Immunol, 2003. **4**(3): p. 217-24.
98. O'Rourke, A.M., J. Rogers, and M.F. Mescher, *Activated CD8 binding to class I protein mediated by the T-cell receptor results in signalling.* Nature, 1990. **346**(6280): p. 187-9.

99. Mittler, R.S., et al., *T-cell receptor-CD4 physical association in a murine T-cell hybridoma: induction by antigen receptor ligation.* Proc Natl Acad Sci U S A, 1989. **86**(21): p. 8531-5.
100. Davis, S.J. and P.A. van der Merwe, *TCR triggering: co-receptor-dependent or -independent?* Trends Immunol, 2003. **24**(12): p. 624-6; author reply 626-7.
101. Irvine, D.J., et al., *Direct observation of ligand recognition by T cells.* Nature, 2002. **419**(6909): p. 845-9.
102. Krogsgaard, M., et al., *Agonist/endogenous peptide-MHC heterodimers drive T cell activation and sensitivity.* Nature, 2005. **434**(7030): p. 238-43.
103. James, J.R., et al., *The T cell receptor triggering apparatus is composed of monovalent or monomeric proteins.* J Biol Chem, 2011. **286**(37): p. 31993-2001.
104. James, J.R. and R.D. Vale, *Biophysical mechanism of T-cell receptor triggering in a reconstituted system.* Nature, 2012. **487**(7405): p. 64-9.
105. Kjer-Nielsen, L., et al., *A structural basis for the selection of dominant alphabeta T cell receptors in antiviral immunity.* Immunity, 2003. **18**(1): p. 53-64.
106. Beddoe, T., et al., *Antigen ligation triggers a conformational change within the constant domain of the alphabeta T cell receptor.* Immunity, 2009. **30**(6): p. 777-88.
107. Kuhns, M.S., M.M. Davis, and K.C. Garcia, *Deconstructing the form and function of the TCR/CD3 complex.* Immunity, 2006. **24**(2): p. 133-9.
108. Kuhns, M.S., et al., *Evidence for a functional sidedness to the alphabetaTCR.* Proc Natl Acad Sci U S A, 2010. **107**(11): p. 5094-9.
109. Dong, et al., *Structural basis of assembly of the human T cell receptor-CD3 complex.* Nature, 2019. **573**(7775): p. 546-552.
110. Martinez-Martin, N., et al., *Cooperativity between T cell receptor complexes revealed by conformational mutants of CD3epsilon.* Sci Signal, 2009. **2**(83): p. ra43.
111. Wang, Y., et al., *A conserved CXXC motif in CD3epsilon is critical for T cell development and TCR signaling.* PLoS Biol, 2009. **7**(12): p. e1000253.
112. Gil, D., et al., *Recruitment of Nck by CD3 epsilon reveals a ligand-induced conformational change essential for T cell receptor signaling and synapse formation.* Cell, 2002. **109**(7): p. 901-12.
113. Risueno, R.M., W.W. Schamel, and B. Alarcon, *T cell receptor engagement triggers its CD3epsilon and CD3zeta subunits to adopt a compact, locked conformation.* PLoS One, 2008. **3**(3): p. e1747.
114. Xu, C., et al., *Regulation of T cell receptor activation by dynamic membrane binding of the CD3epsilon cytoplasmic tyrosine-based motif.* Cell, 2008. **135**(4): p. 702-13.
115. Deford-Watts, L.M., et al., *The cytoplasmic tail of the T cell receptor CD3 epsilon subunit contains a phospholipid-binding motif that regulates T cell functions.* J Immunol, 2009. **183**(2): p. 1055-64.
116. Kuhns, M.S. and M.M. Davis, *The safety on the TCR trigger.* Cell, 2008. **135**(4): p. 594-6.
117. O'Shea, J.J., et al., *Activation of human peripheral blood T lymphocytes by pharmacological induction of protein-tyrosine phosphorylation.* Proc Natl Acad Sci U S A, 1992. **89**(21): p. 10306-10.
118. Secrist, J.P., et al., *Stimulatory effects of the protein tyrosine phosphatase inhibitor, pervanadate, on T-cell activation events.* J Biol Chem, 1993. **268**(8): p. 5886-93.

119. Imbert, V., et al., *Induction of tyrosine phosphorylation and T-cell activation by vanadate peroxide, an inhibitor of protein tyrosine phosphatases.* Biochem J, 1994. **297 (Pt 1)**: p. 163-73.
120. Fernandes, R.A., et al., *What controls T cell receptor phosphorylation?* Cell, 2010. **142**(5): p. 668-9.
121. Springer, T.A., *Adhesion receptors of the immune system.* Nature, 1990. **346**(6283): p. 425-34.
122. Irles, C., et al., *CD45 ectodomain controls interaction with GEMs and Lck activity for optimal TCR signaling.* Nat Immunol, 2003. **4**(2): p. 189-97.
123. Lin, J. and A. Weiss, *The tyrosine phosphatase CD148 is excluded from the immunologic synapse and down-regulates prolonged T cell signaling.* J Cell Biol, 2003. **162**(4): p. 673-82.
124. Choudhuri, K., et al., *T-cell receptor triggering is critically dependent on the dimensions of its peptide-MHC ligand.* Nature, 2005. **436**(7050): p. 578-82.
125. Varma, R., et al., *T cell receptor-proximal signals are sustained in peripheral microclusters and terminated in the central supramolecular activation cluster.* Immunity, 2006. **25**(1): p. 117-27.
126. Chang, V.T., et al., *Initiation of T cell signaling by CD45 segregation at 'close contacts'.* Nat Immunol, 2016. **17**(5): p. 574-582.
127. Cordoba, S.P., et al., *The large ectodomains of CD45 and CD148 regulate their segregation from and inhibition of ligated T-cell receptor.* Blood, 2013. **121**(21): p. 4295-302.
128. Schmid, E.M., et al., *Size-dependent protein segregation at membrane interfaces.* Nat Phys, 2016. **12**(7): p. 704-711.
129. Allard, J.F., et al., *Mechanical modulation of receptor-ligand interactions at cell-cell interfaces.* Biophys J, 2012. **102**(6): p. 1265-73.
130. Hui, E. and R.D. Vale, *In vitro membrane reconstitution of the T-cell receptor proximal signaling network.* Nat Struct Mol Biol, 2014. **21**(2): p. 133-42.
131. Ma, Z., et al., *Surface-anchored monomeric agonist pMHCs alone trigger TCR with high sensitivity.* PLoS Biol, 2008. **6**(2): p. e43.
132. Evans, E.J., et al., *Crystal structure of a soluble CD28-Fab complex.* Nat Immunol, 2005. **6**(3): p. 271-9.
133. Lafferty, K.J. and A.J. Cunningham, *A new analysis of allogeneic interactions.* Aust J Exp Biol Med Sci, 1975. **53**(1): p. 27-42.
134. Beyersdorf, N., et al., *Superagonistic anti-CD28 antibodies: potent activators of regulatory T cells for the therapy of autoimmune diseases.* Ann Rheum Dis, 2005. **64 Suppl 4**: p. iv91-5.
135. Greenwald, R.J., G.J. Freeman, and A.H. Sharpe, *The B7 family revisited.* Annu Rev Immunol, 2005. **23**: p. 515-48.
136. Aruffo, A. and B. Seed, *Molecular cloning of a CD28 cDNA by a high-efficiency COS cell expression system.* Proc Natl Acad Sci U S A, 1987. **84**(23): p. 8573-7.
137. Carreno, B.M. and M. Collins, *The B7 family of ligands and its receptors: new pathways for costimulation and inhibition of immune responses.* Annu Rev Immunol, 2002. **20**: p. 29-53.

138. Beyersdorf, N., T. Kerkau, and T. Hunig, *CD28 co-stimulation in T-cell homeostasis: a recent perspective.* Immunotargets Ther, 2015. **4**: p. 111-22.
139. Esensten, J.H., et al., *CD28 Costimulation: From Mechanism to Therapy.* Immunity, 2016. **44**(5): p. 973-88.
140. Collins, A.V., et al., *The interaction properties of costimulatory molecules revisited.* Immunity, 2002. **17**(2): p. 201-10.
141. Peach, R.J., et al., *Complementarity determining region 1 (CDR1)- and CDR3-analogous regions in CTLA-4 and CD28 determine the binding to B7-1.* J Exp Med, 1994. **180**(6): p. 2049-58.
142. Ikemizu, S., et al., *Structure and dimerization of a soluble form of B7-1.* Immunity, 2000. **12**(1): p. 51-60.
143. Esensten, J.H., et al., *CD28 Costimulation: From Mechanism to Therapy.* Immunity, 2016. **44**(5): p. 973-988.
144. Dennehy, K.M., et al., *Cutting edge: monovalency of CD28 maintains the antigen dependence of T cell costimulatory responses.* J Immunol, 2006. **176**(10): p. 5725-5729.
145. Bhatia, S., et al., *Dynamic equilibrium of B7-1 dimers and monomers differentially affects immunological synapse formation and T cell activation in response to TCR/CD28 stimulation.* J Immunol, 2010. **184**(4): p. 1821-8.
146. Jansson, A., et al., *A theoretical framework for quantitative analysis of the molecular basis of costimulation.* J Immunol, 2005. **175**(3): p. 1575-85.
147. Camperio, C., et al., *CD28 ligation in the absence of TCR stimulation up-regulates IL-17A and pro-inflammatory cytokines in relapsing-remitting multiple sclerosis T lymphocytes.* Immunol Lett, 2014. **158**(1-2): p. 134-142.
148. de Kouchkovsky, D., et al., *microRNA-17-92 regulates IL-10 production by regulatory T cells and control of experimental autoimmune encephalomyelitis.* J Immunol, 2013. **191**(4): p. 1594-605.
149. Guo, F., et al., *CD28 controls differentiation of regulatory T cells from naive CD4 T cells.* J Immunol, 2008. **181**(4): p. 2285-91.
150. Lyddane, C., et al., *Cutting Edge: CD28 controls dominant regulatory T cell activity during active immunization.* J Immunol, 2006. **176**(6): p. 3306-10.
151. Riley, J.L., et al., *Modulation of TCR-induced transcriptional profiles by ligation of CD28, ICOS, and CTLA-4 receptors.* Proc Natl Acad Sci U S A, 2002. **99**(18): p. 11790-5.
152. Bachmann, M.F., et al., *Distinct roles for LFA-1 and CD28 during activation of naive T cells: adhesion versus costimulation.* Immunity, 1997. **7**(4): p. 549-57.
153. Shahinian, A., et al., *Differential T cell costimulatory requirements in CD28-deficient mice.* Science, 1993. **261**(5121): p. 609-12.
154. Holdorf, A.D., et al., *Proline residues in CD28 and the Src homology (SH)3 domain of Lck are required for T cell costimulation.* J Exp Med, 1999. **190**(3): p. 375-84.
155. Raab, M., et al., *p56Lck and p59Fyn regulate CD28 binding to phosphatidylinositol 3-kinase, growth factor receptor-bound protein GRB-2, and T cell-specific protein-tyrosine kinase ITK: implications for T-cell costimulation.* Proc Natl Acad Sci U S A, 1995. **92**(19): p. 8891-5.

156. Sadra, A., et al., *Identification of tyrosine phosphorylation sites in the CD28 cytoplasmic domain and their role in the costimulation of Jurkat T cells.* J Immunol, 1999. **162**(4): p. 1966-73.
157. Kim, H.H., M. Tharayil, and C.E. Rudd, *Growth factor receptor-bound protein 2 SH2/SH3 domain binding to CD28 and its role in co-signaling.* J Biol Chem, 1998. **273**(1): p. 296-301.
158. Boomer, J.S., et al., *Cutting edge: a double-mutant knockin of the CD28 YMNM and PYAP motifs reveals a critical role for the YMNM motif in regulation of T cell proliferation and Bcl-xL expression.* J Immunol, 2014. **192**(8): p. 3465-3469.
159. Bohjanen, P.R., et al., *AU RNA-binding factors differ in their binding specificities and affinities.* J Biol Chem, 1992. **267**(9): p. 6302-6309.
160. Boomer, J.S. and J.M. Green, *An enigmatic tail of CD28 signaling.* Cold Spring Harb Perspect Biol, 2010. **2**(8): p. a002436.
161. Tavano, R., et al., *CD28 interaction with filamin-A controls lipid raft accumulation at the T-cell immunological synapse.* Nat Cell Biol, 2006. **8**(11): p. 1270-6.
162. Fooksman, D.R., et al., *Functional anatomy of T cell activation and synapse formation.* Annu Rev Immunol, 2010. **28**: p. 79-105.
163. Tian, R., et al., *Combinatorial proteomic analysis of intercellular signaling applied to the CD28 T-cell costimulatory receptor.* Proc Natl Acad Sci U S A, 2015. **112**(13): p. E1594-603.
164. Porciello, N. and L. Tuosto, *CD28 costimulatory signals in T lymphocyte activation: Emerging functions beyond a qualitative and quantitative support to TCR signalling.* Cytokine Growth Factor Rev, 2016. **28**: p. 11-19.
165. Frauwirth, K.A., et al., *The CD28 signaling pathway regulates glucose metabolism.* Immunity, 2002. **16**(6): p. 769-77.
166. Boise, L.H., et al., *CD28 costimulation can promote T cell survival by enhancing the expression of Bcl-xL.* Immunity, 1995. **3**(1): p. 87-98.
167. Walker, L.S. and D.M. Sansom, *The emerging role of CTLA4 as a cell-extrinsic regulator of T cell responses.* Nat Rev Immunol, 2011. **11**(12): p. 852-63.
168. Walker, L.S. and D.M. Sansom, *Confusing signals: recent progress in CTLA-4 biology.* Trends Immunol, 2015. **36**(2): p. 63-70.
169. Darlington, P.J., et al., *Hierarchical regulation of CTLA-4 dimer-based lattice formation and its biological relevance for T cell inactivation.* J Immunol, 2005. **175**(2): p. 996-1004.
170. Yu, C., et al., *Rigid-body ligand recognition drives cytotoxic T-lymphocyte antigen 4 (CTLA-4) receptor triggering.* J Biol Chem, 2011. **286**(8): p. 6685-96.
171. Sharpe, A.H. and G.J. Freeman, *The B7-CD28 superfamily.* Nat Rev Immunol, 2002. **2**(2): p. 116-26.
172. Greenwald, R.J., et al., *CTLA-4 regulates induction of anergy in vivo.* Immunity, 2001. **14**(2): p. 145-55.
173. Mandelbrot, D.A., A.J. McAdam, and A.H. Sharpe, *B7-1 or B7-2 is required to produce the lymphoproliferative phenotype in mice lacking cytotoxic T lymphocyte-associated antigen 4 (CTLA-4).* J Exp Med, 1999. **189**(2): p. 435-40.
174. Watanabe, N., et al., *BTLA is a lymphocyte inhibitory receptor with similarities to CTLA-4 and PD-1.* Nat Immunol, 2003. **4**(7): p. 670-9.

175. Gonzalez, L.C., et al., *A coreceptor interaction between the CD28 and TNF receptor family members B and T lymphocyte attenuator and herpesvirus entry mediator.* Proc Natl Acad Sci U S A, 2005. **102**(4): p. 1116-21.
176. Cai, G., et al., *CD160 inhibits activation of human CD4+ T cells through interaction with herpesvirus entry mediator.* Nat Immunol, 2008. **9**(2): p. 176-85.
177. Carreno, B.M. and M. Collins, *BTLA: a new inhibitory receptor with a B7-like ligand.* Trends Immunol, 2003. **24**(10): p. 524-7.
178. Chambers, C.A., et al., *CTLA-4-mediated inhibition in regulation of T cell responses: mechanisms and manipulation in tumor immunotherapy.* Annu Rev Immunol, 2001. **19**: p. 565-94.
179. Derre, L., et al., *BTLA mediates inhibition of human tumor-specific CD8+ T cells that can be partially reversed by vaccination.* J Clin Invest, 2010. **120**(1): p. 157-67.
180. Oya, Y., et al., *Development of autoimmune hepatitis-like disease and production of autoantibodies to nuclear antigens in mice lacking B and T lymphocyte attenuator.* Arthritis Rheum, 2008. **58**(8): p. 2498-510.
181. Deppong, C., et al., *Cutting edge: B and T lymphocyte attenuator and programmed death receptor-1 inhibitory receptors are required for termination of acute allergic airway inflammation.* J Immunol, 2006. **176**(7): p. 3909-13.
182. Steinberg, M.W., et al., *A crucial role for HVEM and BTLA in preventing intestinal inflammation.* J Exp Med, 2008. **205**(6): p. 1463-76.
183. Lin, S.C., C.C. Kuo, and C.H. Chan, *Association of a BTLA gene polymorphism with the risk of rheumatoid arthritis.* J Biomed Sci, 2006. **13**(6): p. 853-60.
184. Murphy, T.L. and K.M. Murphy, *Slow down and survive: Enigmatic immunoregulation by BTLA and HVEM.* Annu Rev Immunol, 2010. **28**: p. 389-411.
185. Mauri, D.N., et al., *LIGHT, a new member of the TNF superfamily, and lymphotoxin alpha are ligands for herpesvirus entry mediator.* Immunity, 1998. **8**(1): p. 21-30.
186. Cheung, T.C., et al., *Unconventional ligand activation of herpesvirus entry mediator signals cell survival.* Proc Natl Acad Sci U S A, 2009. **106**(15): p. 6244-9.
187. Hutloff, A., et al., *ICOS is an inducible T-cell co-stimulator structurally and functionally related to CD28.* Nature, 1999. **397**(6716): p. 263-6.
188. Richter, G., et al., *Tumor necrosis factor-alpha regulates the expression of inducible costimulator receptor ligand on CD34(+) progenitor cells during differentiation into antigen presenting cells.* J Biol Chem, 2001. **276**(49): p. 45686-93.
189. McAdam, A.J., et al., *ICOS is critical for CD40-mediated antibody class switching.* Nature, 2001. **409**(6816): p. 102-5.
190. Riley, J.L., et al., *ICOS costimulation requires IL-2 and can be prevented by CTLA-4 engagement.* J Immunol, 2001. **166**(8): p. 4943-8.
191. Grimbacher, B., et al., *Homozygous loss of ICOS is associated with adult-onset common variable immunodeficiency.* Nat Immunol, 2003. **4**(3): p. 261-8.
192. Bossaller, L., et al., *ICOS deficiency is associated with a severe reduction of CXCR5+CD4 germinal center Th cells.* J Immunol, 2006. **177**(7): p. 4927-32.
193. Moore, T.V., et al., *Protective effector memory CD4 T cells depend on ICOS for survival.* PLoS One, 2011. **6**(2): p. e16529.

194. Zamani, M.R., et al., *PD-1/PD-L and autoimmunity: A growing relationship.* Cell Immunol, 2016. **310**: p. 27-41.
195. Saresella, M., et al., *The PD-1/PD-L1 pathway in human pathology.* Curr Mol Med, 2012. **12**(3): p. 259-67.
196. Chemnitz, J.M., et al., *SHP-1 and SHP-2 associate with immunoreceptor tyrosine-based switch motif of programmed death 1 upon primary human T cell stimulation, but only receptor ligation prevents T cell activation.* J Immunol, 2004. **173**(2): p. 945-54.
197. Chen, L. and D.B. Flies, *Molecular mechanisms of T cell co-stimulation and co-inhibition.* Nat Rev Immunol, 2013. **13**(4): p. 227-42.
198. Agata, Y., et al., *Expression of the PD-1 antigen on the surface of stimulated mouse T and B lymphocytes.* Int Immunol, 1996. **8**(5): p. 765-72.
199. Kinter, A.L., et al., *The common gamma-chain cytokines IL-2, IL-7, IL-15, and IL-21 induce the expression of programmed death-1 and its ligands.* J Immunol, 2008. **181**(10): p. 6738-46.
200. Austin, J.W., et al., *STAT3, STAT4, NFATc1, and CTCF regulate PD-1 through multiple novel regulatory regions in murine T cells.* J Immunol, 2014. **192**(10): p. 4876-86.
201. Kao, C., et al., *Transcription factor T-bet represses expression of the inhibitory receptor PD-1 and sustains virus-specific CD8+ T cell responses during chronic infection.* Nat Immunol, 2011. **12**(7): p. 663-71.
202. Oestreich, K.J., et al., *NFATc1 regulates PD-1 expression upon T cell activation.* J Immunol, 2008. **181**(7): p. 4832-9.
203. Lu, P., et al., *Blimp-1 represses CD8 T cell expression of PD-1 using a feed-forward transcriptional circuit during acute viral infection.* J Exp Med, 2014. **211**(3): p. 515-27.
204. Staron, M.M., et al., *The transcription factor FoxO1 sustains expression of the inhibitory receptor PD-1 and survival of antiviral CD8(+) T cells during chronic infection.* Immunity, 2014. **41**(5): p. 802-14.
205. McPherson, R.C., et al., *Epigenetic modification of the PD-1 (Pdcd1) promoter in effector CD4(+) T cells tolerized by peptide immunotherapy.* Elife, 2014. **3**.
206. Youngblood, B., et al., *Chronic virus infection enforces demethylation of the locus that encodes PD-1 in antigen-specific CD8(+) T cells.* Immunity, 2011. **35**(3): p. 400-12.
207. Voron, T., et al., *VEGF-A modulates expression of inhibitory checkpoints on CD8+ T cells in tumors.* J Exp Med, 2015. **212**(2): p. 139-48.
208. Nishimura, H., T. Honjo, and N. Minato, *Facilitation of beta selection and modification of positive selection in the thymus of PD-1-deficient mice.* J Exp Med, 2000. **191**(5): p. 891-8.
209. Chinai, J.M., et al., *New immunotherapies targeting the PD-1 pathway.* Trends Pharmacol Sci, 2015. **36**(9): p. 587-95.
210. Butte, M.J., et al., *Programmed death-1 ligand 1 interacts specifically with the B7-1 costimulatory molecule to inhibit T cell responses.* Immunity, 2007. **27**(1): p. 111-22.
211. Xiao, Y., et al., *RGMb is a novel binding partner for PD-L2 and its engagement with PD-L2 promotes respiratory tolerance.* J Exp Med, 2014. **211**(5): p. 943-59.
212. Okazaki, T. and T. Honjo, *PD-1 and PD-1 ligands: from discovery to clinical application.* Int Immunol, 2007. **19**(7): p. 813-24.

213. Zhang, X., et al., *Structural and functional analysis of the costimulatory receptor programmed death-1.* Immunity, 2004. **20**(3): p. 337-47.
214. Lazar-Molnar, E., et al., *Crystal structure of the complex between programmed death-1 (PD-1) and its ligand PD-L2.* Proc Natl Acad Sci U S A, 2008. **105**(30): p. 10483-8.
215. Dong, H., et al., *B7-H1, a third member of the B7 family, co-stimulates T-cell proliferation and interleukin-10 secretion.* Nat Med, 1999. **5**(12): p. 1365-9.
216. Freeman, G.J., et al., *Engagement of the PD-1 immunoinhibitory receptor by a novel B7 family member leads to negative regulation of lymphocyte activation.* J Exp Med, 2000. **192**(7): p. 1027-34.
217. Keir, M.E., et al., *Tissue expression of PD-L1 mediates peripheral T cell tolerance.* J Exp Med, 2006. **203**(4): p. 883-95.
218. Scandiuzzi, L., et al., *Tissue-expressed B7-H1 critically controls intestinal inflammation.* Cell Rep, 2014. **6**(4): p. 625-32.
219. Yamazaki, T., et al., *Expression of programmed death 1 ligands by murine T cells and APC.* J Immunol, 2002. **169**(10): p. 5538-45.
220. Francisco, L.M., P.T. Sage, and A.H. Sharpe, *The PD-1 pathway in tolerance and autoimmunity.* Immunol Rev, 2010. **236**: p. 219-42.
221. Yokosuka, T., et al., *Programmed cell death 1 forms negative costimulatory microclusters that directly inhibit T cell receptor signaling by recruiting phosphatase SHP2.* J Exp Med, 2012. **209**(6): p. 1201-17.
222. Parry, R.V., et al., *CTLA-4 and PD-1 receptors inhibit T-cell activation by distinct mechanisms.* Mol Cell Biol, 2005. **25**(21): p. 9543-53.
223. Sheppard, K.A., et al., *PD-1 inhibits T-cell receptor induced phosphorylation of the ZAP70/CD3zeta signalosome and downstream signaling to PKCtheta.* FEBS Lett, 2004. **574**(1-3): p. 37-41.
224. Patsoukis, N., et al., *Selective effects of PD-1 on Akt and Ras pathways regulate molecular components of the cell cycle and inhibit T cell proliferation.* Sci Signal, 2012. **5**(230): p. ra46.
225. Francisco, L.M., et al., *PD-L1 regulates the development, maintenance, and function of induced regulatory T cells.* J Exp Med, 2009. **206**(13): p. 3015-29.
226. Patsoukis, N., et al., *PD-1 alters T-cell metabolic reprogramming by inhibiting glycolysis and promoting lipolysis and fatty acid oxidation.* Nat Commun, 2015. **6**: p. 6692.
227. Barber, D.L., et al., *Restoring function in exhausted CD8 T cells during chronic viral infection.* Nature, 2006. **439**(7077): p. 682-7.
228. Latchman, Y., et al., *PD-L2 is a second ligand for PD-1 and inhibits T cell activation.* Nat Immunol, 2001. **2**(3): p. 261-8.
229. Hofmeyer, K.A., H. Jeon, and X. Zang, *The PD-1/PD-L1 (B7-H1) pathway in chronic infection-induced cytotoxic T lymphocyte exhaustion.* J Biomed Biotechnol, 2011. **2011**: p. 451694.
230. Quigley, M., et al., *Transcriptional analysis of HIV-specific CD8+ T cells shows that PD-1 inhibits T cell function by upregulating BATF.* Nat Med, 2010. **16**(10): p. 1147-51.
231. Ohaegbulam, K.C., et al., *Human cancer immunotherapy with antibodies to the PD-1 and PD-L1 pathway.* Trends Mol Med, 2015. **21**(1): p. 24-33.

232. Pauken, K.E. and E.J. Wherry, *Overcoming T cell exhaustion in infection and cancer.* Trends Immunol, 2015. **36**(4): p. 265-76.
233. Rao, M., et al., *Anti-PD-1/PD-L1 therapy for infectious diseases: learning from the cancer paradigm.* Int J Infect Dis, 2017. **56**: p. 221-228.
234. Tokuhiro, S., et al., *An intronic SNP in a RUNX1 binding site of SLC22A4, encoding an organic cation transporter, is associated with rheumatoid arthritis.* Nat Genet, 2003. **35**(4): p. 341-8.
235. de la Fuente, H., D. Cibrian, and F. Sanchez-Madrid, *Immunoregulatory molecules are master regulators of inflammation during the immune response.* FEBS Lett, 2012. **586**(18): p. 2897-2905.
236. Dmitrieva-Zdorova, E.V., et al., *PDCD1 PD-1.3 polymorphism and allergic bronchial asthma in Russian and Buryat patients.* J Asthma, 2017. **54**(1): p. 46-52.
237. Chan, A.C. and P.J. Carter, *Therapeutic antibodies for autoimmunity and inflammation.* Nat Rev Immunol, 2010. **10**(5): p. 301-16.
238. Finck, B.K., P.S. Linsley, and D. Wofsy, *Treatment of murine lupus with CTLA4Ig.* Science, 1994. **265**(5176): p. 1225-7.
239. Anderson, D.E., A.H. Sharpe, and D.A. Hafler, *The B7-CD28/CTLA-4 costimulatory pathways in autoimmune disease of the central nervous system.* Curr Opin Immunol, 1999. **11**(6): p. 677-83.
240. Bachmaier, K., et al., *Induction of autoimmunity in the absence of CD28 costimulation.* J Immunol, 1996. **157**(4): p. 1752-7.
241. Tada, Y., et al., *CD28-deficient mice are highly resistant to collagen-induced arthritis.* J Immunol, 1999. **162**(1): p. 203-8.
242. Peterson, K.E., et al., *B7.2 has opposing roles during the activation versus effector stages of experimental autoimmune thyroiditis.* J Immunol, 1999. **162**(3): p. 1859-67.
243. Shi, F.D., et al., *Differential requirements for CD28 and CD40 ligand in the induction of experimental autoimmune myasthenia gravis.* Eur J Immunol, 1998. **28**(11): p. 3587-93.
244. Girvin, A.M., et al., *A critical role for B7/CD28 costimulation in experimental autoimmune encephalomyelitis: a comparative study using costimulatory molecule-deficient mice and monoclonal antibody blockade.* J Immunol, 2000. **164**(1): p. 136-43.
245. Salomon, B. and J.A. Bluestone, *Complexities of CD28/B7: CTLA-4 costimulatory pathways in autoimmunity and transplantation.* Annu Rev Immunol, 2001. **19**: p. 225-52.
246. Stuart, R.W. and M.K. Racke, *Targeting T cell costimulation in autoimmune disease.* Expert Opin Ther Targets, 2002. **6**(3): p. 275-89.
247. Perrin, P.J., et al., *Differential requirements of naive and memory T cells for CD28 costimulation in autoimmune pathogenesis.* Histol Histopathol, 1999. **14**(4): p. 1269-76.
248. Beyersdorf, N., et al., *CD28 superagonists put a break on autoimmunity by preferentially activating CD4+CD25+ regulatory T cells.* Autoimmun Rev, 2006. **5**(1): p. 40-5.
249. Hunig, T., *The storm has cleared: lessons from the CD28 superagonist TGN1412 trial.* Nat Rev Immunol, 2012. **12**(5): p. 317-8.

250. Eastwood, D., et al., *Monoclonal antibody TGN1412 trial failure explained by species differences in CD28 expression on CD4+ effector memory T-cells.* Br J Pharmacol, 2010. **161**(3): p. 512-26.
251. Miller, S.D., et al., *Blockade of CD28/B7-1 interaction prevents epitope spreading and clinical relapses of murine EAE.* Immunity, 1995. **3**(6): p. 739-45.
252. Vanderlugt, C.L., et al., *Treatment with intact anti-B7-1 mAb during disease remission enhances epitope spreading and exacerbates relapses in R-EAE.* J Neuroimmunol, 1997. **79**(2): p. 113-8.
253. Lenschow, D.J., et al., *Differential effects of anti-B7-1 and anti-B7-2 monoclonal antibody treatment on the development of diabetes in the nonobese diabetic mouse.* J Exp Med, 1995. **181**(3): p. 1145-55.
254. Butte, M.J., et al., *Interaction of human PD-L1 and B7-1.* Mol Immunol, 2008. **45**(13): p. 3567-72.
255. Alegre, M.L. and F. Fallarino, *Mechanisms of CTLA-4-Ig in tolerance induction.* Curr Pharm Des, 2006. **12**(2): p. 149-60.
256. Riella, L.V., et al., *Deleterious effect of CTLA4-Ig on a Treg-dependent transplant model.* Am J Transplant, 2012. **12**(4): p. 846-55.
257. Tang, A.L., et al., *CTLA4 expression is an indicator and regulator of steady-state CD4+ FoxP3+ T cell homeostasis.* J Immunol, 2008. **181**(3): p. 1806-13.
258. Alvarez-Quiroga, C., et al., *CTLA-4-Ig therapy diminishes the frequency but enhances the function of Treg cells in patients with rheumatoid arthritis.* J Clin Immunol, 2011. **31**(4): p. 588-95.
259. Ko, H.J., et al., *CTLA4-Ig modifies dendritic cells from mice with collagen-induced arthritis to increase the CD4+CD25+Foxp3+ regulatory T cell population.* J Autoimmun, 2010. **34**(2): p. 111-20.
260. van Gelder, M., E.P. Kinwel-Bohre, and D.W. van Bekkum, *Treatment of experimental allergic encephalomyelitis in rats with total body irradiation and syngeneic BMT.* Bone Marrow Transplant, 1993. **11**(3): p. 233-41.
261. Cross, A.H., et al., *Long-term inhibition of murine experimental autoimmune encephalomyelitis using CTLA-4-Fc supports a key role for CD28 costimulation.* J Clin Invest, 1995. **95**(6): p. 2783-9.
262. Wallace, P.M., et al., *CTLA4Ig treatment ameliorates the lethality of murine graft-versus-host disease across major histocompatibility complex barriers.* Transplantation, 1994. **58**(5): p. 602-10.
263. Zimmerman, R., et al., *Advances in the treatment of lupus nephritis.* Annu Rev Med, 2001. **52**: p. 63-78.
264. Racke, M.K., et al., *Distinct roles for B7-1 (CD-80) and B7-2 (CD-86) in the initiation of experimental allergic encephalomyelitis.* J Clin Invest, 1995. **96**(5): p. 2195-203.
265. Martin Mola, E., et al., *Abatacept use in rheumatoid arthritis: Evidence review and recommendations.* Reumatol Clin, 2012.
266. Pilat, N., M.H. Sayegh, and T. Wekerle, *Costimulatory pathways in transplantation.* Semin Immunol, 2011. **23**(4): p. 293-303.

267. Hwang, K.W., et al., *Cutting edge: targeted ligation of CTLA-4 in vivo by membrane-bound anti-CTLA-4 antibody prevents rejection of allogeneic cells.* J Immunol, 2002. **169**(2): p. 633-7.
268. Fife, B.T., et al., *Inhibition of T cell activation and autoimmune diabetes using a B cell surface-linked CTLA-4 agonist.* J Clin Invest, 2006. **116**(8): p. 2252-61.
269. Albring, J.C., et al., *Targeting of B and T lymphocyte associated (BTLA) prevents graft-versus-host disease without global immunosuppression.* J Exp Med, 2010. **207**(12): p. 2551-9.
270. Tajima, N., et al., *JTA-009, a fully human antibody against human AILIM/ICOS, ameliorates graft-vs-host reaction in SCID mice grafted with human PBMCs.* Exp Hematol, 2008. **36**(11): p. 1514-23.
271. Mollweide, A., et al., *Only therapeutic ICOS:ICOSL blockade alleviates acute graft versus host disease.* Klin Padiatr, 2009. **221**(6): p. 344-50.
272. Dempke, W.C.M., et al., *Second- and third-generation drugs for immuno-oncology treatment-The more the better?* Eur J Cancer, 2017. **74**: p. 55-72.
273. Wherry, E.J., *T cell exhaustion.* Nat Immunol, 2011. **12**(6): p. 492-9.
274. Blackburn, S.D., et al., *Coregulation of CD8+ T cell exhaustion by multiple inhibitory receptors during chronic viral infection.* Nat Immunol, 2009. **10**(1): p. 29-37.
275. Kostense, S., et al., *High viral burden in the presence of major HIV-specific CD8(+) T cell expansions: evidence for impaired CTL effector function.* Eur J Immunol, 2001. **31**(3): p. 677-86.
276. Schlaak, J.F., et al., *The presence of high amounts of HBV-DNA in serum is associated with suppressed costimulatory effects of interleukin 12 on HBV-induced immune response.* J Hepatol, 1999. **30**(3): p. 353-8.
277. Wedemeyer, H., et al., *Impaired effector function of hepatitis C virus-specific CD8+ T cells in chronic hepatitis C virus infection.* J Immunol, 2002. **169**(6): p. 3447-58.
278. Gardiner, D., et al., *A randomized, double-blind, placebo-controlled assessment of BMS-936558, a fully human monoclonal antibody to programmed death-1 (PD-1), in patients with chronic hepatitis C virus infection.* PLoS One, 2013. **8**(5): p. e63818.
279. Ozkaynak, E., et al., *Programmed death-1 targeting can promote allograft survival.* J Immunol, 2002. **169**(11): p. 6546-53.
280. Sandner, S.E., et al., *Role of the programmed death-1 pathway in regulation of alloimmune responses in vivo.* J Immunol, 2005. **174**(6): p. 3408-15.
281. Tao, R., et al., *Differential effects of B and T lymphocyte attenuator and programmed death-1 on acceptance of partially versus fully MHC-mismatched cardiac allografts.* J Immunol, 2005. **175**(9): p. 5774-82.
282. Habicht, A., et al., *Striking dichotomy of PD-L1 and PD-L2 pathways in regulating alloreactive CD4(+) and CD8(+) T cells in vivo.* Am J Transplant, 2007. **7**(12): p. 2683-92.
283. Tanaka, K., et al., *PDL1 is required for peripheral transplantation tolerance and protection from chronic allograft rejection.* J Immunol, 2007. **179**(8): p. 5204-10.
284. Ito, T., et al., *Analysis of the role of negative T cell costimulatory pathways in CD4 and CD8 T cell-mediated alloimmune responses in vivo.* J Immunol, 2005. **174**(11): p. 6648-56.

285. Koga, N., et al., *Blockade of the interaction between PD-1 and PD-L1 accelerates graft arterial disease in cardiac allografts.* Arterioscler Thromb Vasc Biol, 2004. **24**(11): p. 2057-62.
286. Keir, M.E., et al., *PD-1 and its ligands in tolerance and immunity.* Annu Rev Immunol, 2008. **26**: p. 677-704.
287. Kitazawa, Y., et al., *Involvement of the programmed death-1/programmed death-1 ligand pathway in CD4+CD25+ regulatory T-cell activity to suppress alloimmune responses.* Transplantation, 2007. **83**(6): p. 774-82.
288. Blazar, B.R., et al., *Blockade of programmed death-1 engagement accelerates graft-versus-host disease lethality by an IFN-gamma-dependent mechanism.* J Immunol, 2003. **171**(3): p. 1272-7.
289. Yang, J., et al., *The novel costimulatory programmed death ligand 1/B7.1 pathway is functional in inhibiting alloimmune responses in vivo.* J Immunol, 2011. **187**(3): p. 1113-9.
290. Ribas, A., et al., *Antitumor activity in melanoma and anti-self responses in a phase I trial with the anti-cytotoxic T lymphocyte-associated antigen 4 monoclonal antibody CP-675,206.* J Clin Oncol, 2005. **23**(35): p. 8968-77.
291. Tumeh, P.C., et al., *PD-1 blockade induces responses by inhibiting adaptive immune resistance.* Nature, 2014. **515**(7528): p. 568-71.
292. Wong, R.M., et al., *Programmed death-1 blockade enhances expansion and functional capacity of human melanoma antigen-specific CTLs.* Int Immunol, 2007. **19**(10): p. 1223-34.
293. Jin, H.T., Ahmed, R., Okazaki, T., *Role of PD-1 in regulating T cell immunity*, in *Negative Co-Receptors and Ligands*, R. Ahmed, Honjo, T., Editor. 2011.
294. Ahmadzadeh, M., et al., *Tumor antigen-specific CD8 T cells infiltrating the tumor express high levels of PD-1 and are functionally impaired.* Blood, 2009. **114**(8): p. 1537-44.
295. Curiel, T.J., et al., *Blockade of B7-H1 improves myeloid dendritic cell-mediated antitumor immunity.* Nat Med, 2003. **9**(5): p. 562-7.
296. Blank, C., et al., *PD-L1/B7H-1 inhibits the effector phase of tumor rejection by T cell receptor (TCR) transgenic CD8+ T cells.* Cancer Res, 2004. **64**(3): p. 1140-5.
297. Iwai, Y., S. Terawaki, and T. Honjo, *PD-1 blockade inhibits hematogenous spread of poorly immunogenic tumor cells by enhanced recruitment of effector T cells.* Int Immunol, 2005. **17**(2): p. 133-44.
298. He, Y.F., et al., *Blocking programmed death-1 ligand-PD-1 interactions by local gene therapy results in enhancement of antitumor effect of secondary lymphoid tissue chemokine.* J Immunol, 2004. **173**(8): p. 4919-28.
299. Terawaki, S., et al., *Specific and high-affinity binding of tetramerized PD-L1 extracellular domain to PD-1-expressing cells: possible application to enhance T cell function.* Int Immunol, 2007. **19**(7): p. 881-90.
300. Borkner, L., et al., *RNA interference targeting programmed death receptor-1 improves immune functions of tumor-specific T cells.* Cancer Immunol Immunother, 2010. **59**(8): p. 1173-83.

301. Brahmer, J.R., et al., *Phase I study of single-agent anti-programmed death-1 (MDX-1106) in refractory solid tumors: safety, clinical activity, pharmacodynamics, and immunologic correlates.* J Clin Oncol, 2010. **28**(19): p. 3167-75.
302. Hamanishi, J., et al., *PD-1/PD-L1 blockade in cancer treatment: perspectives and issues.* Int J Clin Oncol, 2016. **21**(3): p. 462-73.
303. Guo, L., H. Zhang, and B. Chen, *Nivolumab as Programmed Death-1 (PD-1) Inhibitor for Targeted Immunotherapy in Tumor.* J Cancer, 2017. **8**(3): p. 410-416.
304. Pai-Scherf, L., et al., *FDA Approval Summary: Pembrolizumab for Treatment of Metastatic Non-Small Cell Lung Cancer: First-Line Therapy and Beyond.* Oncologist, 2017. **22**(11): p. 1392-1399.
305. van Noort, J.M., et al., *Minor myelin proteins can be major targets for peripheral blood T cells from both multiple sclerosis patients and healthy subjects.* (0165-5728 (Print)).
306. Mueller, D.L., *Mechanisms maintaining peripheral tolerance.* Nat Immunol, 2010. **11**(1): p. 21-7.
307. Fife, B.T. and K.E. Pauken, *The role of the PD-1 pathway in autoimmunity and peripheral tolerance.* Ann N Y Acad Sci, 2011. **1217**: p. 45-59.
308. Atkinson, M.A., *The pathogenesis and natural history of type 1 diabetes.* Cold Spring Harb Perspect Med, 2012. **2**(11).
309. Fife, B.T., et al., *Interactions between PD-1 and PD-L1 promote tolerance by blocking the TCR-induced stop signal.* Nat Immunol, 2009. **10**(11): p. 1185-92.
310. Unger, W.W., et al., *Induction of Treg by monocyte-derived DC modulated by vitamin D3 or dexamethasone: differential role for PD-L1.* Eur J Immunol, 2009. **39**(11): p. 3147-59.
311. Owens, T. and S. Sriram, *The immunology of multiple sclerosis and its animal model, experimental allergic encephalomyelitis.* Neurol Clin, 1995. **13**(1): p. 51-73.
312. Viglietta, V., et al., *Loss of functional suppression by CD4+CD25+ regulatory T cells in patients with multiple sclerosis.* J Exp Med, 2004. **199**(7): p. 971-9.
313. Chen, L., et al., *Constitutive neuronal expression of the immune regulator, programmed death 1 (PD-1), identified during experimental autoimmune uveitis.* Ocul Immunol Inflamm, 2009. **17**(1): p. 47-55.
314. Liang, S.C., et al., *Regulation of PD-1, PD-L1, and PD-L2 expression during normal and autoimmune responses.* Eur J Immunol, 2003. **33**(10): p. 2706-16.
315. Salama, A.D., et al., *Critical role of the programmed death-1 (PD-1) pathway in regulation of experimental autoimmune encephalomyelitis.* J Exp Med, 2003. **198**(1): p. 71-8.
316. Liu, Y., et al., *Neuron-mediated generation of regulatory T cells from encephalitogenic T cells suppresses EAE.* Nat Med, 2006. **12**(5): p. 518-25.
317. Kohm, A.P., et al., *Cutting edge: CD4+CD25+ regulatory T cells suppress antigen-specific autoreactive immune responses and central nervous system inflammation during active experimental autoimmune encephalomyelitis.* J Immunol, 2002. **169**(9): p. 4712-6.
318. Baecher-Allan, C., et al., *CD4+CD25+ regulatory cells from human peripheral blood express very high levels of CD25 ex vivo.* Novartis Found Symp, 2003. **252**: p. 67-88; discussion 88-91, 106-14.

319. Javan, M.R., et al., *Downregulation of Immunosuppressive Molecules, PD-1 and PD-L1 but not PD-L2, in the Patients with Multiple Sclerosis.* Iran J Allergy Asthma Immunol, 2016. **15**(4): p. 296-302.
320. Krupnick, A.S., et al., *Murine vascular endothelium activates and induces the generation of allogeneic CD4+25+Foxp3+ regulatory T cells.* J Immunol, 2005. **175**(10): p. 6265-70.
321. Loftus, E.V., Jr., *Clinical epidemiology of inflammatory bowel disease: Incidence, prevalence, and environmental influences.* Gastroenterology, 2004. **126**(6): p. 1504-17.
322. Katz, J.A., *Management of inflammatory bowel disease in adults.* J Dig Dis, 2007. **8**(2): p. 65-71.
323. Reinecker, H.C., et al., *Enhanced secretion of tumour necrosis factor-alpha, IL-6, and IL-1 beta by isolated lamina propria mononuclear cells from patients with ulcerative colitis and Crohn's disease.* Clin Exp Immunol, 1993. **94**(1): p. 174-81.
324. Uhlig, H.H., et al., *Characterization of Foxp3+CD4+CD25+ and IL-10-secreting CD4+CD25+ T cells during cure of colitis.* J Immunol, 2006. **177**(9): p. 5852-60.
325. Nakazawa, A., et al., *The expression and function of costimulatory molecules B7H and B7-H1 on colonic epithelial cells.* Gastroenterology, 2004. **126**(5): p. 1347-57.
326. Totsuka, T., et al., *Regulation of murine chronic colitis by CD4+CD25- programmed death-1+ T cells.* Eur J Immunol, 2005. **35**(6): p. 1773-85.
327. Song, M.Y., et al., *Protective effects of Fc-fused PD-L1 on two different animal models of colitis.* Gut, 2015. **64**(2): p. 260-71.
328. de Kleer, I.M., et al., *CD4+CD25bright regulatory T cells actively regulate inflammation in the joints of patients with the remitting form of juvenile idiopathic arthritis.* J Immunol, 2004. **172**(10): p. 6435-43.
329. McInnes, I.B. and J.R. O'Dell, *State-of-the-art: rheumatoid arthritis.* Ann Rheum Dis, 2010. **69**(11): p. 1898-906.
330. Muller-Ladner, U., et al., *Mechanisms of disease: the molecular and cellular basis of joint destruction in rheumatoid arthritis.* Nat Clin Pract Rheumatol, 2005. **1**(2): p. 102-10.
331. Keystone, E.C., et al., *Radiographic, clinical, and functional outcomes of treatment with adalimumab (a human anti-tumor necrosis factor monoclonal antibody) in patients with active rheumatoid arthritis receiving concomitant methotrexate therapy: a randomized, placebo-controlled, 52-week trial.* Arthritis Rheum, 2004. **50**(5): p. 1400-11.
332. Nadkarni, S., C. Mauri, and M.R. Ehrenstein, *Anti-TNF-alpha therapy induces a distinct regulatory T cell population in patients with rheumatoid arthritis via TGF-beta.* J Exp Med, 2007. **204**(1): p. 33-9.
333. Wan, B., et al., *Aberrant regulation of synovial T cell activation by soluble costimulatory molecules in rheumatoid arthritis.* J Immunol, 2006. **177**(12): p. 8844-50.
334. Hatachi, S., et al., *CD4+ PD-1+ T cells accumulate as unique anergic cells in rheumatoid arthritis synovial fluid.* J Rheumatol, 2003. **30**(7): p. 1410-9.
335. Myers, L.K., et al., *Collagen-induced arthritis, an animal model of autoimmunity.* Life Sci, 1997. **61**(19): p. 1861-78.
336. Wang, G., et al., *The effects of PDL-Ig on collagen-induced arthritis.* Rheumatol Int, 2011. **31**(4): p. 513-9.

337. Moutsopoulos, H.M., *Sjogren's syndrome: autoimmune epithelitis.* Clin Immunol Immunopathol, 1994. **72**(2): p. 162-5.
338. Nishimura, H., et al., *Development of lupus-like autoimmune diseases by disruption of the PD-1 gene encoding an ITIM motif-carrying immunoreceptor.* Immunity, 1999. **11**(2): p. 141-51.
339. Liu, M.F., C.T. Weng, and M.Y. Weng, *Variable increased expression of program death-1 and program death-1 ligands on peripheral mononuclear cells is not impaired in patients with systemic lupus erythematosus.* J Biomed Biotechnol, 2009. **2009**: p. 406136.
340. Simpson, N., et al., *Expansion of circulating T cells resembling follicular helper T cells is a fixed phenotype that identifies a subset of severe systemic lupus erythematosus.* Arthritis Rheum, 2010. **62**(1): p. 234-44.
341. Kristjansdottir, H., et al., *Lower expression levels of the programmed death 1 receptor on CD4+CD25+ T cells and correlation with the PD-1.3A genotype in patients with systemic lupus erythematosus.* Arthritis Rheum, 2010. **62**(6): p. 1702-11.
342. Daeron, M., *Fc receptor biology.* Annu Rev Immunol, 1997. **15**: p. 203-34.
343. Cheng, X., et al., *Structure and interactions of the human programmed cell death 1 receptor.* J Biol Chem, 2013. **288**(17): p. 11771-85.
344. Minami, Y., L.E. Samelson, and R.D. Klausner, *Internalization and cycling of the T cell antigen receptor. Role of protein kinase C.* J Biol Chem, 1987. **262**(27): p. 13342-7.
345. Smith, K.G. and M.R. Clatworthy, *FcgammaRIIB in autoimmunity and infection: evolutionary and therapeutic implications.* Nat Rev Immunol, 2010. **10**(5): p. 328-43.
346. Nicholas, R. and S.C. Sinclair, *Regulation of the immune response. I. Reduction in ability of specific antibody to inhibit long-lasting IgG immunological priming after removal of the Fc fragment.* J Exp Med, 1969. **129**(6): p. 1183-201.
347. Omasa, T., M. Onitsuka, and W.D. Kim, *Cell engineering and cultivation of chinese hamster ovary (CHO) cells.* Curr Pharm Biotechnol, 2010. **11**(3): p. 233-40.
348. Knox, R., et al., *A streamlined implementation of the glutamine synthetase-based protein expression system.* BMC Biotechnol, 2013. **13**: p. 74.
349. Huntington, J.A., *Molecular recognition mechanisms of thrombin.* J Thromb Haemost, 2005. **3**(8): p. 1861-72.
350. Ooi, A., et al., *A Guide to Transient Expression of Membrane Proteins in HEK-293 Cells for Functional Characterization.* Front Physiol, 2016. **7**: p. 300.
351. Longo, P.A., et al., *Transient mammalian cell transfection with polyethylenimine (PEI).* Methods Enzymol, 2013. **529**: p. 227-40.
352. Jason-Moller, L., M. Murphy, and J. Bruno, *Overview of Biacore systems and their applications.* Curr Protoc Protein Sci, 2006. **Chapter 19**: p. Unit 19 13.
353. Chapman-Smith, A. and J.E. Cronan, Jr., *Molecular biology of biotin attachment to proteins.* J Nutr, 1999. **129**(2S Suppl): p. 477S-484S.
354. Fernandes, R.A., et al., *T cell receptors are structures capable of initiating signaling in the absence of large conformational rearrangements.* J Biol Chem, 2012. **287**(16): p. 13324-35.
355. R.B., B.M.J.R., *Amino acid properties and consequences of substitutions.*

. Bioinformatics for geneticists, 2003. **317**: p. 289.
356. Morgan, D.A., F.W. Ruscetti, and R. Gallo, *Selective in vitro growth of T lymphocytes from normal human bone marrows.* Science, 1976. **193**(4257): p. 1007-8.
357. Lenardo, M., et al., *Mature T lymphocyte apoptosis--immune regulation in a dynamic and unpredictable antigenic environment.* Annu Rev Immunol, 1999. **17**: p. 221-53.
358. Esposito, E. and S. Cuzzocrea, *TNF-alpha as a therapeutic target in inflammatory diseases, ischemia-reperfusion injury and trauma.* Curr Med Chem, 2009. **16**(24): p. 3152-67.
359. Schoenborn, J.R. and C.B. Wilson, *Regulation of interferon-gamma during innate and adaptive immune responses.* Adv Immunol, 2007. **96**: p. 41-101.
360. Hilchey, S.P. and S.H. Bernstein, *Use of CFSE to monitor ex vivo regulatory T-cell suppression of CD4+ and CD8+ T-cell proliferation within unseparated mononuclear cells from malignant and non-malignant human lymph node biopsies.* Immunol Invest, 2007. **36**(5-6): p. 629-48.
361. Quah, B.J. and C.R. Parish, *The use of carboxyfluorescein diacetate succinimidyl ester (CFSE) to monitor lymphocyte proliferation.* J Vis Exp, 2010(44).
362. Hui, E., et al., *T cell costimulatory receptor CD28 is a primary target for PD-1-mediated inhibition.* Science, 2017. **355**(6332): p. 1428-1433.
363. Porciello, N. and L. Tuosto, *CD28 costimulatory signals in T lymphocyte activation: Emerging functions beyond a qualitative and quantitative support to TCR signalling.* Cytokine Growth Factor Rev, 2016. **28**: p. 11-9.
364. Carter, L., et al., *PD-1:PD-L inhibitory pathway affects both CD4(+) and CD8(+) T cells and is overcome by IL-2.* Eur J Immunol, 2002. **32**(3): p. 634-43.
365. Mestas, J. and C.C. Hughes, *Of mice and not men: differences between mouse and human immunology.* J Immunol, 2004. **172**(5): p. 2731-8.
366. He, X., et al., *Anti-human tissue factor antibody ameliorated intestinal ischemia reperfusion-induced acute lung injury in human tissue factor knock-in mice.* PLoS One, 2008. **3**(1): p. e1527.
367. Kuhn, C., et al., *Human CD3 transgenic mice: preclinical testing of antibodies promoting immune tolerance.* Sci Transl Med, 2011. **3**(68): p. 68ra10.
368. Lute, K.D., et al., *Human CTLA4 knock-in mice unravel the quantitative link between tumor immunity and autoimmunity induced by anti-CTLA-4 antibodies.* Blood, 2005. **106**(9): p. 3127-33.
369. Dorfman, D.M., et al., *Programmed death-1 (PD-1) is a marker of germinal center-associated T cells and angioimmunoblastic T-cell lymphoma.* Am J Surg Pathol, 2006. **30**(7): p. 802-10.
370. Linterman, M.A., et al., *Foxp3+ follicular regulatory T cells control the germinal center response.* Nat Med, 2011. **17**(8): p. 975-82.
371. De Silva, N.S. and U. Klein, *Dynamics of B cells in germinal centres.* Nat Rev Immunol, 2015. **15**(3): p. 137-48.
372. Berek, C., A. Berger, and M. Apel, *Maturation of the immune response in germinal centers.* Cell, 1991. **67**(6): p. 1121-9.
373. Blink, E.J., et al., *Early appearance of germinal center-derived memory B cells and plasma cells in blood after primary immunization.* J Exp Med, 2005. **201**(4): p. 545-54.

374. Brown, K.E., et al., *Role of PD-1 in regulating acute infections.* Curr Opin Immunol, 2010. **22**(3): p. 397-401.
375. Fuse, S., et al., *Recall responses by helpless memory CD8+ T cells are restricted by the up-regulation of PD-1.* J Immunol, 2009. **182**(7): p. 4244-54.
376. Allie, S.R., et al., *Programmed death 1 regulates development of central memory CD8 T cells after acute viral infection.* J Immunol, 2011. **186**(11): p. 6280-6.
377. Ladics, G.S., *Primary immune response to sheep red blood cells (SRBC) as the conventional T-cell dependent antibody response (TDAR) test.* J Immunotoxicol, 2007. **4**(2): p. 149-52.
378. Hangartner, L., R.M. Zinkernagel, and H. Hengartner, *Antiviral antibody responses: the two extremes of a wide spectrum.* Nat Rev Immunol, 2006. **6**(3): p. 231-43.
379. Sharpe, A.H., et al., *The function of programmed cell death 1 and its ligands in regulating autoimmunity and infection.* Nat Immunol, 2007. **8**(3): p. 239-45.
380. Attarwala, H., *TGN1412: From Discovery to Disaster.* J Young Pharm, 2010. **2**(3): p. 332-6.
381. Tacke, M., et al., *CD28-mediated induction of proliferation in resting T cells in vitro and in vivo without engagement of the T cell receptor: evidence for functionally distinct forms of CD28.* Eur J Immunol, 1997. **27**(1): p. 239-47.
382. Dennehy, K.M., et al., *Cutting edge: monovalency of CD28 maintains the antigen dependence of T cell costimulatory responses.* J Immunol, 2006. **176**(10): p. 5725-9.
383. Mian, I.S., A.R. Bradwell, and A.J. Olson, *Structure, function and properties of antibody binding sites.* J Mol Biol, 1991. **217**(1): p. 133-51.
384. Horita, S., et al., *High-resolution crystal structure of the therapeutic antibody pembrolizumab bound to the human PD-1.* Sci Rep, 2016. **6**: p. 35297.
385. Tan, S., et al., *An unexpected N-terminal loop in PD-1 dominates binding by nivolumab.* Nat Commun, 2017. **8**: p. 14369.
386. van Zundert, G.C.P., et al., *The HADDOCK2.2 Web Server: User-Friendly Integrative Modeling of Biomolecular Complexes.* J Mol Biol, 2016. **428**(4): p. 720-725.
387. Krissinel, E. and K. Henrick, *Inference of macromolecular assemblies from crystalline state.* J Mol Biol, 2007. **372**(3): p. 774-97.
388. Davies, D.R. and G.H. Cohen, *Interactions of protein antigens with antibodies.* Proc Natl Acad Sci U S A, 1996. **93**(1): p. 7-12.
389. Patsoukis, N., D. Sari, and V.A. Boussiotis, *PD-1 inhibits T cell proliferation by upregulating p27 and p15 and suppressing Cdc25A.* Cell Cycle, 2012. **11**(23): p. 4305-9.
390. Good-Jacobson, K.L., et al., *PD-1 regulates germinal center B cell survival and the formation and affinity of long-lived plasma cells.* Nat Immunol, 2010. **11**(6): p. 535-42.
391. Ferreira, A.P.A. and E. Boucrot, *Mechanisms of Carrier Formation during Clathrin-Independent Endocytosis.* Trends Cell Biol, 2018. **28**(3): p. 188-200.
392. McMahon, H.T. and E. Boucrot, *Molecular mechanism and physiological functions of clathrin-mediated endocytosis.* Nat Rev Mol Cell Biol, 2011. **12**(8): p. 517-33.

393. Doherty, G.J. and H.T. McMahon, *Mechanisms of endocytosis.* Annu Rev Biochem, 2009. **78**: p. 857-902.
394. Mayor, S., R.G. Parton, and J.G. Donaldson, *Clathrin-independent pathways of endocytosis.* Cold Spring Harb Perspect Biol, 2014. **6**(6).
395. Watanabe, S. and E. Boucrot, *Fast and ultrafast endocytosis.* Curr Opin Cell Biol, 2017. **47**: p. 64-71.
396. del Rio, M.L., J. Kaye, and J.I. Rodriguez-Barbosa, *Detection of protein on BTLAlow cells and in vivo antibody-mediated down-modulation of BTLA on lymphoid and myeloid cells of C57BL/6 and BALB/c BTLA allelic variants.* Immunobiology, 2010. **215**(7): p. 570-8.
397. Hurchla, M.A., J.R. Sedy, and K.M. Murphy, *Unexpected role of B and T lymphocyte attenuator in sustaining cell survival during chronic allostimulation.* J Immunol, 2007. **178**(10): p. 6073-82.
398. Chodorge, M., et al., *A series of Fas receptor agonist antibodies that demonstrate an inverse correlation between affinity and potency.* Cell Death Differ, 2012. **19**(7): p. 1187-95.
399. Bardhan, K., et al., *Phosphorylation of Y248 in the ITSM of PD-1 is indicative of PD-1-mediated inhibitory function.* Journal of Immunology, 2017. **198**(1).
400. Goldstein, J.L., et al., *Receptor-mediated endocytosis: concepts emerging from the LDL receptor system.* Annu Rev Cell Biol, 1985. **1**: p. 1-39.
401. Saunders, P.A., et al., *PD-L2:PD-1 involvement in T cell proliferation, cytokine production, and integrin-mediated adhesion.* Eur J Immunol, 2005. **35**(12): p. 3561-9.
402. Wortzel, I. and R. Seger, *The ERK Cascade: Distinct Functions within Various Subcellular Organelles.* Genes Cancer, 2011. **2**(3): p. 195-209.
403. Said, E.A., et al., *Programmed death-1-induced interleukin-10 production by monocytes impairs CD4+ T cell activation during HIV infection.* Nat Med, 2010. **16**(4): p. 452-9.
404. Paluch, C., et al., *Immune Checkpoints as Therapeutic Targets in Autoimmunity.* Front Immunol, 2018. **9**: p. 2306.
405. Raptopoulou, A.P., et al., *The programmed death 1/programmed death ligand 1 inhibitory pathway is up-regulated in rheumatoid synovium and regulates peripheral T cell responses in human and murine arthritis.* Arthritis Rheum, 2010. **62**(7): p. 1870-80.
406. Gao, W., et al., *Stimulating PD-1-negative signals concurrent with blocking CD154 co-stimulation induces long-term islet allograft survival.* Transplantation, 2003. **76**(6): p. 994-9.
407. Hirata, S., et al., *Prevention of experimental autoimmune encephalomyelitis by transfer of embryonic stem cell-derived dendritic cells expressing myelin oligodendrocyte glycoprotein peptide along with TRAIL or programmed death-1 ligand.* J Immunol, 2005. **174**(4): p. 1888-97.
408. Brown, G.R., et al., *IL-12-independent LIGHT signaling enhances MHC class II disparate CD4+ T cell alloproliferation, IFN-gamma responses, and intestinal graft-versus-host disease.* J Immunol, 2005. **174**(8): p. 4688-95.
409. Dixon, K.O., et al., *Functional Anti-TIGIT Antibodies Regulate Development of Autoimmunity and Antitumor Immunity.* J Immunol, 2018. **200**(8): p. 3000-3007.

410. He, W., et al., *Galectin-9 significantly prolongs the survival of fully mismatched cardiac allografts in mice.* Transplantation, 2009. **88**(6): p. 782-90.